

# **Path Planning, Modelling and Simulation for Energy Optimised Mobile Robotics**

By

Cong Niu

This Thesis is submitted to the Department of Design, Manufacture and  
Engineering Management, University of Strathclyde, for the degree of  
Doctor of Philosophy.

# Declaration of Authenticity and Author's Rights

## AUTHOR'S DECLARATION

This thesis is the result of the author's original research. It has been composed by the author and has not been previously submitted for examination which has led to the award of a degree.

The copyright of this thesis belongs to the author under the terms of the United Kingdom Copyright Acts as qualified by the University of Strathclyde Regulation 3.50. Due acknowledgement must always be made of the use of any material contained in, or derived from, this thesis.

Signed:

A handwritten signature in black ink, appearing to read 'C. J. M.', written over a horizontal line.

Date: 05/JUNE/2021

## Acknowledgements

There are many important people who have provided help and are supportive in the research process of my Ph.D study.

First, I would like to thank Prof. Yan not only for giving me an opportunity and platform for my research, but more importantly his dedicated professionalism has been an inspiration to me as a researcher.

I would like to thank my parents, as they have provided all the funding and expenses for and during my Ph.D. I am very glad and lucky to have them as my parents. I would like to thank Dr. Yang who has given me great advice and showed me how to be a good researcher during the start of my Ph.D., when I was fortunately working in a similar project. I would also like to thank Ms Youhua Li, who has always given me good advice, and not only in an academic context.

To my friends and colleagues, Alessandro Bianco and Gwenole Henry, thank you for all the help you have provided for me during the long and difficult process of field tests for my Ph.D. research, and Dr. Mark Post during the start of my Ph.D.

I would like to thank Duncan Lindsay, Dino Bertolaccini and all the technical colleagues who have provided technical support for my research.

I would like to thank Mrs Caroline McGuire and all the colleagues who helped me in the department office, where they have always provided support.

Finally, to all my family and friends thank you for all the great support and comfort you have given me as an individual who is far away from his own home country. Also, thanks for all the others who have spent time and made effort for me during my PhD.

## **Publications**

### **Published**

Niu C, Yan X. Energy optimization path planning for battery-powered agricultural rover[C]//MATEC Web of Conferences. EDP Sciences, 2018, 173: 02001.

Yan X, Bianco A, Post M, et al. The AgriRover: a mechatronic platform from space robotics for precision farming[M]//Reinventing Mechatronics: Proceedings of Mechatronics 2018. University of Strathclyde, 2018: 112-119.

Yan X T, Bianco A, Niu C, et al. The AgriRover: a reinvented mechatronic platform from space robotics for precision farming[M]//Reinventing Mechatronics. Springer, Cham, 2020: 55-73.

### **Accepted**

Niu C, Yan X Sustainable mechatronic solution to agricultural precision farming inspired by space robotics technologies//Eco-Mechatronics – Mechatronic applications in respect of sustainability & climate change, 2021

X-T Yan, C Niu, Y Li and Gwenole Henry Capturing and integrating agricultural soil data using AgriRover for smart farming //Field Navigation and Autonomous Tractors, 2021

### **Awaiting Outcome**

Niu C, Yan X. Multi-Perspective Dynamic Modeling and Simulation of a Mobility System for Wheel Based Robotic Platform AgriRover// Journal of Information Science and Systems Science, 2021

## **Abstract**

This thesis is concerned with an investigation of a solution for mobile robotic platforms to minimize the usage of scarce energy that is available and is not wasted following traditionally planned paths for complex terrain environments. This therefore addresses the need to reduce the total energy cost during a field task or mission. A path planning algorithm is designed by creating a new approach of artificial potential field method that generates a planned path, utilising terrain map. The new approach has the capability of avoiding the local minimum problems which is one of the major problems of traditional potential field method. By solving such problems gives a reliable solution to establish a required path. Therefore the approach results in an energy efficient path of the terrain identified, instead obvious straight line of the terrain.

A literature review is conducted which reviews the mainstream path planning algorithms with the applications in mobile robotic platforms was analysed. These path planning algorithms are compared for the purpose of energy optimized planning, which concludes the method of artificial potential field as the path planning algorithm which has the most potential and will be further investigated and improved in this research.

The methodology of designing, modelling and simulating a mobile robotic platform is defined and presented for the purpose of energy optimized path planning requirement. The research is to clarify the needs, requirements, and specifications of the design. A complete set of models which include mechanical and electrical modelling, functional concept modelling, modelling of the system are established. Based on these models, an energy optimized path planning algorithm is designed. The modelling of force and the kinematics is established to validate and evaluate the result of the algorithm through simulations. Moreover a simulation environment is

established which is constructed for multi-perspective simulation. This also enables collaborative simulation using Simulink and ADAMS to for simulating a path generated by the path planning algorithm and assess the energy consumption of the driven and steering mechanism of an exemplar system called AgriRover. This simulation environment allows the capture of simulated result of the total energy consumption, therefore outlines the energy cost behaviour of the AgriRover. A total of two sets of paths was tested in the fields for validation, one being generated by the energy optimized path planning algorithm and the other following a straight path. During the field tests the total cost of energy was captured . Two sets of results are compared with each other and compared with the simulation. The comparison shows a 21.34% of the energy saving by deploying the path generated with the energy optimized path planning algorithm in the field test.

This research made the following contribution to knowledge.

A comparison and grading of mainstream path planning algorithms from energy optimisation perspective is undertaken using detailed evaluation criteria, including computational power required, extendibility, flexibility and more criteria that is relevant for the energy optimized planning purpose. These algorithms have not been compared from energy optimisation angle before, and the research for energy optimised planning under complex terrain environments have not been investigated.

Addressing these knowledge gaps, a methodology of designing, modelling and simulating a mobile platform system is proposed to facilitate an energy optimized path planning. This , leads to a new approach of path planning algorithm that reduces unnecessary energy spend for climbing of the terrain, using the terrain data available. Such a methodology derives several novel methods: Namely, a method for avoiding local minimum problem for artificial potential field path planning using the approach of approximation; A method of achieving high expendability of the path planning

algorithm, where this method is capable of generate a path through a large map in a short time; A novel method of multi perspective dynamic simulation, which is capable of simulating the behaviour of internal mechanism and the overall robotic mobile platform with the fully integrated control, The dynamic simulation enables prediction of energy consumption; Finally, a novel method of mathematically modelling and simplifying a steering mechanism for the wheel based mobile vehicle was further investigated.

# Table of Contents

1	Introduction.....	1
1.1	Development Needs and Background.....	3
1.2	Agricultural Intelligence .....	4
1.2.1	Excessive Fertilisation .....	6
1.2.2	Soil Sampling.....	7
1.2.3	Agricultural Rover .....	8
1.3	Path planning applications and challenges.....	8
1.4	Research approach and methodology.....	9
1.4.1	Research Methodology.....	9
1.4.2	Research Questions .....	10
1.4.3	Research Hypothesis .....	11
1.4.4	Aims and Objectives .....	13
1.5	Thesis Organisation.....	15
2	Literature Review.....	17
2.1	Rover and Mobile Robotic Systems.....	17
2.1.1	Space Rovers.....	17
2.1.2	Industrial Mobile Robotic Systems.....	20
2.1.3	Agricultural Rovers.....	22
2.1.4	Autonomous Cars.....	25
2.2	Approaches and Modelling Language for Path Planning .....	26
2.3	Planning Approaches and Algorithms.....	28
2.3.1	A* Algorithm .....	28
2.3.2	Rapidly-Exploring Random Tree (RRT) algorithm .....	30
2.3.3	Pure Pursuit Path Planning Algorithm .....	32
2.3.4	Artificial Potential Field Path Planning Algorithm.....	35

2.3.5	Particle Swarm Optimisation .....	37
2.3.6	Ant Colony Planning Algorithm .....	38
2.3.7	Genetic Algorithm for Energy Optimised Path Planning.....	40
2.3.8	Neural Network (Multi-layer perceptron) for Energy Optimised Path Planning .....	42
2.3.9	Reinforcement Learning for Path Planning.....	43
2.3.10	Kalman Filtering .....	44
2.3.11	Model Predictive Control Algorithm .....	45
2.4	Simulation and Modelling.....	46
2.4.1	Multi-Perspective Approach .....	47
2.4.2	Energy Modelling and Dynamic Simulation.....	48
2.4.3	Battery Simulation and Modelling.....	50
2.5	Algorithm Comparison for Energy Optimised Path Planning .....	51
2.6	Summary and Identification of Knowledge Gaps.....	55
3	Design Methodology for Energy Optimised Path Planning of Mobile Robotics (EO- PPMR).....	60
3.1	Introduction.....	60
3.2	Energy Optimised Planning Design Methodology .....	65
3.2.1	Task Clarification .....	66
3.2.2	Conceptual Design .....	67
3.2.3	Embodiment Design.....	69
3.2.4	Function Design Process .....	69
3.3	Evaluation .....	71
3.4	Summary .....	73
4	Energy Modelling and Energy Optimised Path Planning .....	74
4.1	Introduction.....	74
4.2	Energy Modelling of the AgriRover .....	75

4.3	Energy Optimised Planning .....	78
4.3.1	Introduction of the Algorithm for Energy Optimisation Planning .	78
4.3.2	The Advantages of the Artificial Potential Field.....	79
4.3.3	Description of the Energy Optimisation in Path Planning .....	80
4.4	Potential Field Representation and Generation.....	81
4.4.1	Accessing and Processing the Map .....	81
4.4.2	Potential Field Representation .....	83
4.4.3	A Generic Artificial Potential Field Generation Algorithm .....	84
4.5	Generating the Generic Field for the Farming Fields From Maps.....	87
4.6	Multi-Artificial Potential Field Representation and Merging.....	89
4.6.1	Path Finding with the Merged Potential Field .....	91
4.6.2	Difficulty and Solutions using the Artificial Potential Field Method	
	96	
4.7	Energy Cost Estimation Implemented in MATLAB.....	97
4.8	Case Demonstrations and Algorithm Validation .....	97
4.9	Expanding the Artificial Potential Field.....	101
4.10	Summary .....	103
5	The Mathematical Modelling of the AgriRover Steering Mechanism.....	105
6	Dynamic Modelling and Analysis of the Rover Driving Wheels .....	116
6.1	Introduction .....	116
6.2	Definition and Classification of the Field Surface Irregularities .....	116
6.3	Relationship between Current and Torque of the Rover Motors .....	117
6.4	Kinetic Response of the Rover on Different Surfaces .....	122
6.5	Analysis of the Relationship between Torque and the Capacity of the Rover	125
6.6	Summary .....	127
7	Motion Analysis of the Rover .....	128

7.1	Mechanism Motion Modelling Aim and Objectives.....	128
7.2	AgriRover Kinematic Motion Model.....	131
7.3	Mechanism and Motion Simulation and Analysis .....	131
7.3.1	Linear Motion on Solid Flat Surface.....	131
7.3.2	Linear Motion on a Soft Flat Surface.....	133
7.3.3	Linear Motion with Different Speeds .....	135
7.3.4	Linear Motion with Slopes in the Farmland Field .....	138
7.3.5	Linear Motion with Obstacles.....	139
7.3.6	Linear Motion with a Trench.....	140
7.3.7	Linear Motion with Sinusoidal Surface .....	141
7.4	Summary .....	142
8	ADAMS and Simulink Co-Simulation .....	143
8.1	Aim of the Co-Simulation.....	143
8.1.1	Aim and Objectives.....	143
8.1.2	Variables of the Simulation .....	143
8.1.3	Control .....	145
8.2	ADAMS and MATLAB Co-Simulation Overview.....	146
8.2.1	Co-Simulation Overview .....	146
8.2.2	Co-Simulation Principle.....	148
8.2.3	Co-Simulation Setup Process.....	149
8.3	Mechanical System Setup for the AgriRover.....	150
8.3.1	3D Model .....	150
8.3.2	Kinematic Pairs .....	151
8.3.3	Definition of the Contact Force .....	152
8.3.4	Navigation Angle Measurement Module .....	153
8.3.5	Setup ‘Measures’ with Rover Orientation and Motion Status Measurement.....	154

8.4	ADAMS Model Parameter Settings.....	155
8.4.1	Variable Definitions .....	155
8.5	MATLAB Simulink Block Diagram .....	158
8.5.1	Control Model Setup.....	158
8.5.2	Control Scheme Setup in Simulink.....	160
8.5.3	Simulink Function Block and Path Tracking .....	161
8.5.4	Front Wheel Steering Angle Control Module .....	168
8.6	PID Parameters Tuning .....	168
8.7	Simulation Verification and Debugging.....	169
9	Validation and Evaluation Through Field Tests .....	172
9.1	Field Test Task Descriptions .....	172
9.2	Field Test Setup Description .....	173
9.2.1	Power Consumption Test in UK from Point A to B .....	173
9.2.2	Power Consumption Test in Multi-Point Planning .....	175
9.3	Path Planning Before the Test .....	176
9.3.1	Path Planning in UK Field Tests .....	176
9.3.2	Multiple Target Point Path Planning .....	182
9.4	Overview of the Rushyhill Farm Field Test .....	188
9.5	Result and Data Analysis .....	190
9.5.1	Rushyhill Farm field Test.....	190
9.5.2	Field Test in China .....	195
9.6	Summary .....	195
10	Discussion and Conclusion .....	197
10.1	Contribution to Knowledge.....	197
10.2	Discussion .....	203
10.2.1	Hypothesis Discussion .....	203
10.2.2	Aims Discussion .....	205

10.2.3 Overall Discussion .....	206
10.3 Future Work and Improvement .....	207
10.3.1 An Energy Optimised Path Planning Method for Multiple Robots 207	
10.3.2 AgriRover Hardware Update .....	208
10.3.3 GPS Accuracy .....	209
10.4 Conclusion .....	209
References .....	211
Appendix A: Co-Simulation.....	220
Notes for the Co-Simulation Setup for Future Reference .....	220
Variable Setup .....	220
Links between MATLAB Simulink and ADAMS .....	223
Co-Simulation Result Data Processing .....	225
Problems and Solutions of Co-Simulation.....	227

## Table of Figures

Figure 1. (A) UN 2012 (solid red line), with 80% PI (dark shaded area), 95% PI (light shaded area), and the traditional UN high and low variants (dashed blue lines). (B) UN 2012 population projections by continent. In both graphs, the vertical dashed line denotes 2012. (Gerland <i>et al.</i> , 2014).....	1
Figure 2. AgriRover, prototype with soil sampling and analysis system in a field .....	3
Figure 3 Research process flow chart by (Kothari, 2004) .....	10
Figure 4. Opportunity rover traverse map, Western rim of Endeavour, 3,328th Martian day (NASA, 2013).....	20
Figure 5. Division of areas and micro areas into nodes (Kusuma <i>et al.</i> , 2019). ..	29
Figure 6. Modified RRT algorithm for exploration by Umari (Umari <i>et al.</i> , 2017) .....	31
Figure 7. Geometric explanation of the Pursuit path (BačÍK <i>et al.</i> , 2017) .....	32
Figure 8. All-Purpose Remote Transport System (Wit, 2000).....	33
Figure 9. Pure pursuit relationships between speed and look-ahead distance (Wit, 2000) .....	34
Figure 10. Safe path selected (Warren, 1989) .....	36
Figure 11. Particle Swarm Optimisation with iterations (Bansal, 2019) .....	37
Figure 12. Ant colony planning (Blum, 2005).....	39
Figure 13. Ant colony size compared (bars on the curve for every 5 iterations shows the standard deviation) (Blum, 2005) .....	40
Figure 14. Basic structure of the battery simulation framework by Reiter (Reiter <i>et al.</i> , 2019) .....	51
Figure 15. Yan’s mechatronic system design concept (Xiu-Tian Yan <i>et al.</i> , 2010) .....	63

Figure 16. A generic design process model for energy optimised mechatronic rover system .....	64
Figure 17. Conceptual design stages (Christophe <i>et al.</i> , 2014).....	68
Figure 18. Design process of the energy optimised path planning algorithm....	70
Figure 19. A the dynamic total cost of transport plot example. Running for 18.3 m with an average speed of 0.3 m/s. ....	78
Figure 20. Geology terrain map .....	82
Figure 21. OS Terrain™ 5 DTM tiles .....	83
Figure 22. Map process flowchart.....	84
Figure 23. Farmland field terrain .....	84
Figure 24. Plot of a two-dimensional slice of the gravitational potential in and around a uniform spherical body. The inflection points of the cross-section are at the surface of the body. (Tikhonov <i>et al.</i> , 2013) .....	86
Figure 25. Distance potential field of a farm land .....	87
Figure 26. Height difference potential field.....	89
Figure 27. Merged potential field.....	90
Figure 28. Merged potential field when the interval of both fields is matched .	91
Figure 29. <code>distance_p</code> decision code .....	93
Figure 30. Waypoints on the map.....	94
Figure 31. Simplified flow chart of the algorithm .....	95
Figure 32. Energy cost estimation code .....	97
Figure 33. Straight-line path and height change graph .....	98
Figure 34. Energy optimised path and height change graph.....	99
Figure 35. Downhill condition compared. ....	100
Figure 36. Randomly generated surface roughness map .....	102
Figure 37. Large map planning result .....	103
Figure 38. Block diagram of Equation 29 .....	108

Figure 39. Block diagram of Equations 29 and 30.....	108
Figure 40. Block diagram of Equation 32.....	109
Figure 41. Merged diagrams of Figure 39 and Figure 40 .....	109
Figure 42. Merged diagram of Equation 33 and Figure 41 .....	109
Figure 43. Merged diagram of Equation 36 and Figure 42.....	110
Figure 44. System Block diagram.....	110
Figure 45. Transformation of Figure 44.....	111
Figure 46. Transformation of Figure 45.....	111
Figure 47. System block diagram with output of $\theta_m$ .....	112
Figure 48. System block diagram including mass .....	112
Figure 49. Steering mechanism modelled in Simulink .....	113
Figure 50. Steering system block diagram.....	115
Figure 51. Performance parameters of the 940D1001 motor.....	118
Figure 52. Wheel hub transmission of the first-generation rover .....	119
Figure 53. Driving wheel simulation setup.....	120
Figure 54. Road surface Class D simulation of the rotating torque on each wheel .....	121
Figure 55. Total driving current .....	122
Figure 56. Simulation results of the torque on each wheel on a Class D field surface .....	123
Figure 57. Simulation results of the torque on each wheel on a Class E field surface .....	123
Figure 58. Simulation results of the torque on each wheel on a Class F field surface .....	124
Figure 59. Relationship between maximum torque and mass on a Class E surface .....	127
Figure 60. Left: the rover, Right: the model .....	129

Figure 61. AgriRover front cabin CAD model.....	131
Figure 62. Rover travel displacement versus time curve .....	132
Figure 63. Car speed versus time curve .....	132
Figure 64. Actuator support force versus time curve .....	133
Figure 65. Driving torque versus time curve .....	133
Figure 66. Rover traveling speed vs time curve.....	134
Figure 67. Supporting force of the actuator provided by the steering mechanism .....	134
Figure 68. (1) Driving torque on the wheel, (2) Driving torque after stabilisation .....	135
Figure 69. Relationship between time and rover displacement .....	137
Figure 70. Relationship between time and speed.....	137
Figure 71. Supporting force provided by steering actuator under different speeds .....	138
Figure 72. Rover speed versus time graph.....	139
Figure 73. Geometry of the Obstacle .....	139
Figure 74. Rover speed versus time graph when passing an obstacle .....	140
Figure 75. Geometry of the trench .....	140
Figure 76. Rover speed versus time curve when passing over the trench.....	141
Figure 77. Speed versus time curve on sinusoidal field.....	142
Figure 78. The model of the AgriRover .....	144
Figure 79. Waypoints generated by the path planning algorithm. ....	144
Figure 80. Terrain imported for the co-simulation.....	145
Figure 81. Co-Simulation Principle .....	148
Figure 82. Simplified AgriRover model.....	151
Figure 83. Joint in ADAMS after simplification.....	151
Figure 84. Rover and the terrain contact force parameters .....	152

Figure 85. ADAMS simulation .....	153
Figure 86. Navigation angle measurement module.....	154
Figure 87. ADAMS measure settings.....	154
Figure 88. Input and output variables set .....	155
Figure 89. The complete construction of the control syste .....	160
Figure 90. Speed control block diagram .....	162
Figure 91. Control block diagram of the trajectory tracking .....	163
Figure 92. Trajectory data entry module .....	164
Figure 93. Function Block Parameters ‘Selector’ module .....	165
Figure 94. Expected steering angle block diagram .....	165
Figure 95. Cycle counting module .....	167
Figure 96. Judgment of loop breaking module .....	167
Figure 97. Front wheel steering angle control module .....	168
Figure 98. PID control parameters tuning.....	169
Figure 99. Second co-simulation Second Co-simulation results of an optimal path in comparison with a standard path: (1) the optimised path, (2) intermediate energy for the path in (1), (3)hight changes for the path(1), (4) straight or normal path, (5) intermediate energy for the path in (4), (6) hight changes for the path (4).....	170
Figure 100. Field test of current and voltage data validation.....	174
Figure 101. Test power data validation characteristic comparison .....	175
Figure 102. Energy optimised waypoints plotted on satellite map .....	178
Figure 103. Energy optimised path and height change .....	179
Figure 104. Straight path and height change.....	180
Figure 105. Straight path with waypoints plotted on satellite map.....	182
Figure 106. An example plan for soil sampling generated for a target farm at NERCITA.....	183

Figure 107. Plan for soling sampling at NERCITA’s National Demonstration Base .....	184
Figure 108. An alternative AgriRover robotic path plan.....	184
Figure 109. A complete robotic soil sampling plan for the NERCITA selected farms.....	185
Figure 110. A complete robotic soil sampling plan for the NERCITA selected farms.....	187
Figure 111. A complete robotic soil sampling plan for the NERCITA selected farms.....	188
Figure 112. Rushyhill farm field test setting.....	189
Figure 113. Rushyhill farm field test with water and ice. ....	190
Figure 114. Field test power output from each driving and steering module, planned path compared to the straight path.....	192
Figure 115. Field test power at a given time for the planned and straight paths .....	193
Figure 116. Trapezoidal numerical integration zoomed in .....	194
Figure 117. Relationships between each contribution .....	199
Figure 118. Variable torque_vr1 setup .....	220
Figure 119. Set input variables.....	220
Figure 120. Set the torque .....	221
Figure 121. Acceleration settings.....	222
Figure 122. Link the model with the variable .....	223
Figure 123. Function Block Parameter: ADAMS Plant window .....	224
Figure 124. Simulation window .....	226
Figure 125. The Result Set box selecting torque_pos.....	226
Figure 126. Power curve generation .....	227



## Table of Tables

Table 1. Suitability for energy optimised path planning .....	53
Table 2. Work on path planning completed by others.....	58
Table 3. Energy optimised planning algorithm design process needs and tasks	66
Table 4. Time needed to complete the planning.....	101
Table 5 Time needed to complete the planning for a large map .....	103
Table 6. Road Classification (Andren, 2006) (Nguyen <i>et al.</i> , 2019) .....	117
Table 7. Simulation Parameters.....	120
Table 8. Road surface class D simulation and calculation results.....	121
Table 9. Calculation results of different surfaces .....	124
Table 10. Relationship between torque and capacity for the rover .....	126
Table 11. Parameters used in the Mechanism motion modelling.....	130
Table 12. Input and output variables .....	156
Table 13. Output variable .....	158
Table 14. Energy optimised waypoints set in GPS coordinates.....	177
Table 15. Straight path waypoint set .....	181
Table 16. A potential plan for soil sampling, consists of GPS coordinates and distance information between points.....	186

## **List of Acronyms**

**APF: Artificial Potential Field**

**ADAMS: Software for Multibody Dynamics Simulation Solution**

**GPS: Global Positioning System**

**RRT: Rapidly-Exploring Random Tree**

**UAV: Unmanned Aerial Vehicle**

**AUV: Autonomous Underwater Vehicle**

**NASA: US National Aeronautics and Space Administration**

**JPL: NASA Jet Propulsion Laboratory**

**LIBS: Laser Induced Breakdown Spectroscopy**

**FINER: Feasibility, interest, novelty, ethics, and relevance**

**MMRTG: Multi-Mission Radioisotope Thermoelectric  
Generator**

**KMR QUANTEC: mobile industrial robot system from KUKA**

**OPTIC: Optimising Preferences and Time-Dependent Costs**

**TCoT: Total Cost of Transport**

**EO- PPMR: Energy Optimised Path Planning of Mobile  
Robotics**

# 1 Introduction

In 2018 the world population reached and exceeded 7.6 billion people around the world. It took over 200,000 years to reach 1 billion people, but only 200 years to exceed 7 billion people, with more than an 80% possibility that the world population will be over 9.6 billion in 2050 (Gerland *et al.*, 2014). Figure 1 shows the world population growth projection.

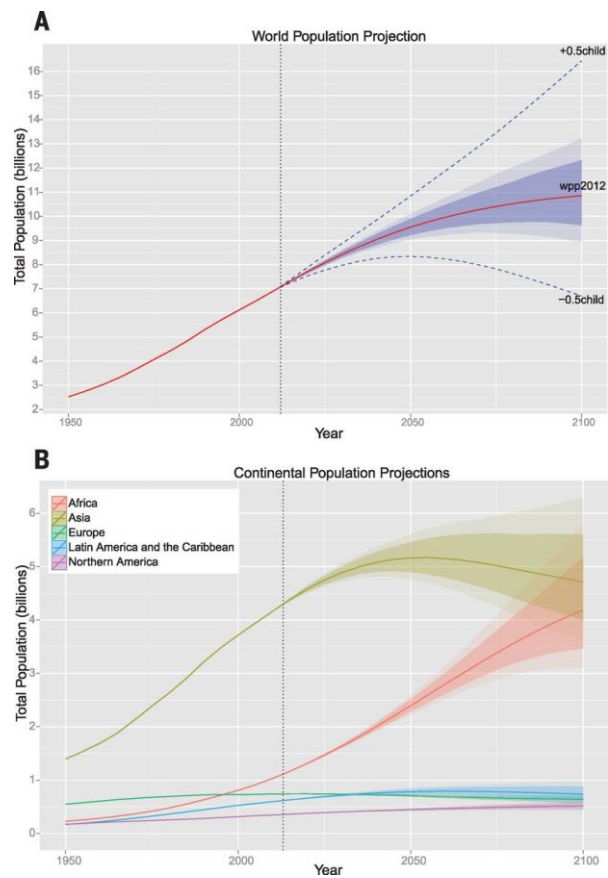


Figure 1. (A) UN 2012 (solid red line), with 80% PI (dark shaded area), 95% PI (light shaded area), and the traditional UN high and low variants (dashed blue lines). (B) UN 2012 population projections by continent. In both graphs, the vertical dashed line denotes 2012. (Gerland *et al.*, 2014)

According to the FAO (United Nations' Food and Agriculture Organization), the food production must improve by 60% to meet the demand of basic food for the population need by 2050 (Jayaraman *et al.*, 2016). A more efficient agricultural

process will be beneficial for the world population. It is a tendency that objects and processes around us, such as lights, TV, kitchenware, cars, and manufacturing processes, are all getting smarter. However, for farming processes in the field, improvements still can be made. Two major factors that prevents the autonomously-operated farming platforms to be widely used is the cost and the effectiveness. These two factors are related to each other, the effectiveness of the farming platform and the cost are under the same considerations, a better platform should have a lower cost and a high effectiveness, but normally a lower cost farming platform will not be as effective as the higher cost farming platform. Hence, if the cost is limited, hardware of the platform would be hard to improve, but the software on the farming platform can be improved with a smaller cost increase.

The software for a robotic autonomous farming platform requires many different algorithms . Firstly, an interface has been developed for the user, the farmer can use this to set the mission and tasks for the robot platform. Then the mission planning system will set the tasks for the robot. After the mission has been planned, the path planning will start finding the path for the robot from point to point. The path planning algorithm then can find a path between two points with different planning goals whether it is a goal of optimised energy or time.

Sustainable development is becoming a tendency and is one of the most important elements for future development, without the consideration of sustainability the environmental problem will become a “contemporary issue” as introduced by Klarin (Lakshmanan *et al.*, 2020). Even though the coal consumption for generated electricity has decreased since 2003 from 38.4% to 22.4% in 2019, the electricity generated from fossil fuels still contributes to 53.8% of all electricity generated, according to the International Energy Organization (IEA) in 2020. Subsequently, energy efficient

designs and projects are becoming more important to comply with the idea of sustainability.

## 1.1 Development Needs and Background

In a development process for a robotic farming platform, compromises have been made due to a confined size and budget. For a lower budget, an electric driven wheel-based rover is more suitable than some of the other options, such as a full-sized robotic-controlled tractors. The AgriRover has been designed and made with the maximum total weight of 25 kg with a load. Figure 2 shows the AgriRover running in a field.



Figure 2. AgriRover, prototype with soil sampling and analysis system in a field

If a task path point has been decided for the rover, a path planning algorithm will find the shortest path in space, which is the projection of a straight line on the terrain when no obstacles. But, in the UK, a lot of the farm fields are not flat, so a projection of a straight path on the terrain may not be the most energy efficient path when the field is not flat. Terrain will have lower and higher points when running in the real world.

These lower terrains have a tendency of being inside of a shaded area, which could accumulate water, resulting in the surface around these points being softer. This will have the potential danger of getting the rover trapped, thus these potentially dangerous areas should be avoided. Secondly, as this rover is battery powered, the total amount of energy that can be used before the battery is depleted are limited, so a more energy efficient and safer path planning algorithm needs to be developed.

There are many types of battery powered autonomous vehicles know as mobile robotic vehicle can benefit from such path planning, modeling and simulation design process and methodology. This algorithm is be developed with versatility in mind, which make it possible to use on other mobile robotic vehicle and platforms that have limited onboard energy source. For example, in a lunar rover with a battery and solar cell as the energy source. Furthermore, the energy optimisation path planning algorithm should not only be focused on maximising the effectiveness of the mission, but also on increasing the reliability of the vehicle by lowering the load on the onboard driving actuators.

Finally, there should be comprehensive and systematic modelling and simulations to give a guideline for the effectiveness of the algorithm during field tests. The simulation should focus on generating an energy consumption profile with the detailed controllable vehicle model and the real-world terrain data.

## **1.2 Agricultural Intelligence**

During recent years, mechanical, electronic and electrical devices are becoming more and more intelligent. But for some of the agricultural applications, such as soil sampling and analysis in the UK and China, it has not been fully automated. Soil sampling and analysis is mostly done every two years, this results in only a report with 100 m resolution (Niu *et al.*, 2018) given to the farmer, along with the soil nutrients.

Producing a higher resolution of this soil sampling nutrients data is time consuming and highly labor intensive work if it is done manually, therefore the analysis fee is expensive. However, for precision agriculture this data is important, as not only are the correct nutrients levels of the soil essential for the crop growth, but also the different levels of the soil nutrients are required for different crops. So, to increase the yield of crops the soil nutrients need to be controlled in a suitable range, depending on the crops. This measurement process is normally done every two years which is infrequent, therefore the precise fertilisation can only be carried out every two years according to the measurement data. So, a more frequent soil sampling and nutrients analysis will improve the precision of the fertilisation, therefore improving the yield of the crops. For organic farming, informatisation of the crops are important for tracking and monitoring purposes, as the traceability of the organic farming is essential, and the nutrients levels need to be recorded.

Ecological footprints can be reduced by utilising technics from smart farming. Fertilisers and pesticides can be applied with higher precision and in lesser quantities depending on the specific farming site. A precision agricultural system can extenuate leaching problems, as well as the emissions of greenhouse gasses (Georgakopoulos *et al.*, 2016).

For smart farming applications accessibility, accuracy, and timeliness of the fertilisation are important and indispensable informatisation. As such, for a more timeliness informatisation, the fertilisation needs to be tested more often than the traditional laboratory methods with reduced costs. For a farm that is far away from any soil nutrients laboratory this method can allow the test on site, which makes it more flexible, less time consuming and allows it to be more real time. This is more useful and useable by the farmers. As the space of the arable field is limited, the changes are advancing significantly to produce enough crops for human consumption. Positioning

and smart farming a solution for a such problem has always been a consideration for mankind. By utilising technics from positioning and smart farming, the crops yielded per unit area are improved (Prathibha *et al.*, 2017) (Kempenaar *et al.*, 2016) .

There are many methods of smart farming and agricultural intelligence ranging from sensing, data collection, data processing, fertilisation, crop harvesting, pest control and soil nutrients analysis. Firstly, for agricultural sensing there are both remote sensing and local sensing. For example, in remote sensing in agricultural intelligence: multispectral remote sensing has been used for estimation of the green leaf area index (Curran, 1983). Vegetation indexing is a transformation of light in two or more wavelengths, by measuring these bands of light the contribution of vegetation properties can be determined as the vegetation index in order to describe the spatial and temporal inter-comparisons of photosynthetic activity of the field and canopy structural variations (Huete *et al.*, 2002). This method is used for gaining the vegetation index of a given area, such as a forest or agricultural field. By utilising the vegetation index, agricultural practitioners have the tools to monitor the growing status of the plant from a macro perspective. With remote sensing, a vegetation index map over a time period can be generated. Using this map, agricultural practitioners can observe overall changes during the months, seasons, and even years. Information like this will help them to predict the crop growth status and for future planting. By using the soil nutrient data over time combined with the remote sensing data, a higher level of precision agriculture can be produced.

### 1.2.1 Excessive Fertilisation

One problem caused by excessive fertilisation is eutrophication (G Fred Lee *et al.*, 1978) (Jones *et al.*, 1982). The urgency of reducing eutrophication by lowering nutrient input into aquatic ecosystems “*in order to protect drinking-water supplies and to reduce eutrophication, including the proliferation of harmful algal blooms and*

“dead zones” in coastal marine ecosystems has been widely recognized (Conley *et al.*, 2009)”. One of the most problematic nutrients causing the eutrophication is the organic nitrogen compound where the Planktonic N<sub>2</sub>-fixing cyanobacteria are blooming, causing pollution in fresh water (Conley *et al.*, 2009). However, for agricultural purposes fertilisers that are rich in organic nutrient compounds are essential, where nitrogen nutrients are the most important nutrients for the growth of agricultural crops, and also the hardest to manage (Gaskell *et al.*, 2007). Traditionally, farmers use excessive amount of fertiliser to ensure the nutrient levels in the farmland field is sufficient for the growth of crops, causing eutrophication. With the idea of sustainability and precision farming in mind, this problem can be reduced and finally solved by utilising an autonomous unmanned vehicle that is capable of analysing the soil in real time and apply the fertilising compound according to the nutrient data.

### 1.2.2 Soil Sampling

The more frequently an accurate soil sampling and analysis is completed is an important step forward for balancing the growth of agricultural crops and the prevention of over fertilisation. A search system capable of doing this task was designed and built in the form of a prototype robotic mobile vehicle as shown in Figure 2. With the drill on board attached to the rear section of the AgriRover, the soil sampling process will be able to be performed autonomously in the field. After the sampling of the soil, a process of Laser Induced Breakdown Spectroscopy (LIBS) (Xiu T Yan *et al.*, 2018) is performed, which will give a unique absorption spectrum, depending on the composition of elements in the soil. Finally, according to this absorption spectrum data, the nutrients in the soil can be calculated. By repeating the sampling and LIBS process, the report can be generated with flexibility in the sampling point, defined by the user.

### 1.2.3 Agricultural Rover

The AgriRover was designed as a multipurpose autonomous robotic mobile platform, specifically for agricultural applications, such as soil sampling, crop picking and mapping. This multipurpose agricultural robotic mobile platform is designed with inspiration from the concept and mindset of interplanetary Rovers, while maintaining a favourable economical cost. Utilising the rechargeable lithium battery as the energy source with full electrical actuators and motors for the mobility system, the AgriRover is designed with the focus of an eco-friendly and sustainable development, as it is important both environmentally for the wellbeing of ourselves and financially makes sense in long term. One of the design perspectives is to make the AgriRover energy efficient during its operation, this can be achieved by following an energy efficient pathway. The design and validation of the energy optimised path planning algorithm will be the focus of this thesis.

## 1.3 Path planning applications and challenges

Path planning applications include mostly two types, one is for mobile robotic platforms and the other one is for robotic arms. In this paper the path planning algorithm in discussion is focused on the mobile robotic platforms. Such mobile robotic platforms path planning applications include the robotic platforms running on the ground, such as the AgriRover or Perseverance Rover on mars, and can be expanded to UAVs, AUV. When running autonomously a path planning algorithm will need to function correctly, which is not always the case. For example, the Opportunity Rover had to end it's mission because of the path taken was on soft sand, lead to the it being stucked, this has been further discussed in Chapter 2. Performance of the path planning algorithm is evaluated differently depending on the applications, but can include aspects such as time losses, energy costs, real time performance and reliability.

So, the main changes for the path planning are to increase the performance and reliability with the data available, and reduce the requirement of computational power. Finally, a simulation for such a plan path is beneficial for evaluation and to reduce the cost of experimentation. In this case the path planning algorithm are designed for the general mobile robotic platform in this case the AgriRover, which is a battery powered autonomous mobile platform designed to work in agriculture applications. The challenges faced with this path planning application, like many other battery-powered small size mobile robotic platforms, is the total amount of energy that can be carried on the platform. To solve this challenge, a path planning algorithm that is focused on generating an energy efficient path is required.

## **1.4 Research approach and methodology**

This chapter describes important research questions in the field of mobile robotics, more specifically on their path planning, with an aim for the consideration of maximising energy utilisation. In order to answer these questions a research methodology is followed. First hypothesis is made to prove or disprove it. These lead to the formal definition of the research aims and objectives through which the research questions are answered.

### **1.4.1 Research Methodology**

Research methodology is a scientific and systematic way of solving the research problem which is adopted by researchers for the study of the problem with logic behind them. Certain procedures and techniques identified as methods are only applicable to certain problems, research methodology considers the logic behind the methods. (Kothari, 2004)

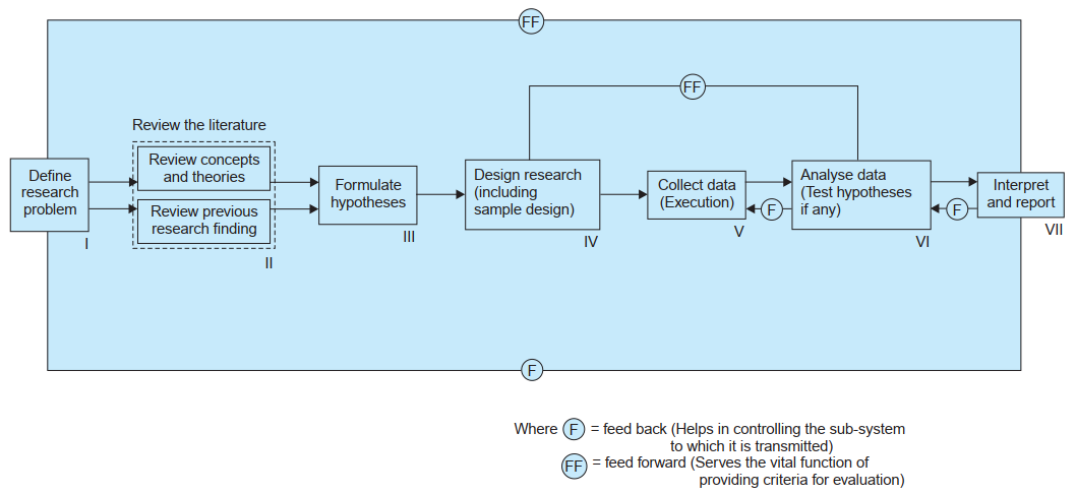


Figure 3 Research process flow chart by (Kothari, 2004)

Figure 3 shows the research process developed by Kothari, which has more than thirty thousand citations and is widely adopted among researchers. From left to right in Figure 3 are stages I to VII, which covers the whole research process. Stage I is the definition of the research problem, which is proposed and discussed in this chapter under sections 1.4.1 and 1.4.2. Stage II covers the review of literature and knowledge gap identification which is done in chapter 2. Stage III formulates the hypotheses presented in this chapter under section 1.4.3. Stages IV to VI is the main body of the research, which includes research design moulding simulation and testing covered in Chapters 3 to 9. The final stage VII is covered in Chapter 10 with the discussion and conclusion interpreted in the report in Figure 3.

### 1.4.2 Research Questions

In general, the research questions need to be able to define two questions. First is to answer what kind of research that the researcher will be looking for and where to look for it. The second is to identify the objectives of the research that will be studied (Gregar, 1994). For the first question, the kind of research in this thesis is both a

qualitative and quantitative matter, this is discussed in Chapter 3. For the second question, the aims and objectives of the research is discussed in Section 1.4.4.

More specifically, research questions are described in single sentences that can achieve new insights, with answers to a new field of mobile robotics and its energy efficient planning. These questions can specify a study design, predictor, or outcome to the needs of knowledge, as Hulley introduced in (Hulley, 2007). Hulley also proposed an evaluation method named “FINER criteria”. For the topic of this thesis, the following research questions can be asked:

What constitutes a feasible approach to designing an energy optimized path planning algorithm for mobile robotic platforms? This would provide new knowledge to advance next generation agricultural mobile robotics to address the increasing demands for more efficient food production.

How such a design for this kind of energy optimised path planning algorithm for a mobile robot should be derived? Furthermore, how does this specific design of the energy optimised planning algorithm cope with the varying terrains for the mobile robotic platforms? Both of these questions are answered with a new approach based on the literature review. The literature review first shows the current knowledge of past planning algorithms for different platforms within different applications. Therefore, the review gives an evaluation to these search algorithms proposed. Through the process of identifying the knowledge gaps, the novelty of this research can be determined.

### 1.4.3 Research Hypothesis

A hypothesis is a description on the expectancy of research outcomes, not a random guess, but a prediction using the knowledge available. The first step for the question

of the hypothesis should be specific and researchable (Crick *et al.*, 1994). For this thesis, the first part of the hypothesis is: How to extend the mission duration of a wheel-based mobile robotic platform without spending money or requiring upgrading of the hardware. The second step of hypotheses is formed after the preliminary research. For this thesis, the second part of hypothesis is: Upgrading the past planning algorithm with the goal of extending the mission duration should be achievable. The third step of proposing a complete set of hypotheses are to formulate the questions. For this thesis, the third part of hypothesis is: There is an algorithm that can be designed to solve the problem of unnecessary energy losses, therefore extending the mission duration when a mobile robotic platform, such as the AgriRover, is running in an undulating terrain environment.

The fourth step for proposing a complete set of hypotheses is to refine the hypothesis, ensuring it to be specific and testable, while also containing the relevant variables and predicted outcomes. For this thesis, the fourth part of hypothesis is: By utilising design of the energy optimised path planning algorithm, it is more likely to lower the total energy cost during the operation of a mobile robotic platform, such as the AgriRover, in an undulating terrain environment. Step five of proposing a complete set of hypotheses is to make a comparison. For this thesis, the fifth part of hypothesis is: The total energy costs of the same planning task when using the energy optimised path planning algorithm, utilising the AgriRover in an undulating terrain environment, is lower than when the AgriRover is running in a straight-line. The last step of proposing a complete set of hypotheses is to set the null hypotheses, which is the opposite of the expected result. For this thesis, the final part of the hypothesis is: Even with the energy optimised path planning algorithm utilised by the AgriRover, the total energy cost is the same or higher than the straight-line planning under the same planning task running in an undulating terrain environment.

#### 1.4.4 Aims and Objectives

The aim of this project is to investigate a methodology to design a path planning algorithm for mobile robotic platform, such as the AgriRover, that lowers the total energy losses when running in a terrain rich environment. This new algorithm designed must be expandable, with new needs and functions, as the multifunction mobile robotic platform evolves. In addition, the algorithm designed should be adaptable with minimum modifications for other mobile robotic platforms. Finally, a complete and comprehensive modelling and simulation of the AgriRover as an example needs to be implemented as the evaluation guideline for the energy optimised path planning algorithm.

The objectives of the project are identified as follows: the first step of the objective definition process is to propose valid and researchable questions as shown in section 1.4.2, which followed a framework of the “FINER criteria” as Hulley introduced (Hulley, 2007). This step will check if the topic that needs to be researched can pass the criteria of ‘Feasible’, ‘Interesting’, ‘Novel’, ‘Ethical’ and ‘Relevant’, therefore becoming a valid research topic that can continue to proceed. Secondly, a set of hypotheses needs to be presented, which are shown in Section 1.4.3, and these hypotheses set the expected result and unexpected result, therefore it can be used as the proof conditions for this project. After this, the following objectives are identified to achieve the research aim:

- Designing the path planning algorithm for a mobile robotic platform, such as the AgriRover, that is focused on the energy consumption of the AgriRover being the first planning priority, except the safety.
- Using the terrain data of the test farmland field for the major considerations of the path planning, in order to achieve a planned path for a mobile robotic

platform that avoids passing through the terrains unnecessarily, and therefore saving more energy compared to going in a straight path.

- Modelling and simulating the energy consumption of a mobile robotic platform needs to be done. This is so that when operating in the field during its mission, these simulated results can be used as evidence for the performance of the energy optimised path planning algorithm.
- Comparing and evaluating the results of the field test needs to be completed, which include the comparison of the results generated by the energy optimised path planning against the energy losses when a mobile robotic platform is operating in a straight line.
- Finally, an evaluation and conclusion will be drawn according to the results of the comparison, which should give a percentage of the total energy saved and the energy saved per unit distance travelled.

After specifying the design objectives, the literature review can be ensued, with the aim to find a novel solution that is suitable and efficient to solve the problem of energy optimised planning, which is shown in Chapter 4. The objective of this review is to identify the information gap by analysing the current methods and approaches of the path planning methods for mobile robotic platforms, and identify suitable approaches that can be used to solve the problems of energy optimised path planning.

Following the literature review, a research methodology is presented in Chapter 3. This lays the foundation for generating a new method of the path planning algorithm, which can help to model and simulate mobile platforms, such as the AgriRover, to generate paths. The field tests of the algorithm can then be carried out and the results of the power consumption can be recorded for the analysis and comparison purposes. Based on these, it is possible to draw conclusions from the findings and define future research work, according to the results of the simulation and verified field tests, for the improvement of the design process and associated methodology.

## **1.5 Thesis Organisation**

### Chapter 1 – Introduction

Introduction and overview of the problems needing to be solved from the perspective of path planning, modelling and simulation, as well as the thesis research methodology.

### Chapter 2 – Literature Review

Review and knowledge gap identification in the literature on path planning with energy optimisation, modelling and simulation for a mobile robotic platform.

### Chapter 3 – Design Methodology for Energy-Optimised Path Planning for Mobile Robotics

Design methodology for a general mobile robotic platform with the goal of energy-optimised design criteria and considerations.

### Chapter 4 – Energy Modelling and Energy-Optimised Path Planning

Energy modelling frameworks for a general mobile robotic platform – AgriRover and the energy-optimised path planning algorithms design and implementation on actual farmland.

### Chapter 5 – The Mathematical Modelling of the AgriRover Steering Mechanism

The static modelling of the steering mechanism for a general mobile robotic platform – AgriRover.

### Chapter 6 – Dynamic Modelling and Analysis of the Rover's Driving Wheels

The dynamic modelling and analysis of the driving wheels for a general mobile robotic platform – AgriRover.

## Chapter 7 – Motion Analysis of the Rover

The motion analysis of a general mobile robotic platform – the AgriRover under different surface conditions and mission payload.

## Chapter 8 – ADAMS and Simulink Co-Simulation

A collaborative simulation between ADAMS and Simulink of a general mobile robotic platform – the AgriRover with the task of following a specific path on specific terrain.

## Chapter 9 – Validation and Evaluation Through Field Tests

Validation and evaluation of energy-optimised path planning, modelling and simulation using a general mobile robotic platform – AgriRover.

## Chapter 10 – Discussion and Conclusion

Discussions, conclusions and future research on energy-optimised path planning, modelling and simulation for mobile robotic platforms.

## **2 Literature Review**

This chapter describes a thorough literature review of the state of the art robotic systems, focusing on their broad applications and associated challenges. A particular research focal area has been identified to address the planning of these systems by investigating the existing work, methods and algorithms developed for general robotic system planning, with a particular focus on energy consideration. This is to address the challenge that many similar mobile robotic systems face when they are deployed in its application fields. Modelling and simulation work have also been reviewed to gain insight into these system's behavior. Finally, a map of information gaps have been identified to provide a solid foundation for the research questions and the scope of the research.

### **2.1 Rover and Mobile Robotic Systems**

Mobile robotic systems have been widely used in many industrial applications and they can be in the form of legged or platform-based mobile systems, which are also referred as rovers. In each of these application fields there exists challenges and requirements. This section will review the identified relevant applications and mobile robotic systems. Space and agricultural rovers have a more similar working environment compared to other robotic platforms, therefore, they will be reviewed in more detail in this section.

#### **2.1.1 Space Rovers**

During recent years, the public and the government regained interest in space exploration, as several Lunar Rovers and Mars Rovers have been launched successfully for scientific missions. One of the most important applications for mobile

robotic systems is in interplanetary space exploration missions. These missions aim to find potential evidence of life in other planets, as demonstrated by Curiosity, the Perseverance missions, Tianwen-1 or Change 5, which returned soil samples from the Moon to study the formation of the moon on the dark side. There is a high cost involved in space missions; for exploring Mars alone NASA spent \$21 billion before 2020 and an additional \$2.4 billion was budgeted for NASA's 2020 Perseverance Rover mission (Williford *et al.*, 2018), which later proved to be insufficient. One of the most important design criteria for such missions is the life span of the vehicle under extreme and sometimes unknown conditions. These systems are normally designed to be as durable and as effective as possible.

One of the improved design features on the Mars Perseverance Rover is the wheel and mobility system. This is based on knowledge gained from the Perseverance Rover's predecessor, the Curiosity Rover, which only has a designed life expectancy of 90 days, according to NASA. However, Curiosity is still in operation after 8 years. This is partly attributed to the effort that the engineers were manually rerouting the path for the Curiosity Rover to avoid more wear and allow them to extend the mission duration longer. Despite this significantly increased life span, it is not without problems: the wheel and driving system on the Curiosity Rover are severely worn due to the harsh surface and terrain of Mars.

Both the Perseverance and Curiosity Rovers are powered by a Multi-Mission Radioisotope Thermoelectric Generator (MMRTG), being 66.8 centimeters long and 64.2 centimeters in diameter (Bechtel, 2013). The MMRTG are designed to generate heat and electricity, with heat generated by the decaying effect of plutonium 238 using the Peltier effect. The electrical energy is then stored into two onboard batteries for further use, as "the peak power consumption of the Rover is 900 Watts", and the MMRTG has only "about 110 Watts of output and declining few percent every year",

according to the Jet Propulsion Laboratory in NASA. Although the MMRTG is a very good solution for the Rover, with the size similar to an SUV 3 metres long, 2.7 metres wide and 2.2 metres tall, it is not a good solution for a smaller craft. This is due to the size constraint that the MMRTG cannot be too small or the natural decaying of the plutonium-238 will create less heat, therefore being less efficient for the electricity generation. In addition, the ionising radiation and heat shielding required also limit how small the MMRTG can be in order to maintain a reasonable efficiency (Bechtel, 2013). Furthermore, the safety of such a device is another major factor, where if not utilised carefully a nuclear disaster could occur (Cochran *et al.*, 2020).

For rovers smaller than the Curiosity and Perseverance ones, such as the Spirit and Opportunity rovers, as well as many Lunar rovers, a solar panel is typically used for power, which has very limited power available. It is therefore important that an energy optimised planning is generated for a longer exploration path.

For example, the Opportunity Mars Rover landed on Mars in 2004 and had been in service until the middle of 2018, which has the longest service life for an interplanetary exploration rover of 14 years and 136 days, far exceeding the expectancy of life for the Opportunity Mars Rover which was designed for 90 Martian days (24 hours, 39 minutes). Powering the Opportunity Rover is purely dependent on solar cells, which provides 900-Watt hours of energy each day at the start of the mission and it recharges the two on-board lithium batteries. The power generation capability of the solar cell dropped to 730 Watt hours after 316 Martian days from the landing (Crisp *et al.*, 2003). The limited power requires that the path planned for the Opportunity Mars Rover are energy efficient and optimised. Figure 4 shows a path taken by the Opportunity Rover on the 3,328th Martian day (NASA, 2013).



smart city sensing and robot mode, is developed for the testing of algorithms and sensors. One of the scenarios is used for is as a collaborative robotic test-pad, such as for the testing of warehouse robots, which move differently shaped pallets during operation. This test-pad was also designed to utilise the trial version of the algorithm before it can be deployed on a particular robotic system. Such a robotic system can include onboard wireless communication actuators and a rich set of sensors. For flexibility and an extendable evolution of the system, the Dockers Containers and ROS2 DDS middleware was used for the software architecture of the mobile robotic test-bed platform. This has the flexibility of supporting future sensor and network upgrades as the technology improves. This provides an open test-bed to support further research and experimentation for swarm robots and different uses of the Industrial Internet of Things (Farnham *et al.*, 2021).

Kumar (Kumar *et al.*, 2019) developed a mobile robot with manipulators that is for picking up and placing objects in a working warehouse environment. The design goal of this project was to make a robotic platform with two 4-degree-of-freedom specially designed robotic manipulators, that is capable of fulfilling the customer orders by picking the goods from a location and placing them in a designated area. Where the trajectory planning are done with the inverse kinetic approach, which is controlled by Arduino Mega microcontroller. The traverse of the mobile platform is achieved by utilizing ROS, which enables it to move from one location to another. Finally, the two arm mobile robotic platform is tested to transport goods from the designed locations to their targeted places (Kumar *et al.*, 2019). What has been achieved with this is the design and prototype of an economic robotic platform that is inspired by cutting edge technology. A robotic arm design RA improvement is made for pick-and-place activities compared to a platform that has only one arm.

For platforms such as presented, the energy optimised path planning method is not essential, due to the availability of indoor charging stations, but still energy optimised path planning improves the effectiveness of the system, by considering the extended period of operation and also makes possible the lowering of the time taken for charging the battery. Therefore, an energy and time balanced optimisation path planning specifically designed for each case is argued in this research as necessary, and can make such platforms more effective.

### 2.1.3 Agricultural Rovers

During recent years the technologies have improved and the cost of them have reduced. Increasingly more previously state-of-the-art, cutting-edge technology has been explored for use in more conventional, commercial markets, such as industrial and agricultural markets, instead of only for military and space use. One of the represented technologies is mechatronics with robotic control, where a system has the structure of one, or a complex combination, of mechanical, hydraulic, numerical, or control systems, which are controlled by electronics. In recent years, it has especially gained popularity for use in agricultural cases. Robotic systems have been developed for agricultural use and they provide the possibility of precision farming, which can create benefits for improving sustainability and productivity, as well as liberating workers from hard labor in food production.

Łukowska presented a robotic platform design for the purpose of soil sampling, where the goal is to optimise the usage of fertilisers, in order to lower the possibility of over fertilisation and improve the cost effectiveness of the fertilisation process. The purpose of the project was to make an autonomous robotic platform that is able to perform soil sampling for the agriculture purposes. The sample is analysed to determine the compositions of the nutrient levels for the soil, and this is then accessed finally by the farmers via a handheld test set, or available for large-scaled farmlands

on a platform which samples the soil without direct interaction from the farmer (Łukowska *et al.*, 2019). Although there was a prototype built and field tests have been conducted, with photos showing the drilling process in Europe and North America presented in the article, there is a lack of a quantitative conclusion, as the sample report provided only states the test conditions: weather, speed of the Rover, and the GPS coordinates, but the report doesn't provide information on the sampling points' coordinates and results.

Xaud presents another mobile robotic rover designed for bioenergy agricultural applications. The work reported sugarcane farms are heavily covered with vegetation, compared to regular non-bioenergy farms, which makes the working environment for the robotic Rover different. The project produced and developed an autonomous mobile robotic system designed for a number of tasks in sugarcane farms, with many use cases. The goal was to design a semi-autonomous waterproof and low-cost vehicle capable of working in an environment which is inside of plantation tunnels, with dense vegetation coverage. It also allows the capability of collecting samples and mapping the areas that are hard to access with the onboard sensing systems. Xaud presented an overview of the mechanical design of the onboard embedded electronics, the software architecture of the rover, and the construction of the prototype. Finally, the results after the field tests have been obtained and analysed, where the proposed conceptual design challenges of the robots are addressed. Additionally, the future work of a full autonomous navigation concept and a new prototype design is proposed (Xaud *et al.*, 2019). In conclusion, the design construction and field test results of this robotic rover is a low cost solution that gives a good motivation for future approaches. The environment, where this type of mobile systems is designed to operate in, is challenging, as most of the conventional sensors such as cameras and LIDAR could struggle due to the thick vegetation. He authors, however, that used low-cost thermal-

imaging cameras as a method for mapping is able to address perception requirements for this situation, with a certain level of effectiveness.

Another agricultural rover called AgriRover was presented and developed by Yan and his team (Xiu-Tian Yan *et al.*, 2020). This is a multi-functional mobile platform that is novel and is designed for agricultural applications. AgriRover is inspired and designed by investigating space robotic technology and transforming these ideas into the development of a set of technology suitable to terrestrial applications. The prototype of the AgriRover is a testament to innovative space technology utilised in precision farming for the first time. The energy optimised planning strategy is implemented, and the total cost of transport is proposed and validated with dynamic consideration. An autonomous navigation framework has been established, which enables the AgriRover to operate safely and unsupervised in a farming environment. A novel agricultural object-recognition system designed specifically for agriculture was implemented and evaluated. A soil sampling system, with the capability of an onboard real-time nutrient measurement system, was design and prototyped, which is inspired by interplanetary Rovers. The design process of the system followed a design methodology of a mechatronic system model, which reshaped the planetary exploration Rover into the AgriRover, a platform specifically for agricultural applications. Finally, multiple field trials have been conducted and some of the results were reported (Xiu-Tian Yan *et al.*, 2020).

In conclusion, the AgriRover system opened a possibility of real time soil quality sampling and analysis, which is quick and cost effective, combined with the energy optimised path planning method, which eliminates the unnecessary work of the Rover. The coverage area of the AgriRover when measuring the soil quality can be extended further, as well as the longevity of the mobility system can be ensured. Finally, the

obstacle detection system utilises onboard sensors to ensure the safe operation of the Rover.

#### 2.1.4 Autonomous Cars

Autonomous cars are becoming a very popular research topic and transportation reality. Companies have invested heavily in and achieved different levels of autonomous-assisted driving, yet a fully autonomous self-driving vehicle is yet to be seen driving on public roads safely, thus still requiring further development. With improved technology, such as communication, image recognition, LIDAR sensing, GPS navigation and high-performance ASIC (Application-Specific Integrated Circuit) being made more affordable and more accessible, a fully autonomous vehicle is making progress to becoming a fully functional reality.

Hussain reported self-driving cars with difficulty and issues that needs to be solved. Because of the recent development and achievement of many technologies, autonomous cars are becoming a reality, with prototypes created by many corporations, with test driving already comprising millions of miles. A staggering amount of investment of both money and time are dedicated to the development of autonomous vehicles by many leading technology companies and car manufacturers. They are believed to make a commercially viable autonomous car a reality in the coming years. Such a goal is achievable. There exists many challenges, including technical difficulties such as real-time high-speed data analysis, stability of complex software system testing, validation for safety, and other greater technical difficulties. There are arguably more important nontechnical problems, such as insurance policies, as well as ethical and moral concerns, which will require careful and thoughtful solutions, so that the government requirements, regulations and policies can be fulfilled. This report discusses the issues and possible solutions, and for development for the autonomous cars they also highlight the applications that could be beneficial to

the customers and sector. Finally, to make cost effective and efficient autonomous cars a reality, this report discusses what challenges and difficulties must be addressed, and gives a suggestion for implementers, designers, regulatory organisations, political makers, and manufacturers (Hussain *et al.*, 2018). In addition, not only does saving of the energy during the movement of the electric car extend the range, but it also mentions that even though the car is fully electric, the electricity used currently is still mostly from non-renewable energy sources, therefore making it is necessary to save the energy used.

In conclusion, although the development progress of fully autonomous cars has been fast during recent times, it has still largely remained in the level of automation of the NHTSA (initially established as the Society of Automotive Engineers) level 2 (Zacherl *et al.*, 2020, Rödel *et al.*, 2014), which is limited automation with supervision. However, as the available technology develops it will be achieve level 3, which is limited automation without supervision, and level 4, which is fully automated, soon in the future (Albers *et al.*, 2020).

## **2.2 Approaches and Modelling Language for Path**

### **Planning**

There are a number of approaches and tools which have been developed for mobile robots, and this is reviewed in terms of path planning strategies for navigation in Patle *et al.* A method to avoid obstacles in known environments is reported, and uses free segments and turning point algorithms in Hassani. Among these approaches, Optimising Preferences and Time-Dependent Costs (OPTIC) is highly relevant to this work, which is a temporal planner design tool for solving the path planning problem, where the cost is determined by the time dependent performance and the cost of goal collection. These kinds of path planning problems are applied in a range of

applications, such as the delivering of fresh goods to meet a specific delivering requirement, or to fulfill orders from customers that require a narrow delivery time frame. This is not specifically limited to the delivery of agriculture products, medical supplies also need to search optimal plans as deliveries of vaccines and organs must meet a strict time frame for a valuable service (Carreno *et al.*, 2020, Benton *et al.*, 2012).

Papadimitriou represented a method of adaptive planning that has the ability to combat hardware faults during the mission by utilising the concept of Ontologies (Papadimitriou *et al.*, 2015). Adaptive mission planning requires a lot of computational resources during the operation. The high-level mission priorities also have the possibility of changing with adaptive mission planning. Papadimitriou introduced a new way of increasing persistent autonomy for Autonomous Underwater Vehicles (AUVs) with the ontological approach, which is done when part of the hardware fails and threatens the integrity of the current mission, where the mission priority needs to be incorporated into the decision making method. This is achieved by utilising a well-established planning language (Hoffmann *et al.*, 2020) Planning Domain Definition Language (Haslum *et al.*, 2019) with the Optimising Preferences and Time-Dependent Costs (OPTIC). *“The results demonstrate the power of an ontology-based knowledge representation and reasoning approach in driving adaptation”* (Papadimitriou *et al.*, 2015). The energy efficiency is also achieved by mission planning, which is done by changing the order of execution, with the possibility of readopting the mission during operation.

This method presented an increased energy efficiency of the overall mission, by changing the order execution based on distance during the mission, which required the real-time computational evaluation and re-planning as Papadimitriou introduced.

## 2.3 Planning Approaches and Algorithms

There are two major types of path planning for wheel-based autonomous robots, and they can be classified as implicit path planning algorithms and explicit path planning algorithms. An explicit path planning algorithm generates a parametric curve or way points (Montes *et al.*, 2007) and is mostly seen in global path planning: using a global map and mission points, a set of way point for the robot is generated. Implicit path planning algorithms do not give a clear and complete set of way points or parametric curve at once, instead the path is generated based on the robot's onboard sensors. The geometric model of the environment is processed from the information that is collected by the sensors (Wong *et al.*, 2020) (Arras *et al.*, 2001). This is mostly used in local path planning environments. There are other explanations on implicit path planning by other researchers in (Martinez *et al.*, 1998).

### 2.3.1 A\* Algorithm

Although the a-star algorithm is a classic algorithm widely used for multiple missions and purposes. There is a topic that has gained popularity during recent years that is full coverage planning, used in cleaning robots. The work by (Le *et al.*, 2018) is a path planning utilising the a-star algorithm that is focused on efficient coverage. Le presented methods of navigating a morphological robot, which is reconfigurable during its mission, in a complex environment (Le *et al.*, 2018), where the performance of coverage planning is significantly degraded. During operation of the coverage planning, the morphology of the robot is considered, and the objectives is to maximise the coverage area while going through narrow paths. Finally, the test is recorded in an environment where robot operates using the robotic operating system (ROS) system.

More applications for the a-star planning algorithm are aimed for care robots. Unlike coverage planning, this planning objective is to go from one point to another.

As the a-star algorithm is used to find the shortest path from one point to the other in this scenario (Kusuma *et al.*, 2019), the objective is for the path planning continue to work even after the robot is moved by the user or misses an objective. Kusuma represented a method for division of areas and micro areas in two dimensions as shown in Figure 5. Following this, a look-up table with weighted value is calculated. The weighted value is calculated based on the distance to the destination point, and the weighted values for the obstacles are set for calculation using the heuristic distance function  $h(n)$ .

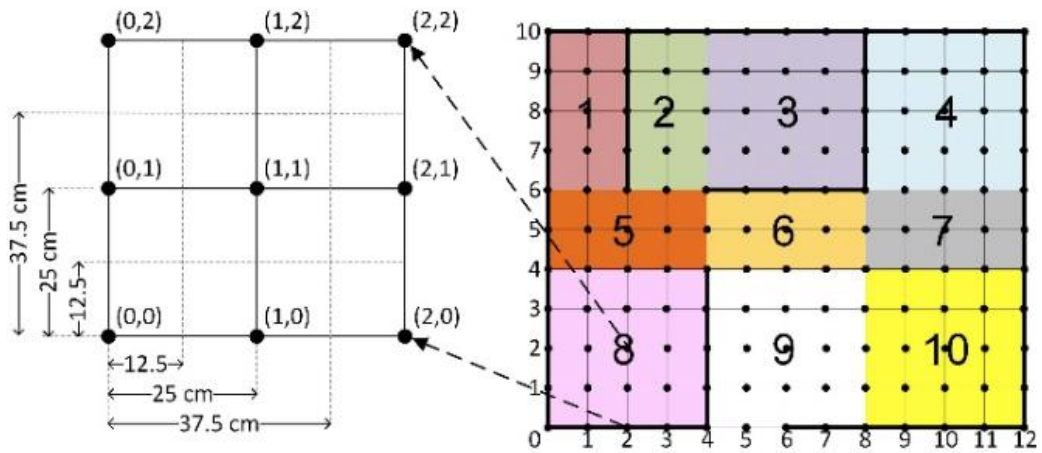


Figure 5. Division of areas and micro areas into nodes (Kusuma *et al.*, 2019)

Then the a-star path finding procedure begins, where the next waypoint is decided based on the calculation of the heuristic distance function  $h(n)$ . The total cost is calculated using a sum of the heuristic function plus actual distance. After the next waypoint is decided, the weighted value look-up table is modified. Once the waypoint has been visited, their weighted value changes. After many steps, when the next waypoint is the destination point, the algorithm stops. When a plan is modified by introducing a possibility for the user to change the position of the robot, the algorithm can still find the path.

The a-star algorithm is a well-established, classic heuristic search algorithm for path planning tasks. The advantage is that the optimal shortest path is guaranteed to be found from one point to the other. This is achieved by sequentially expanding the nodes with the smallest heuristic function  $h(n)$ , prioritising the expansion of nodes that can make the function value smaller (Chen *et al.*, 2018). The disadvantages of this algorithm are the relatively low effectiveness and execution speed of the algorithm, which depends on the calculation of heuristic distance function  $h(n)$  which is defined by the designer of the algorithm.

### 2.3.2 Rapidly-Exploring Random Tree (RRT) algorithm

The rapidly-exploring random tree (RRT) pathfinding algorithm is an effective method for path planning, which is heavily biased towards unexplored and unvisited regions, and has the capability of working with more than two dimensions (Kleinbort *et al.*, 2018).

The problem with the traditional random tree algorithm, when used for exploration, is overlapping. Using RRT, the robots can revisit the map area that was previously explored, because the branch is grown randomly, which means with the different time steps it could overlap. Researchers are addressing this problem with Sensor-based Random Tree (SRT) (Keidar *et al.*, 2012), where the SRT algorithm grows the branch only one at a time. A robot follows this branch until there is an obstacle that stops the extension of the tree branch. However, search methods will not entirely avoid the possibility of revisiting, because when the branch cannot extend further, the robot has to backtrack in order to continue the exploration. When doing so, the revisiting problem is still present.

Umari introduced a method of utilising the RRT algorithm to achieve path planning in a partially unknown environment, and improve the efficiency by reducing the

possibility of revisiting. This method was implemented and tested using ROS (Umari *et al.*, 2017). Furthermore, the algorithm has the capability of detecting the environment boundaries, or otherwise known as frontier points, which is completed by using the local and global tree branches, giving a possibility of robotic exploration. The robot does not immediately follow the branch when it is generated, instead the random tree branch is generated separately, with the movement distance of the robot observed using the robot onboard sensors. After all the branches reach the boundary of the detection sensor distance, a filter is applied to classify the obstacle's frontier and space that the robot can move to. Then, one of the possible routes for the robot is sent to the driving system to execute the movement. Finally, by running this algorithm repeatedly, a complete mapping of the region can be produced and is shown in Figure 6 as seen in (Umari *et al.*, 2017).

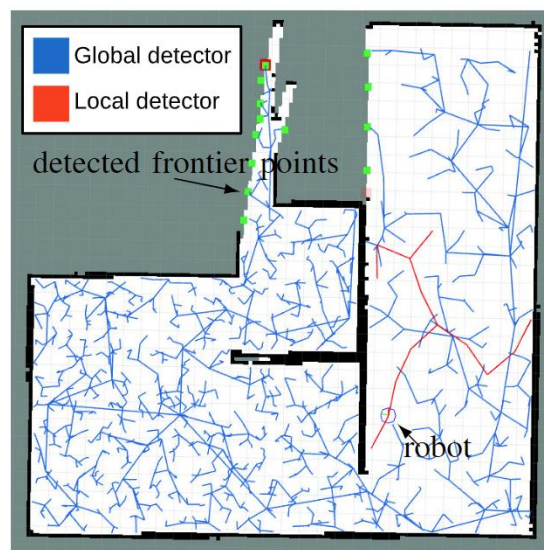


Figure 6. Modified RRT algorithm for exploration by Umari (Umari *et al.*, 2017)

Although the RRT algorithm is very effective for robotic exploration and mapping of a region, it is less suitable for an energy optimised planning, because the branches are randomly generated, which does not optimise energy efficiency.

### 2.3.3 Pure Pursuit Path Planning Algorithm

The Pursuit algorithm is a geometric path and trajectory planning method (Peralta *et al.*, 2020) that is commonly used with a good level of effectiveness (Amidi *et al.*, 1991). According to the current position, a set point is chosen at a set distance looking-ahead, which is the chord length of the arc  $L$  (Samuel *et al.*, 2016) as shown in Figure 7. This path planning algorithm was first developed in 1985, where the pure-pursuit path planning algorithm was used in the field of robotics. This algorithm was used to estimate the steering for the robot in order to keep it on the path (Wallace *et al.*, 1985).

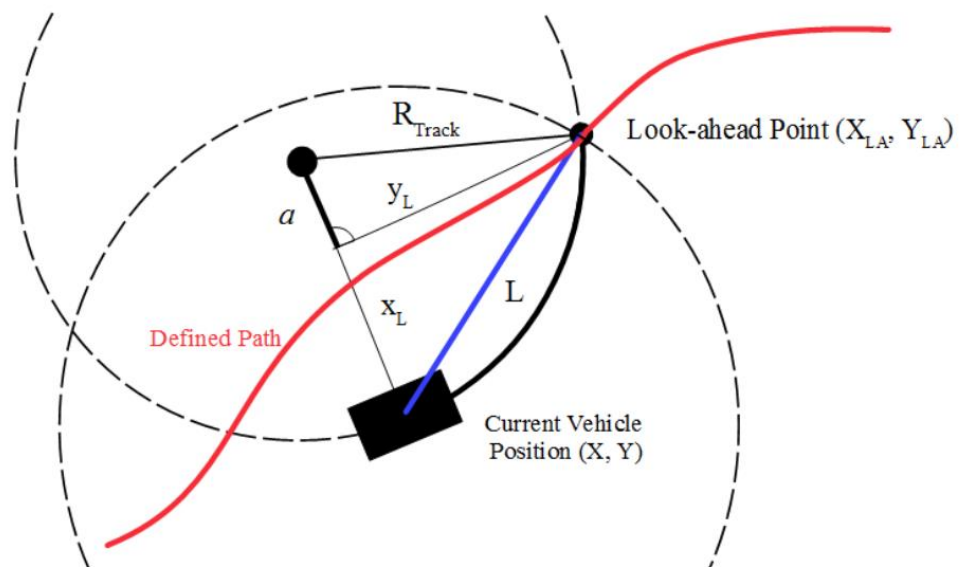


Figure 7. Geometric explanation of the Pursuit path (BačÍK *et al.*, 2017)

The following steps are taken for the pursuit path. Firstly, the current location  $(X,Y)$  of the robot is found. Then, with a predefined look ahead distance  $(L)$ , the goal point  $(X_{LA},Y_{LA})$  is found and the difference is calculated. Thirdly,  $R_{track}$  is calculated using (1). (BačÍK *et al.*, 2017).

$$R_{track} = \frac{L^2}{2X_l} \quad (1)$$

Accordingly,  $R_{track}$  is an arc radius that the robot needs to follow, and the path can be corrected (Scharf *et al.*, 1969, Coulter, 1992).



Figure 8. All-Purpose Remote Transport System (Wit, 2000)

According to the work on vector pursuit path tracking for autonomous ground vehicles (Wit, 2000), the pure pursuit path planning is used on all-purpose remote transport systems, such as that shown in Figure 8.

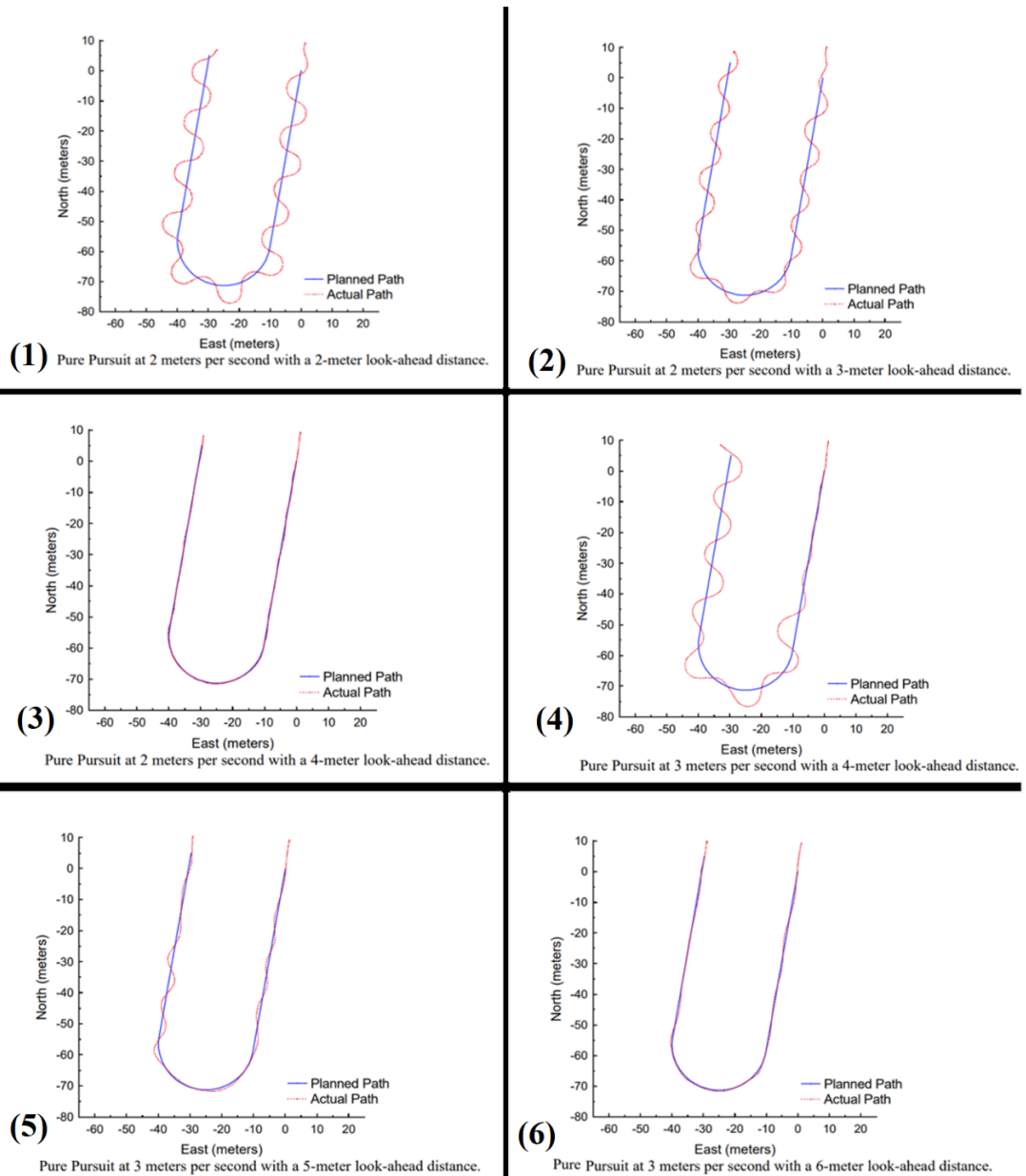


Figure 9. Pure pursuit relationships between speed and look-ahead distance (Wit, 2000)

As Figure 9 shows a characteristic of the pure pursuit algorithm, the look-ahead is related to the speed of the vehicle when following the planned path shown in blue. Figure 9 (1), (2) and (3) show the trajectories of a vehicle movements at a speed of 2 meters per second with the look-ahead distance of 2, 3 and 4 meters respectively, which show that other than with the look-ahead distance of 4 meters, the vehicle path is in oscillation.

For the faster speed of 3 meters per second of the vehicle shown in Figure 9 (4), (5) and (6), the oscillation only stops with the look-ahead distance of 6 meters shown in Figure 9 (6). In summary the pure pursuit path planning algorithm is curved and depends on differing speeds and paths where the vehicle runs.

Such a method is mostly in use on trajectory planning aimed at generating a smooth path for the platform to follow. The way point is connected smoothly with position error when implemented in real-world applications. The Pure Pursuit Path Planning is very well developed and used in many applications.

#### 2.3.4 Artificial Potential Field Path Planning Algorithm

There are many applications of path planning which have used the artificial potential field algorithm, also sometimes known as the Virtual Force Field (VFF) Method. Mostly this algorithm is used for obstacle avoidance planning. The algorithm works on one attractive and one repulsive field to represent the destination point and the obstacles. Some early research uses the artificial potential field as the basis of the planning (Khatib, 1986) (Warren, 1989), but newer work uses an assembly of many methods, such as the Evolutionary algorithm, Simulated Annealing, or other algorithms (Mollazade *et al.*, 2012) (Orozco-Rosas *et al.*, 2019, Qixin *et al.*, 2006, Vadakkepat *et al.*, 2000).

Figure 10 shows the results of a typical artificial potential field path planning algorithm (Warren, 1989) . The aim of the work is to “*develop an artificial potential field technique for planning the path of a robot. The focus of the work is to avoid local minima than other potential field Methods by establishing a trial path and modifying the entire path under the influence of the potential fields*” (Warren, 1989). This early research is a classic piece of work focusing on the artificial potential field for obstacle avoidance planning.

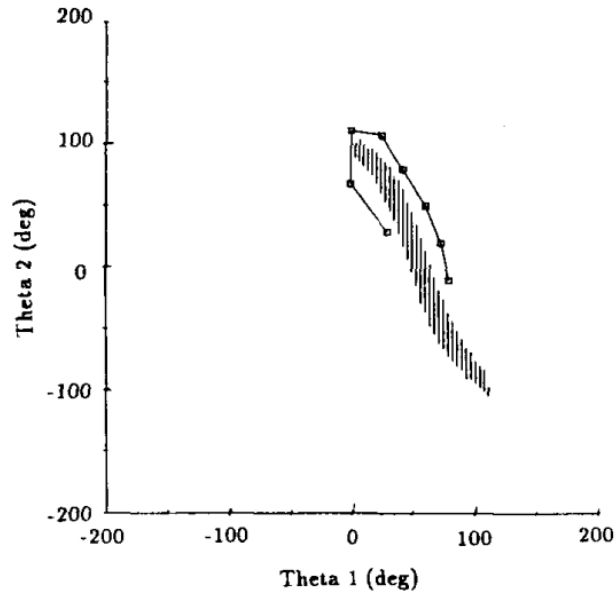


Figure 10. Safe path selected (Warren, 1989)

The artificial potential field algorithm is less susceptible to local minima that has the capability of finding a path around a hard and insurmountable obstacle.

Not only are the artificial potential field algorithms used in offline planning, but also for online planning. Bounini showed development of a modified potential field method for the mobile robot to perform local navigation through obstacles (Bounini *et al.*, 2017). The work details a way of eliminating the local minimum by calculating additional potential fields with single global minimums, which is additional destinations of the robot. This new potential field is a repulsive potential field and it is generated according to the local minimum parameters. This is achieved by increasing the repulsive values round the obstacles for the local minimum problems to be solved. The method has its limitations, namely where if the obstacle is closer together, an increased repulsive potential field results in a path through the obstacles which cannot be found. This is, however, a good way to use artificial potential field to navigate a robot through a narrower and obstacle rich environment.

### 2.3.5 Particle Swarm Optimisation

Particle Swarm Optimisation is an optimisation algorithm based on study of a population of insects, inspired by bionics and was originally proposed by Kennedy and Eberhart in 1995 (Kennedy *et al.*, 1995), and has been cited more than sixty thousand times. Particle Swarm Optimisation was widely used in a wide range of applications that is non-linear not only for path planning, but also in design and optimisation of infinite impulse response digital filters (Slowik *et al.*, 2007). The technique improves the stability of a single-machine-infinite-bus (Hassan *et al.*, 2005).

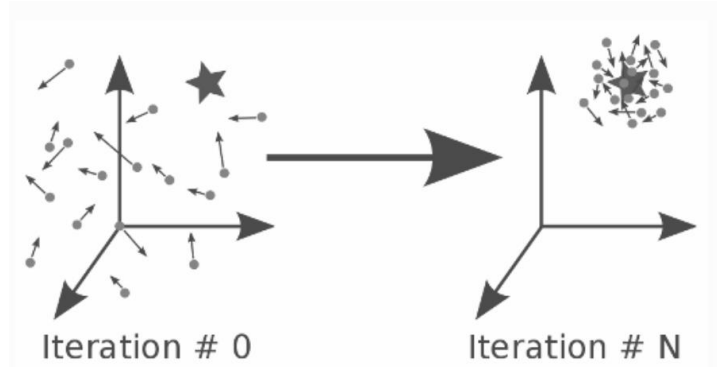


Figure 11. Particle Swarm Optimisation with iterations (Bansal, 2019)

The Particle Swarm Optimisation algorithm was inspired by the foraging behavior of a swarm of animals (Bansal, 2019). Each point has a memory of their locations where they achieved the best performance  $\mathbf{x}_i^l$  and the best decision vector  $\mathbf{x}^g$ . The position is then updated using the ) (Bansal, 2019), where  $\mathbf{x}$  is the location,  $\mathbf{v}$  is the speed, and  $\omega$ ,  $\eta_1$  and  $\eta_2$  are user defined.

$$\begin{aligned} \mathbf{v}_{i+1} &= \omega (\mathbf{v}_i + \eta_1 \mathbf{r}_1 \cdot (\mathbf{x}_i - \mathbf{x}_i^l) + \eta_2 \mathbf{r}_2 \cdot (\mathbf{x}_i - \mathbf{x}^g)) \\ \mathbf{x}_{i+1} &= \mathbf{x}_i + \mathbf{v}_i \end{aligned} \quad (2)$$

After a number of iterations, the particles converge around the point which is predefined, as shown in Figure 11.

In conclusion, Particle Swarm Optimisation is mostly suited for solving and optimising problems that are non-linear with multiple input and output preferences. For single or a small number of rovers, which is the focus of this research, Particle Swarm Optimisation is less relevant.

### 2.3.6 Ant Colony Planning Algorithm

Similar to the Particle Swarm Optimisation planning, the ant colony planning algorithm is another path planning method inspired by nature, which is even more popular and known as an effective tool to solving path planning problems. The difference is that the ant colony planning algorithm is inspired by ants' behaviour of finding a path from A to B with Artificial Pheromone Reinforcement, and the behaviour of following the stronger pheromone (Dorigo *et al.*, 2006). Particle Swarm Optimisation planning, instead works by positioning and vectors that impersonate the foraging behavior of a swarm of animals.

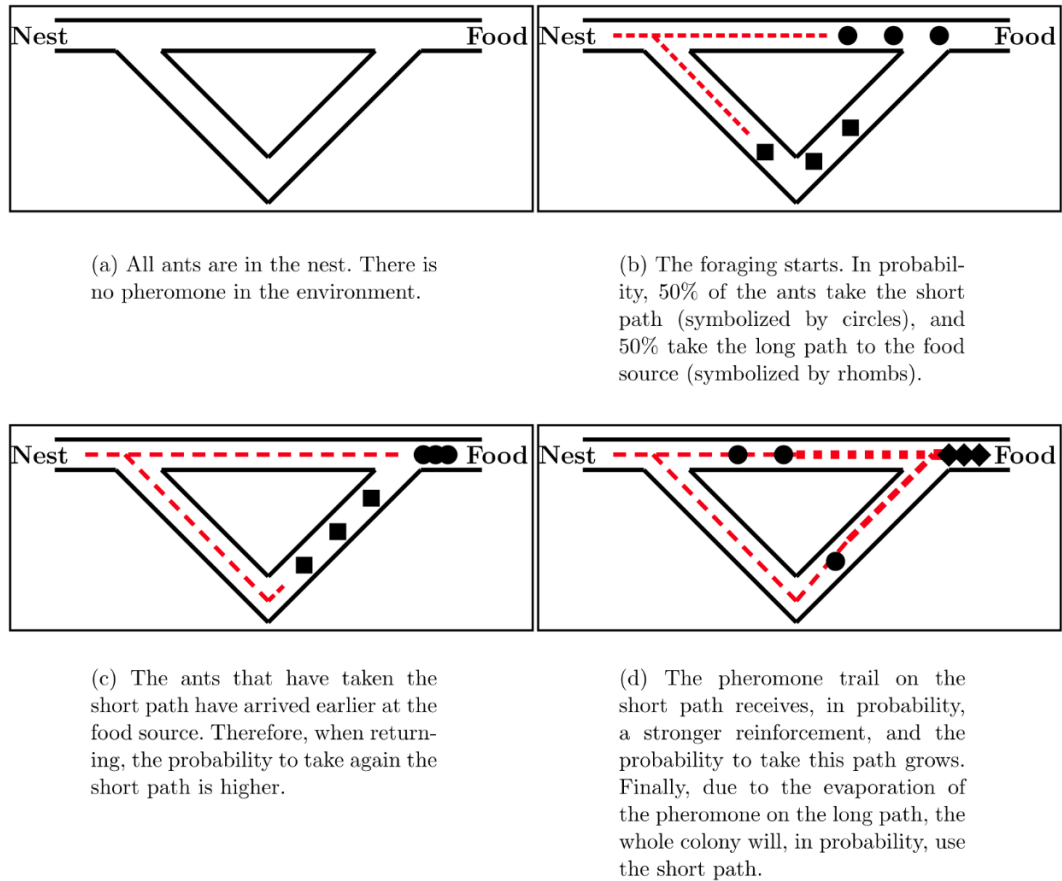
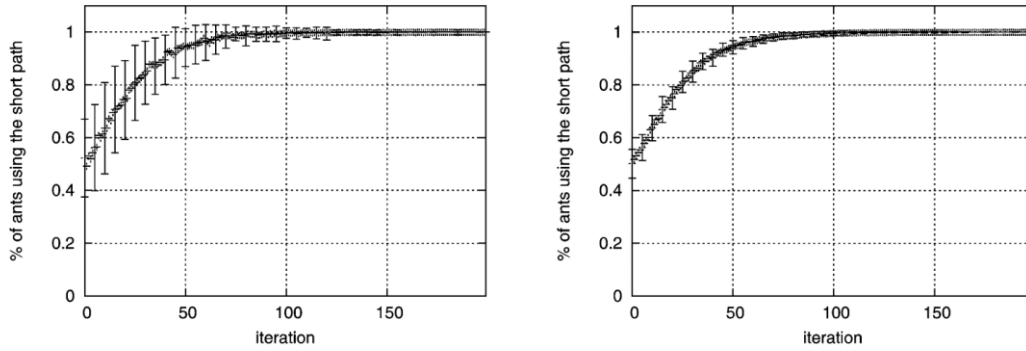


Figure 12. Ant colony planning (Blum, 2005)

Figure 12 shows the principle of the Ant colony planning algorithm. Figure 12 (a) shows a set up with two paths, the bent one longer than the top path. The starting position is marked as nest and the destination point marked as food. In the first iteration the Artificial Ants are moving towards the destination with random distribution shown in Figure 12 (b). The artificial ants who have taken the shorter path arrives first and when they are going back to the nest they have a higher probability in taking the same shorter path as they release pheromones as shown in Figure 12 (c). Finally, as the iteration goes on the Artificial Pheromone Reinforcement grows higher and higher and after a number of iterations all the artificial ants follow the shorter path as shown in (d) (Blum, 2005, Dréo *et al.*, 2002).



(a) Colony size: 10 ants

(b) Colony size: 100 ants

Figure 13. Ant colony size compared (bars on the curve for every 5 iterations shows the standard deviation) (Blum, 2005)

Figure 13 shows the planning results of the algorithm, including statistical information. This clearly shows the converging of all ants using the shorter path after about 100 iterations when the size of the colony size is at 10, shown in Figure 13 (1), and Figure 13 (2) shows when the colony size is at 100 it takes less iterations with a better distribution.

### 2.3.7 Genetic Algorithm for Energy Optimised Path Planning

A battery-powered unmanned aerial vehicle is another platform that requires energy saving, and a higher energy efficiency means longer mission durations and more effective operations. Genetic algorithms are used for energy-cost focused UAV path planning, where both the speed and altitude of the vehicle needs to be considered. Optimised paths for a UAV normally has less turns and less changes in directions during the coverage flight, since changing the direction and speed of the vehicle requires more energy compared to flying straight. Shivgan proposed a method for UAV coverage flight path planning utilising a genetic algorithm, and compared the result between an energy optimised route to a shortest distance route (Shivgan *et al.*, 2020). During a simulation, two to five times less energy was lost utilising the genetic algorithm, reducing the number of turns while still maintaining coverage to all the

waypoints. For UAV path planning, most of the research work focuses on only obstacle avoidance in flying through buildings and terrains. With a battery-powered UAV the flight time is limited, so deciding how to use the limited energy to cover a surveyed area is a problem that needs further research (Hirahara *et al.*, 2018). In addition, the waypoints and coverage for different missions can be formatted as a classical traveling salesman problem, which is a NP-hardness (non-deterministic polynomial-time hardness), where only the correct answer of the problem can be verified by a polynomial, and not vice versa (Hirahara *et al.*, 2018).

The genetic algorithms follows the following procedure. First, the number of people that is the possible solution of the problem was selected and defined, where the size of the population is determined by testing and trials, after generating the population randomly. There is a fitness value based on an optimised solution, the better fitted chromosome, which consumes less power is kept, then more chromosomes are randomly generated. The next step is the crossover where the next generation is produced. The fourth step is mutations, where random sections of the chromosomes are swapped before finally, the optimised result is generated.

In comparison, the genetic algorithm normally requires more computational power compared to traditional methods, such as potential field and A\*algorithm. This increases the on-board power consumption and probably increases the cost of the on-board computer system. Although this paper represents a method that is suitable for a UAV, it would not be suitable for a ground-based vehicle with energy consumption and cost constraints, such as an agricultural Rover, where cost is an important factor. In addition, the complexity of representing spatial and agricultural related information in such an algorithm increases the challenge of implementation.

### 2.3.8 Neural Network (Multi-layer perceptron) for Energy Optimised Path Planning

Neural network approaches are gaining popularity in research fields and are usually used to solve a problem that is difficult to precisely define with mathematical equations, or a problem lacking a good understanding. Combined with machine learning, a neural network can be trained to solve problems that is random in nature and complex, such as the classification and recognition of images, texts and sound. The neural network has thus become a very popular topic during recent years. In this section the possibility of using neural networks for path planning is discussed.

Introduced by Das is a path planning strategy for robots using six layered neural networks (Das *et al.*, 2018). The work analyses and discusses a six-layer neural network methodology for path planning in a high-density environment. The input for the network consists of the front, left, and right distances from the obstacle, as well as the target angle. The output is a steering angle, and this is an output parameter for the neural network. The results generated from experimentation and numerical analysis had a difference of only 6% (Das *et al.*, 2018). In conclusion, although the problem-solving ability of the neural networks is very good, in most cases the neural networks are trained with mostly trial and error. This is due to the neural network system being mostly a black box with parameters trained for this specific case. Such a setup needs to be changed when the platform that it is calculating for changes. Therefore, this makes the flexibility of the overall system relatively low, which means new training needs to be undertaken again when the mobile robotic platform receives an upgrade, or receives any modifications to the total weight or it's mobility system, requiring additional time. In addition, the dataset for training may not always be available for agricultural applications, where conditions such as terrains, weather, etc. can change constantly, making the trained algorithm potentially unsuitable for a new scenario.

Where other researchers, such as Sun (Sun *et al.*, 2018), used the approach of the Neural Network Algorithm for the coverage planning, the energy consumption was mentioned, but no research was done on energy optimised path planning.

### 2.3.9 Reinforcement Learning for Path Planning

Reinforcement learning is one of the two most important research areas in artificial intelligence and it is a very popular topic, with multiple fields of applications, such as image and sound recognition and processing, statistics and forecasts, behaviour analysis and many more. Presented by Lakshmanan is a method of reinforcement learning for full coverage path planning, designed for the Tetromino robot (Lakshmanan *et al.*, 2020). This algorithm provides a complete coverage planning algorithm for a tiling robot used for surface painting, floor cleaning, building maintenance, and building inspection. One of the elements of the tiling robots is a reconfigurable polyomino-based platform, which has the capability of overcoming the limitation of fixed form robots, therefore providing a better coverage area. Intelligent decisions can be made during operation by reconfiguring the shape of the robot in real-time for optimal strategies in order to maximise the coverage area and minimise the energy consumption. The proposed algorithm for path planning is a method using trained deep black reinforcement learning, applied on a robotic platform named hTetro. The use of this method results in an optimal set of shapes depending on the environment and generates a trajectory planning result with overall less power consumption. With the use of Long Short Term Memory (LSTM) layers a Convolutional Neural Network (CNN) was trained with the method reinforcement learning algorithm, called Actor Critic Experience Replay (ACER). The final result was compared with the existing method based on traditional theory of the tiling model, which includes spiral, zigzag and greedy search schemes. It is also compared with the Travelling Salesman Problem (TSP) with a GA approach and Ant Colony

Optimisation (ACO). The results show the proposed algorithm has an overall lower energy consumption and requires less time to generate the solution in the simulated environments in comparison with the traditional tiling model and TSP (Lakshmanan *et al.*, 2020). The results of the reported method of reinforcement learning for the application of coverage planning, with a reconfigurable robot platform, proves to be effective. This is further supported by examples of reinforcement learning being used in many applications, such as the AlphaGo. Although the method of reinforcement learning is a very effective way of solving complex problems compared to unsupervised machine learning, as it has a lower requirement of data samples, it still needs accurate sample data at the training input of the system.

### 2.3.10 Kalman Filtering

Kalman filtering is an algorithm that is used with the assumption of unknown variables and inputs of previous measurements gathered over time. The common filtering algorithms are widely used in different applications and only requires a limited amount of computational power. Applications using the Kalman filter include global navigation satellite systems, tracking spotting of the radar system and linear navigations with an expanded Kalman filter (Govaers, 2019). Not only are they common filters used for navigation and path planning, but also for Speculate, the state-of-charge for lithium-ion batteries as reported by Shrivastava presented in (Shrivastava *et al.*, 2019).

Khamseh presented a use of the Kalman filter with the state estimation for manipulating unmanned aerial vehicles, which is a type of robot equipped with the manipulative mechanism that enables and gives them the capabilities of interaction with the environment. The state estimation of this type of robot is especially challenging, due to the inherent couplings, nonlinear and uncertain behavior of the proposed system, creating a complex dynamic problem, which typically means the

extended Kalman filter may not be a possible solution. However, Khamseh introduced two Kalman filters using general and spherical unscented transformers to resolve this dynamic problem. These open the possibility of examining the quality of the overall control performance. The experimental vehicle is a quadcopter with a robotic manipulator attached, which has the linear–quadratic–Gaussian (LQG) control designed with the goal to simultaneously control the quadcopter and the manipulator. The performance of the filter algorithm is compared, which includes overall control performance, estimation accuracy and execution time. Finally, more parameters, such as total loss of sensory data, were examined with the case of an increased noise level. Kalman filtering is a filtering method that is effective for onboard sensor data processing, which requires previous states of the data as the input. For the task of online trajectory planning, Kalman filtering is effective.

### 2.3.11 Model Predictive Control Algorithm

Unlike some of the existing path planning methods, which use a high-level rule based on the decision-making approach, the Model Predictive Control (MPC) algorithm uses a unified path planning method without explicit rules. The MPC algorithm operates by deciding the maneuvers automatically.

Liu introduced a method of the MPC algorithm for full size vehicles with constraints for safety, where collision is avoided between the controlled vehicle with other vehicles and the surroundings. Furthermore, a lane-associated potential field is introduced to ensure the movement of the vehicle is smooth. Finally, the simulation of the path planning method was tested for different man-made scenarios to evaluate the effectiveness and safety of this algorithm (Chang Liu *et al.*, 2017).

Williams introduced a method of the MPC algorithm with predictive path integral control, which is based on an importance sampling scheme utilising a generalised

algorithm with parallel optimisation developed on a GPU (graphic processing unit) (Williams *et al.*, 2017). Generalised importance sampling schemes possess the capability of allowing changes, such as diffusion and drift terms of random diffusion processes, which is important in the performance of the MPC algorithm. This new algorithm proposed is compared in simulation to an algorithm using MPC with nonlinear dynamic differential programming. Finally, the proposed algorithm was utilised by multiple vehicles with navigation tasks inside an obstacle dance environment. (Williams *et al.*, 2017)

This paper describes a resulting performance profile of the MPC algorithm, which shows the suitability of such an algorithm for an environment such as a highly clustered area. The shortcoming of such a method is that one of the key parameters' variance of the sampling distribution impacts the performance of the algorithm directly. More frequent sampling generates smoother and more precise manoeuvres, but with a higher cost of more computational power required, or less frequent sampling generates trajectories that are less optimal and more aggressive.

## **2.4 Simulation and Modelling**

Having reviewed all relevant applications and algorithms for path planning, modelling in particularly complex systems is an important consideration, as the robotic systems, including mobile rover systems, are complex and typically require a systematic approach to designing and modelling these systems in order to produce a robust and intellectual design solution. With adequate modelling consideration, simulation techniques and environments are also crucial to this research in order to generate accurate and reliable results in this virtually developed environment. This section provides an overview of the reviews results on these topics. These reviews focus on energy related modelling and simulation. (Hou *et al.*, 2019a)

### 2.4.1 Multi-Perspective Approach

Depending on the application of the robotic mobile platforms, there is a multi-perspective approach to the set goals of the path planning, where the goals can be set differently. For a cleaning robot, floor coverage planning is required to consider the environment it operates in, e.g. a full coverage of the given space. These include consideration of mechanical elements, so that the system is able to reach all locations of the target environment, enabled by actuation and perception. Similarly, this is true for robots that transfer time sensitive goods, where time taken is the most important aspect of the planning. Finally, for Rovers that have limited energy available, energy optimised planning needs to be implemented.

Proposed by Yan (Xiu-Tian Yan *et al.*, 2010) is a design process model for mechatronic system designs. As a methodology framework for systematic mechatronic design, it defines the key steps and a set of guidelines for considering multiple perspectives of designing a mechatronic system. Conventionally, the engineering design of a mechatronic system is a process that is sequential, where the problem is generated during the process of the design, and then explored and evaluated as the design process evolves. These relatively prescriptive design approaches are found in traditional design models, which are used in many classic design textbooks, including French's *Conceptual Design* (Michael J French *et al.*, 1985), systematic design (Pahl *et al.*, 2007), which has a wider mechatronic context by (Bradley *et al.*, 2000), and Schemebuilder (Sharpe, 2012). Proposed is a new design process model for mechatronics systems, where it is intended with a holistic view in mind, and the lifecycle issue during the designing phase is considered. Then, the design process methodology proposed is implemented with an application of a mechatronic system that has a low flow rate, high position mechatronic oil dispensing system. Finally, the life cycle issues is set to be carried out in (Borg *et al.*, 2000) . This paper details a new

approach to the design methodology for mechatronics system design. This approved an implementation of a well thought-out methodology to improve the effectiveness of mechatronics system design. Design processes for low volume high position oil dispensing systems originally took seven years, and has had its design duration decreased to only one year. This shows a design methodology for a multi-perspective design approach.

#### 2.4.2 Energy Modelling and Dynamic Simulation

As mentioned in the last section, the battery-powered robotic platforms have a limited amount of energy at their disposal. As an example, the space rovers are powered by solar cells, and agricultural and industrial robotic platforms are powered by batteries, where the energy is a limiting factor for the duration of the mission. Energy modelling of the robotic system is not only important for the purpose of predicting the search duration of the mission, but also for a energy efficient route, as mentioned in Section 2.1.1. A less energy optimised route taken by the mobile robotic platform places more stress on their mobility system, which decreases their operational life and increases the possibility of the platform being out of service due to mechanical failure. Therefore, energy modelling and simulation of the battery-powered mobile robotic platform is important. (Hou *et al.*, 2019b)

Presented by Datouof is an energy-efficient trajectory planning method for mobile robots, where a modification has been made for the a-star algorithm. The energy model of the three-wheeled Omnidirectional mobile robots was created. Then the A\* algorithm is modified according to the result from the modelling, where the calculation of the heuristic function is modified, specifically. The heuristic function has been discussed in Section 2.3.1. With the modified heuristic function, the modified a-star algorithm can find an energy efficient path. The optimum velocity is calculated by solving the Sequential Quadratic Problem. Finally, the path generated by the algorithm

is simulated using a three-wheeled mobile robotic platform named the Omnidirectional Mobile Robot. This platform uses the different speeds and directions of the three wheels to control the trajectory of the robot, without a steering mechanism. The simulation environment is set up with 3 artificially-placed, high-friction zones of the same height (Datouo *et al.*, 2017). The energy modelling of three-wheeled robot is validated by the results of the simulation. The energy cost of a smooth and unsmooth path, with two different approaches, are compared. However, the energy cost of the shortest distance path against the path generated by the proposed algorithm has not being compared, which does not give a solid conclusion of the effectiveness of the energy efficient path planning. Nevertheless, the algorithm presented with the modified heuristic function has a potential for further investigation. The a-star path planning algorithm in Section 2.3.1 with its advantages and disadvantages is analysed.

The second article presented by Canfield is a validation of a power consumption model for a skate steer mobile robot (SSMR), which has two tracks instead of wheels. SSMRs have advantages compared to wheel-based robots, it is more robust with a simpler driving and steering mechanism. However, it also has disadvantages, such as when steering unnecessary friction is generated and the driving system has a lower efficiency in terms of electrical energy transferred to kinetic energy. The SSMRs have a larger power consumption when the robot is turning due to the corresponding slipping friction while inducing a larger load on the driving system. The behavior of the slipping motion is generally characterised through Instantaneous Centers of Rotation (ICR), where the friction model is established dynamically. However, the existing power models for the SSMRs generally constructed at a kinematic level assumes the slipping motion has a motion equation extracted from empirical data, which may not be accurate. The paper presented introduced a method of modelling the power consumption of the SSMR based on slip parameters, which is calculated with

differential equations extracted from motion equations. The dynamic power model is then validated by the implementation of 2 practical applications of manufacturing. The first application is where the mobile robot is set to climb a steel surface with the primary power consumption for overcoming gravity and turning. The second application is set to show the dynamic ICR model can predict the power consumption with good accuracy. Finally, the results of the experiment validate the energy model, which could be used for optimal trajectory planning to minimise the energy consumption during the mission (Canfield *et al.*, 2019). In conclusion, this report has achieved most of the work claimed, with energy modelling of the SSMR in great detail, however, there is a lack of dynamic simulation and the real-world tests do not show the energy consumption data.

### 2.4.3 Battery Simulation and Modelling

The rover modelled and simulated in this review uses lithium-polymer batteries for their operation. A review of battery modelling and simulation is given.

As Reiter introduced, the thermal and electrical behaviour of a system during its operation using lithium-ion batteries is a complex and systematic problem. To ensure the wellbeing off the vehicle and safety of the surroundings this must be understood (Reiter *et al.*, 2019). A modular simulation framework was proposed, which allows the simulation to perform on different types of batteries, with different electrical and thermal properties. He proposed a framework that contains 3 layers: the cell level, the system level and the monitoring level, as shown in Figure 14.

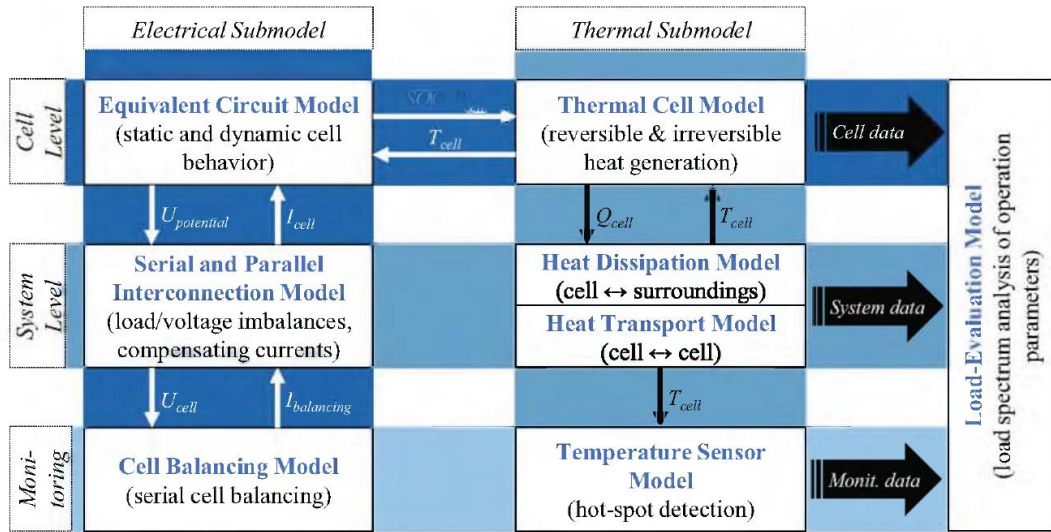


Figure 14. Basic structure of the battery simulation framework by Reiter (Reiter *et al.*, 2019)

Reiter used Simulink to establish the simulation framework for the modelling and simulation of the batteries. Reiter achieved an average accuracy of voltage within 60 mV and an accuracy of current within 40 mA during the simulation. There is, however, no report on the overall power consumption.

## 2.5 Algorithm Comparison for Energy Optimised Path Planning

Having reviewed all relevant path planning methods, it is necessary to compare their suitability and ability to generate an energy optimised path for a wheel based robotic platform within a given terrain. For the purpose of this comparison, it is essential for the algorithms to be able to cope with several factors. These include: the suitability for modelling and representing energy, computational efficiency, suitability to optimise energy dynamically, ability of expanding the modelling for additional requirements in the future, flexibility of the algorithms in dealing with different application scenarios, and how robust the algorithm is. With the possibility of running in real-time onboard the robotic platform, these are important factors for consideration.

Table 1 shows the results of a comparison for path planning methods and algorithms reviewed in Section 2.3, with the characteristics and performances of them specifically compared for the application of energy optimised path planning. The number of stars awarded to each algorithm is based on an assessment of the papers relating to the algorithm by the author, and is based on information from papers in the literature.

Table 1 shows all the mainstream path planning algorithms for mobile robotic platforms with the all their differences. Different path planning algorithms have different characteristics on the applicability of their applications and the objectives of the path planning. Some path planning algorithms are more suitable for specific applications, such as for coverage, point-to-point, exploration or trajectory planning. The path planning algorithms are graded in stars on the different aspects shown in the Table 1.

First is the terrain and ground roughness modelling suitability, and this is evaluated based on the path planning principles of the algorithms. For example, RRT or A\* plan the path according to a dynamic matrix, which changes every step as the waypoint is generated. The fixed terrain and ground roughness will therefore need to be made to matching the dynamic characteristic of the evaluation matrix, which require extra complexity and computation power, being less suitable for terrain and ground roughness modelling. Noreen has compared the Computational power needed / Execution time in his research for a performance comparison of path planning algorithm (Noreen *et al.*, 2019). Liu has stated the achievement of robust and extensibility while designing a path planning algorithm (Gengqian Liu *et al.*, 2005). Boroujeni demonstrated the flexibility of the path planning algorithm performing the task for the autonomous vehicles (Boroujeni *et al.*, 2017). In addition of all above, for the purpose of evaluate the suitability of energy optimised path planning algorithm on

terrain, the terrain roughness modelling suitability has been added as a evaluation target.

Table 1. Suitability for energy optimised path planning

<b>Name</b>	<b>Terrain and Ground Roughness Modelling Suitability</b>	<b>Computational power needed</b>	<b>Extensibility</b>	<b>Flexibility</b>	<b>Robustness</b>
A*, D* algorithm	Low	High	High	Medium	High
RRT	Low	High	Extra high	High	High
Pure Pursuit	Low	Low	Medium	Low	Extra high
Artificial Potential Field	High	Low	High	High	Medium
Particle Swarm	Medium	Extra high	Medium	Low	Medium
Ant colony	High	Extra high	Medium	Medium	Medium
Genetic Algorithm	High	Extra high	Low	Low	Low
Neural Network (Multi-layer perceptron)	Low	Extra high	Low	Low	Low
Reinforcement Learning	Low	High	Low	Medium	Medium
Model Predictive	Low	High	Medium	Low	High

The second evaluation is the computational power needed. This is based on the computational resources required when the path planning algorithm is running, and those required when the map is being expanded. Some path planning algorithms, such as Reinforcement learning or Neural Networks, will require new training when the map is changed, which requires high computational resources. Furthermore, when the

map size is expanded, the computational resources for the training will increase nonlinearly and by greater. Less stars means the computational power requirement and the map size scaling has a better relationship of linearity and a smaller slope.

The extendibility is the third evaluation of the possibility of extending the capability of the algorithm as needed. For example, when more environmental elements needs to be considered, such as the hardness of the surface that a larger robotic vehicles will need to consider such as crop planting robotic vehicles, irrigation or pesticide-applying robotic vehicles. Adding more environmental elements for some planning algorithms such as the Genetic Algorithm will require a complete redesign and reconfiguration of the algorithm. This would require similar amounts of manpower as compared to designing a completely new algorithm, which will waste time and money and should be avoided. Thus, more stars indicate a better suitability for extending the functions of the algorithm.

Flexibility is an evaluation based on the possibility of implementing existing fully-developed algorithms from the platform that it is designed to work in to a new platform. For example, the fully developed energy optimised path planning algorithm for the AgriRover has the requirement of being reused in a UAV. How much the original code needs to be altered and modified is the level of flexibility, where more start means better flexibility. The possibility of changing the accuracy and performance of the algorithm in exchange for the required computational power is also considered. For example, varying the size and the frequency of updating the pathfinding matrix, some of the algorithms have the capability of changing its performance by lowering the updated frequency or size of the pathfinding matrix in exchange for quicker and better real-time response of the system.

Finally, the robustness is evaluated based on the stability of the algorithm when it is used during real-world applications. This is whether or not they have been reported

unreliable in the source papers referenced in this chapter, as some of the algorithms that are more complex will have a tendency of being less stable during experimentation.

In conclusion, for the application of designing an energy optimised path planning algorithm for application in the prototype of the agricultural autonomists mobile robotic platform, the AgriRover, considering the above five aspects a balanced choice is made. The Artificial Potential Field is the most suitable for this application. Firstly, as the potential field can be superimposed and combined with the seated rules, the extensibility and suitability of using the terrain as a part of the planning is achievable. Secondly, the pathfinding process in the Artificial Potential Field Method is based on the attraction and repulsion of the artificial field. The size of the search field is changeable, making it more flexible in accuracy, which makes it suitable for online and onboard real-time path planning if needed. Finally, the problem of the artificial potential field algorithm being less reliable, due to the problems of local minimum, is one of the focuses of this thesis.

## **2.6 Summary and Identification of Knowledge Gaps**

As electric powered devices and vehicles are being used more often for the purpose of sustainability, both from an energy and environmental perspective, the path planning algorithm that takes a mobile robotic platform from one point to another, with only the consideration of obstacle avoidance, will need to be improved and expanded. As the design purpose of electrical vehicles and mobile robotic platforms is for sustainability, the path planning algorithm itself needs to have the method of reducing the energy consumption as an important design criteria. Khan has given an explanation of the necessity for energy efficient planning (Khan *et al.*, 2018).

Table 2 shows that other researchers have developed and presented methods and algorithms for path planning tasks, designed for mobile robotic platforms, from small-scale platforms, such as trajectory robots (Lakshmanan *et al.*, 2020) and drones to the large scale All-Purpose Remote Transport System (Wit, 2000). Most of the methods and algorithms have presented solutions only for obstacle avoidance, but they have not given a systematic solution for other challenging problems faced by path planning tasks, such as the energy costs of the path generated for ground vehicles based on information such as terrains and roughness of the ground. There was path planning algorithms for UAVs that focused on minimising the energy consumption using the model of minimising the change of speed and travel directions of the UAV. However, for a slow moving robotic platform that is focused on precision, such as interplanetary exploration and agricultural rovers, minimising the change of speed and travel directions has a limited result of minimising the energy consumption due to the already slower speed of the platform. In such cases, the terrains that the robotic platform operates on have to be considered when generating paths. Considering terrain data when selecting a path for the robot is not only important for minimising the energy consumption, but can also, more importantly, be used to ensure the safety of the robotic platform by avoiding extreme inclines and declines, therefore minimising the risk of tipping and rolling the mobile robotic vehicle. This can also avoid overloading the actuators onboard. An energy optimised path planning utilising terrain conditions has versatility and expandability that can be used for agricultural and interplanetary rovers, and even low fly UAVs. By utilising energy-optimisation focused algorithms will not only save energy consumption, but also reduce and eliminate high torque output situations, therefore producing less electrical, thermal and mechanical long-term wear of the mobile robotic platform. This will extend the longevity of the platform, increasing reliability and reducing costs.

In addition, most of the research done on path planning do not have complete dynamic energy modelling and simulations regarding the vehicles they were researched with. A complete dynamic energy-focused model that has interaction between each mechanism of the actual vehicles, that is also capable of being controlled, and representing dynamic behavior in a simulation environment has never been done. With such completed processes of dynamic energy modelling and simulations, with the complete representation of the mechanisms, a relatively precise likelihood of the energy consumption behaviour can be proposed. This would be a judging criterion for the performance of the further energy optimised path planning algorithm.

Furthermore, the design process and methodologies of such energy-focused modelling and simulation has a consultation value that can be used as a reference for any related future research that wants an energy consultation behaviour estimate of a robotic mobile platform. The methodologies and design process of the energy optimised path planning algorithm based on terrain will also provide a guideline for any future needs of developing path planning algorithms that is focused on minimalising the energy consumption which has not been done before.

In conclusion, even with this need, there is still a lack of a published energy-focused path planning algorithm based on the terrain for autonomous mobile platforms, such as the AgriRover. Additionally, there is a lack of a complete energy model and simulation that has the capability of dynamic control implementation, where the result of this simulation can be used as evaluation and validation tools for an energy optimised path planning algorithm.

Table 2. Work on path planning completed by others

Type of Algorithm	Type of Application	Researchers	Optimisation of Energy Cost	Obstacle Avoidance	Consideration of Terrain	Experimentation	Robot Lifespan Extension	Dynamic Energy Modelling and Simulation
A* algorithm	Ground robot Coverage planning	Le	No	Yes	No	Yes	No	No
	Ground robot Point-to-point	Kusuma	No	Yes	No	No	No	No
RRT	Ground robot Exploration	Kim	No	Yes	No	No	No	No
	Ground robot Exploration	Umari	Yes	Yes	No	Yes	No	No
Pure Pursuit	Ground trajectory robot planning	BAČÍK	No	Yes	No	Yes	No	No
	Tracked vehicle trajectory planning	Wit	No	Yes	Yes	Yes	No	No
Particle Swarm	UAV Trajectory planning	Roberge	No	Yes	Yes	No	No	No
Ant colony	Ground robot point-to-point	Blum	No	Yes	No	No	No	No
	Ground multi robot planning	Wong	No	No	No	No	No	No

<b>Type of Algorithm</b>	<b>Type of Application</b>	<b>Researchers</b>	<b>Optimisation of Energy Cost</b>	<b>Obstacle Avoidance</b>	<b>Consideration of Terrain</b>	<b>Experimentation</b>	<b>Robot Lifespan Extension</b>	<b>Dynamic Energy Modelling and Simulation</b>
Genetic Algorithm	UAV Coverage planning	Shivgan	Yes	Yes	No	No	No	Partial, only static modeling
Neural Network (Multi-layer perceptron)	Ground robot point-to-point	Das	No	Yes	No	Yes	No	No
Reinforcement Learning	Ground Tetromino robot point-to-point	Lakshmanan	Yes	Yes	No	Yes	No	No
Model Predictive	UAV trajectory planning	Williams	No	Yes	No	No	No	No

# **3 Design Methodology for Energy Optimised Path Planning of Mobile Robotics (EO- PPMR)**

## **3.1 Introduction**

Based on the literature review, it is clear that mobile robotic systems require energy efficient path planning in navigating fields. This is especially the case when the mobile robots are deployed in an unknown environment, as demonstrated in the literature review of Section 2.1.1.

Before generating an algorithm for energy efficient path planning, it is necessary to investigate common methodology considering all the important aspects of the system and environmental factors, in order for the proposed work to be generic and applicable in additional applications. In this chapter, a purpose-generated design methodology is presented for path planning of mobile robotics. An energy optimisation algorithm can then be derived for detailed modelling and path optimisation to improve energy efficiency and long-distance operations. The algorithm design is modelled and developed based on Figure 15.

The proposed design process model consists of three pillars, namely the information repository pillar, design process pillar and energy pillar. The information repository pillar is concerned with the representation of the design information expansion process, as more design decisions are made, more design parameters values are committed, hence more information is decided. The design process pillar represents the conventional process of designing mechatronic systems, such as a mobile rover. These processes flow from top to bottom and help a designer to progress to a satisfactory design. Building on this established work, this work proposes to have a new pillar and focuses on the consideration of energy conservation and external impact factors onto a field robot. This is further considered to include the dynamic

changing environment and its impact on the energy consumption of a mobile robotic system. These factors include the elevation of the terrain, the surface unevenness of the terrain, and the hardness of the surfaces that a mobile rover will travel on. With this considered in the design process model, detailed in this chapter, it is believed that a full and comprehensive consideration can be made to ensure a mobile robot is designed to be energy efficient.

In the information repository pillar in Figure 15, from top to bottom, it shows the information of the mechatronic system design process expands as the system develops, and the relationships between each part interconnects, which is shown on the left using the evolving information flow arrow. This information can be categorised into four blocks of information from top to bottom. These include information on design initialisation and task clarification, which can be further divided into the parts that describe the system level needs of the customers, and specifications through analysis, as well as market intelligence for commercialising a mobile robot in a researched market. The information becomes richer, as shown in Figure 15, by the darkening colour of the product design specification. This is an evolving information flow for the existing information, which are the statements of the customers' needs and marked research results.

In the second pillar in Figure 15, from the top to the bottom, it shows the mechatronic system design process and activities for generating a final design solution. It involves both concepts of generation and qualitative modelling. In this step concepts are generated and evaluated according to specific working principles using the existing information of design specifications produced in step one. After that, a fully developed concept model is created for further evaluation.

The information from the concept which was generated and evaluated is passed to the third step, which is the embodiment design and quantitative modelling for evaluation. Embodiment and detail design are first undertaken so that all components

are specified, then the evolving information is passed for the embodiment models, and then also the fully developed solution models. These models can then be simulated and quantitatively evaluated.

Finally, the last part of the mechatronic system design process in the middle pillar is about multi-perspective modelling and simulation, in which a mobile robot solution is fully modelled and simulated from several perspectives, as illustrated in the last part of the information repository pillar. All these multi-perspective models provide a full representation of a mobile system for exhaustive evaluation. There are more intertwined relationships and trade-offs required and considered at this stage for an optimal solution, as shown in the Figure 15. In this step, many models are designed, as shown in the bottom part of Figure 15. Building on the library of simulation models, as well as simulation and visualisation, a mechatronic system can be fully generated, evaluated and validated in this virtual modelling world. This forms the basis of Yan's mechatronic system design process model, as shown in Figure 15.

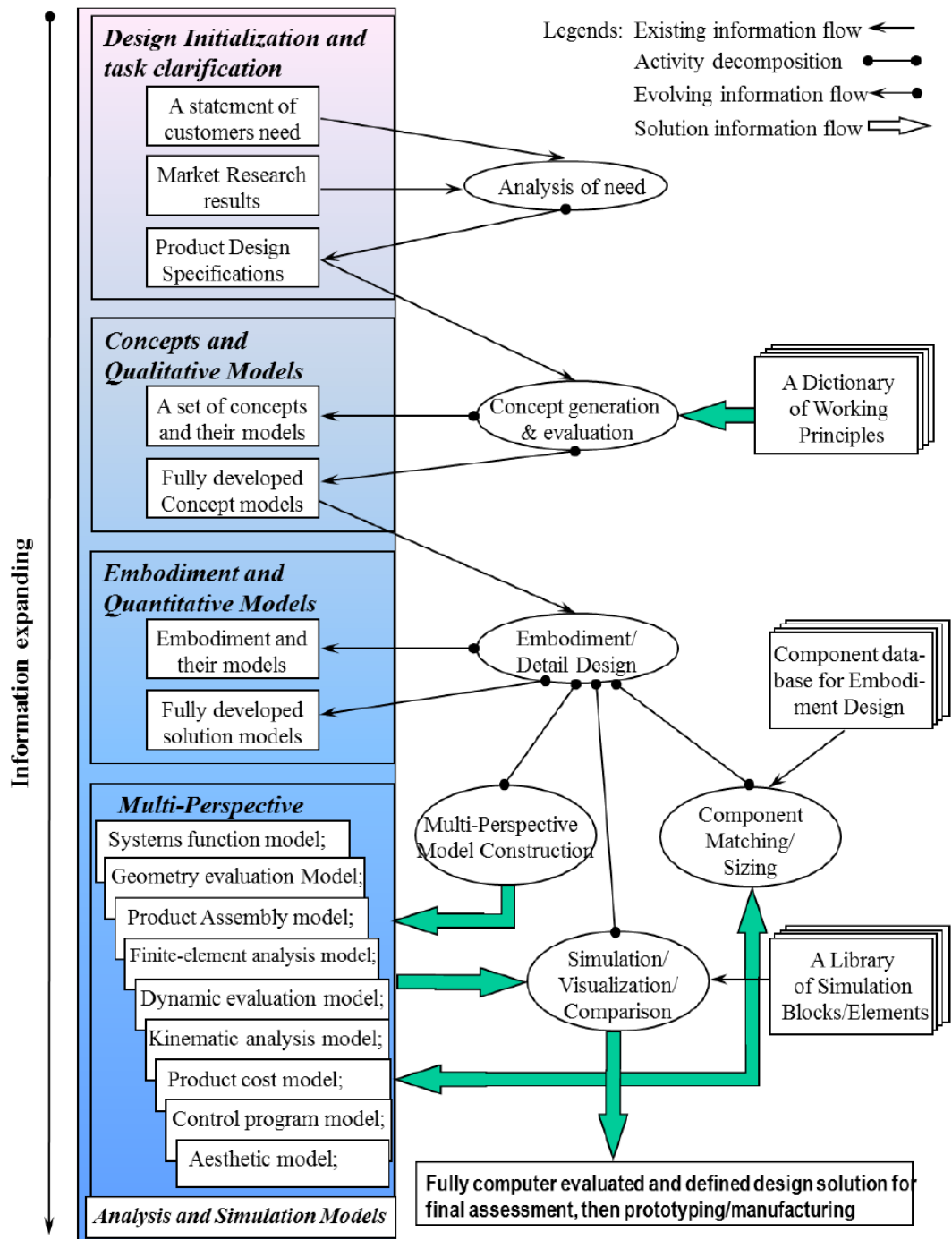


Figure 15. Yan's mechatronic system design concept (Xiu-Tian Yan *et al.*, 2010)

Reviewing the model represented in Figure 15, it is clear that energy was not a focal viewpoint for consideration, and this was left for further investigation. This work builds on this aspect and proposes an enhanced specific design process by considering

energy of the mechatronic system. In aiming to enhance the design process, a newly created pillar can be found in Figure 16.

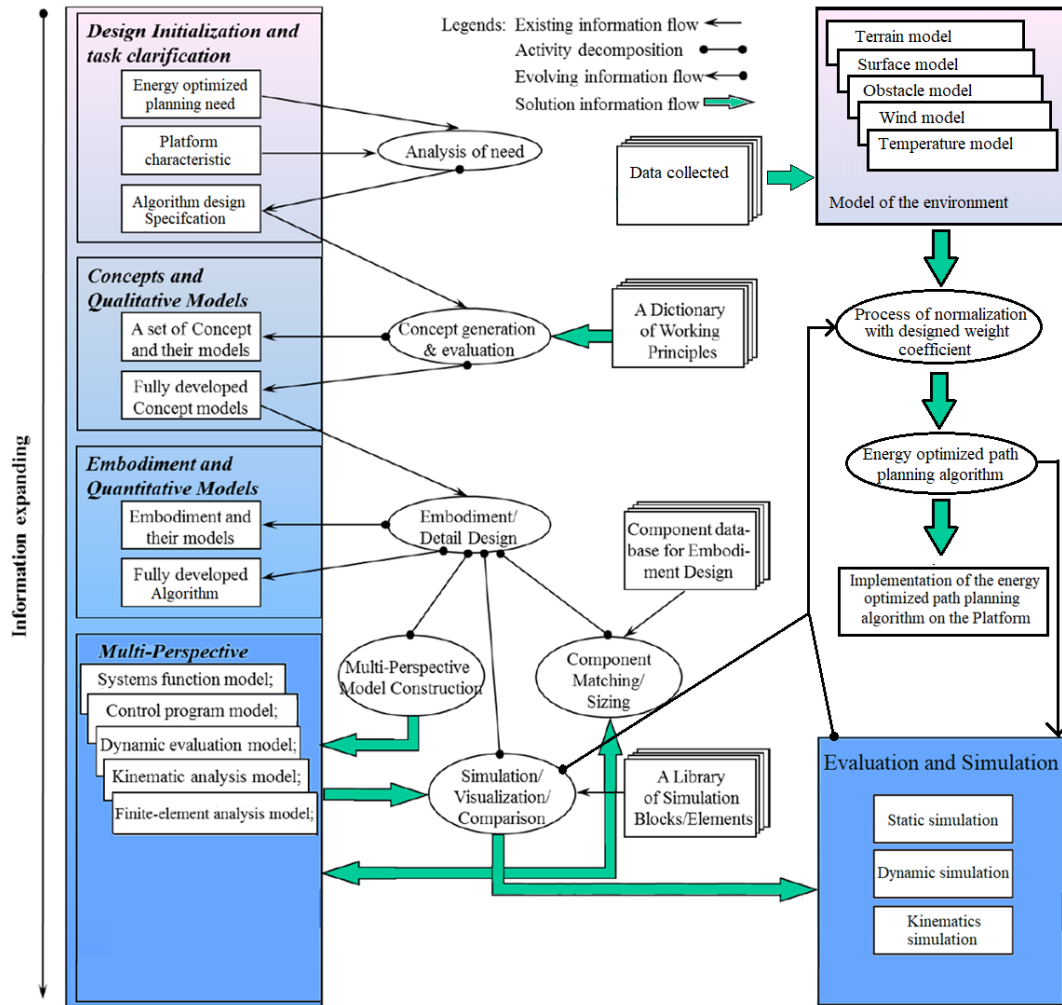


Figure 16. A generic design process model for energy optimised mechatronic rover system

From the energy optimised path planning modouling and simulation , the design process model, as shown in Figure 16, considers the following aspects: environment, path planning and terrain.

Surface modelling shows the difference between between ideal uniform surface and the real world complex ground surface if used. On the top left it is seen that the planning first needs to be formulated, such as considering how the planning algorithm will be focused on the ratio between the shortest path and lowest energy cost. Moving down to the second part, the platform characteristic needs to be considered, depending

on the difference between each platform's characteristic for each type, a different path planning method will need to be utilised. After the first part, moving down to the second and third parts of Figure 15, it remains the same for both the concept and qualitative design step, and the embodiment and quantitative design step.

In the last part, as this is a energy optimised planning design concept, the models required are less when compared to the universal design concept shown in Figure 15.

Finally, shown on the right is the design of the path planning algorithm. It is seen at the top that data is collected using various methods, such as data collected by the onboard and offboard sensors, weather station, and satellite, will be modelled according to the requirement of the application, which could include air-, ground- or water-based scenarios. After the modelling of the environment, there is a processing algorithm for each of the environmental models that gives different priorities according to the objectives of the specific platform, which could include maximum distance travelled, full coverage, exploration and more. According to these objectives, each of the environmental models will be processed and selected. With these selected inputs, the designed energy optimised algorithm will generate a path for the specific platform independently, making it flexible and expandable. The result of the path generated is then simulated again, the parameters of the planning algorithm can be tweaked and the performance off the energy optimised path planning algorithm can be improved. The performance is determined as satisfied when the algorithm can be implemented to the individual platform and the field test can then be preceded with.

### **3.2 Energy Optimised Planning Design Methodology**

For an energy efficient mobile rover design, a list of considerations have been compiled based on the literature review and fields studies. Table 3 shows the detailed design tasks that is requires investigation on the left and the specific outcomes that needs to be generated on the right. These can then be used to help build a

comprehensive representation of the energy models of a mobile rover design. This tabel is inspired by the Li's haptic design process (Li, 2019).

Table 3. Energy optimised planning algorithm design process needs and tasks

<b>Tasks required for energy perspective design and modelling</b>	<b>Outputs</b>
Task clarification through analysis of needs.	Inspiration and research review
	Requirements and specifications
Mechanical/Electrical modelling to enable detailed energy conversion representation. Functional concepts modelling.	Limitations and capabilities analysis of the platform
	Key power component energy models for simulation
	Key functional models for behaviours representations and simulation
Detailed functional modelling. Software development modelling. Algorithms development for control, e.g. PID control	Control methods and software analysis for the implementation of the algorithm
	Specific energy efficient control algorithms
Force modelling Kinematics modelling	Analysis for the platform on force and kinematics models for validation and simulation
Simulation	Performance evaluation on simulation results
Field test	System performance data captures
	Field data analysis for validation

### 3.2.1 Task Clarification

Firstly, the path planning tasks will need to be identified and clarified. This is mostly dependent on the type of platform the energy optimised planning algorithm is required to be implemented on and the objectives that the algorithm needs to achieve. It is important to have a clear understanding and specification for the path planning, as there are many kinds of vehicles and each kind is different in their path planning. These

different kinds of vehicles include the Lunar rover, Mars rover, Agricultural rover, or any other type of vehicle like the Autonomous Underwater Vehicle, Unmanned Aerial Vehicle, or Unmanned Surface Vehicle. They all have a limited stored power supply, or a power output limited by electricity and mechanical structure. This is the case not only for those mentioned, but also for similar types of vehicles. Moreover, the path planning objectives can also be different. For example, a Lunar rover could be used for exploration, mapping, sampling, retrieving or transportation. For different missions, different yet comparable energy optimised planning algorithms are required for the same principles, but they are different in their execution. For example, in a mapping mission the global map of the environment could be largely unknown, but the surrounding terrains and structures can be captured by the onboard sensors, in which case a dynamic energy optimised planning algorithm needs to be utilised. For each different mobile robotic platform, there are different characteristics, requirements and specifications, which are considered and needed for the development of an energy optimised planning algorithm.

### 3.2.2 Conceptual Design

Conceptual design is an early stage of the design process for the high-level, overall function of a project, or in this case an algorithm, that can work in different specified cases.

More specifically, conceptual design is the phase where engineering, science, practical knowledge and commercial aspects are brought together, and where the most important decisions are made (Michael J French *et al.*, 1985).

Shown in Figure 17, the conceptual design stage can be divided into 3 parts and they have an interconnected relationship as shown. First, the needs and ideas will be transferred into a functional definition. Following this, a concept is generated according to the functional definition. Finally, the concept will need to be validated

and evaluated, with the results feed back to the beginning and the functional definitions can thus be changed with new functional definitions presented.

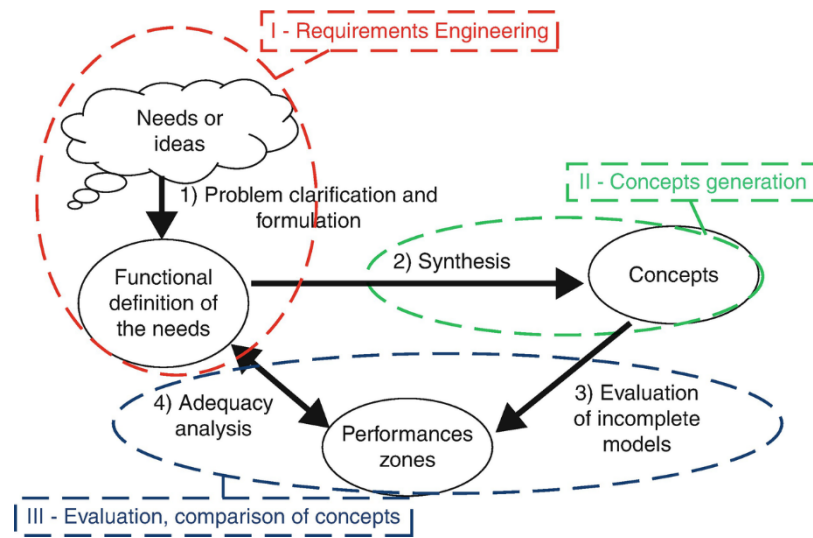


Figure 17. Conceptual design stages (Christophe *et al.*, 2014)

For this particular algorithm’s conceptual design, the integrability and compatibility, between the energy optimised planning algorithm and the platform that the algorithm will be deployed on, are very important. For example, a lightweight and low power consumption platform, such as a small lunar rover, have less processing power compared to a heavier and higher power consumption platform, such as an autonomous underwater vehicle. This high-power consumption platform requires a lower processing planning algorithm that is more suitable for such an application. In addition, the environment also needs consideration, which has different impacts for different types of platforms. The algorithm needs to be designed specifically for the platforms within a particular environment they will work in so that they achieve true energy optimisation.

The conceptual design for the energy optimised path planning algorithm therefore needs to define and describe a full picture of understanding of the mobile platforms and the environment for the algorithm’s conceptual design. Following this process, the type of planning algorithm then can be selected, validated and evaluated as described in the next section of embodiment design.

### 3.2.3 Embodiment Design

Embodiment design is a more specific design process compared to the conceptual design. Embodiment design is the part of the design process which starts from the principle solution or concept of a technical product (Pahl *et al.*, 1996).

First, the key requirements and constraints of the embodiment design for the energy optimised planning algorithm need to be determined. The limitations and constraint requirements are laid in and associated with the hardware structure. A planning algorithm, therefore, needs to be designed with the consideration of such limitations and requirements. The principle that makes the energy optimised planning algorithm work needs to be created and generalised. It is particularly important to ensure it is compatible with all the systems onboard the platform, which can include, but is not limited to, mechanical, electronic, sensor, hydraulic, and pneumatic sub-systems. Therefore, it is important to produce and reference an information base so that these concepts can be supported, depending on the selection of working principles. Finally, the working principle of the energy optimised path planning algorithm design process can be confirmed, followed by the embodiment and conceptual design model being generated and assessed.

### 3.2.4 Function Design Process

Unlike a product design, the Function Design Process for energy optimisation is mostly a software and algorithm design. The function of the energy optimised path planning algorithm needs to find a path for the platform which is both safe and the most energy efficient, where the least amount of processing power is utilised.

This step of the design will be break down into functions, sub functions and modules. As the process develops, changes and improvements need to be made on the functional modules, but the framework remains the same during development.

Finally, the energy optimised path planning algorithm can be coded and tested. This design process is shown in Figure 18.

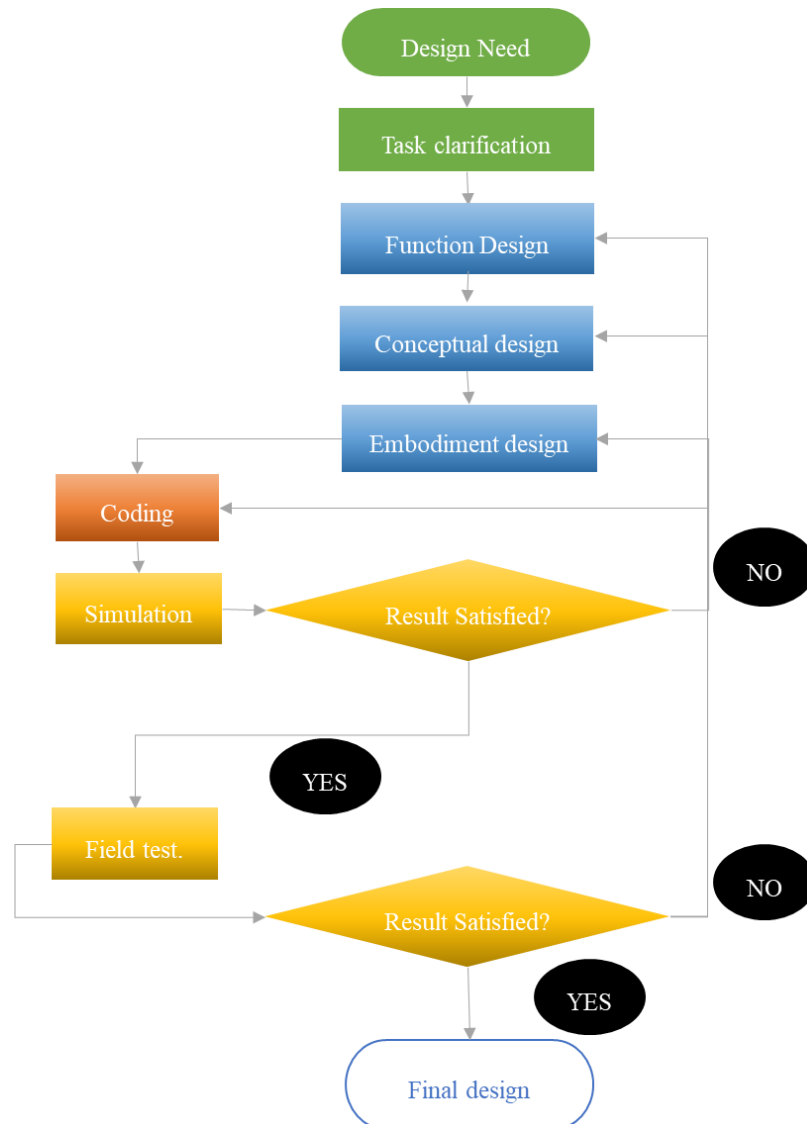


Figure 18. Design process of the energy optimised path planning algorithm.

In Figure 18, green shows the definition of the application, blue shows the process of design, red shows the process of implementation and yellow shows the process of evaluation. First, the design needs are decided and the tasks of design is identified. Then, the design process begins with the conceptual, embodiment and function designs, which will give a detailed design of the algorithm. The next step of the design process is to programme the algorithm, which aims to make it implementable on the platform that is designed for. The final steps shown in yellow is the process of

evaluation, where the results of planned path will first be simulated and then this will be evaluated. If the result is satisfactory, the process will proceed to the next step of field test. If not, the process will go back as the arrows show and according to the aspect of the dissatisfied areas. If the field test is preceded with, the results of the field test is captured and evaluated. If the result is satisfactory, the design can be implemented on the platform, and if the result is unsatisfactory, the design process will go back to the design and coding process, as shown in Figure 18.

### **3.3 Evaluation**

Evaluations should be conducted constantly during the entire design process, as mentioned in French's design model (Richard H French, 1985). After finishing each step of the design process, an evaluation should take place. Both the performance and compatibility should be considered. If any performance is deemed unsatisfactory, or a solution is incompatible, the current design process should be backtracked and improvement on the solution shall be made, or an alternative solution should be generated. A methodology of evaluation methods need to be developed. From the literature review represented by Davidson (2005), as well as Howe and Eisenhart (1990), while considering the mobile platform design, the following evaluation approach is proposed for this study. As the book (Davidson, 2005) mentions, 4 key points need to be addressed. The solutions are followed.

1. The identification of the right criteria for the energy-focused design evaluation.

The criteria that is important is what defines the functionality and robustness of the energy optimised path planning algorithm. This includes but is not limited to, all the necessary factors for the design of the algorithms, the type of path planning algorithms selected, the efficiency of the code, the number of bugs in the code, the testing and debugging procedure, and the modifications done according to the testing results. For this study, it is considered that the energy costs of transportation is a key criterion in

addition to other mechatronic system design criteria, such as power rating, functionality, cost, weight, etc. The focus will be on the total cost of energy of transportation.

2. The level of importance for each criterion and the balance between them.

The factors for evaluating an energy optimised path planning algorithm are as follows: safety of the surroundings, safety of the platform, energy cost, time cost and process power needed. The level of importance of these considerations vary between different platforms and different missions. It is therefore proposed in this study to leave this decision to determine the level of importance to a mechatronics system designer.

3. The qualitative and quantitative standards of the designs.

As is mentioned in (Howe *et al.*, 1990), quantitative is statistic or metric, and it is a quantifiable and measurable in numbers with units. In this case: how much energy is saved, how much time it takes to finish the path, and what is the maximum peak drive current in the energy optimised path planning algorithm design process.

In contrast, the qualitative is unmeasurable in numbers, which includes the usability of the energy optimised path planning algorithm, the quality of the model used in each step, and the human-computer interaction, if applicable.

In this study, a combination of these two evaluation approaches is adopted to enable a balanced evaluation. When it is possible, as much as possible, a quantitative evaluation of an energy-focused design solution is made and results are reported. If this is not possible, in cases of field studies on the performance of a system, a qualitative approach is adopted for evaluation.

- 4. Weaknesses of the design

The weaknesses of the algorithm design is a measurement of the robustness under working conditions, and with simulations it can be improved to a better level. Furthermore, with appropriate field tests the working platform can be improved even

more. This is an important measurement for improving a design. Given the challenge in an unstructured environment, while being intended for multiple mobile platforms using a generic approach, this study promotes this aspect of the methodology for evaluation in order to identify the weaknesses and improve the solution.

### **3.4 Summary**

A new methodology of designing an energy optimised path planning algorithm is presented in this chapter. First, Yan's mechatronic system design concept (Xiu-Tian Yan *et al.*, 2010) is exhibited and explained in detailed steps, as shown in Figure 15 in page 63. A new pillar focusing on the energy consideration is introduced for consideration, as well as supporting design concept exploration for the energy optimised path planning algorithm, as shown in page 64 Figure 16.

Then energy optimised planning design methodology is introduced with 4 parts which define the design process methodology. This includes task clarification, conceptual design, embodiment design and function design. Finally, the evaluation of the design solution, for energy consideration of mechatronic systems and its processes, is introduced.

Building on this investigation and proposal, an energy optimised planning design methodology is used for the design of this energy optimised path planning algorithm for the AgriRover, with evaluation and simulation described in Chapter 8. Further field tests and results are described Chapter 9.

# 4 Energy Modelling and Energy Optimised Path Planning

## 4.1 Introduction

This chapter describes the work of energy modelling of a mobile rover system and its application in the AgriRover. The main concept of modelling the key performance parameter of energy is called the Total Cost of Transport (TCoT), and is defined as the total energy used per unit weight, per unit distance travelled. This is a further development of the work by (Bhounsule *et al.*, 2012), which considers only the movement of the vehicle on flat ground.

After the introduction on the establishment of a generic energy model for a rover platform, the energy optimised path planning algorithm for the rover is introduced. And energy cost when using the energy optimized path planning algorithm and not using the algorithm are calculated compared and evaluated on the targeted test platform AgriRover which has been mentioned in introduction.

From the system integration point of view a field mobile robotic platform, such as an agricultural or space rover, normally contains a local and global planner where the local planner is used for local tasks, such as dynamic obstacle avoidance, sometimes with dynamic motion planning, and the global planner is tasked with global applications, which includes the global path planning based on static elements obtained before the deployment of the mobile robotic platform.

The energy-optimised path planning in this thesis is focused on offline planning, with the available data on terrain size being 385m by 330m. This energy-optimised path planning algorithm is a global planner utilising the available terrain data. According to the reviewed literature, online local planning for mobile robotic platforms is mostly focused on obstacle avoidance and motion optimisation. In the

field of obstacle avoidance, a significant amount of research has been published. Therefore, this research will not be focused on such a subject.

For online planning research is done for dynamic obstacle avoidance and motion planning on mobile robotic platforms and autonomous automobile platforms, which was reviewed in 2.1.2 and 2.1.4. Research was reviewed on the energy-optimised local motion planning for UAV's, which will not be beneficial for the use of mobile robotic platforms with reasons mentioned in section 2.6.

The goal of research for path planning in this case is to find an energy-optimised path in rich terrain with static data. In conclusion, offline global path planning is selected to ensure the novelty and the performance of the energy-optimised path planning in a rich terrain environment for mobile robotic platforms.

## **4.2 Energy Modelling of the AgriRover**

Given the unstructured and known or unknown environments which typically mobile platform faces, e.g. a rover, will operate in, it is important to model the power consumption to ensure the system meets the affordability and operational time requirements. Affordability in this work is defined as the delivery of the minimal energy cost for a given rover operation, while also considering that the rover needs to be able to return to its base for charging safely and avoiding unnecessary costs of fetching or searching for it due to a total energy loss of the rover. Operational time and understanding of the energy consumption, in order to predict energy consumption during an operation in an unstructured environment, is also an important feature for the modelling of a rover. To address these crucial needs, a new method for measuring the energy efficiency of a mobile platform is proposed in order to provide an accurate and timely measurement of the power consumption during its operation. The model is also intended and can be applied to any mobile technology using legs or wheels. The model consists of two aspects: static and dynamic modelling.

Due to the changing nature of power consumption of rovers in unstructured environments, the dynamic energy consumption and its efficiency of any rover is derived, in order to establish the key energy performance characteristics of the mobile platform. This will allow for the evaluation of the instantaneous and peak performance characteristics of the mobile platform in typical soil sensing operations. In these applications, it is insufficient to measure only the static energy efficiency, and as such the new approach includes both time and overall performance analysis which will provide new intellectual features to the rover modelling.

The instantaneous power of dynamic modelling for a rover is derived from first principles. This approach takes a systematic approach and captures the total power of the rover system so that it has a holistic view of the power that has been used, is being used and will likely be used. This approach is therefore capable of potentially covering all energy used and enabling a predictive energy management of the onboard energy system. Referring to Equation 3, the instantaneous power  $P$  in any sub-system is given by the average power,  $P_{avg}$ , as the time interval,  $\Delta t$ , approaches zero of that particular system.

$$P = \lim_{\Delta t \rightarrow 0} P_{avg} = \lim_{\Delta t \rightarrow 0} \frac{\Delta W}{\Delta t} = \frac{dW}{dt} \quad (3)$$

Power  $P_T$  is the total power required at any instantaneous moment. Power  $P_m$  is the power used for the displacement of the rover. This is a value which will be different with differing acceleration and is calculated as shown in Equation 4.  $P_s$  is the power used for the steering of the rover. To overcome the friction between the rover and contact surface,  $P_f$  is introduced. During operation, there will be heat generated due to mechanical friction and the electrical energy to mechanical rotation conversion. The power due to the heat loss by the propulsion system can be defined by  $P_h$ . This portion of the power is proportional with the power that is passed through the rover and can

be further integrated by sub-systems. Finally,  $P_e$  is the power required for the on-board electronic equipment.

$$P_T = P_m + P_s + P_f + P_h + P_e \quad (4)$$

$P_m$  is the summation of the power on each wheel and at any given time, calculated as  $P_m = F \cdot V_l$ . Furthermore,  $P_s$  is the summation of the power consumed by the steering system, calculated using  $P_s = \tau \cdot \omega$ .

For the driving motors, heat loss  $P_{hd}$  is considered and at any given time.  $P_{hd}$  is a function of  $P_m$ . The heat loss  $P_{hd}$  is calculated as demonstrated in Equation 5, where  $\eta$  is the product of the efficiencies of the rover motor and the motor driver.

$$P_{hd} = P_m \cdot (1 - \eta) \quad (5)$$

For steering motors, the heat loss  $P_{hs}$  can be calculated as shown in Equation 6.

$$P_{hs} = P_s \cdot (1 - \eta) \quad (6)$$

Consequently, the total heat loss,  $P_h$ , will be the summation of  $P_{hs}$  and  $P_{hd}$ .

At an instantaneous moment the power  $P(t)$  can be defined as in Equation 7.

$$P_{(t)} = \frac{dW}{dt} \quad (7)$$

According to the total power required at any instantaneous moment, the energy cost of the rover  $E_T$  can be defined as in 8.

$$E_T = \int P \cdot dt \quad (8)$$

By merging Equation 4 and Equation 8, in any one given time interval from  $t_1$  to  $t_2$ , the AgriRover's energy consumption  $E_T$  is given by the integral as shown in Equation 9.

$$E_T = \int_{t_1}^{t_2} (P_m + P_s + P_f + P_h + P_e) \cdot dt \quad (9)$$

Applying Equation 9, it is proposed to define the total cost of transport as the ratio of the power consumption to the product of weight and velocity in real time, enhancing the static measurement, as shown in 10.

$$TCoT = \frac{E_T(t)}{W(t) \cdot V(t)} \quad (10)$$

Where W and V are the weight of the AgriRover and the velocity it travels at, respectively. Applying 10, it is possible to estimate the dynamic total cost of transport of any rover. One example of such dynamic behavior over a period of time is shown in Figure 19. This is an estimated modelling result and the detailed calculation is show below.

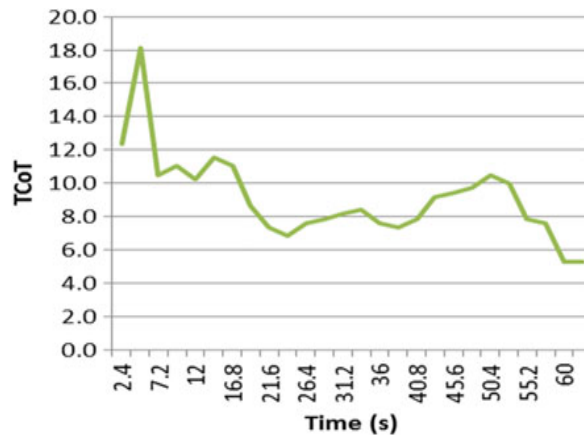


Figure 19. A the dynamic total cost of transport plot example. Running for 18.3 m with an average speed of 0.3 m/s.

## 4.3 Energy Optimised Planning

### 4.3.1 Introduction of the Algorithm for Energy Optimisation Planning

In this part of the thesis a path planning algorithm, with energy optimisation as the goal, is explained and demonstrated. This energy optimised path planning algorithm

is developed based on an Artificial Potential Field algorithm with modifications, and an extension of the Artificial Potential Field algorithm. The modifications and extension of the factors of the Artificial Potential Field corresponding with the criteria of an energy optimised path planning is explained. The energy optimised path planning algorithm's code is then shown and explained. Lastly, the result of the total cost of energy is calculated and compared for the optimised path and a straight point-to-point path.

### 4.3.2 The Advantages of the Artificial Potential Field

The Artificial Potential Field algorithms have been investigated widely and have several advantages as follows. Firstly, the Artificial Potential Field algorithms, with many modifications or adaptations, are well tested and used (Bing *et al.*, 2011, Hwang *et al.*, 1992, Pamosoaji *et al.*, 2013, Qi *et al.*, 2008, Qixin *et al.*, 2006, Raja *et al.*, 2015). Despite these research works reported, for most cases such algorithms are used for avoiding obstacles, path finding in predefined indoor spaces, and locally to avoid rough terrains. This research will extend this algorithm into a new application in an unstructured and open environment. The work will also extend its potential for path planning and optimisation. Thus, the main features and potential advantages of the Artificial Potential Field path planning are summarised as follows:

- Lower cost of the computing performance compared to more intelligent and bionic path planning algorithms, such as genetic algorithms, neural networks, ant colonies, which makes it more suitable for an onboard computer with limited power and available space.
- The required computing power will not increase to the power of 2, or sometimes to the power of 3, as the size of the map increases, such as seen in the Fractal Tree path planning algorithm (Pinzi *et al.*, 2019) or A\* algorithm (Tseng *et al.*, 2014). Instead, the required computing power will increase linearly as the size of the map increases. This is particularly suitable for unstructured environments, as the map could be significantly extended.

- Lastly, the Potential Field has the feature of being a modifiable algorithm. This will enable the operation of a new Potential Field algorithm, which could be modified on demand during operation without requiring completion, which makes the algorithm much more flexible.

Overall, the Potential Field algorithm is more suitable for a generic rover to use for the energy optimised path planning which are possible for Online Planning in the future with limited onboard Computing performance.

### 4.3.3 Description of the Energy Optimisation in Path Planning

Normally the moving path of the rover is a straight line, as this will minimise the steering effort. It is a good strategy to travel in a straight line, as it is normally the shortest distance for the rover to travel, but sometimes a straight path is not the most energy efficient path when the terrain is not flat. Instead, going around hills in an optimised fashion may be more energy efficient. By applying the proposed path planning algorithm, as shown in page 95 Figure 31, a new path can be found. This generated path would save more energy than a straight-line path. When moving the rover at a fixed speed, the energy spent on going up and down a hill will be wasted as typical heat loss. Even with a very highly-efficient energy recovery braking system, over 50 percent of the energy will be wasted. However, by going around the hill the energy could be saved (Niu *et al.*, 2018).

Firstly, presume when the rover climbs, additional energy is needed and the kinetic energy cannot be converted back to electrical energy, as the design of the rover driven by electrical motors are typically not reversible, due to the high gear ratio in the system. Furthermore, potential energy gained from a higher position of the rover can't be easily recovered during a downhill descent.

As Equation 4 and Equation 9 in Chapter 4.2 shows,  $P_m$  is the power used for the displacement of the rover, and the multiplication of  $P_m$  by the unit time,  $E_T$  can be subdivided into Equation 11 (Ooi *et al.*, 2009). In Equation 11,  $E_m$  is the total kinetic energy when moving.  $E_c$  is the energy needed when changing the state of movement, such as speeding up, slowing down, or steering.  $W_r$  is the work needed to overcome the resistance.

$$\int E_T = \int E_m + \int E_c + \int W_r \quad (11)$$

$E_m$  and  $E_c$  are mainly dispensed on the mass of the rover.  $W_r$  is composed of two parts, the work needed to overcome resistance when moving, and the work needed when ascending. The descending stage could be counteracted by the gravity component in the direction of the movement (Shuang Liu *et al.*, 2013).

## 4.4 Potential Field Representation and Generation

### 4.4.1 Accessing and Processing the Map

Before the algorithm can be proceeded with, the terrain map of the field is accessed on Digimap EDINA, which is a web mapping and online data delivery service developed by the EDINA national data center for UK academia (Morris *et al.*, 2000) (Millea, 2003).

The terrain data used in this algorithm are all accessed and obtained from this platform. Figure 20 shows the two farmland fields indicated by the red boxes, which are located on the Rushyhill farm close to Auchinairn Rd, Glasgow, G64 1UR. These farmland fields are two of the main testing fields for the AgriRover around the Glasgow area. This energy optimised path planning algorithm maps out the waypoints for the rover on the field located in the bottom left, shown by an arrow in Figure 20.

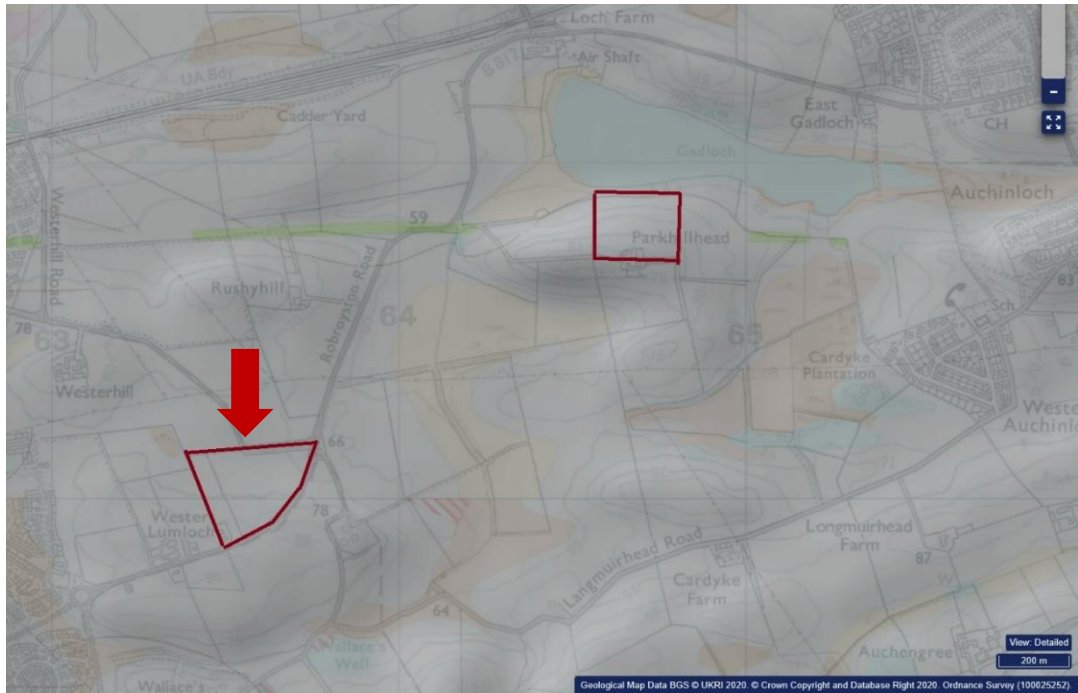


Figure 20. Geology terrain map

The farmland field terrain is then downloaded from the EDINA Digimap, known as the OS Terrain™ 5 DTM data, which has one height data point every 5 meters. For this specified farmland field, Ordnance Survey tiles NS66NW and NS67SW are downloaded and merged. This is because the specified farmland field is on the edge of two tiles. Each OS Terrain™ 5 DTM tile has a size of 5 by 5 kilometers, thus after the merge there are 2000 by 1000 data points, as shown in Figure 21.

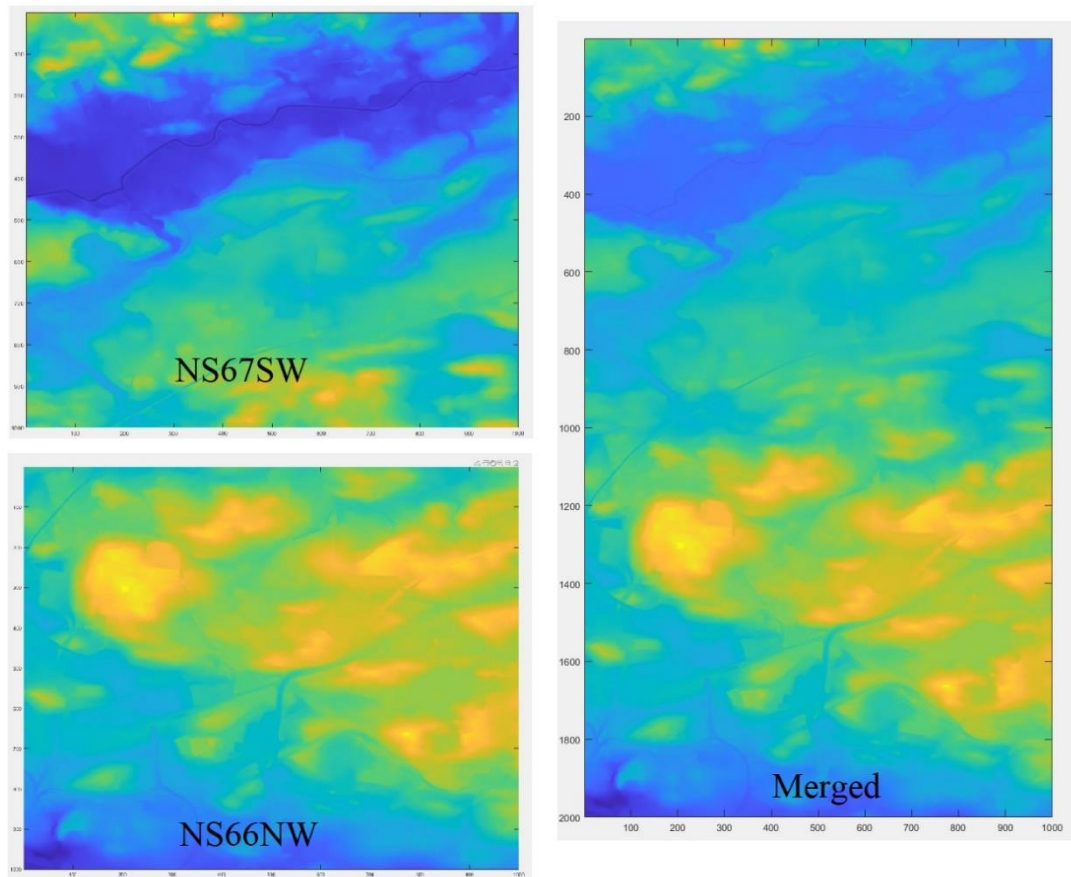


Figure 21. OS Terrain™ 5 DTM tiles

#### 4.4.2 Potential Field Representation

The farmland field terrain is cut from the merged map with the top of the map facing south opposite the common map, shown in Figure 23. The map has a size of 66 by 76 data points, specifying 330 by 380 meters with a height difference of 20.37 meters. This covers the farmland field process shown in Figure 22.

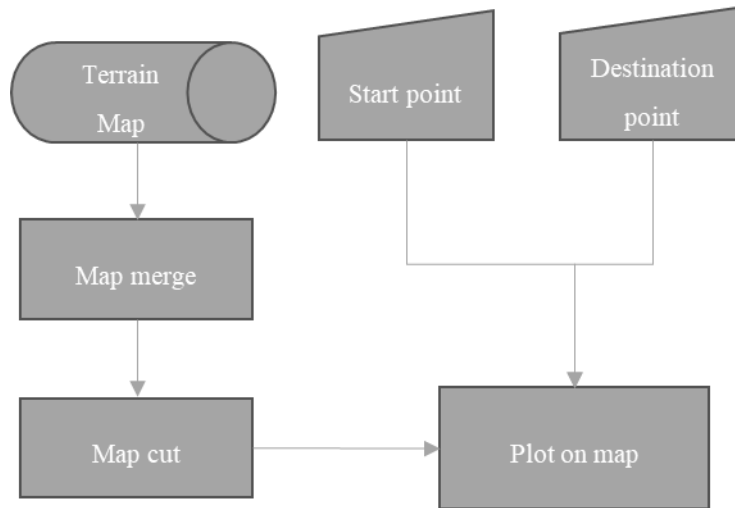


Figure 22. Map process flowchart

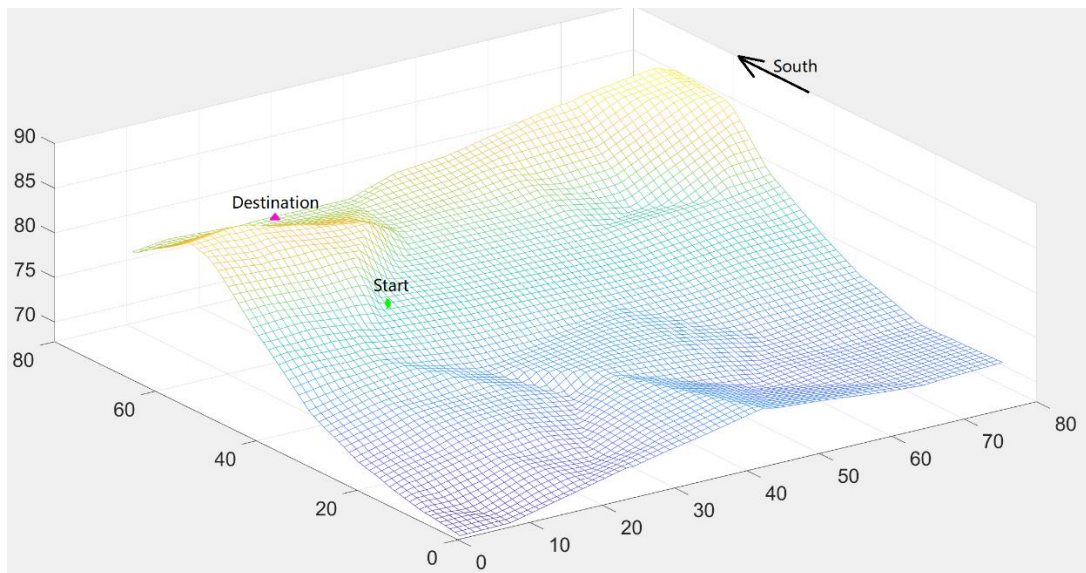


Figure 23. Farmland field terrain

#### 4.4.3 A Generic Artificial Potential Field Generation

##### Algorithm

The algorithm is based on the artificial potential field with modifications and improvements. Every environmental variable has a corresponding artificial potential field calculated by an independent equation. Variables that can be calculated include a topographic map and obstacle map. The first two potential fields considered are the

distance and height difference potential fields. The distance potential field is calculated based on the coordinates of the points on the map.

Firstly, the start point and destination point is set on the map, as shown in Figure 23 by the green circle for the start point and magenta parallelogram for the destination point.

The distance potential field  $E_p$  is calculated as Equation 12. The  $X$  and  $Y$  are horizontal and vertical coordinates for any given point.  $X_d$  and  $Y_d$  are horizontal and vertical coordinates for the destination point, and  $G$  is the gravity.

$$E_p = G/\sqrt{(X - X_d)^2 + (Y - Y_d)^2} \quad (12)$$

Equation 12 is inspired by the gravity potential, which can be expanded in a series of Legendre polynomials. The denominator in the integral is expressed as shown in Equation (13) in order to achieve the gravitational potential  $V$  at a distance  $x$  (Tikhonov *et al.*, 2013). The  $x$  and  $r$  points are represented as position vectors relative to the center of mass. Figure 24 shows this is a gravitational potential.

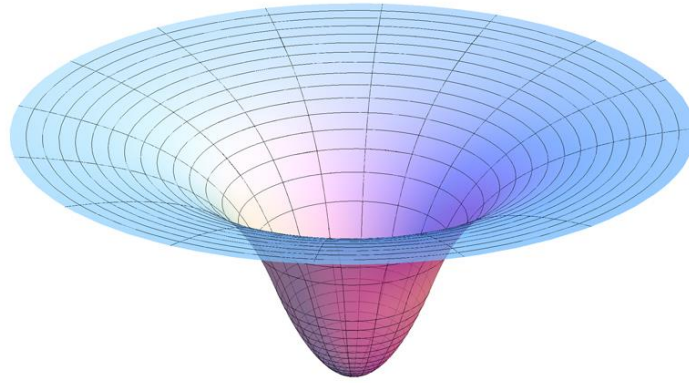


Figure 24. Plot of a two-dimensional slice of the gravitational potential in and around a uniform spherical body. The inflection points of the cross-section are at the surface of the body. (Tikhonov *et al.*, 2013)

$$V(\mathbf{x}) = - \int_{\mathbb{R}^3} \frac{G}{\sqrt{|\mathbf{x}|^2 - 2\mathbf{x} \cdot \mathbf{r} + |\mathbf{r}|^2}} dm(\mathbf{r}) \quad (13)$$

By applying Equation 13 to each point using the pseudocode shown below. A sharp function with a single extremum is created as shown in Figure 25.

```

start a loop with x from 1 to 66

    give a reset value y=1

    start a loop with y from 1 to 76

        Distance potential field =1/(9.8/ Square root of(Absolute
        value of(x- x coordinate of destination point)^2+ Absolute
        value of (y - y coordinate of destination
        point)^2))*distance_p;

    end the loop

```

## 4.5 Generating the Generic Field for the Farming Fields From Maps

This is a variable  $distance_p$ , which is a unique modification to solve the problem of the local minimum, which will be discussed later. The closer the distance, the higher the potential, as shown in both Equation (13) and Figure 24. This is the reciprocal of the distance potential field.

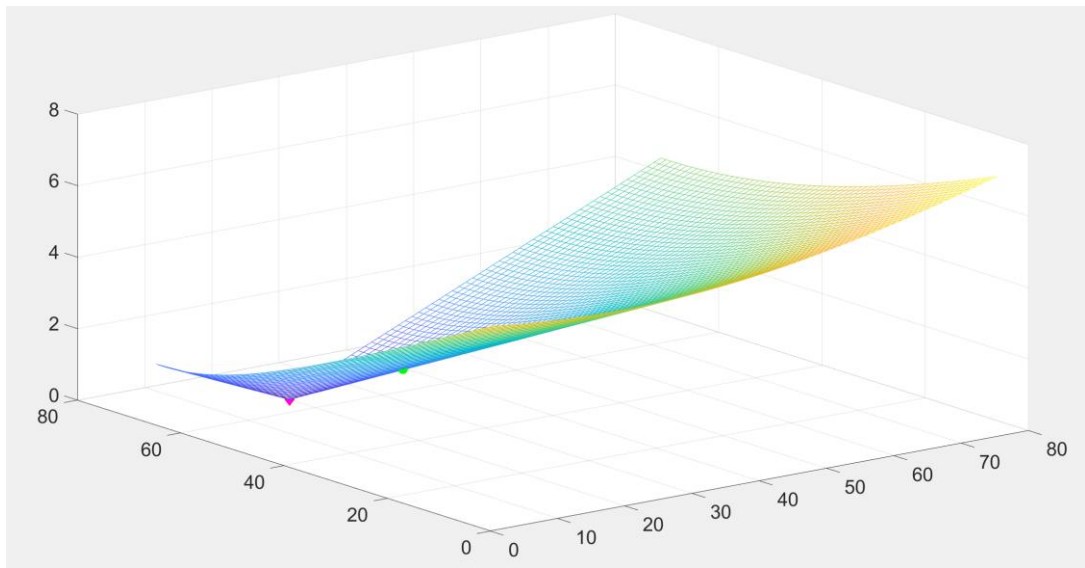


Figure 25. Distance potential field of a farm land

This is the first artificial potential field which is used for attraction of the waypoints, as shown in Figure 25. The destination point has the lowest potential by searching. Setting a round ball with mass, but no inertia, from any point on the map other than the destination point, under gravity the round ball will start rolling and end up at the destination point with no other forces applied. This is the artificial potential field created due to the attraction of an artificial potential field. When increasing the  $distance_p$ , the weight due to the attraction of the artificial potential field in the total potential field will increase to ensure that the destination point is reached. The merging process of the fields will be discussed in Section 4.6, when several artificial potential fields are applied.

Equation 14 is inspired by the potential energy for a linear spring (Tipler *et al.*, 2007), and is defined as shown in the equation (Tipler *et al.*, 2007).

$$W = \int_0^t \mathbf{F} \cdot \mathbf{v} dt = - \int_0^t kxv_x dt = - \int_0^t kx \frac{dx}{dt} dt = \int_{x(t_0)}^{x(t)} kx dx = \frac{1}{2}kx^2 \quad (14)$$

*For convenience, consider contact with the spring occurs at  $t = 0$ , then the integral of the product of the distance  $x$  and the  $x$ -velocity,  $xv_x$ , is  $x^2/2$  (Tipler *et al.*, 2007).*

A simplified expression is shown in Equation 15 (Tipler *et al.*, 2007). So by setting the  $k$  equal to 1 and according to the condition that the height change, no matter an increase or decrease, will all be a potential energy increase, as a height decrease does not result in power generation or charging of the AgriRover battery.

$$U(x) = \frac{1}{2}kx^2 \quad (15)$$

The height difference potential field is calculated. The height difference potential is based on topographic maps and elastic potential energy formulas. The height difference potential field  $E_p$  is calculated as shown in 16, where  $H_p$  is the height for a given point  $p$ , and  $H_D$  is the height of the destination point.

$$E_p = \frac{1}{2}|H_p - H_D|^2 \quad (16)$$

By applying Equation 16 to each point using the pseudocode shown below. The height difference potential field is created in Figure 26.

```

give a value x=1

give a value y=1

start a loop with x from 1 to 66

    give a reset value y=1

        start a loop with y from 1 to 76

            height difference potential field =1/2*[(Absolute value of
            (each map point on coordinates(x,y)- height of the way point
            1))]^2;

```

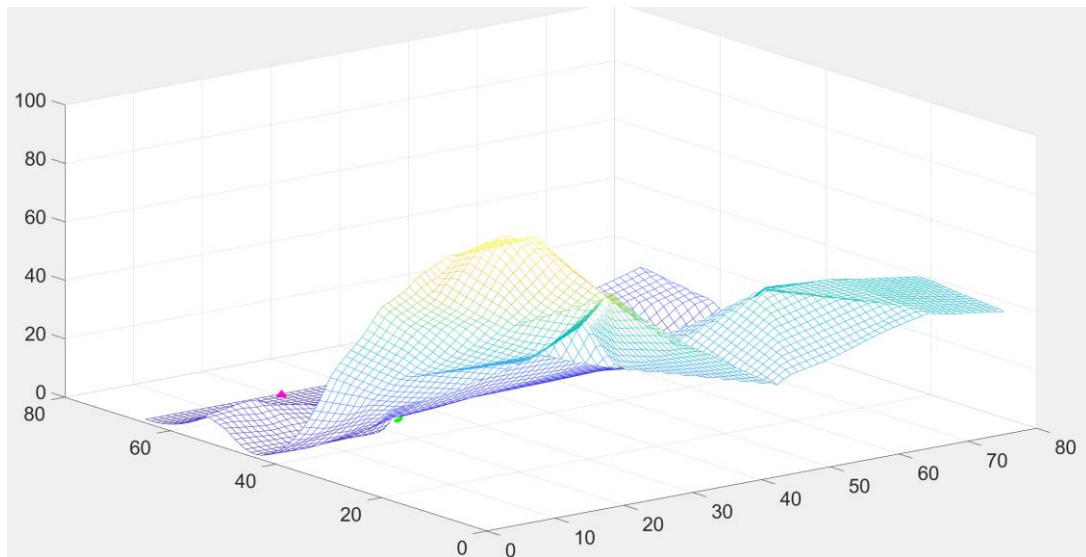


Figure 26. Height difference potential field

## 4.6 Multi-Artificial Potential Field Representation and Merging

The next step is merging all the potential fields, and the pseudo code used is shown below.

```
potential_mesh_all= coefficient of height * height difference
                    potential field + coefficient of distance *
                    Distance potential field;
```

The potential\_mesh\_all is the merged potential field of all the potential fields which is multiplied by a weight factor and then added. Figure 27 is thus generated.

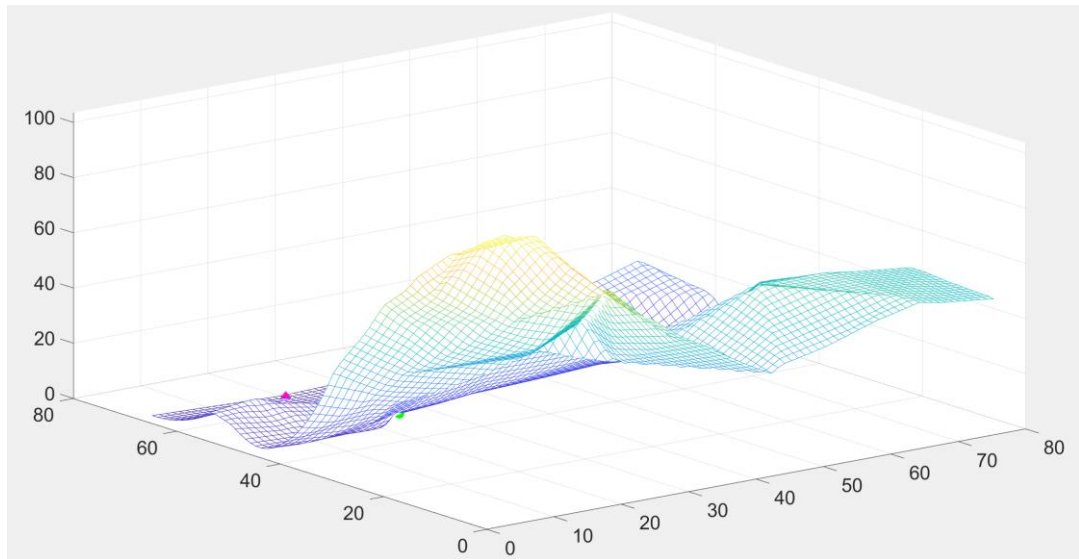


Figure 27. Merged potential field

Visually Figure 26 and Figure 27 are difficult to distinguish between, because Figure 25 only has an interval from 0 to 7, which is a smaller weight when compared to the height difference potential field. However, as mentioned, increasing the distance\_p will increase the interval of the distance potential field, therefore making the merged field more distinguishable and smoother, as seen in Figure 28.

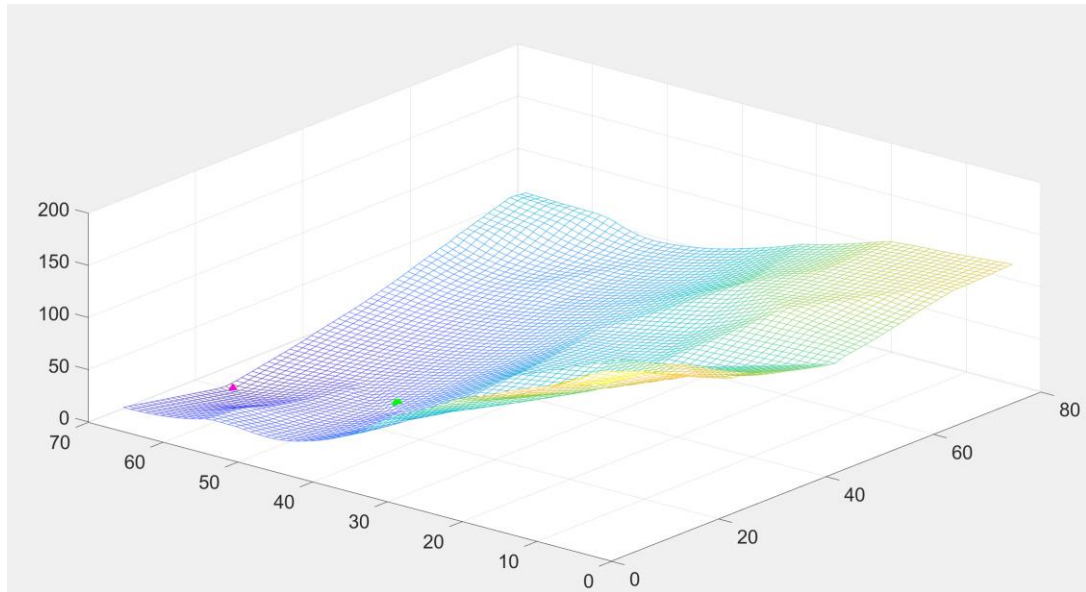


Figure 28. Merged potential field when the interval of both fields is matched

The  $distance_p$  is decided by the path finding algorithm, which will be discussed in the next part of this chapter.

#### 4.6.1 Path Finding with the Merged Potential Field

The path finding algorithm is designed to find a path between the start point and the destination point, according to the merged potential field, which is explained in Section 4.4.3. From the green circle as the start point to the magenta parallelogram as the destination, shown in Figure 28, a path is found by applying a series of algorithms shown below.

First, the maximum number of waypoints are set using Equation 17), and the code shown in the first line. This is calculated using the distance between the green circle start point and the magenta parallelogram destination point. The Round to positive infinity before multiplied by square root of 2  $\lceil \sqrt{2} \rceil$ , which is set as the maximum number of waypoints in this path finding algorithm. The reason for the multiplication of the square root of 2, is to ensure the number of waypoints are more than the distance of the square root of 2, which allows the path finding algorithm a greater number of waypoints. In other words, when point1 is (1,1) and point2 is (2,2), the maximum

number of waypoints is the square root of 2 multiplied by square root of 2, which results in 2 waypoints. Thus, the path finding can take 2 steps to get to the destination.

$$steps = \lceil \sqrt{2} \times \sqrt{(P_{1x} - P_{2x})^2 + (P_{1y} - P_{2y})^2} \rceil \quad (17)$$

```
steps=ceil(sqrt(2)*(sqrt((point1(1)-point2(1))^2+(point1(2)-
point2(2))^2)));%%max number of steps which will be needed to find
all waypoints.
```

Ideally, using the 8 points around the start point, a 3-by-3 matrix is formed. A bubble sort of the matrix elements is applied, and the lowest value is selected. By finding the coordinates of the lowest value points, and if the coordinates are inside the map, it is then saved into a number array called `local_1`. This algorithm is then applied by the maximum number of waypoints discussed before. The number array will thus contain all the waypoints from the start point to the destination.

In most cases, due to complex navigation in an unstructured environment, the number of waypoints will exceed the maximum number of waypoints defined initially in the system, which is intended to minimise the computational burden. This limitation is addressed, and a flag for the algorithm is set to allow the algorithms to break in the next loop. The weight modifier, `distance_p`, will be increased and Figure 25 will thus increase.

```

125 %% Distance Potential field modify parameter
126 flag1=0; % reset flags for indication of destination way reach the point2
127
128 potential_mesh_mean=abs(mean(potential_mesh(:)));
129
130 distance_p_a= sqrt((point1(1)-point2(1))^2+(point1(2)-point2(2))^2);
131
132 distance_p_step=potential_mesh_mean/distance_p_a/100;
133
134 distance_p=0;
135 while flag1==0
136
137
138
139 distance_p=distance_p+distance_p_step;

```

Figure 29. distance\_p decision code

distance\_p is decided with the above code in Figure 29, which is the beginning of the code loop. As the code shows in line 128, the average value of the height difference potential field is calculated with the absolute value. Then, the distances between the start point and the destination point is calculated as shown in line 130. Following this, the step of distance\_p is set with the resolution of 1/100, as shown in line 132. The resolution is interchangeable, where a finer resolution may increase the effectiveness of the algorithm and decrease the energy cost. But then as the test that has been done showed, any resolutions finer than 1/100 will be mostly ineffective and cause unnecessary calculation loads. Finally, distance\_p will increase as the step is set when the loop starts.

Also, when the path is close to the map boundary the 8 points around the current waypoint will have a 0 in the 3-by-3 matrix, and this will cause the bubble sort of the matrix elements to find the 0 as outside the map boundaries. To prevent this from ever happening, a judge code is added as shown below. This line of code will prevent the path from being outside the map boundaries and then skip the rest of the steps when the destination point is reached.

```
if flag1==0 && next_way_point(1)-1>0 && next_way_point(2)-1>0 &&  
next_way_point(1)+1 <=66 && next_way_point(2)+1<=76 % Prevent the  
matrix from exceeding boundary
```

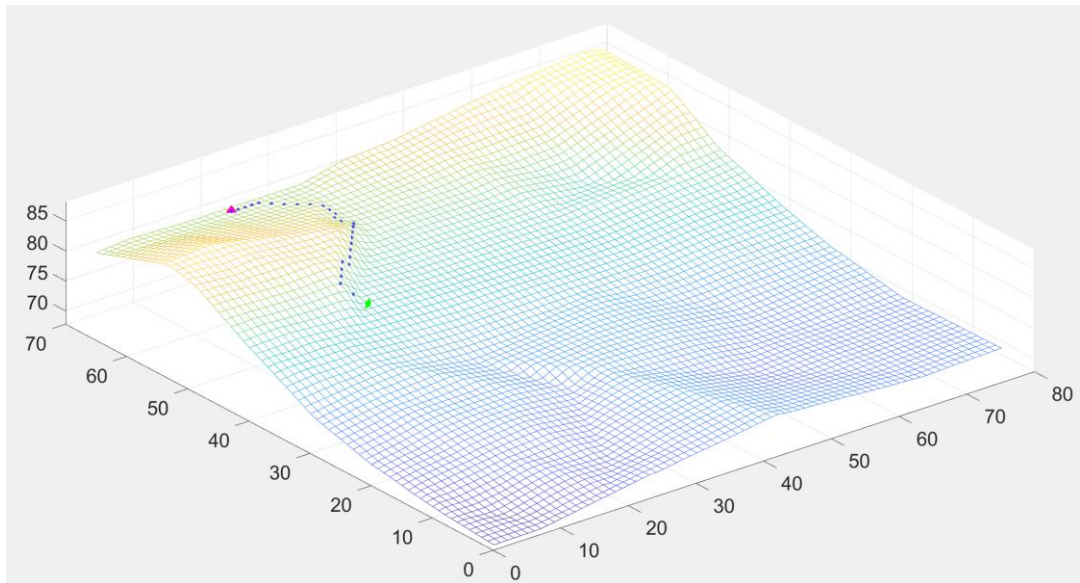


Figure 30. Waypoints on the map

The last step is to plot the waypoints on the map as shown in Figure 30. Followed by this is a simplified flowchart of the algorithm shown in Figure 31.

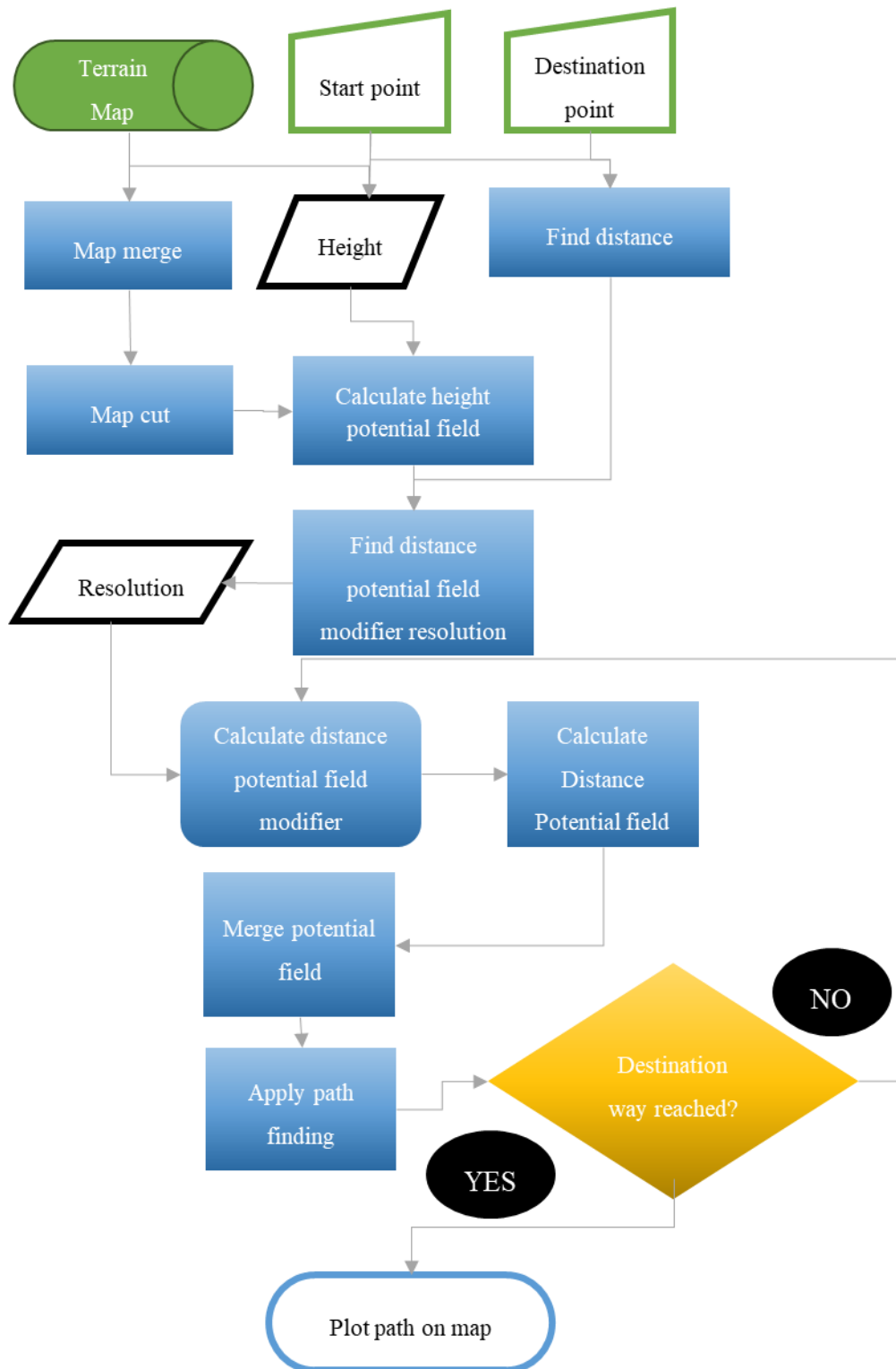


Figure 31. Simplified flow chart of the algorithm

In Figure 31 the color green shows the inertial data, with solid green showing the matrix and green which is outlined shows individual points. Furthermore, outlined

black shows intermediate values, solid blue shows the process, yellow shows the evaluation, solid black shows the evaluation result, and outlined blue shows the end process.

#### 4.6.2 Difficulty and Solutions using the Artificial Potential Field Method

The local minimum is one of the major difficulties of any Artificial Potential Field path planning method (Min Cheol Lee *et al.*, 2003), and to solve such difficulties, 3 methods are designed and used.

First, the maximum number of steps are set to stop the trapping and oscillation of the path finding algorithm. This is introduced in the last part of this chapter. By setting a limiting factor so that when exceeding the maximum number of steps the algorithm will break the loop, the oscillations and infinite loop problem during execution will therefore stop.

The second method, as mentioned in the previous chapter, is a weight modifier of the distance potential field. In combination with the max number of set steps, if the max number of steps is reached after the breaking of the loop, the modifier will increase to the step set, as introduced in the last part of this chapter.

Lastly, there is a sharpening process of the merged potential field so that the destination point has the lowest point of the 8 surrounding points, ensuring the last step of the pathfinding is always the destination point, instead of a local oscillation near the destination point. If the height around the destination point is similar to the starting point, the oscillation often happens near the destination point when the path came close to the area around the destination due to the lower value of the height potential field. Sharpening the destination point of the potential field increases the effectiveness of the path planning and lowers the overall energy cost.

## 4.7 Energy Cost Estimation Implemented in MATLAB

After a path is found the energy cost is estimated. This is done by using the code shown in Figure 32. This estimation is under ideal circumstances, where the only cost of energy is a high increase. A detailed modelling and simulation is done and introduced in Chapter 8.

```
420 %% The energy needed to overcome gravity is calculated W=mgh; if rover is 25 kg
421 j=1;
422 i=1;
423 energy=[];
424 for j=j:n;
425
426     a=[heightdata(j)];
427     d=[heightdata(j+1)];
428
429     h_diff=d-a;
430
431
432     if h_diff>=0 %if inclined
433
434         energy_in=h_diff*25*9.8;
435
436         energy=[energy, energy_in];
437
438     end
439
440
441 end
442
443 energy_T=sum(energy)
```

Figure 32. Energy cost estimation code

First, the height difference between each point is calculated and plotted. Then, if the height is increased the energy cost to overcome gravity is calculated and saved in an array. Lastly, each number of the array is summed, and the energy cost estimation to overcome gravity is calculated.

## 4.8 Case Demonstrations and Algorithm Validation

The energy cost comparison between a straight-line path and energy optimised path is discussed in this part of the thesis. The green circle is the start point and magenta parallelogram is the destination point. The energy cost is only calculated to overcome gravity, as in the code of Figure 32.

The first case is an uphill condition. As shown by the pathline in Figure 33, the map indicates the height has increased from 79 meters to 83 meters at the first peak, and then increased to more than 84 meters to reach the maximum height, after reducing to 82 meters with further travel on decent. This trajectory has resulted in a total cost of energy of 1379.4 joules.

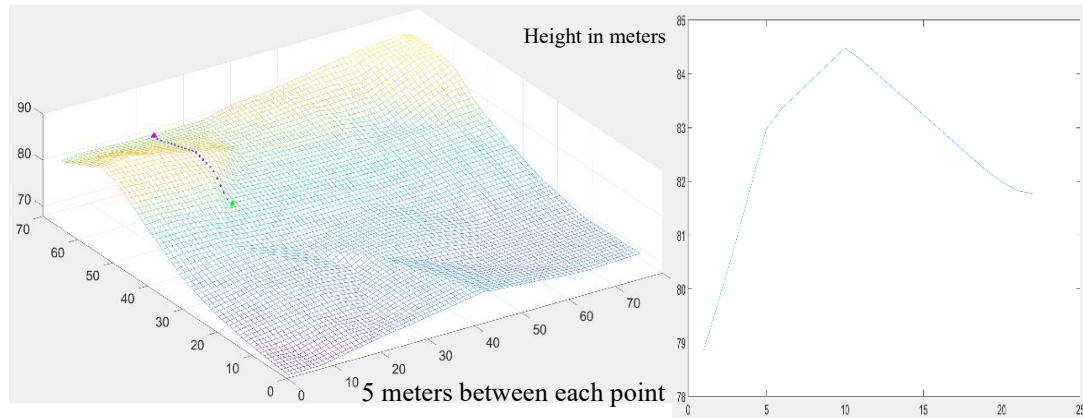


Figure 33. Straight-line path and height change graph

An energy optimisation has been performed based on the algorithms proposed. This is shown in the pathline in Figure 34, and as one can see, the height has increased from 79 meters to 82.2 meters then the height changes remain between 81.43 and 82.25 metres. The total cost of energy of 972.65 joules can be observed in this case.

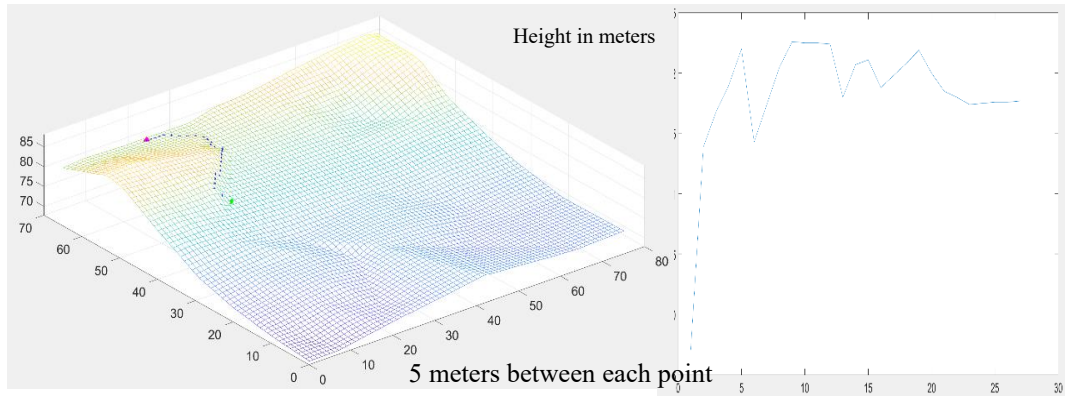


Figure 34. Energy optimised path and height change graph

In this case, the energy reduction to overcome gravity is 406.75 joules when comparing between the straight-line path and the energy optimised path, implying that the energy saved is over 30% with the height change.

The second case is a downhill condition, with the start and destination points exchanged, as shown in Figure 35.

In this case the final energy reduction is 242.55 joules when compared to the straight-line path and energy optimised path, the energy saved is over 37% on the height change. Finally, shown in Table 4 is the time required to complete the planning, which is 0.638 s.

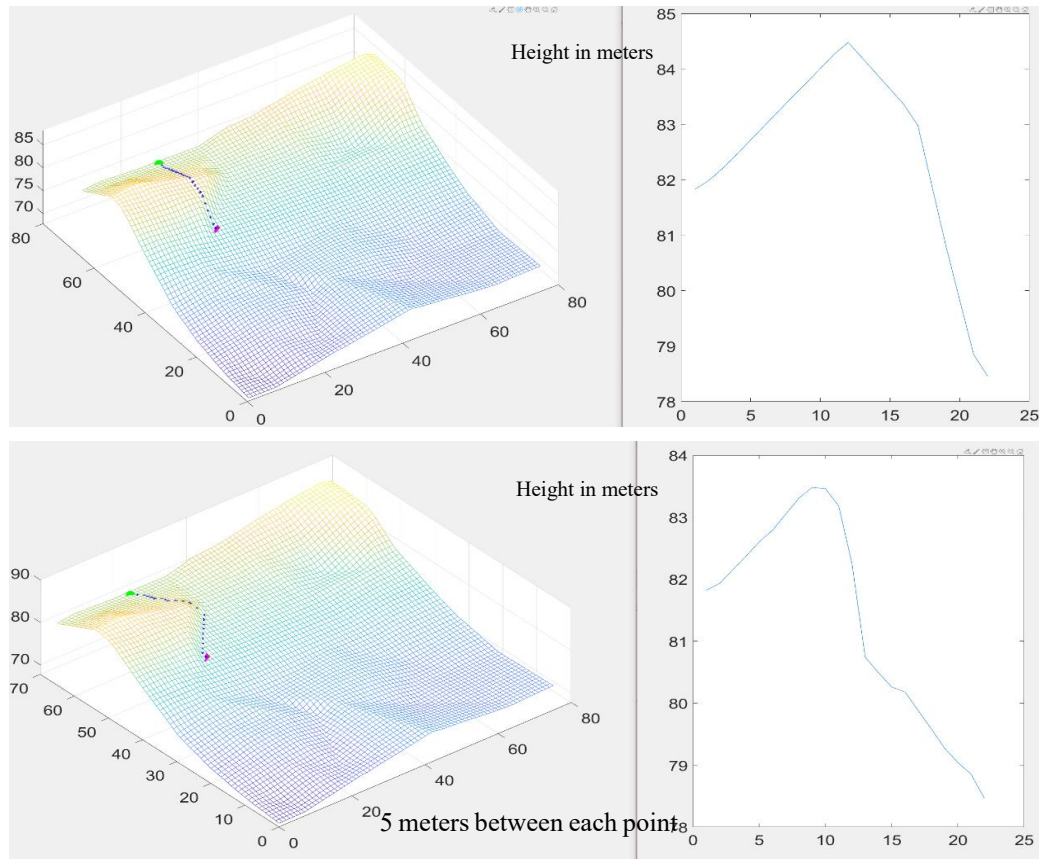


Figure 35. Downhill condition compared.

Table 4. Time needed to complete the planning

Function Name	Calls	Total Time
planning	1	0.586 s
unix	1	0.184 s
mesh	3	0.124 s
newplot	52	0.051 s
newplot>ObserveAxesNextPlot	52	0.022 s
grid	3	0.021 s
cla	4	0.017 s
Surface.Surface>Surface.Surface	3	0.012 s
configureAxes	3	0.012 s
configureAxes>checkChildren	3	0.010 s
graphics\private\clo	4	0.009 s

## 4.9 Expanding the Artificial Potential Field

With more information or additional needs, the artificial potential field is expandable by adding an element to the sum of the total artificial potential fields, such as a potential field of the surface roughness grading and a potential field for uncrossable obstacles. The surface roughness grading is mentioned in Section 6.2. If the data is available or collectable, an artificial potential field can be generated, such as shown in Figure 36.

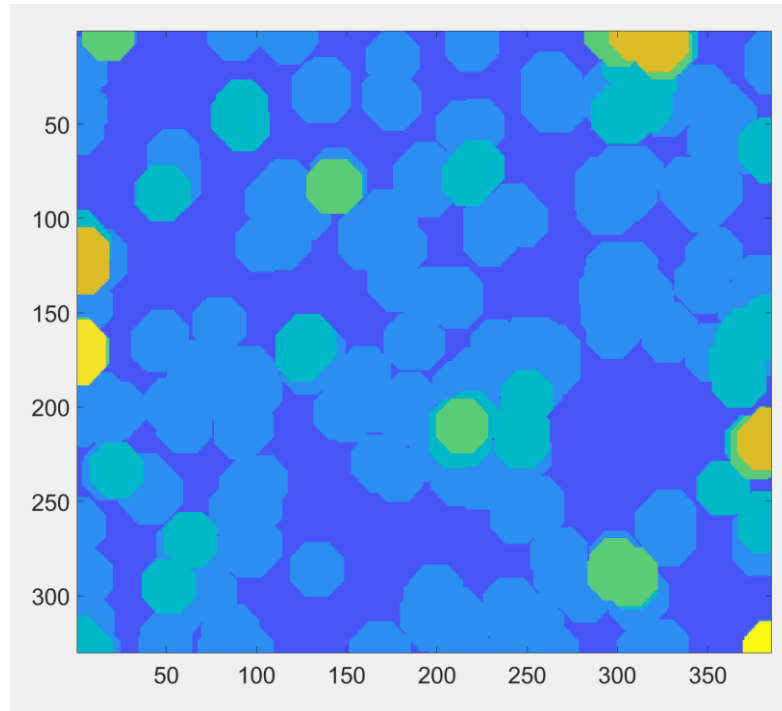


Figure 36. Randomly generated surface roughness map

Also, as a benefit of the modified Artificial Potential Field, the map size is expandable with a lower requirement of computational power. Shown in Figure 37 is the energy optimised path planning used on a map that is 5-by-5 km, where a 1000-by-1000 data point is in computation, with a time cost of only 2.081s, as shown in Table 5. Furthermore, the energy to overcome gravity is only 970.2 joules, compared to 1646.4 joules if the rover went in a straight line.

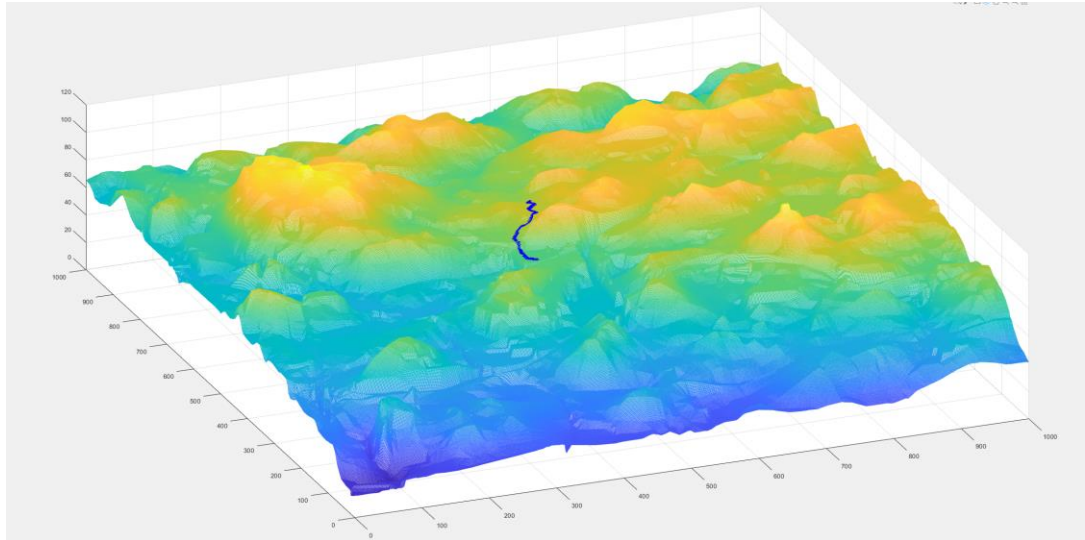


Figure 37. Large map planning result

Table 5 Time needed to complete the planning for a large map

Function Name	Calls	Total Time
largemap_ planning	1	2.116s
newplot	349	0.193 s
mesh	4	0.181 s
newplotwrapper	345	0.098 s
CanvasPlugin.createCanvas	5	0.084 s
CanvasSetup.createScribeLayers	5	0.049 s
ScribeStackManager.getLayr	20	0.044 s
ScribeStackManager.createLayer	15	0.038 s
newplot>ObserveAxesNextPlot	349	0.029 s
gobjects	710	0.024 s

## 4.10 Summary

This chapter described a novel energy modelling and energy optimised path planning approach for an autonomous mobile robotic platform, the AgriRover. This approach uses a dynamic and adaptive Artificial Potential Field that has given a

solution on the problem of local minimum while finding a energy optimised path with limited time. The energy optimised path has the energy reduction for overcome the terrain reduced from 972.65 joules to 730.1 joules, a total decrease of 242.55 joules is observed. This comparison between a straight-line path and the energy optimised path sees an energy saving of over 37% with the height change. This reduction ratio is only applicable to the change of the altitude (Z Axis), without the consideration of the XY Axis. However, the full simulation has been designed and proceeded with in Chapter 8. Furthermore, the expandability of the designed energy optimised path planning algorithm is demonstrated with a map that is 5-by-5 km in size.

Although from a control perspective, every mobile robotic platform is different. But from the point of view of energy consumption models and patents, all wheel-based mobile robotic platforms are inter-related. Therefore, the global energy consumption behaviour across all mobile robotic platforms is similar, so the developed energy-optimised path planning method is a generalised approach to solve mobile robotic platform problems. Also the research proceeded and was validated using AgriRover as the research platform because it was the only mobile robotic platform available at a reasonable cost of time and money.

## 5 The Mathematical Modelling of the AgriRover Steering Mechanism

First, the voltage of the motor of the steering system at a given time  $t$ , also known as the balanced voltage equation, can be described as Equation 18 (Sharma *et al.*, 2017).

$$V_a(t) = l_a \frac{di_a(t)}{dt} + R_a i_a(t) + E_a \quad (18)$$

where

$V_a(t)$  is the total voltage of the motor at the time  $t$ ,

$l_a$  is the inductance of the motor,

$i_a$  is current of the motor,

$R_a$  is the internal resistance of the motor,

$E_a$  is the back electromotive force (EMF) given by Equation 19).

$$E_a = C_e \omega_m(t) \quad (19)$$

where

$C_e$  is the coefficient of the back EMF,

$\omega_m$  is the angular speed of the motor.

Then the torque in the motor at the given time  $t$  is described as  $M_m(t)$ , and is calculated as shown in Equation 20.

$$M_m(t) = C_m i_a \quad (20)$$

where

$C_m$  is the torque constant.

Finally, the balanced equation of torque at a given time  $t$  can be written as shown in Equation 21.

$$J_m \frac{d\omega_m(t)}{dt} + f_m \omega_m(t) = M_m(t) - M_c(t) - M_d(t) \quad (21)$$

where

$J_m$  is the total rotary inertia of the motor shaft,

$f_m$  is the coefficient of friction of the system,

$M_c(t)$  is the interference output from the outside of the system, and

$M_d(t)$  is the force on the motor shaft generated when the ground.

The equation of torque on a planetary gearbox when contacting the ground is shown in 22

$$M_g(t) = R_g K_g x_g(t) \quad (22)$$

where

$R_g$  is the equivalent radius with the torque on the gearbox generated from contacting the ground,

$K_g$  is the coefficient of elasticity of the tire when contacting the ground,

$x_g$  is the displacement generated when the tire contacts the ground due to the elasticity of the tire, and

$M_g$  is the force generated on gearbox shaft when contacting the ground.

The force generated on the motor shaft when contacting the ground is calculated as shown with Equation 23.

$$M_d(t) = \frac{M_g(t)}{j_0} \quad (23)$$

where

$j_0$  is the reduction rate of the gearbox.

The displacement generated when the tire contacts the ground, due to the elasticity of the tire, is calculated as shown in Equation 24.

$$x_g(t) = R_g \int_0^t \frac{\omega_m(t)}{j_0} dt \quad (24)$$

Finally, the output angle of the motor is calculated as shown in Equation 25.

$$\theta_m(t) = \int_0^t \omega_m(t) dt \quad (25)$$

The next step is to transform these equations and generate the steering mechanism system block diagram. From Equation 18 and 19, Equation 26 can be formed.

$$V_a(t) = l_a \frac{di_a(t)}{dt} + R_a i_a(t) + C_e \omega_m(t) \quad (26)$$

Applying a Laplace transform to Equation 26, Equation 27 is generated.

$$V_a(s) = l_a s i_a(s) + R_a i_a(s) + C_e \omega_m(s) \quad (27)$$

After this, a Laplace transformation is applied to calculate  $i_a(s)$ , as shown in Equation 28.

$$i_a(s) = \frac{1}{l_a s + R_a} V_a(s) - \frac{C_e}{l_a s + R_a} \omega_m(s) \quad (28)$$

Equation 28 is then adjusted to find the value for  $i_a(s)$  as shown in Equation 29.

$$i_a(s) = \frac{1}{l_a s + R_a} [V_a(s) - C_e \omega_m(s)] \quad (29)$$

Equation 29 can be transformed into the block diagram shown in Figure 38.

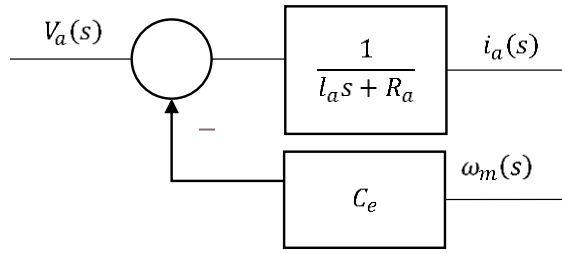


Figure 38. Block diagram of Equation 29

Applying a Laplace transform to Equation 20, Equation 30 can be generated. Equation 30 can then be used to create Figure 39.

$$M_m(s) = C_m i_a(s) \quad (30)$$

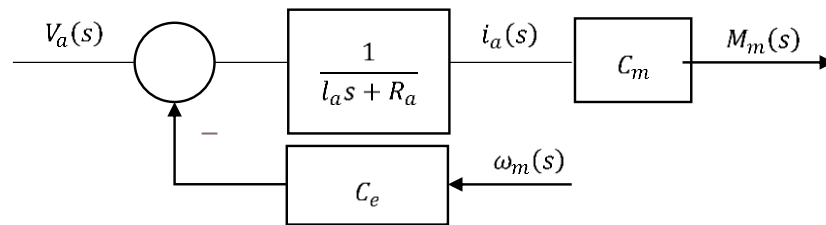


Figure 39. Block diagram of Equations 29 and 30

Equation 31 can be generated by applying the Laplace transform to Equation 21, where  $M_c$  is the interference input and is set to 0.

$$j_m s \omega_m(s) + f_m \omega_m(s) = M_m(s) - M_d(s) - 0 \quad (31)$$

Equation 31 is thus arranged to find  $\omega_m(s)$  as shown in Equation 32.

$$\omega_m(s) = \frac{1}{j_m s + f_m} [M_m(s) - M_d(s)] \quad (32)$$

The block diagram of Equation 32 can thus be created, and is shown in Figure 40.

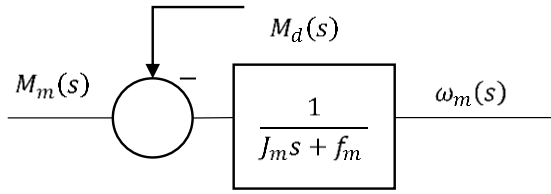


Figure 40. Block diagram of Equation 32

Merging the two block diagrams in Figure 39 and Figure 40 is shown in Figure 41.

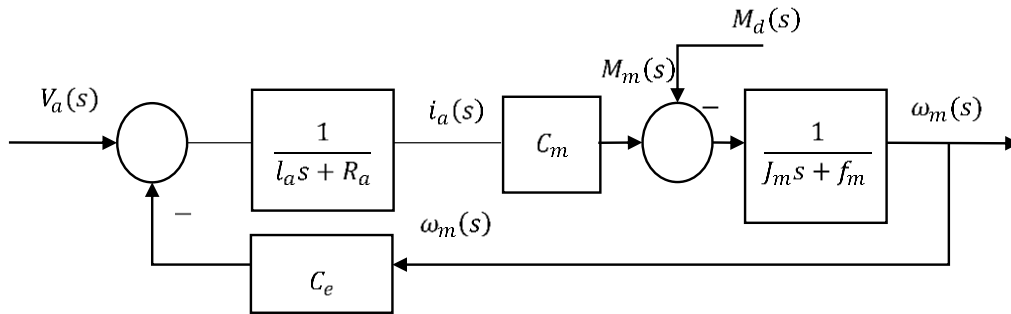


Figure 41. Merged diagrams of Figure 39 and Figure 40

Applying the Laplace transform to Equation 24 results in Equation 33.

$$x_g(s) = \frac{R_g}{j_0 s} \omega_m(s) \quad (33)$$

Following from this, merging Equation 33 and Figure 41 results in Figure 42.

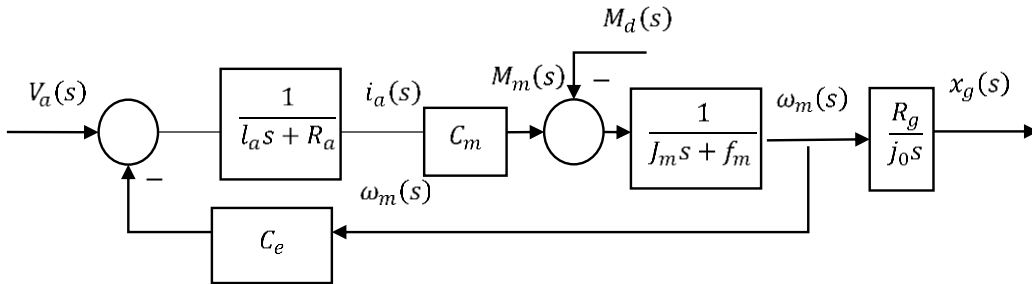


Figure 42. Merged diagram of Equation 33 and Figure 41

Applying the Laplace transform to Equations 22 and 23 results in Equations 34 and 35, respectively.

$$M_g(s) = R_g K_g x_g(s) \quad (34)$$

$$M_d(s) = \frac{M_g(s)}{j_0} \quad (35)$$

Merging Equations 34 and 35 together results in Equation 36.

$$M_d(s) = \frac{R_g K_g}{j_0} x_g(s) \quad (36)$$

Combining Equation 36 and Figure 42 results in Figure 43.

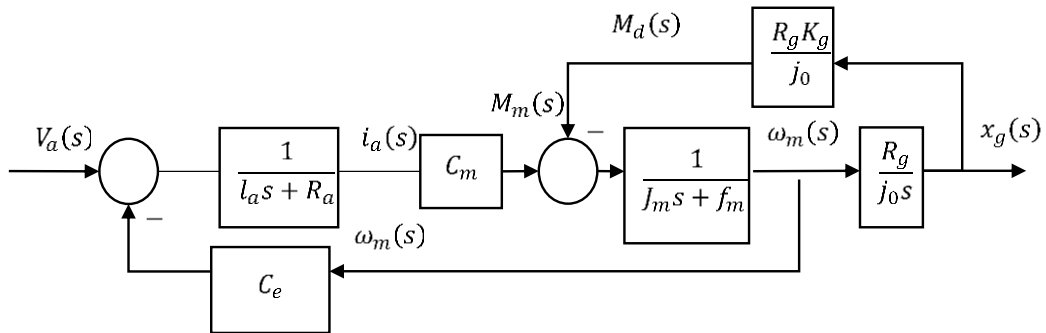


Figure 43. Merged diagram of Equation 36 and Figure 42

Because  $l_a$  and  $f_m$  are low values, they can be set to 0 in this case, with the resulting System Block diagram in Figure 44.

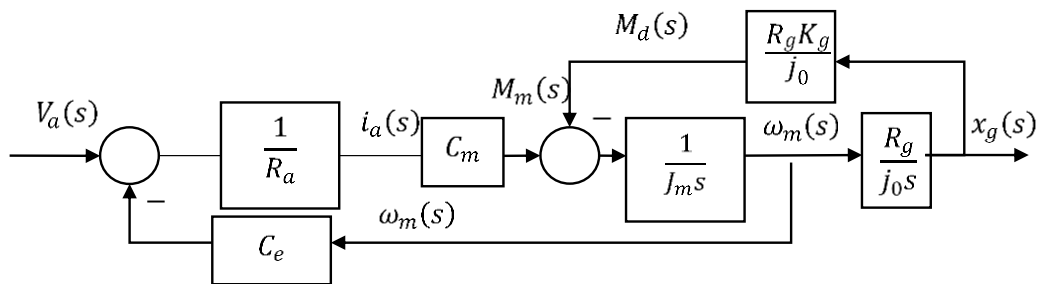


Figure 44. System Block diagram

Transforming Figure 44 in order to simplify the system block diagram results in Figure 45. Simplifying Figure 45 yet again then results in Figure 46.

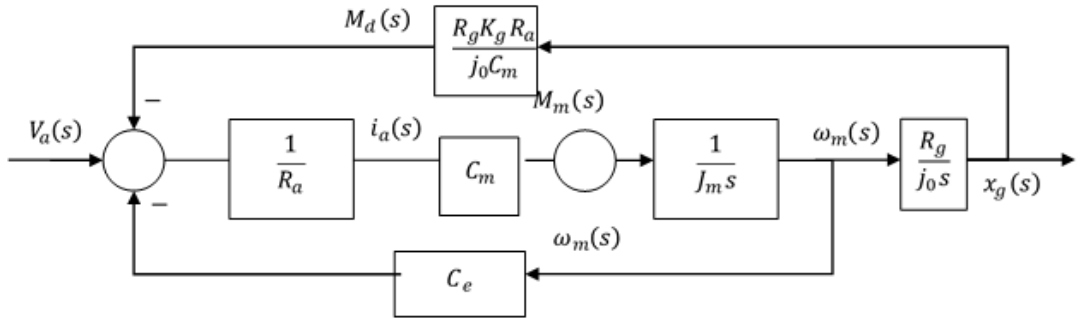


Figure 45. Transformation of Figure 44

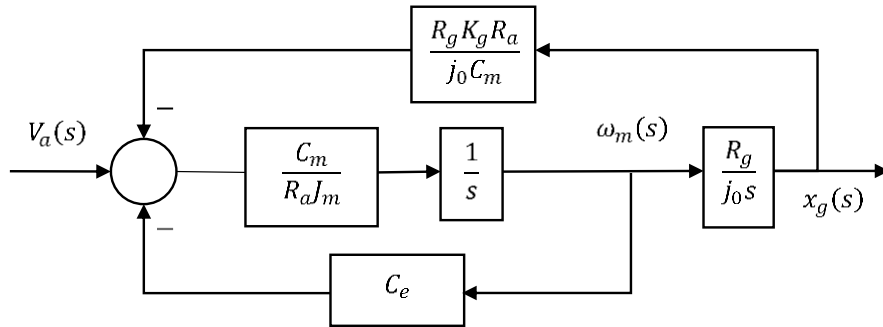


Figure 46. Transformation of Figure 45

To get the output angle of the steering mechanism the following steps are thus taken. First, apply the Laplace transform to Equation 25 to achieve Equation 37.

$$\theta_m(s) = \frac{\omega_m(s)}{s} \quad (37)$$

Merging Equations 37 and 33 results in Equation 38.

$$x_g(s) = \frac{R_g}{j_0} \theta_m(s) \quad (38)$$

The block diagram can then be generated by merging Equation 38 into Figure 46 to result in the diagram that has the steering angle as an output, as seen in Figure 47.

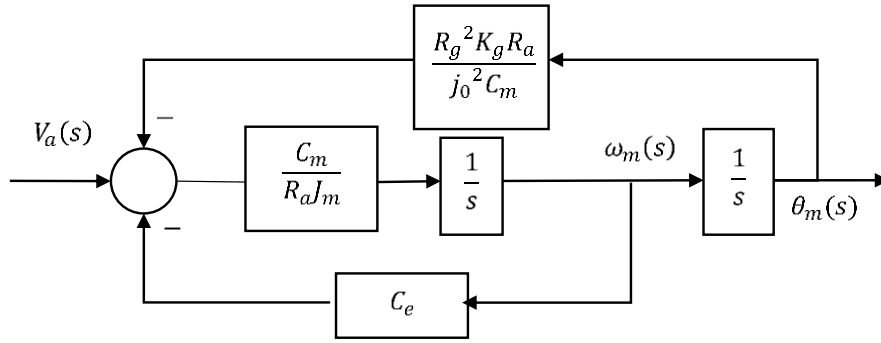


Figure 47. System block diagram with output of  $\theta_m$

Finally, adding the mass  $m$  of the rover into the system block diagram of Figure 47 generates the diagram seen in Figure 48.

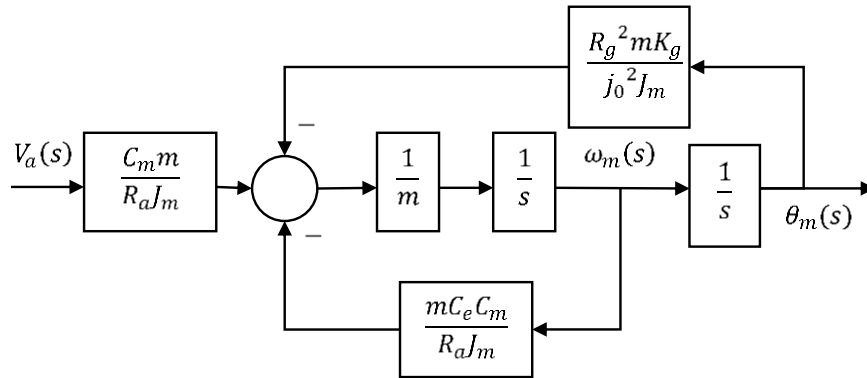


Figure 48. System block diagram including mass

The steering mechanism is simplified and then modelled as a Mass-Spring-Damper in Simulink, as shown in Figure 49, with the parameters of the coefficient of elasticity,  $K$ , calculated with Equation 39 and the coefficient of damping calculated using Equation 42.

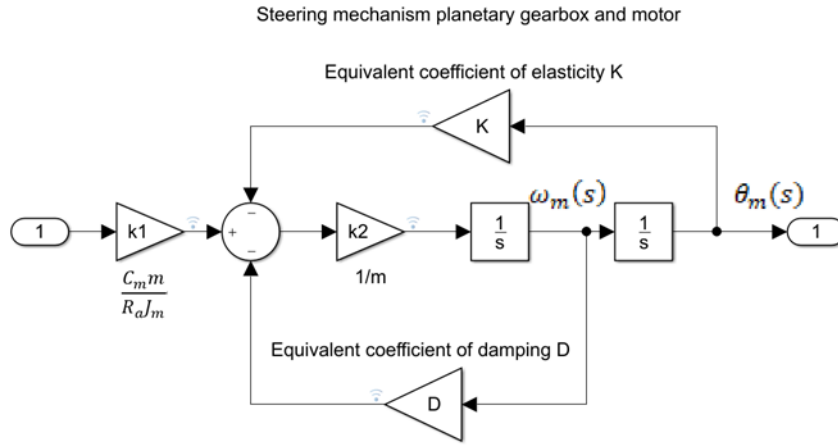


Figure 49. Steering mechanism modelled in Simulink

Consequently, the equivalent coefficient of elasticity is shown in Equation 39 which is used in the top loop of Figure 48 and Figure 49.

$$K = \frac{mR_g^2 K_g}{J_m j_0^2} \quad (39)$$

Where  $R_g$  is the equivalent radius from the shaft of the gearbox to the steering torque generated from contacting the ground. This is 80mm, or 0.08m.  $j_0$  is gearbox reduction rate, which is 113 according to the data sheet for the Maxon 203126 gearbox (Maxongroup, 2021).  $K_g$  is the stiffness of the tire, which is calculated according to Equation 40 (Lines, 1991).

$$K_g = 172 - 1.77R + 5.6A + 0.34WRP \quad (40)$$

Where  $R$  is the radius of the tire, which is 80 millimetres for the rover, and  $A$  is the age, which is 1 year as a base line value mentioned in the article.  $W$  is the radius of the wheel, which is 80 millimetres, and  $P$  is pressure, which is 5 bar. So, the stiffness of the tire is calculated as 177.4652 KN/M.

$J_m$  is the total rotary inertia of the motor shaft and is calculated with Equation 41 (Galvagno *et al.*, 2011).

$$J_m = J_z + J_0 + J_1 \left(\frac{n_1}{n_2}\right)^2 \quad (41)$$

Where  $J_z$  is the rotary inertia of the motor,  $135 \text{ g cm}^2$ ,  $J_0$  is the rotary inertia of the gearbox,  $9.4 \text{ g cm}^2$ , and  $J_1$  is the rotary inertia of the wheel, which has a weight total of  $500\text{g}$  and the inertia is then calculated as a pendulum ( $mr^2$ ) (Serway, 1986) with an arm length of  $80\text{mm}$ .  $n_1$  is the input's number of teeth, which is  $3$ , and  $n_2$  is the number of teeth of the output, which is  $338$  according to the the data sheet of the Maxon 203126 gearbox.

So  $J_m$  (Equation 41) is calculated as:

$$J_m = 135 + 9.4 + (500 \times 8^2) \left(\frac{3}{338}\right)^2 = 146.92 \text{ g cm}^2 = 1.4692 \times 10^{-5} \text{ kg m}^2$$

Thus,  $K$  (Equation 39) is calculated as:

$$K = \frac{20 \times 0.08^2 \times 177.4652 \times 1000}{1.4692 \times 10^{-5} \times 113^2} = 121083.61$$

The equivalent coefficient of damping is shown in Equation 42, which is the bottom loop of Figure 48.

$$D = \frac{mC_e C_m}{R_a J_m} \quad (42)$$

where  $C_e$  is the back EMF constant, which is calculated by the speed constant  $600 \text{ rmp/v}$  which is equal to  $62.832 \text{ rad/s/v}$ . So, the back EMF constant is:  $1/62.8=0.0159 \text{ v/rad/s}$ .  $C_m$  is the orque constant and is calculated by the nominal torque divided by nominal current:  $59.4 \text{ mNm}/1000/2.06\text{A}= 0.0262\text{Nm/A}$ .  $R_a$  is the internal resistance of the motor and will be set at  $1 \text{ ohm}$ , which is a common value of internal resistance of motors with similar size and power.

$$D = \frac{20 \times 62.832 \times 0.0262}{1.4692 \times 10^{-5}} = 2240945.28$$

Finally,  $k_1$  in Figure 49 is calculated according to Figure 48:

$$k1 = (C_m m)/(R_a J_m) = 35665.67.$$

Thus, the final steering system block diagram is shown in Figure 50.

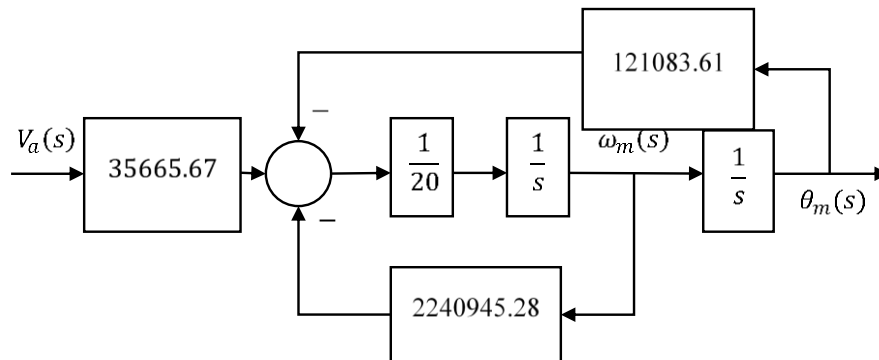


Figure 50. Steering system block diagram.

The transform of Control System Block Diagram shown is based on (Golnaraghi *et al.*, 2017) chapter 3, (Gajic *et al.*, 1996) chapter2 ando (Kani, 1998) chapter1.

In summary this is a complete process on the simplification of the steering mechanism of a mobile robotic platform. This provide a complete method of modelling and simplification for such platform which is used as a guideline for further simulation and investigation.

## 6 Dynamic Modelling and Analysis of the Rover Driving Wheels

### 6.1 Introduction

This chapter introduces the work done on the dynamic modelling of the AgriRover driving wheels, which was the other part of the AgriRover mobility system designed to meet the needs of soil sampling and harvesting in a farming field. This chapter provides a detailed analysis of the movements of the AgriRover, in order to demonstrate the technical feasibility of the design. First, a classification of the road surfaces are introduced. Then, a simulation is preceded with under the different conditions in the road surface classification. Finally, there is a profile of the AgriRover, under different surface roughness conditions during operation, provided.

### 6.2 Definition and Classification of the Field Surface Irregularities

#### Irregularities

According *ISO 8608* (ISO, 1995) (Dodds *et al.*, 1973) “*Mechanical vibration -- Road surface profiles -- Reporting of measured data*” random road surface irregularities is defined. Road irregularities is defined as  $G_q(n)$ , which can be shown in Equation 43 (Agostinacchio *et al.*, 2014) (Tudón-Martínez *et al.*, 2015).

$$G_q(n) = G_q(n_0) \left(\frac{n}{n_0}\right)^{-2} \quad (43)$$

Where  $n$  is the spatial frequency measured in cycles/meter, and  $G_q(n_0)$  is the power spectral density of the road surface irregularities, and this has been classed as levels A to H, shown in Table 6 below.

Table 6. Road Classification (Andren, 2006) (Nguyen *et al.*, 2019)

Road Class	<i>Power Spectral Density</i> $G_q(n_0)/(10^{-6}\text{m}^3)$ ( $n_0=0.1\text{m}^{-1}$ )
A	16
B	64
C	256
D	1024
E	4096
F	16384
G	65536
H	262144

### 6.3 Relationship between Current and Torque of the Rover Motors

First generation rovers use 4 of the 940D1001 Planetary Geared Motors for the output of the driving wheels as shown in Figure 52. The output torque of the motor is converted into the torque for the wheel through a planetary reduction transmission, with a reduction value from 100 to 1. The performance parameters of the 940D1001 motor is shown in Figure 51 below.

940D51	(4.5v - 15v)	RATIO 5:1
940D271	(4.5v - 15v)	RATIO 27:1
940D511	(4.4v - 15v)	RATIO 51:1
<b>940D1001</b>	<b>(4.5v - 15v)</b>	<b>RATIO 100:1</b>
940D1391	(4.5v - 15v)	RATIO 139:1
940D2641	(4.5v - 15v)	RATIO 264:1
940D5161	(4.5v - 15v)	RATIO 516:1
940D7211	(4.5v - 15v)	RATIO 721:1

MODEL	VOLTAGE		NO LOAD		AT MAXIMUM EFFICIENCY						STALL TORQUE	
	OPERATING RANGE	NOMINAL	SPEED	CURRENT	SPEED	CURRENT	TORQUE		OUTPUT	EFF	STALL TORQUE	
			R.P.M.	A	R.P.M.	A	oz - in	g - cm	W	%	oz - in	g - cm
RE - 385	6.0 - 15.0	<b>12v CONSTANT</b>	11646	0.18	9869	<b>0.99</b>		<b>78.4</b>	7.98	66.1		513.5

Figure 51. Performance parameters of the 940D1001 motor

Setting the force conversion factor of the motor as  $K_{em}$  in Equation (44).

$$K_{em} = \frac{78.4 \text{ g}\cdot\text{cm}}{0.99 \text{ A}} = 79.2 \text{ g}\cdot\text{cm}/\text{A} \times 0.0000980665 = 0.007767 \text{ N}\cdot\text{m}/\text{A} \quad (44)$$

Thus, the relationships between the turning torque of each wheel and the corresponding drive current is as follows in Equation 45.

$$T_{wheel} = K_{wheel} \times K_{em} \times I_{wheel} \times n_1 \times n_2 \times \eta_1 \times \eta_2 \quad (45)$$

$T_{wheel}$  is the torque of each wheel,  $K_{wheel}$  is the correction parameter,  $I_{wheel}$  is the driving current of the motor,  $n_1$  is the transmission ratio of the motor (which is 100 for the 94D1001 motor), and  $n_2$  is the transmission ratio of the wheel hub transmission (which is 1.1). Finally,  $\eta_1$  is the total efficiency of the motor and its transmission, which is 0.55, and  $\eta_2$  is the efficiency of the wheel hub transmission, which is close to 0.9. So, after substituting these into Equation 45, Equation 46 below is found.

$$T_{wheel} = 0.4229 K_{exp} I_{wheel} \quad (46)$$

After test driving the wheels on the ground, each wheel is observed to require 0.05A of current in order to overcome internal friction. Therefore, Equation 46 has been corrected to Equation 47, as shown below.

$$T_{wheel} = 0.4229 K_{exp} (I_{wheel} - 0.05) \quad (47)$$



Figure 52. Wheel hub transmission of the first-generation rover

$K_{exp}$  is determined by numerical simulation results and experimentally measured driving currents. The parameters shown in

Table 7. Simulation Parameters

Parameter Name	Parameter Value
Rover mass (i.e., chassis + load mass in kg)	20
Coefficient of rolling resistance between the tire and field	0.2* (Study, 2006)
Coefficient of sliding friction between the tire and field	0.7* (Study, 2006)

, is used for the simulation.

The driving wheels' simulation is carried out, using the setup as shown in Figure 53, with simplified models of the rover driving system and suspension.

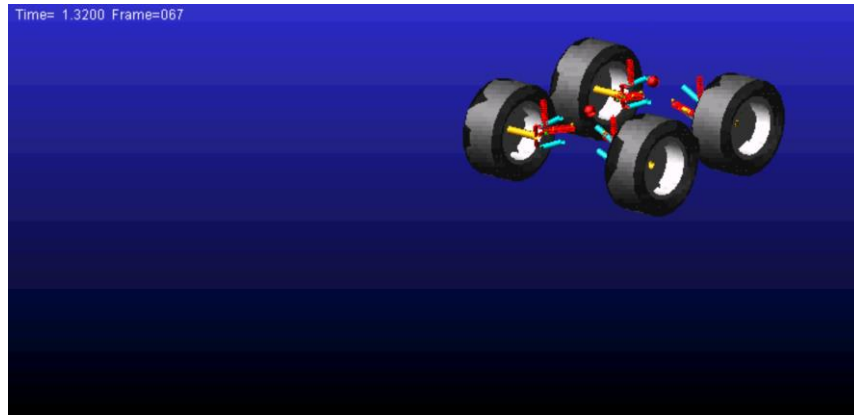


Figure 53. Driving wheel simulation setup

The first case of the simulations is done on a random, uneven class D road surface. The rotational torque of a 20kg agricultural rover (including both the trolley and top-loading equipment) travelling at a speed of 0.3m/s in the field has been simulated. The simulation time was 30 seconds. The wheels on the road surface are independently shown in Figure 53, with fl and fr as the front left and right wheels, and rl and rr as the rear left and right wheels. Shown below in Table 8 is the calculation results, followed by the resulting graph of the torque in Figure 54.

Table 7. Simulation Parameters

Parameter Name	Parameter Value
Rover mass (i.e., chassis + load mass in kg)	20
Coefficient of rolling resistance between the tire and field	0.2* (Study, 2006)
Coefficient of sliding friction between the tire and field	0.7* (Study, 2006)

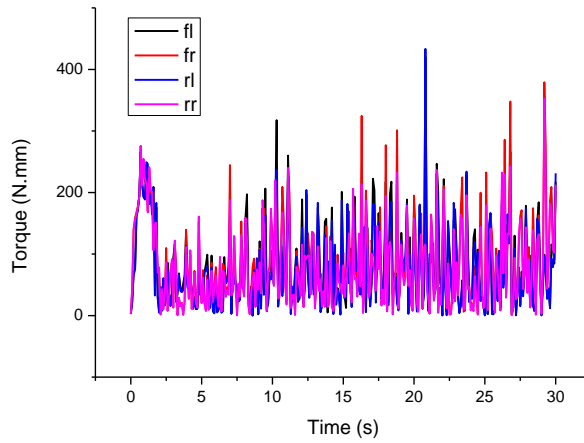


Figure 54. Road surface Class D simulation of the rotating torque on each wheel

Table 8. Road surface class D simulation and calculation results

class	fl Maximum torque (N.mm)	fl average torque (N.mm)	fr Maximum torque (N.mm)	fr average torque (N.mm)	rl Maximum torque (N.mm)	rl average torque (N.mm)	rr Maximum torque (N.mm)	rr average torque (N.mm)	Four- wheel average torque sum (N.mm)
D	420.6698	79.71624	379.1472	86.22094	433.3723	73.51059	352.2251	78.13444	317.5822

Figure 55 below shows the total driving current measured in the experiment under the working conditions, which equals an average of 2.021A.

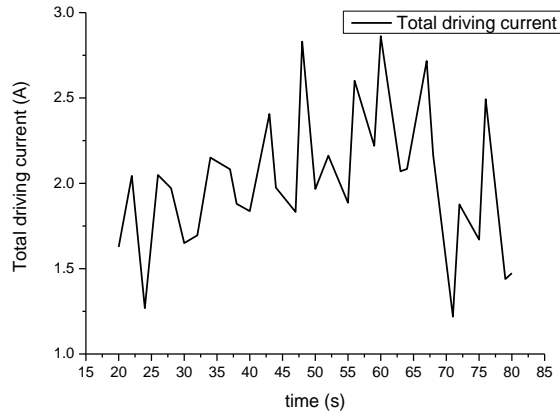


Figure 55. Total driving current

By substituting  $T_{wheel} = 0.3175822$  N.m and  $I_{wheel} = 2.021$  A into Equation 48, the correction parameter  $K_{exp}$  is calculated to equal 0.381. So, the relationship between the rotating torque of each wheel and the drive current is determined as Equation 49.

$$T_{wheel} = 0.1611 \times (I_{wheel} - 0.05) \quad (49)$$

For the second version of the rover, the  $K_{exp}$ ,  $K_{em}$ ,  $n_1$ ,  $\eta_1$  and  $\eta_2$  values are the same. However, it uses a different wheel hub transmission, thus  $n_2 = 55/12 = 4.58$ . For the second version of rover, the relationship between the rotating torque of each wheel and the drive current is shown in Equation 50 below.

$$T_{wheel} = 0.6713 \times (I_{wheel} - 0.05) \quad (50)$$

## 6.4 Kinetic Response of the Rover on Different Surfaces

According to the farmland field studied, the road classes D, E and F was established. These surfaces have been modelled for the first generation rover that weighs 20 kg. On each surface, the rover will be operating at 0.3 m/s and the torque on each wheel is simulated under duration of 30s. The results are shown in Figure 56, Figure 57, and Figure 58 below.

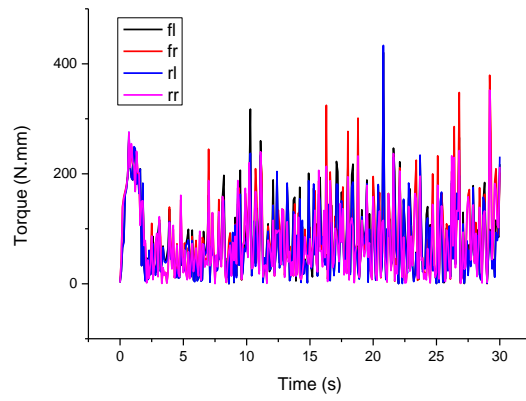


Figure 56. Simulation results of the torque on each wheel on a Class D field surface

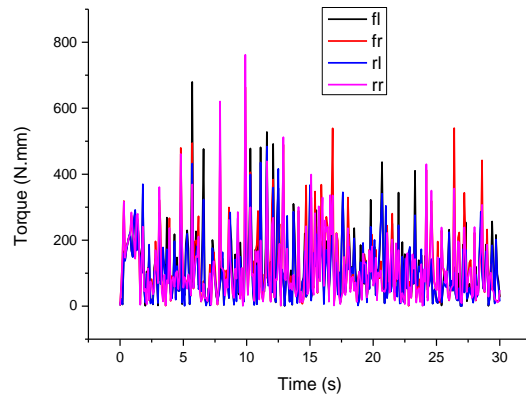


Figure 57. Simulation results of the torque on each wheel on a Class E field surface

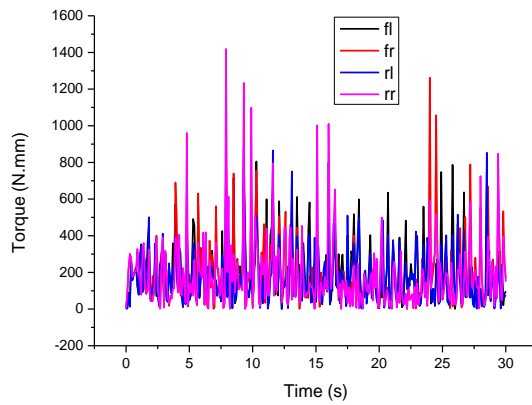


Figure 58. Simulation results of the torque on each wheel on a Class F field surface

The wheels on the road surface are independently shown above on different surfaces, where fl and fr are the front left and right wheels, and rl and rr are the rear left and right wheels. Shown below in Table 9 is the calculation results.

Table 9. Calculation results of different surfaces

class	fl Maximum torque (N.mm)	fl average torque (N.mm)	fr Maximum torque (N.mm)	fr average torque (N.mm)	rl Maximum torque (N.mm)	rl average torque (N.mm)	rr Maximum torque (N.mm)	rr average torque (N.mm)	Four-wheel average torque sum (N.mm)
D	420.6698	79.71624	379.1472	86.22094	433.3723	73.51059	352.2251	78.13444	317.5822
E	679.7207	115.9798	663.8044	122.79	483.9662	105.4658	761.8855	112.3931	456.6287
F	805.171	192.6974	1262.464	190.6752	870.7737	175.7024	1419.463	184.6702	743.7452

According to the equations above, the driving current of the rover on different surfaces can be calculated. For class D surfaces, the average driving current of the rover is 2.021A. Furthermore, for class E surfaces the average driving current of the

rover is 2.884A, and for class F surfaces, the average driving current of the rover is 4.667A.

The surface roughness has thus a positive correlation to the driving wheel torque required, in order to achieve the same speed in a unit time. The driving current increases as the level of roughness increases. More specifically, when the surface roughness increased from D to E to F, the driving current also increased from 2.021A to 2.884A to 4.667A. These are 30% and 38% increases, respectively. Subsequently, the path planning tasks will need to avoid the higher roughness surface classes, and select the surfaces that has a lower level of roughness, when energy optimisation is a planning requirement.

## **6.5 Analysis of the Relationship between Torque and the Capacity of the Rover**

The simulation is now set where the rover has different masses, which is 30kg, 45kg and 60kg. With each mass the rover is simulated on both of the surface classes E and F, with a speed of 0.3m/s. The results from this are shown in Table 10 below.

Table 10. Relationship between torque and capacity for the rover

Mass/ Class	fl Maximum torque	fr Maximum torque	rl Maximum torque	rr Maximum torque	Maximum torque on wheel
<b>30_E</b>	679.7207	663.8044	483.9662	761.8855	761.8855
<b>45_E</b>	798.8926	1091.517	612.0694	669.3103	1091.517
<b>60_E</b>	1650.696	1099.001	1458.202	1207.825	1650.696
<b>30_F</b>	805.171	1262.464	870.7737	1419.463	1419.463
<b>45_F</b>	1626.988	2188.954	1134.27	1446.209	2188.954
<b>60_F</b>	2718.722	2172.303	2372.859	2608.057	2718.722

As the table shows, when the mass increases, the maximum torque needed to drive the rover will increase. Setting the maximum torque on the wheel as a function of the mass when the rover is operating on a class E surface, Equation 51 can be found for the maximum torque on wheel  $T_{E_{max}}$  as shown below.

$$T_{E_{max}} = A_1 m^2 + B_1 m + C_1 \quad (51)$$

Where  $m$  is the mass, and  $A_1$ ,  $B_1$  and  $C_1$  are the fitting coefficient numbers. Using the 3 sets of data in the table on Class E and Equation 52 above, the following is found:

$$A_1=0.5101;$$

$$B_1=-16.2825;$$

$$C_1=791.265;$$

Equation 51 can be simplified to Equation 52 below.

$$T_{E_{max}} = 0.5101m^2 - 16.2825m + 791.265 \quad (52)$$

Using this simplified equation, a graph of the relationship between maximum torque and mass can be generated as shown in Figure 59 below.

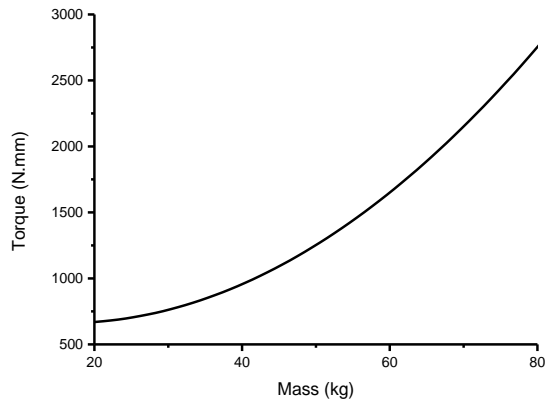


Figure 59. Relationship between maximum torque and mass on a Class E surface

## 6.6 Summary

In this chapter the rover driving energy is analysed with the established ISO 8608 field surface classes. Secondly, the kinetic model of the rover has been simulated on different field surface classes and the driving current has been calculated. Thirdly, the relationship between the driving current and the torque has been simulated and analysed for different surface roughness classes. Lastly, with different masses of the rover, a relationship between maximum torque and mass has been created. This all gives a detailed discussion of the Rover driving wheel power consumption under different conditions, and therefore provides a guideline for the design of the path planning algorithm.

## **7 Motion Analysis of the Rover**

In this chapter, the motion analysis of the rover is completed, where the movement is simulated under different loading and speed conditions. The motion analysis is carried out for obstacles in different shapes and under different speeds, where the impact of the speed is plotted.

### **7.1 Mechanism Motion Modelling Aim and Objectives**

In this section, the motion of the mechanism on the rover has been modeled in detail, such as the steering mechanism and suspension system. Compared to the previous chapter, this chapter gives a more detailed and isolated simulation of the rover mechanism, where the specific forces on each mechanism are analysed.

Establishing a full rover model, according to the functions, mainly includes the front cabin, rear cabin, suspension bow assemblies (a total set of 8), shock absorber dampers (a total set of 8), wheels (a total set of 4), and steering actuators (4 sets in total). No fasteners have been modelled. In the prototype, all connections with fasteners are replaced by "fixed pairs" in the modeling process. A total of 195 part models, with specific functions and dimensions, were created and these parts are assembled as the Rover.

When combined, all the parts have the same material and without relative movement, the final number of parts is 68. The material properties, geometric dimensions, physical characteristics, etc. of these parts are created in SolidWorks according to the prototype, as shown in Figure 60 below.

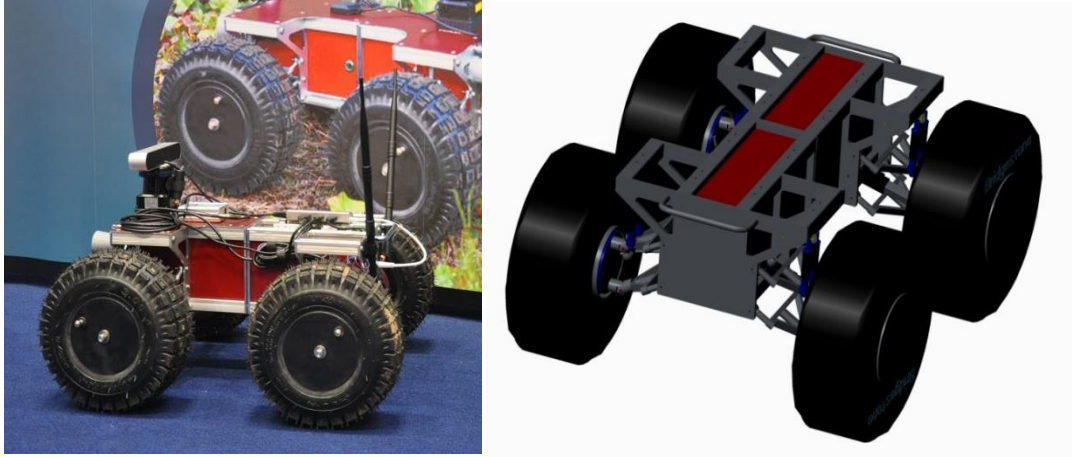


Figure 60. Left: the rover, Right: the model

The weight is added to the rover model, so that the weight of the Rover after the weight increases is the same as the actual prototype's maximum weight. In addition, some

parameters used in the mechanism motion modelling simulation is shown in Table 11.

Table 11. Parameters used in the Mechanism motion modelling

<b>Parameter name</b>	<b>Parameter value</b>
Rover full load mass (robot mass, kg)	20
Actuator spring rate (N/mm)	129.8
Actuator damping coefficient (N.s/mm)	6000
Shock absorber stiffness (N/mm)	129.8
Damping coefficient of shock absorber (N.s/mm)	6000
Coefficient of rolling resistance between tire and cement	0.012*
Coefficient of sliding friction between tire and cement	1*
Coefficient of rolling resistance between tire and field	0.2*
Coefficient of sliding friction between tire and field	0.7*
Coefficient of rolling resistance between tire and sand	0.3*
Coefficient of sliding friction between tire and sand	0.35*
Wheel radius (mm)	80
* is referenced from (Iwashita <i>et al.</i> , 1998) (Rabinowicz, 1951) (Domenech <i>et al.</i> , 1987)	

## 7.2 AgriRover Kinematic Motion Model

The model of the AgriRover in ADAMS is imported from the CAD model, which is shown is the front cabin of the AgriRover in Figure 61. Where all the parts was imported into the ADAMS software and the relationship of the assembly is defined, and this is introduced in Chapter 8.

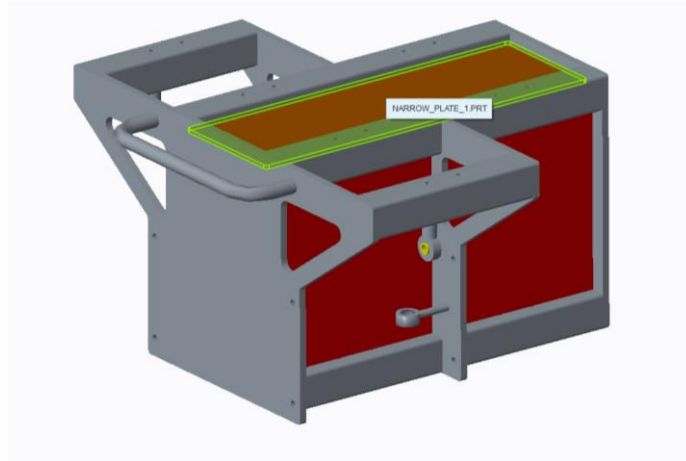


Figure 61. AgriRover front cabin CAD model

## 7.3 Mechanism and Motion Simulation and Analysis

### 7.3.1 Linear Motion on Solid Flat Surface

First, simulate the linear motion of a fully loaded rover on a flat road in the field (without an inclination angle). At the initial moment, the rover will start from the stationary position, and the movement speed of the rover is 0.3m/s, with a simulation time of 10s. The wheels of the rover have been set to a constant speed.

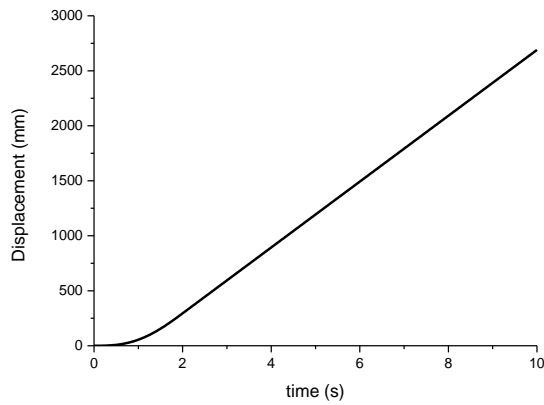


Figure 62. Rover travel displacement versus time curve

As shown above in Figure 62, the curve shows the displacement of the rover in the direction of travel (referred to as the Y direction) versus the time. It can be seen from the graph that the displacement of the car during the startup process (before 2s) is a non-linear increase, due to the sliding motion between the ground and the wheels. After the speed is stabilised (i.e. after 2s), the travel displacement is linearly related to the travel time.

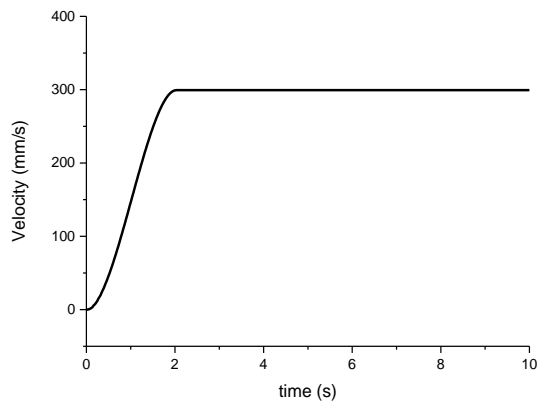


Figure 63. Car speed versus time curve

Figure 63 shows that the speed increases from 0 to 0.3 m/s in 2s time. Figure 64 shows the support force on the steering mechanism, which increased from 0N to more than 6N, with oscillation, within the first 1s, and then decreased to 0 at 2s as the speed of the rover stabilised. Figure 65 shows the torque on the wheels during the simulation, which has a similar tendency as support force on the steering mechanism, as in Figure

64. This is because the support force on the steering mechanism is directly generated by the corresponding driving torque on the wheels.

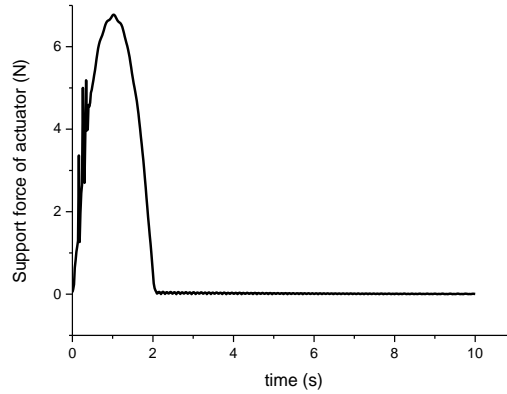


Figure 64. Actuator support force versus time curve

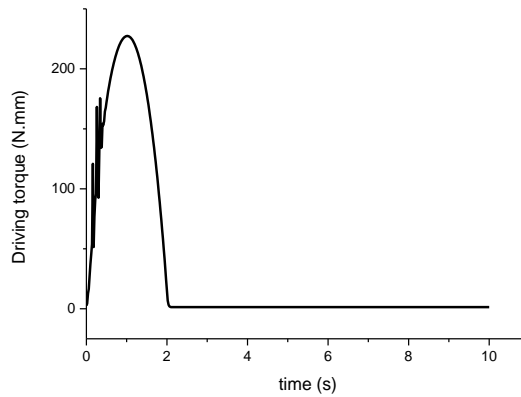


Figure 65. Driving torque versus time curve

### 7.3.2 Linear Motion on a Soft Flat Surface

The linear motion, without inclination, of the fully-loaded rover is simulated on cement, sand, and farm field surfaces. The rover is static at the start of the simulation, after it accelerates to reach a steady speed of 0.3m/s, and the simulation time is 10s. Figure 66 shows the speed curves of the rover on each surface. It can be seen from the figure that the speed curves of the rover during acceleration are different, due to the

different friction coefficients between the tires and the different road surfaces. The acceleration on the farm field is better than that on sand.

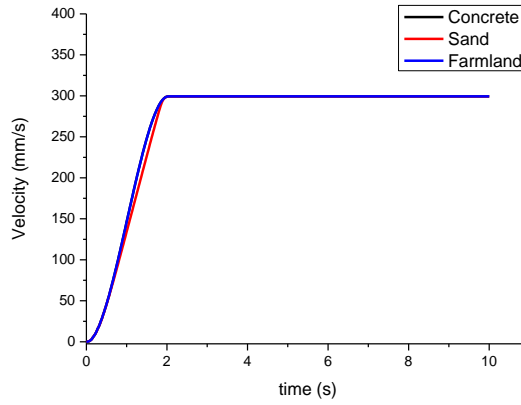


Figure 66. Rover traveling speed vs time curve

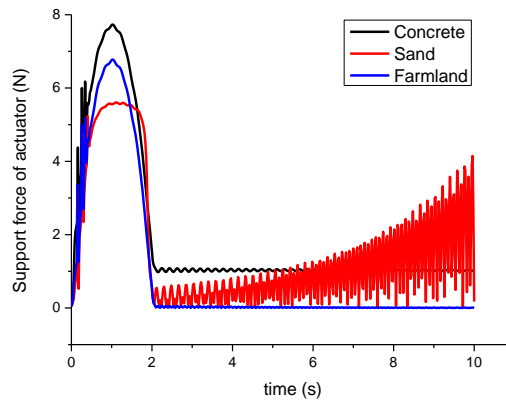


Figure 67. Supporting force of the actuator provided by the steering mechanism

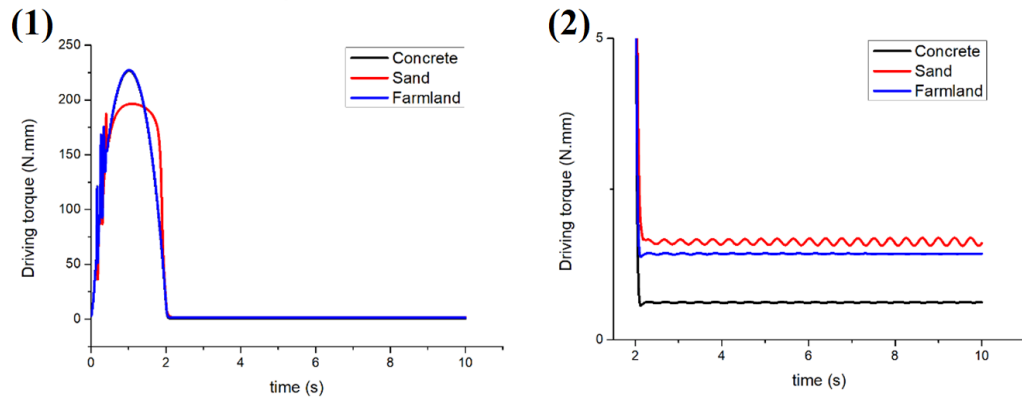


Figure 68. (1) Driving torque on the wheel, (2) Driving torque after stabilisation

Figure 67 demonstrates the supporting force provided by steering mechanism, Figure 68 (1) shows the driving torque on wheel, and Figure 68 (2) shows a magnified view of the driving torque after stabilisation under different surface conditions.

Figure 67 shows the supporting force provided by each steering actuator, in order to maintain straight driving during the travel of the rover on different surfaces. Figure 68 (1) shows that the supporting force provided by the steering actuators, which have a relationship of cement > farmland > sand. After the speed is stabilised shown in Figure 68 (2), the supporting force on the steering actuators for cement and farmland are stabilised, while the force required by the steering actuators on sand oscillates and increases with time. From Figure 68 (1) the relationship of the driving torque during the starting of the car is: farmland > cement > sand, and after the speed is stabilised, the driving torque has this relationships sand > farmland > cement. Finally, the driving torque oscillates at different levels after the speed is stabilised.

### 7.3.3 Linear Motion with Different Speeds

This part is designed for the simulation of a fully loaded rover with different speeds on a solid flat farmland field. The speeds simulated are 0.1m/s, 0.3m/s, 0.5m/s and 1m/s. The rover is static at the start of the simulation, after acceleration its steady speed is reached will be at 0.1m/s, 0.3m/s, 0.5m/s and 1m/s, and the simulation time for this is 10s.

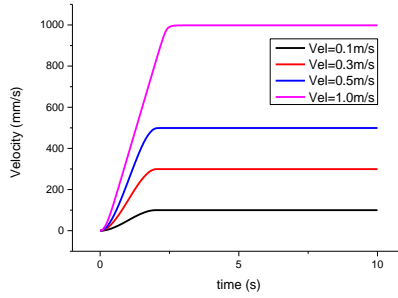


Figure 70. Relationship between time and speed

below shows the curve portraying the relationships between time and rover displacement.

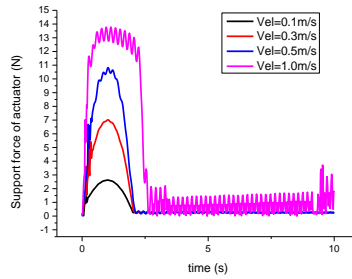


Figure 71. Supporting force provided by steering actuator under different speeds

then shows the curve of the relationships between time and speed. The final figure, Figure 71, shows the supporting force provided by each steering actuator under different speeds.

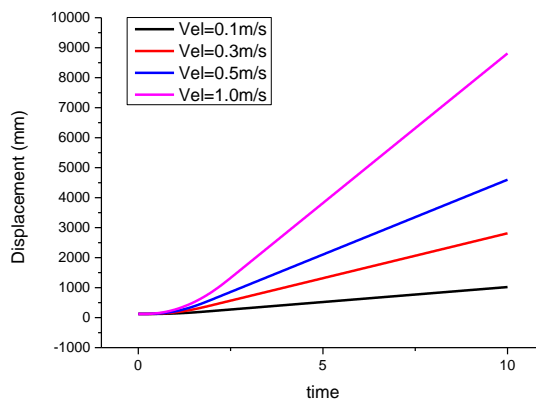


Figure 69. Relationship between time and rover displacement

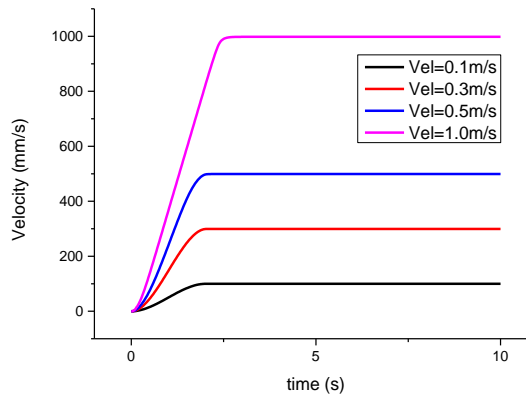


Figure 70. Relationship between time and speed

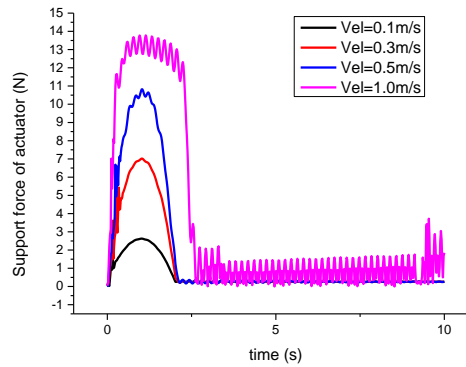


Figure 71. Supporting force provided by steering actuator under different speeds

As shown in the last figure (Figure 71) above, the supporting force provided by the steering actuator under different speeds is different for the linear motion. From the start, the supporting force required for keeping the wheel facing forward has a relationship with different speeds. As the last figure above shows, the forces are bigger when the acceleration is faster at the start of the rover. With the speed below 0.5m/s, the forces stabilise after a similar time, but when the speed is 1m/s the forces are oscillating.

### 7.3.4 Linear Motion with Slopes in the Farmland Field

For this part of simulation, the rover has been set on the farmland field with different slope angles. The angles are  $0^\circ$  (flat),  $15^\circ$  (uphill),  $30^\circ$  (uphill),  $45^\circ$  (uphill),  $-15^\circ$  (downhill),  $-30^\circ$  (downhill), and  $-45^\circ$  (downhill). The rover is static at the start of the simulation, after the acceleration its steady, the speed is 0.3m/s with a simulation duration of 10 seconds.

Figure 72 below shows the rover speed versus time curve. It can be seen from the figure that no matter the slope angle, the speed of the rover will decrease in the initial stage of climbing uphill. The steeper the slope, the greater the speed drop, and the longer it takes for the speed to return to a steady speed.

When the the rover is going downhill, the speed will rise in the initial stage. The steeper the slope, the greater the speed rise. Regardless of it being uphill or downhill, the speed will oscillate from entering the slope section to gaining steady speed again.

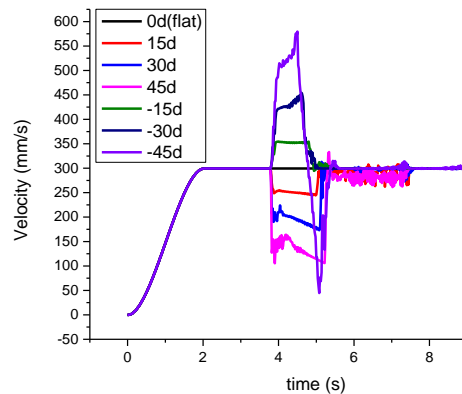


Figure 72. Rover speed versus time graph

### 7.3.5 Linear Motion with Obstacles

For this part of simulation, the rover has linear movement when crossing obstacles on the farmland field at different speeds. The speeds simulated are 0.1m/s, 0.3m/s, 0.5m/s and 1m/s. The rover is static at the start of the simulation.

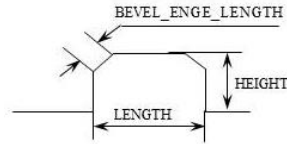


Figure 73. Geometry of the Obstacle

The geometry of the obstacle is shown in Figure 73, it has a HEIGHT of 20mm, LENGTH of 200mm and BEVEL\_ENGE\_LENGTH of 5mm, obstacle and the rover travel direction is set to an angle of 45°.

Figure 74 below shows the speed of the rover for the duration of the simulation. As the curves in the figure shows, when the rover passes the obstacle, it causes a speed oscillation, and the duration of the oscillation is less than the speed increase from 0.1m/s to 1m/s.

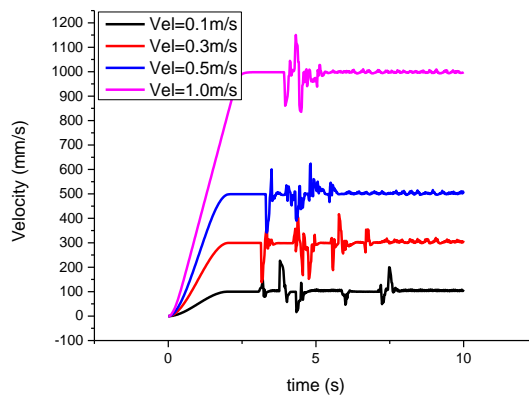


Figure 74. Rover speed versus time graph when passing an obstacle

### 7.3.6 Linear Motion with a Trench

For this part of simulation, the rover does linear movement crossing a trench on a farmland field. The rover is static at the start of the simulation and the speed is 0.3m/s.

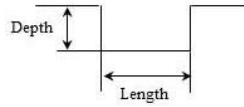


Figure 75. Geometry of the trench

Geometry of the trench is shown in Figure 75. It has been set with a Depth of 20mm and Length of 200mm. The rover is set to go in a straight line directly facing the trench, and the speed change is logged.

Figure 76 demonstrates the rover speed versus time curve when passing through the trench. As the curves in the figure shows, when the rover passes the trench the speed is reduced to 0m/s at point A and then increases sharply after.

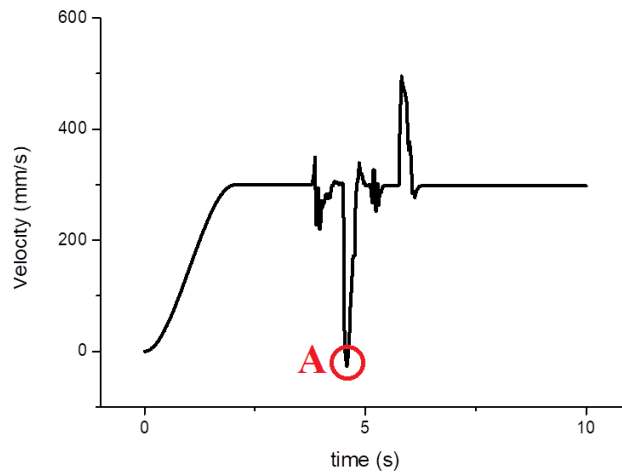


Figure 76. Rover speed versus time curve when passing over the trench

### 7.3.7 Linear Motion with Sinusoidal Surface

For this part of simulation, the rover does linear motion crossing a sinusoidal farmland field. The rover is static at the start of the simulation and the speed is set to 0.3m/s. The Sinusoidal road surface has a wavelength of 3000mm and amplitude of 50mm.

Figure 77 below shows the rover speed versus time curve. As the figure shows, the rover is skidding at first then followed by an oscillation, and finally the rover has a sinusoidal speed curve after 10s.

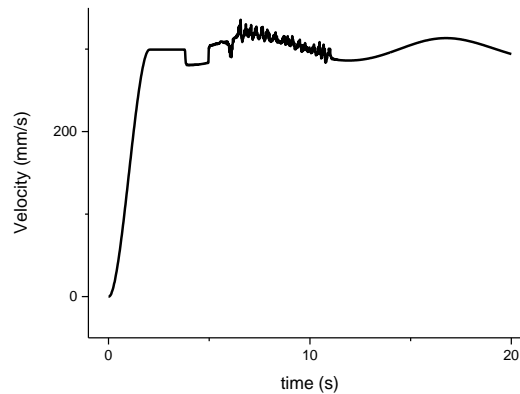


Figure 77. Speed versus time curve on sinusoidal field

## 7.4 Summary

In this chapter the rover is analysed and simulated when driving in ADAMS without trajectory control, and trajectory control has been made in both ADAMS and Simulink Co-Simulation. In this chapter, the dynamic model of the rover is established. The linear motion of the rover on a flat field under full load is simulated. The linear motion of the flat field for different working surfaces, the linear motion at different speeds, the linear motion of different slopes in the field, the linear motion of crossing obstacles in the field, and the linear motion of a sinusoidal surface in the field are all simulated. The response curves of these simulations for the displacement, speed, actuator support forces, and driving torques are obtained, demonstrated and analysed. All the simulations in this chapter give a break-down and detailed representation of the characteristics of the AgriRover when passing certain types of obstacles. The impact of certain types of obstacles are simulated, which shows the trench obstacles have a higher impact to the speed of the AgriRover compared to protruding obstacles with the same dimensions.

## **8 ADAMS and Simulink Co-Simulation**

In this chapter the collaborative simulation between ADAMS and Simulink is presented for the purpose of energy consumption prediction, where the control module of following a specific path is established by Simulink and the physical simulation is done in ADAMS.

### **8.1 Aim of the Co-Simulation**

#### **8.1.1 Aim and Objectives**

The objectives include: controlling the speed of wheels as the input, in order to make the robot have a constant speed, and following the specified path between the start and end points in a 3-dimensional space. Furthermore, the torque and speed of each wheel will be outputted when the robot is moving through the entire path. The collaborative simulation method between MATLAB Simulink and ADAMS is used. The MATLAB Simulink will be used as a control module that provides the required output of the rover, and ADAMS will provide a 3-dimensional space with detailed modelling of both the terrain and the rover, that will be used for the dynamic simulation. The two systems work collaboratively together to give a solution according to the needs of the systematic detailed dynamic modelling.

#### **8.1.2 Variables of the Simulation**

Firstly, the robot model has been exported as compressed binary 3D files and has been imported into ADAMS as shown in Figure 78, which is the physical model of the AgriRover.



Figure 78. The model of the AgriRover

Secondly, the starting and destination points have been generated by the path planning algorithm, and this can be imported to the simulation, as shown in the example in Figure 79.

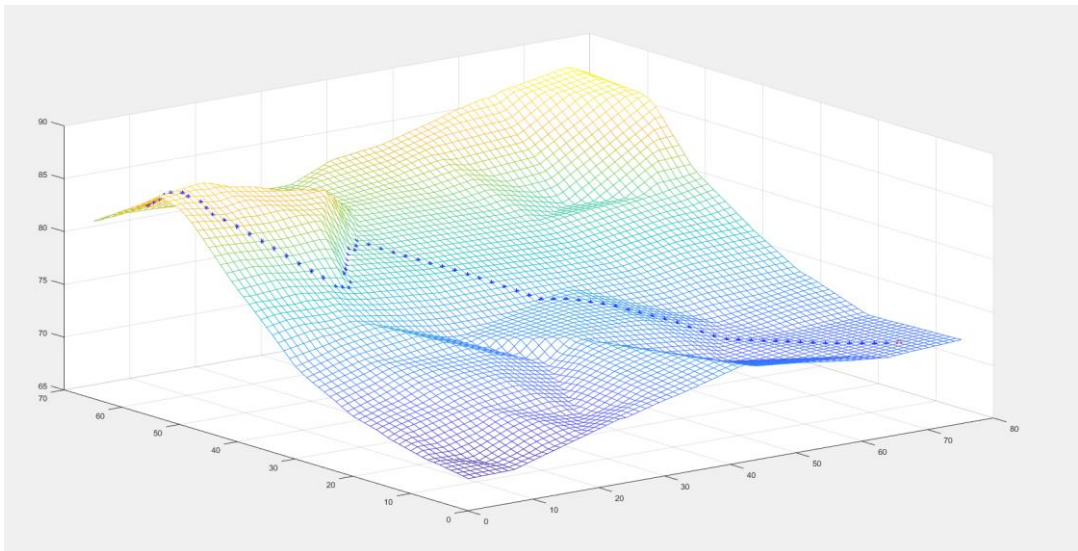


Figure 79. Waypoints generated by the path planning algorithm.

Lastly, the terrain map has been imported into ADAMS as shown in Figure 80.

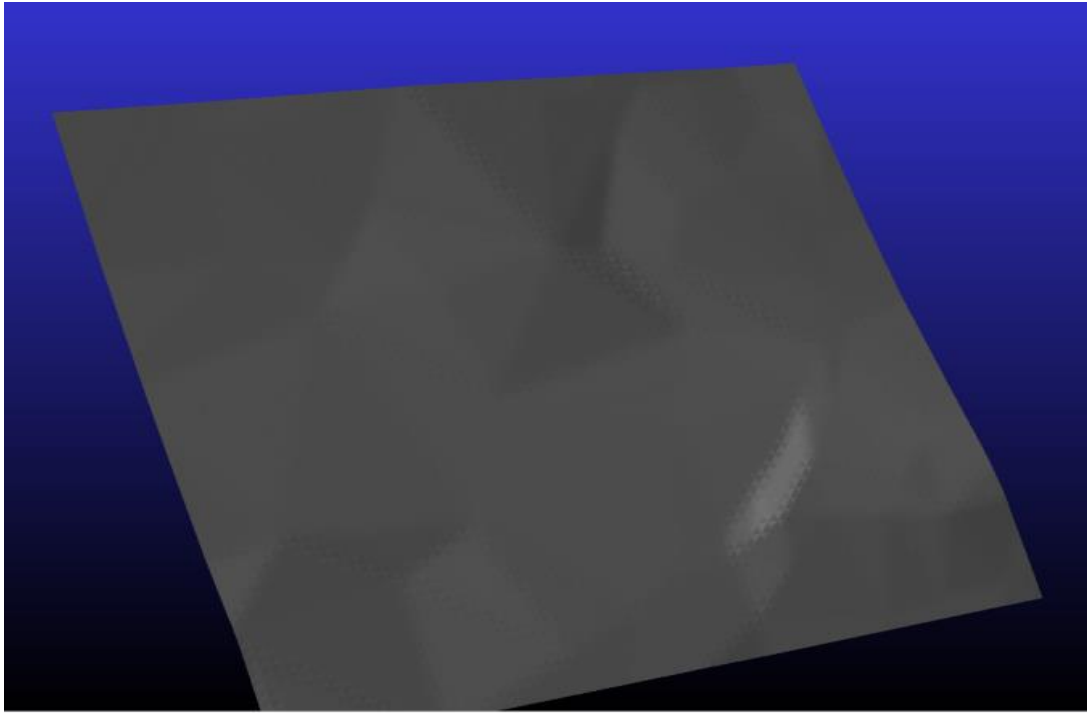


Figure 80. Terrain imported for the co-simulation

### 8.1.3 Control

#### 8.1.3.1 Control Objectives

The objectives for control are as follows:

1. Control the speed of each wheel to maintain the robot speed at 0.5m/s
2. The upper limit of acceleration for each wheel is  $0.5\text{m/s}^2$ .
3. The steering angle of each wheel is set between  $-30^\circ$  to  $+30^\circ$ . The rotational acceleration upper limit is set to  $15^\circ/\text{s}^2$ .
4. The robot needs to follow each waypoint generated by the path planning algorithm.
5. A control method to ensure the robot achieves the above objectives is chosen. The PID (Proportional Integral Derivative) method was chosen.

#### 8.1.3.2 Control Objectives Analysis

According to the control objectives, the physical characteristics of the robot, the effectiveness, and the running speeds of the co-simulation, the following simplification has been made to accommodate that mentioned above.

The rover has been simplified to front wheel steering only, instead of all the wheels steering, in order to lower the resources needed for running the co-simulation. Front wheel drive has been adopted due to the conflict that was caused when running both front and rear wheel drive, because the wheel speed control of the co-simulation is not synchronous,. Then, to further reduce lag and instability, the two front wheels are synchronised and they move with the same control inputs for the robot, which include only two forces, the torque on the ground and the torque for steering. Lastly, the friction coefficient is set as a constant value, instead of the randomly generated matrix, because ADAMS dose not have such a function.

## **8.2 ADAMS and MATLAB Co-Simulation Overview**

### **8.2.1 Co-Simulation Overview**

For complex electromechanical systems, if the traditional design method is followed, such as repeatedly testing and improving the prototypes, it is not only difficult to effectively make improvements of the product performance, but also require a lot of materials, which cost money and time to manufacture. Thus, it is necessary to use the computer simulation by building a 3D model as a virtual prototype first, before manufacturing many physical prototypes.

By testing the virtual prototype first, the deficiencies of the system can be identified and improved, which can effectively shorten the development cycle of the algorithm and improve algorithm performance.

The kinematics and dynamics simulations of multi-rigid-body systems can be achieved by using ADAMS. ADAMS is a mechanical systems and dynamics simulation software. The model established by ADAMS can reflect the actual physical model precisely, and ADAMS simulation results can also have a high level of accuracy when compared to actual physical models (Gao *et al.*, 2012).

However, ADAMS lack more complex control functions. For a complex application which have control needs, the simulation will require software that is capable of implementing the function of control, such as in MALAB, MATRIX, or EASY 5 (Gao *et al.*, 2012). MATLAB has many powerful and convenient control functions, which makes the construction of the control systems possible. The Simulink module in MATLAB can be used to model, analyse and simulate the interactive environment of various dynamic systems, which include continuous, discrete and hybrid systems. Simulink can also be used to integrate the state-flow of the model and simulate complex event-driven logical states of the system (Agrawal *et al.*, 2004).

By using these two softwares together works as the junction of co-simulations, not only can a joint system of the robotic arm be simulated and analysed for the kinematics and dynamics of the model, but the control system of the model can also be established. This will provide a technical basis for the development of the physical prototype (Cheraghpour *et al.*, 2011). This application search method is used to simulate the system of the autonomous mobile robotic platform, the AgriRover.

## 8.2.2 Co-Simulation Principle

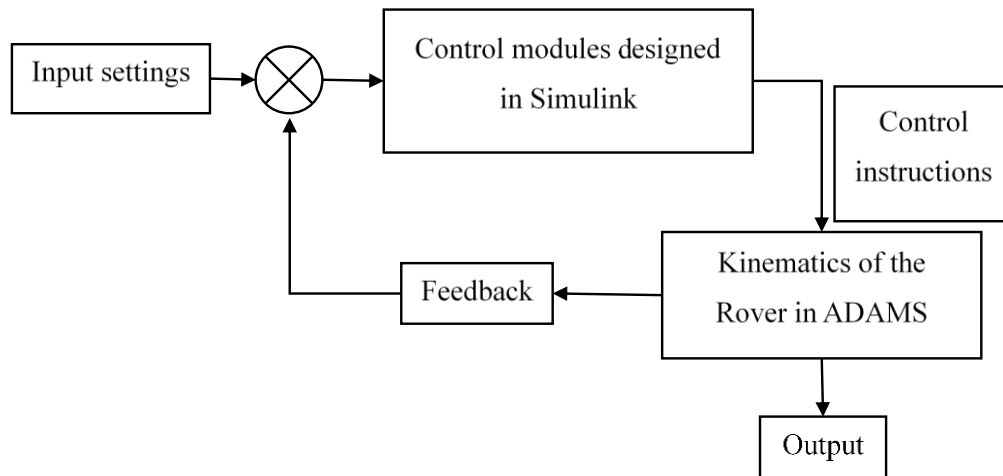


Figure 81. Co-Simulation Principle

In the junction of the co-simulation between ADAMS and MATLAB, ADAMS is mainly responsible for the execution of the control instructions and the measurement of the parameters that are concerned with. MATLAB is mainly responsible for the generation of the control instructions.

After the mechanical system of the vehicle model is established in ADAMS, the position, speed, steering angle, and other motion state parameters of the vehicle are set as the output in ADAMS, with the driving torque of the wheels and the steering torque as the input of ADAMS for the control of the vehicle.

Correspondingly, for MATLAB, after receiving the motion state parameters of the vehicle from ADAMS, the driving torque of the wheels and the steering torque of the steering motion pair are calculated by the tracking control system in Simulink, with other control variables also fed back to ADAMS (Gao *et al.*, 2012). Co-Simulation Principle is shown in Figure 81.

### 8.2.3 Co-Simulation Setup Process

The simulation environment is setup in the ADAMS-view properties window: the start position and the startup parametric was set. Then in MATLAB, the start position was set in the software properties window, which is set as the same as the ADAMS-view start position. The simulation setup is based on the ADAMS-MATLAB Co-simulation for Industrial Robot Analysis, provided by the Mscsoftware official website and the ADAMS/Controls under Third-Party Products & Services on Mathworks official website (Ángel *et al.*, 2012).

First, the file was copied to the "co\_simulink\_example1" folder, which is in the workspace of the project. Then in MATLAB the working directory is changed to the same workspace, as it is mandatory to be set as the same as the existing files. Then, by entering the file name "controlspid" in the MATLAB command window and pressing enter, the command window will display the input and output characteristics of ADAMS, and this is important for the setup in ADAMS. Then by entering `adams_sys` in the command window, a .mdl file will be generated in subfolders, which will be named as `tcontrol_model.mdl`. By running this file, the ADAMS software and simulation will start, with a warning window which it can be ignored.

After the simulation process is complete, the ADAMS window will close. By opening the .bin file in the ADAMS-view, the postprocessor then opens in the ADAMS-view, thus the simulation data will be loaded. Following this, animation can be loaded in the canvas window. Lastly, the plot is loaded, where the curves for various parameters can be plotted.

## **8.3 Mechanical System Setup for the AgriRover**

### **8.3.1 3D Model**

The 3-dimensional model created by software, such as Solidworks, can be converted into sn x\_t format and then imported into ADAMS. During the process of modelling, the origin of the axis name and the direction of the axis of the model will be different between the modelling software and ADAMS. Therefore, a conversion of the axis was done to align the direction and the name of the axes. The axis of the model is changed in the 3D modelling software, because the axes are not easily changeable in ADAMS.

The model of the rover is simplified, and unnecessary parts are deleted. The parts without relative movement are merged, reducing the number of parts that can facilitate the calculations in ADAMS. This improves the efficiency and reduces the time taken for the simulation operations. The simplified vehicle is shown in Figure 82. The body, terrain, and steering angle measurement (shown in next section) has been simplified into 11 parts, as shown in the figure.

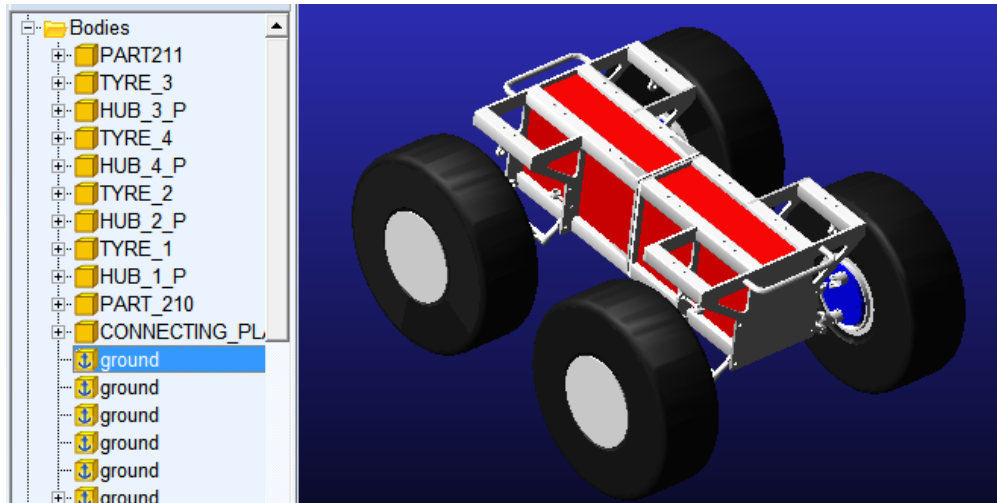


Figure 82. Simplified AgriRover model

### 8.3.2 Kinematic Pairs

The four wheels of the AgriRover have a total of 4 driving rotating pairs and 4 steering rotating pairs. Figure 83 (1) shows the steering pair and Figure 83 (2) shows driving pair.

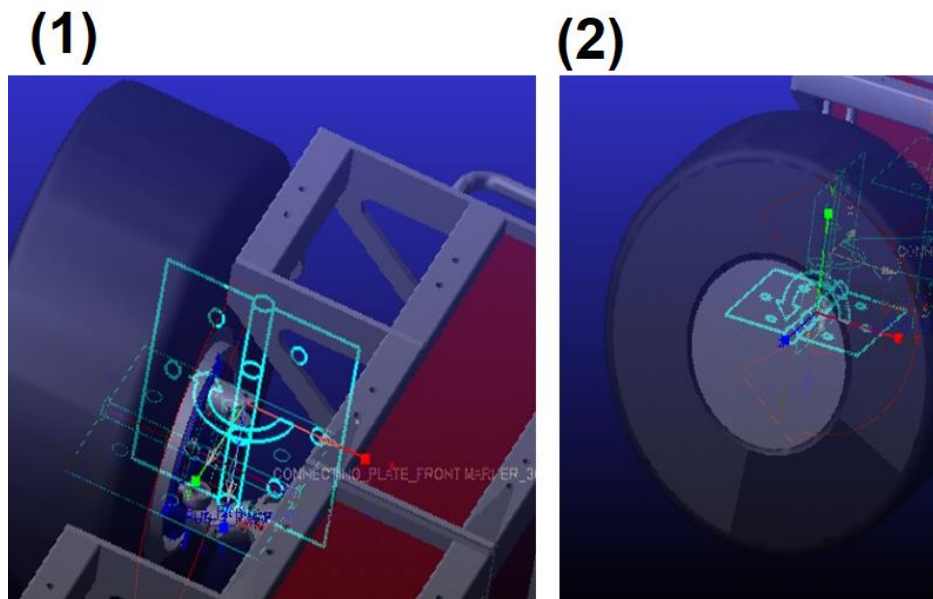


Figure 83. Joint in ADAMS after simplification

In order to simplify the control, a parallel pair is added between the steering wheels of the two front wheels to keep the steering completely aligned.

The direction of the rotary joint was incorrect when first setting up, and this is changed in the settings of the working grid to solve this problem. A few attempts were taken to set the position and direction correctly. Furthermore, a fixed joint is added between the terrain module and the ground in ADAMS.

### 8.3.3 Definition of the Contact Force

The module of the contact force between the four wheels of the rover and the terrain is established, which was done by using the Special Forces category. The contact force between the four wheels of the vehicle and the terrain module, as well as the settings of the parameters are shown in the Figure 84. The normal force needs to be set as Impact, otherwise the penetration problem will happen during the simulation process. Then, the gravity force and direction were set.

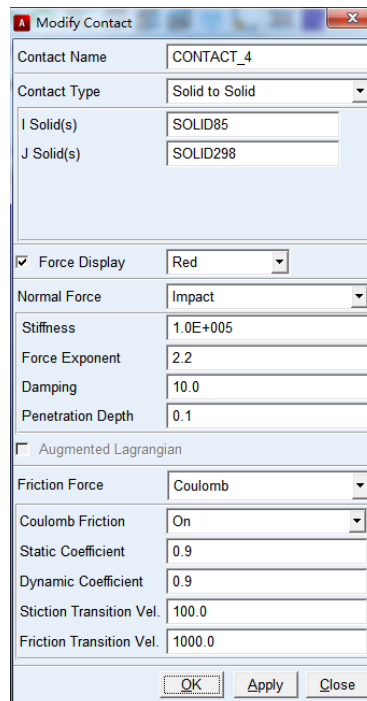


Figure 84. Rover and the terrain contact force parameters

After completing the above, the simulation is started as shown in Figure 85. Observation of the rover state will be needed, when the contact setting is correct the vehicle will stay on top of the terrain without the problem of penetration or singularity;

if an anomaly occurs. The problem could be as follows: the initial distance of the tire from the ground is too close, there is a problem with the force setting, or the steering and driving was moving uncontrolled due to no added control.

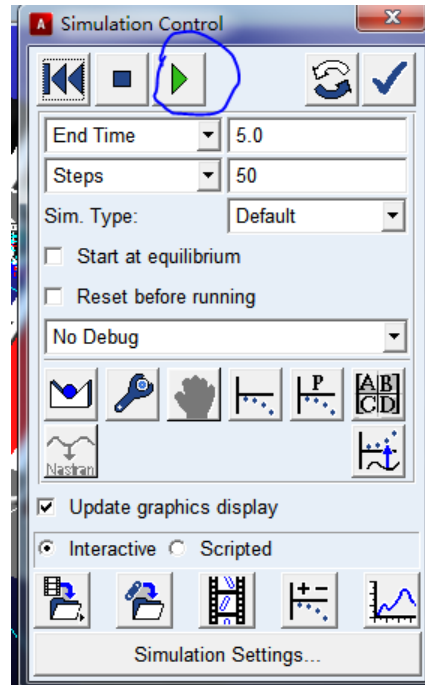


Figure 85. ADAMS simulation

### 8.3.4 Navigation Angle Measurement Module

In order to accurately feed back the steering angle of the vehicle during the movement, a part is added on the frame of the Rover model as the navigation angle measurement module. This is shown in Figure 86 as highlighted red cylinder.

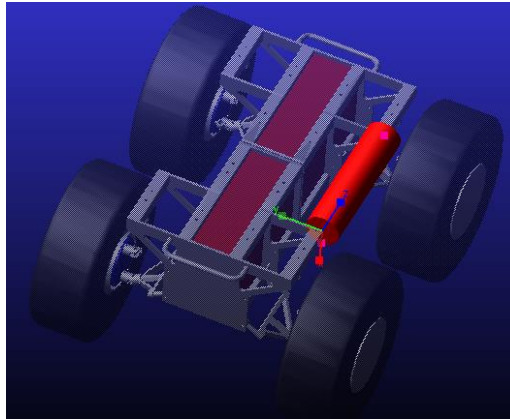


Figure 86. Navigation angle measurement module

### 8.3.5 Setup ‘Measures’ with Rover Orientation and Motion Status Measurement

The two variables of the front wheel steering angle and acceleration of the steering angle was measured by using the measure function in ADAMS, which was set as shown in Figure 87 for a joint named joint\_52. Then measure is selected with the characteristics of the relative angular velocity.

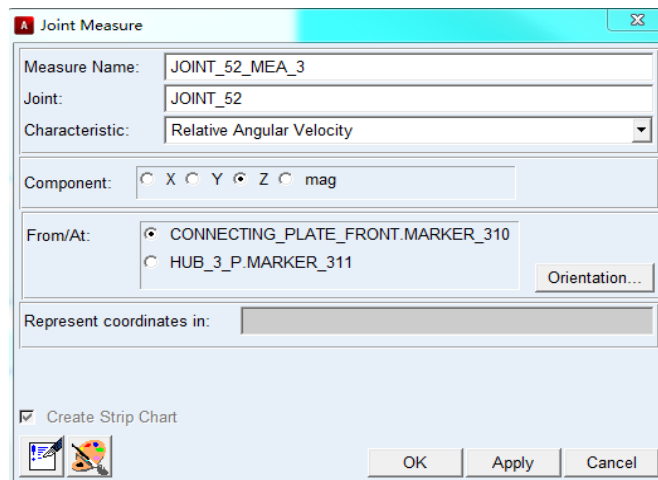


Figure 87. ADAMS measure settings

The front right wheel angular velocity measurement and front right wheel angle measurement were completed using the same method. The orientation needs to be changed, as due to the fact that the wheels are facing each other, the coordinate system is the opposite of each other.

## 8.4 ADAMS Model Parameter Settings

When running the co-simulation, data exchange between ADAMS and MATLAB is required. This section explains the establishment of the input and output variables between the ADAMS and MATLAB softwares.

### 8.4.1 Variable Definitions

The rover model in this case has a total of 9 set input variables and 7 output variables. The communication link block diagram in Figure 88 was automatically generated by Simulink. Each of the input and output variables are then shown in Table 12.

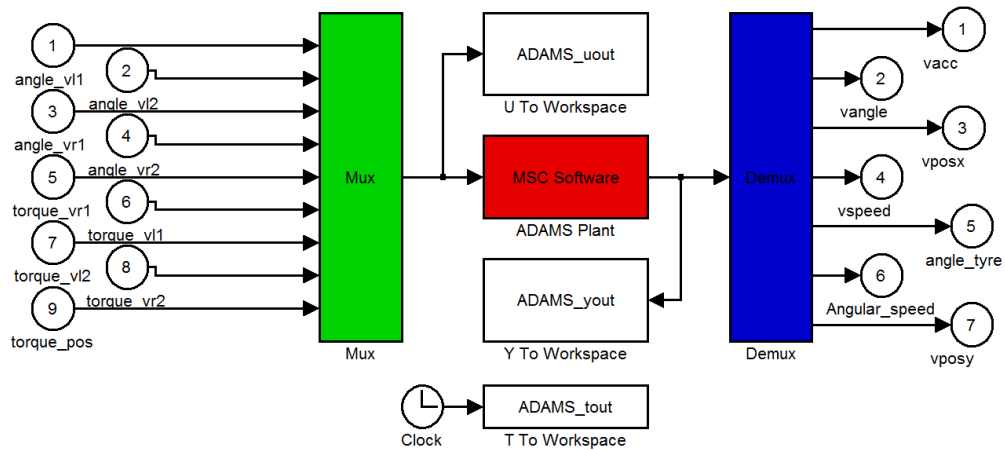


Figure 88. Input and output variables set

Table 12. Input and output variables

Input Variables			Output Variables		
№	name	Functions	№	name	Functions
1	angle_vl1	Front left wheel steering angular acceleration	1	vacc	Rover acceleration
2	angle_vl2	Left rear wheel steering angular acceleration	2	vangle	Rover steering angle
3	angle_vr1	Right front wheel steering angular acceleration	3	vposx	Rover x-direction coordinates
4	angle_vr2	Right rear wheel steering angular acceleration	4	vspeed	Rover speed
5	torque_vr1	Right front wheel torque	5	Angle_tyre	Front wheel steering angle
6	torque_vl1	Left front wheel torque	6	Angular_speed	Front wheel steering angular speed
7	torque_vl2	Left rear wheel torque	7	vposy	Vehicle y-direction coordinates
8	torque_vr2	Right rear wheel torque	— —	—	—
9	torque_pos	Absolute value of input torque	— —	—	—

In order to simplify the control model and improve the simulation efficiency, as mentioned before, the steering only controls the right front wheel angular acceleration, and the remaining three wheels angular accelerations are set to 0, of which the left

front wheel has set constraints to ensure the two steering wheels are synchronised at any time. The wheel speed control only drives the torque of the two wheels in the front, and the torque of the two rear wheels is set to 0.

The input variable `torque_pos` is the value of the front wheel driving torque, which is not involved in the control module, it is only used for the energy consumption calculation. Furthermore, The x- and y-directions in the `vposx` and `vposy` variables refer to the x- and y- coordinatew on the ground in ADAMS, which is the opposite of the x and y in the terrain. Finally, the rest of the output variables are set as shown in Table 13.

Table 13. Output variable

Variables	Functions	F (time) settings	Description
vacc	Rover acceleration	ACCM(CONNECTING_PLATE_FRONT.cm,MARKER_342)	Output the total acceleration between the two coordinate systems
vangle	Rover steering angle	AZ(MARKER_340,MARKER_339)	Output the rotation angle between the two coordinate systems around the Z axis.
vposx	Rover x-direction coordinates	DX(CONNECTING_PLATE_FRONT.cm,MARKER_342)	Output the distance of the two coordinate systems along the X axis.
vspeed	Rover speed	VM(CONNECTING_PLATE_FRONT.cm,MARKER_342)	Output the total speed between the two coordinate systems
Angle_tyre	Front wheel steering angle	.model_car.ORIENT_MARKER_310_MARKER_311_MEA_1	Output the measure variable
Angular_speed	Front wheel steering angular speed	.model_car.JOINT_52_MEA_3	Output the measure variable
vposy	Vehicle y-direction coordinates	DY(MARKER_342,CONNECTING_PLATE_FRONT.cm)	Output the distance of the two coordinate systems along the y-axis direction.

## 8.5 MATLAB Simulink Block Diagram

### 8.5.1 Control Model Setup

First, the working directory of MATLAB is set to the same working directory of ADAMS. In the MATLAB command window, Controls\_Plant\_1.m has been entered. Then ADAMS\_sys has been entered, which is the interface command between ADAMS and MATLAB. After entering the ADAMS\_sys command, the selection window of MATLAB/Simulink for the S-Function box represents the nonlinear model of ADAMS, which is the model used for dynamic simulations. This shows the State-Space, and represents the linearised model in ADAMS, and ADAMS\_sub contains nonlinear equations with all the selected variables.

Figure 89 shows the system block diagram of the inputs and outputs set in ADAMS and the control block diagram in Simulink, which will be explained after this section.



### 8.5.3 Simulink Function Block and Path Tracking

The control block diagram contains many scopes and numerical display modules, which are used for debugging the display of various variables during the simulation process.

#### 8.5.3.1 Speed Control Module

The control block diagram for the speed control is shown in Figure 90, with the control blocks divided.

The lower left corner of Figure 90 is the speed controller. In this case, it is set to 0.5m/s. On top in this model is the proportional integral control that is used, and the appropriate proportional coefficient is adjusted through experiments, the next section will show parameter adjustments. The unit used is millimeters due to the unit used for the modelling of the Rover also being millimeters, therefore the units are correctly corresponding to each other.

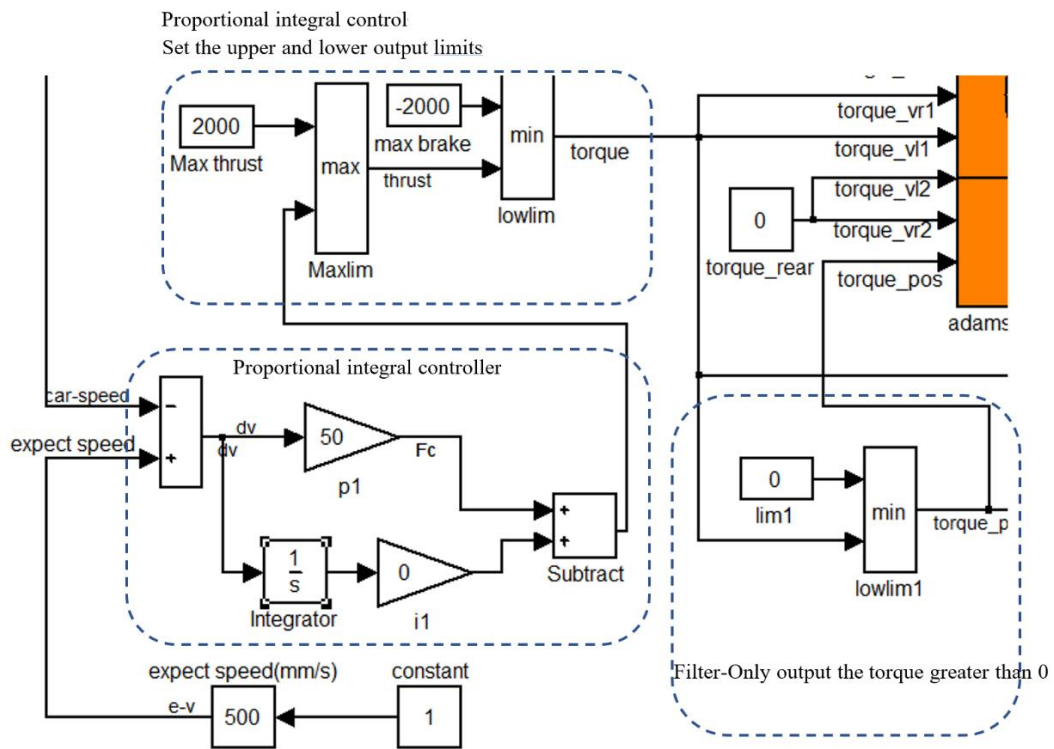


Figure 90. Speed control block diagram

At the top of the speed controller is the torque controller, which is used to set the upper and lower limits of the output values by comparing the largest and smallest numbers in each module. At the same time, the output signal is divided into other channels through filtering, so only the number of the torque that is greater than 0 is outputted. The default torque number which is less than 0 will be filtered and therefore no energy is lost when it is used for calculations of the energy consumption. Then, all the variables are outputted into ADAMS.

### 8.5.3.2 Trajectory Tracking and Steering Control Module

The control block diagram of the trajectory tracking and steering control module is shown in Figure 91, which will be introduced in detail in the next section. This module includes trajectory data entry, distance judgment, expected steering angle calculations, cycle counting, and judgment of the loop breaking module.

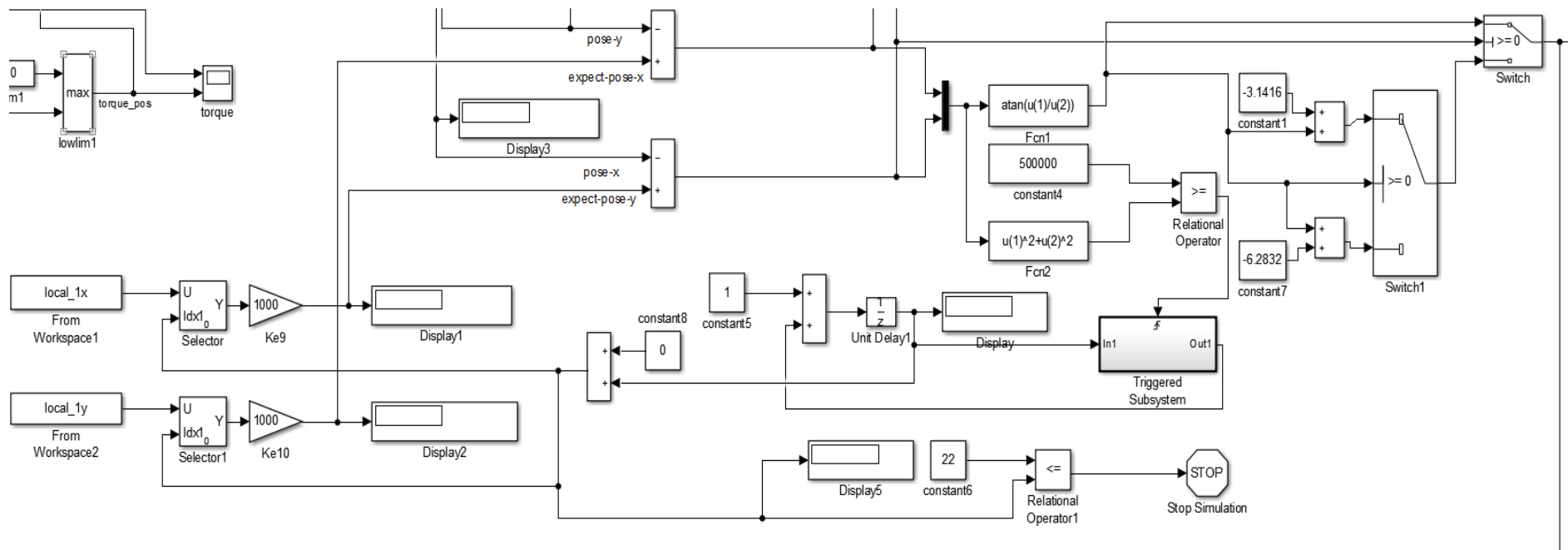


Figure 91. Control block diagram of the trajectory tracking

### 8.5.3.3 Trajectory Data Entry Module

The block diagram of the trajectory data entry module is in Figure 92.

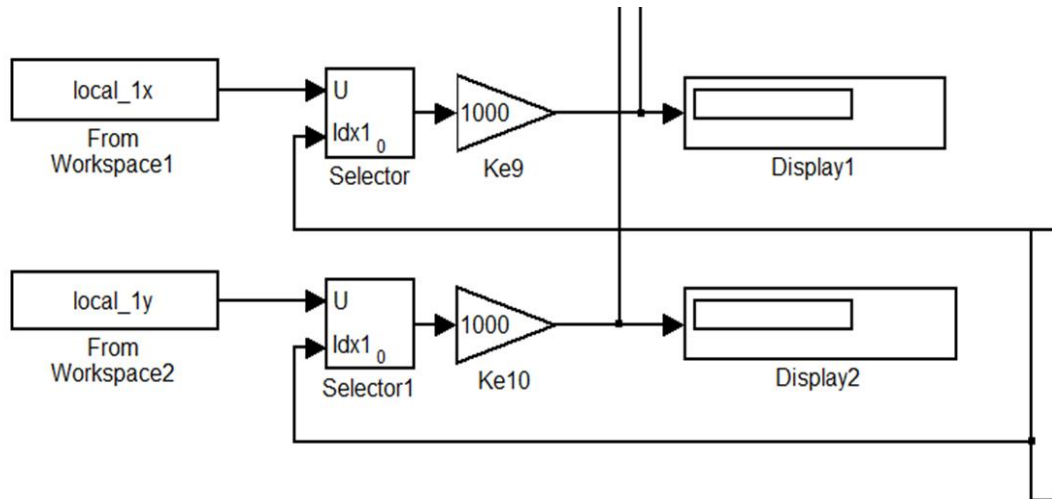


Figure 92. Trajectory data entry module

The function of the ‘from workspace1’ module is set for reading the array named local\_1, which was generated in Chapter 4, and contains the sets of the waypoints for the planned path in MATLAB. This module is used for importing the x- and y-coordinates data into the control module.

The Function Block Parameters ‘Selector’ and ‘Selector1’ modules are used to select which number of the waypoint coordinates are selected, and it functions according to the number generated by the cycle counting module shown in Figure 95.

The parameter of the ‘Selector’ module is set as shown in the Figure 93. The index mode is set to ‘Zero-based’ and the index is set to ‘index vector (port)’, it indicates which external signal is responsible for selecting which number in the output array. The number for the ‘Input port size’ is set to the number of tracking points minus one, for this case the set of waypoints is 23, thus 23-1 is 22, which will be entered as shown in Figure 93.

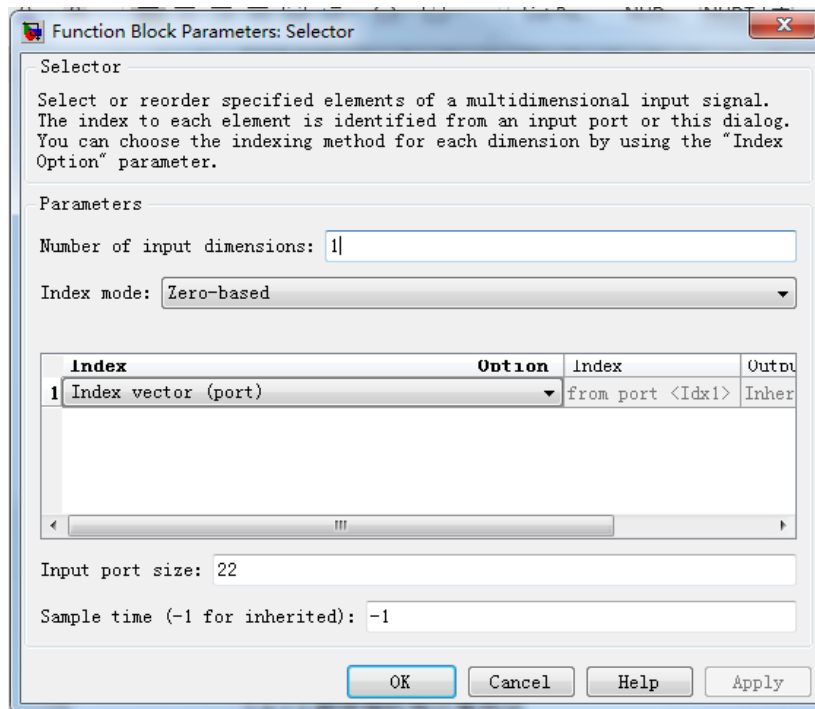


Figure 93. Function Block Parameters ‘Selector’ module

#### 8.5.3.4 Front Wheel Steering Control Module

The control block diagram for the expected steering angle is shown in Figure 94, outside of the red box.

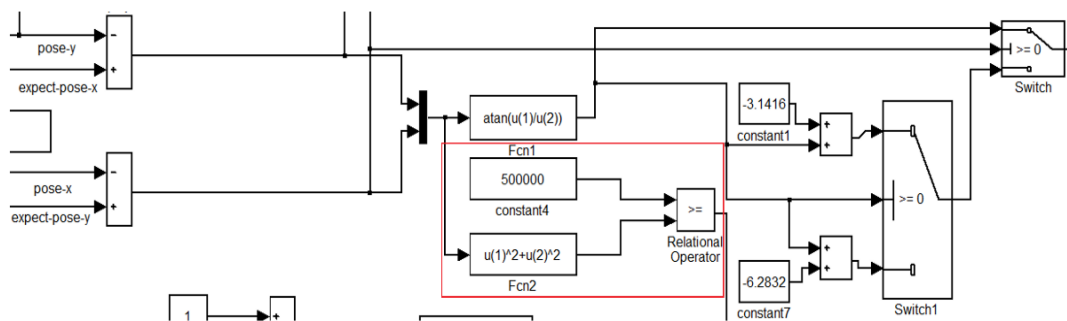


Figure 94. Expected steering angle block diagram

After the x- and y-coordinates acquired target points are transferred into this module, and they are compared with the x- and y-coordinates of the current positions of the Rover in ADAMS. As mentioned before, because of the coordinate direction of the 3D Rover model, the x-coordinate output by ADAMS is the y-coordinate of the terrain model, and the output of the y-coordinate is the x-coordinate of the terrain model. This comparison is done on the left of Figure 94.

After the difference has been calculated between the target coordinates and the current coordinate, the "arctan (u (1) / u (2))" trigonometric function in the 'Fcn1' module is used to obtain the rover's steering angle.

The two switch modules are used to judge the relationship between the target point and the current position point, because when the calculated steering angle is in the third or fourth quadrants of the coordinate system it is the same as if the steering angle is in the first or second quadrants. Thus, the switch needs to be used to determine which quadrant the calculated steering angle is in, and the expected steering angle is converted to polar coordinates by two constant modules, 'constant1' and 'constant7'.

#### 8.5.3.5 Distance Judgment Module

'Fcn2' is the function for calculating the distance between the current point and the next waypoint by using ' $u(1)^2 + u(2)^2$ ', without the extraction of a root, as shown in the red box in Figure 94. Following this, this calculated value is compared with the number 50,000, which is roughly the square of 224mm, and 224 mm is the distance between the center of mass to the front of the modelled rover. The judgment for the distance of the next waypoint is done by the block function of 'relational operation'. If the distance between the current point to the next waypoint is smaller than 224 mm, the judgment block will give an output of true, otherwise the output will be false. If the output of this module is true, it means the next waypoint is reached and the cycle counting module will be triggered.

#### 8.5.3.6 Cycle Counting Module

The block diagram of the cycle counting module is shown in Figure 95.

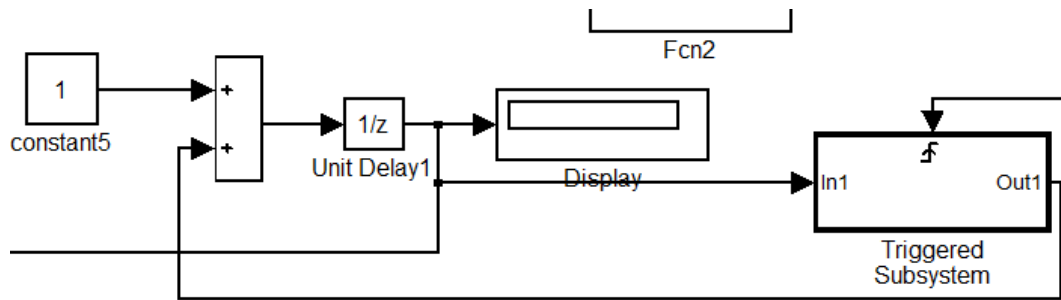


Figure 95. Cycle counting module

The 'Triggered Subsystem' module is a response module that can be triggered when the top input is on a racing edge, and the input 'In1' is 1, and only when the counter will be counting to plus 1. This counter is used to track the waypoint number, so that the simulation can proceed to the next waypoint, and is also used for judgement and breaking the loop when the counter is more than 22.

#### 8.5.3.7 Judgment of Loop Breaking Module

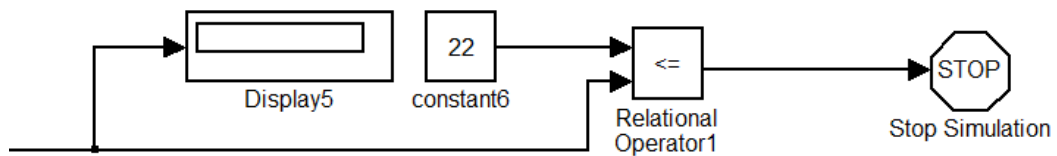


Figure 96. Judgment of loop breaking module

The judgment of loop breaking module is shown in Figure 96. The current waypoint number will be used as the input, and the logic comparison module is used to determine if the last waypoint has been reached. If so, the simulation will stop as the destination point is reached, and therefore the program will stop.

### 8.5.4 Front Wheel Steering Angle Control Module

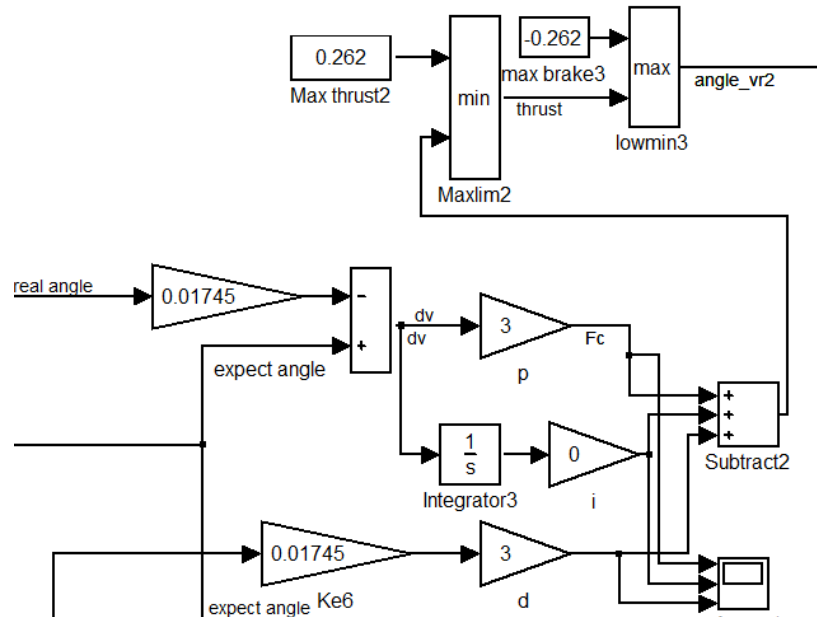


Figure 97. Front wheel steering angle control module

The control block diagram of the front wheel steering angle is shown in Figure 97. The control method used is a Proportional–Integral–Derivative (PID) control method. The output is the angular acceleration of the steering angle for the front wheels. The upper and lower limits of the output value is set to  $15^\circ/s^2$ , where  $1^\circ=0.01745\text{rad}$ .

## 8.6 PID Parameters Tuning

PID control has been used for the front wheel steering angle in this system, and the P, I and D parameters are tuned, with the results as shown in Figure 98. The test started with a given expected steering angle of -0.1, as the goal step. PID parameters have been tested, as shown below in Figure 98. In summary, the best result is when  $P=3$ ,  $i=0$ , and  $d=3$ , as it is has the lowest steady-state error.

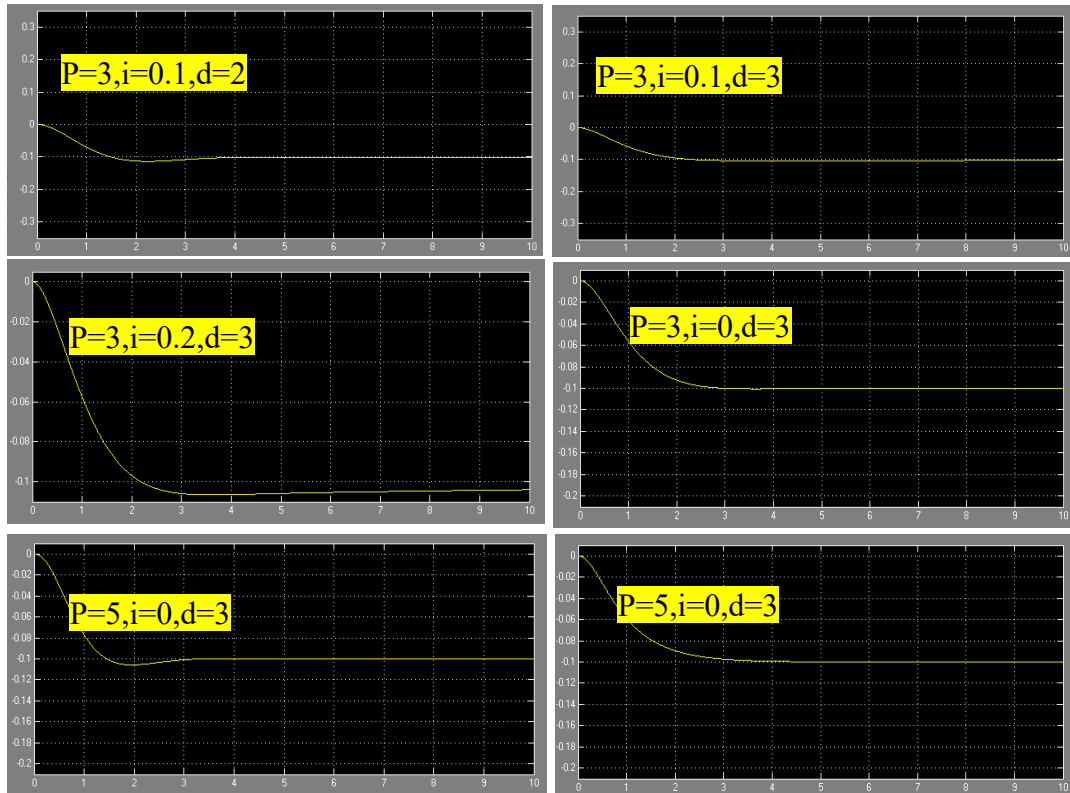


Figure 98. PID control parameters tuning

## 8.7 Simulation Verification and Debugging

The rover mass is 9.2kg. The simulation uses millimeters for length, newton for force, kilograms for mass, seconds for time, and rad for angles.

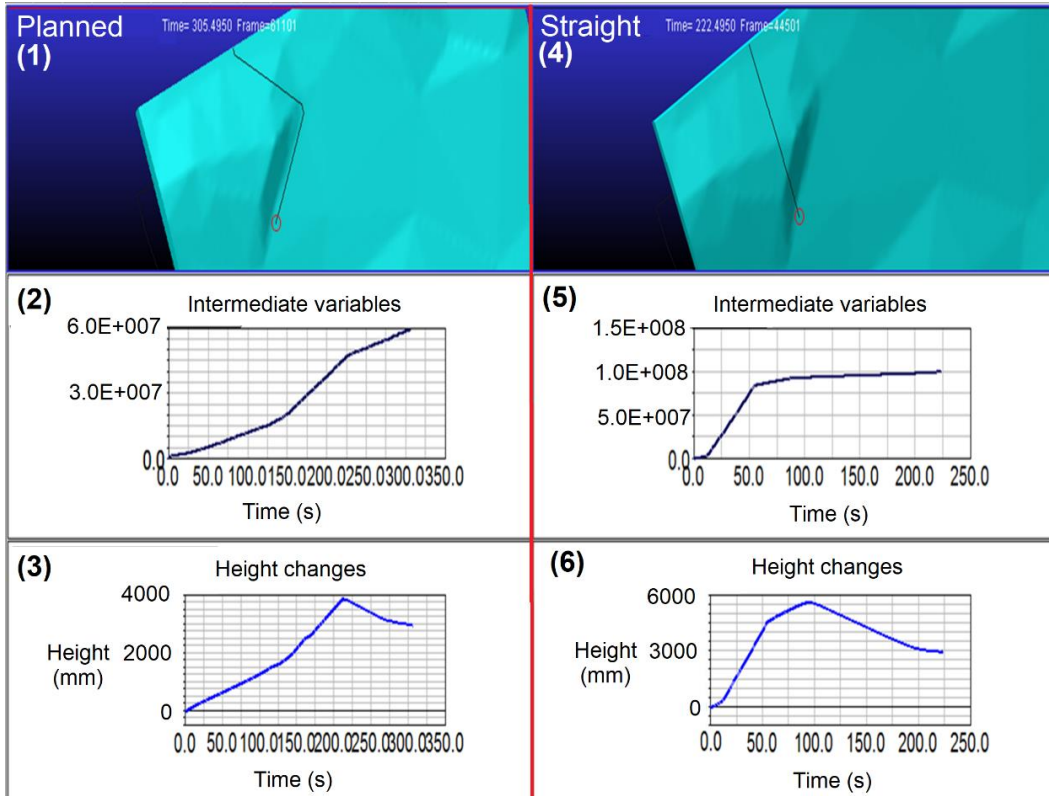


Figure 99. Second co-simulation Second Co-simulation results of an optimal path in comparison with a standard path: (1) the optimised path, (2) intermediate energy for the path in (1), (3) height changes for the path(1), (4) straight or normal path, (5) intermediate energy for the path in (4), (6) height changes for the path (4)

In this co-simulation the path generated with the path planning algorithm has the goal set to the lowest power consumption. The start point is indicated as a green circle. For a given terrain, it is necessary to optimise a path and a result is shown in Figure 99 (1), From the co-simulation, the total power consumption of the planned path shown in Figure 99 (2) which is lower than the straight-line path one shown in Figure 99 (5) And the height change of planned path has a lower slope shown in Figure 99 (3) compared to Figure 99 (6) straight-line path.

As shown in (1),(2) and (3) of the Figure 99 is the energy optimised path, the total run time is 305 seconds and the total intermediate energy cost is  $6.268139 \times 10^7$  by each wheel this variable is an integral of time with  $\tau \times v$  where the speed unit is in mm/s.

To calculate the final total energy consumption into joules, the following conversion 54 is used which is a derive of the 53(Kleppner *et al.*, 2014).

$$W = \int_{\theta_1}^{\theta_2} \tau d\theta \quad (53)$$

$$Work = \int_{t_2}^{t_1} \tau \omega = \int_{t_2}^{t_1} \tau \times \frac{v}{r} \quad (54)$$

Where is the radius of the Rover wheel has a radius of 80 millimeter, as the Rover have two driving wheels when simulated, the final energy cost will be in result of 1568.54 joules( $\frac{6.268139 \times 10^7}{80} / 1000 \times 2$ ).

As shown on the right of the Figure 99 (4-6) for the straight path, the total run time is 223s, which is shorter than the planned path's 305s shown in Figure 99(1-3). The total length of the path is less using the straight path. However, the total power cost shown is  $1.012932 \times 10^8$  N · mm · s, which is higher due to the work done by the rover against gravity is higher. So, by using the same 54 with the same procedure as before, the power cost is calculated to be 2532.33 joules, which indicates a saving of 38.12% .

Appendix A has additional guide notes for co-simulation in setting up, data processing and problems and solutions.

## 9 Validation and Evaluation Through Field Tests

There are a number of field tests undertaken to validate the theoretical work done during the modelling and simulating of the AgriRover behaviour reported in Chapter 9. This chapter details the setup of these tests and the results from them. Conclusions are also drawn in terms of the validation of the theoretical work.

### 9.1 Field Test Task Descriptions

The first field test was conducted at a farmland field called Rushyhill Farm, near Glasgow in the UK. The test has been split into two groups of tests. The first group's tests are focused on the energy optimised planning. The second set of field tests took place in Beijing, which focused on multi-point planning from an energy perspective. Due to technical problems of the AgriRover, the full results based on the original plan were not obtained.

The first set of tests are designed to perform the following tasks:

1. The test is to demonstrate the capability of the planning algorithm by identifying an optimal path for any given points, e.g. from point A to point B.
2. By utilising the energy optimised path planning, another path from point A to point B can be found.
3. Obtaining sufficient data of two tests for comparison:
  - a). the first test is to capture the data set of the energy consumption between a direct, straight or shortest path between the set points,
  - b) the second test is to obtain the data set of energy consumption on a path that has been generated with the designed energy optimised planning algorithm.
4. The results of the two paths are compared and conclusions are drawn.

The second set of field tests is to investigate the scenarios where there are needs for multiple waypoints, and the terrain is also relatively flat. In this case, a path is generated where the task is to transverse multiple points during a field soil sampling operation, which is one of the key functions of the AgriRover.

Similar to the first set of tests, the second set also aims to undertake a comparison study between different ways of multi-point planning. First, the algorithm will find a path for the AgriRover with a straight line, then turning 90 degrees at the edge of the waypoint, forming a rectangular shape. Secondly, the designed algorithm finds a path for the AgriRover with a triangular shape, with the waypoint connected forming an angle of 60 degrees at the edge of the field. The results of these two strategies of planning are compared and conclusions are drawn.

## **9.2 Field Test Setup Description**

### **9.2.1 Power Consumption Test in UK from Point A to B**

Before the field tests, there are functions required to ensure the accuracy and consistency of the tests results of the energy consumption measurements. A voltage and current monitoring module has been designed and implemented onboard the AgriRover for an earlier version of the rover, and this was made available. For the new version of the AgriRover, the voltage and current monitoring PCB are unnecessary, as the new version of the rover has the voltage and current monitoring built into the Pololu jrk 21v3 motor driver. As the motor driver's current and voltage measurement have not been tested before, a validation step has thus been conducted. Figure 100 shows two multimeters attached to the AgriRover, and the total current and voltage data of the of the AgriRover is collected and logged. After the collection of the current and voltage, a multiplication of them is performed to calculate the power consumed.



Figure 100. Field test of current and voltage data validation

Figure 101 (1) shows the total power output in each second that is collected by the multimeters, and Figure 101 (2) shows the power output from the four wheels that is collected by the motor drivers, which shows the calibration field test run. The result has characteristic matches shown by these red circles. As the figure shows, the total power consumption of the rover in Figure 101 (1) is different from that in Figure 101 (2), which is due to the driver output power of the rover as the onboard electronics also have a contribution to the power consumption, such as the search GPS module, IMU module communication module, and onboard computer. Furthermore, the top figure has more power consumption, even during the idling of the rover, because the rover has an onboard computer running, regardless of the speed of the wheels, even during idling and without communication or driver output. However, for this test the goal is to compare the power consumption of the path planning algorithms, therefore only the

motor power consumption will be compared, without the comparison of the rest of the onboard electronics. This is because the onboard electronics, such as the communication module and onboard computer, will have unpredictable power consumption during the field test, due to the communication distance and the calculation loads.

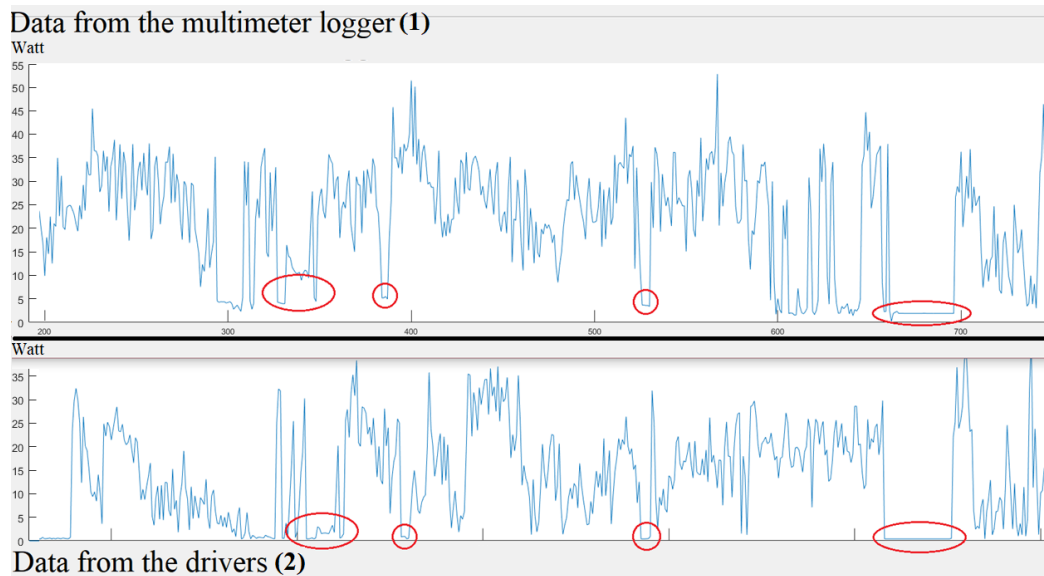


Figure 101. Test power data validation characteristic comparison

The first part of the test that took in place in Rushyhill farm utilises the AgriRover, with added weight to bring the total weight of the AgriRover to 20 kilogram. It traveled at a speed of 0.3 m/s. Before running, with each set of waypoints generated by the algorithm, the voltage of the battery is logged to ensure the power consumption calculations after the test is accurate and valid.

### 9.2.2 Power Consumption Test in Multi-Point Planning

As part of the SmartFarm construction plan, the UK team have demonstrated its latest robotic technology in autonomous soil sampling.

This demonstration is therefore arranged as part of a visit. The key purpose is to show the feasibility of the AgriRover-Sense in autonomous soil sampling at the

National Demonstration Base for Precision Agriculture Research at Xiatoangshan, Beijing.

## **9.3 Path Planning Before the Test**

### 9.3.1 Path Planning in UK Field Tests

As mentioned in Chapter 4, the energy optimised path planning algorithm generates a path from any point A to point B. Then, the waypoints are converted from the National Grid (British National Grid System) to GPS coordinates, which can be used by the AgriRover. The conversion has been done by utilising a MATLAB function named 'OS2LL'. All the waypoints are converted as shown in Table 14, and then they are plotted on the satellite map, as shown in Figure 102. This is the path for the Rover to follow.

Table 14. Energy optimised waypoints set in GPS coordinates

<b>Points</b>	<b>Latitude</b>	<b>Longitude</b>	<b>Points</b>	<b>Latitude</b>	<b>Longitude</b>
1	55.90361	-4.1826	12	55.90395	-4.1835
2	55.90365	-4.18268	13	55.9039	-4.18358
3	55.90369	-4.18277	14	55.90386	-4.18365
4	55.90374	-4.18285	15	55.90381	-4.18373
5	55.90378	-4.18293	16	55.90376	-4.18381
6	55.90382	-4.18301	17	55.90372	-4.18389
7	55.90387	-4.1831	18	55.90367	-4.18396
8	55.90391	-4.18318	19	55.90362	-4.18404
9	55.90395	-4.18326	20	55.90358	-4.18412
10	55.904	-4.18334	21	55.90353	-4.1842
11	55.904	-4.18342	22	55.90353	-4.18428



Figure 102. Energy optimised waypoints plotted on satellite map

Figure 103 shows the 3D view of the energy optimised path starting from the green circle to the destination shown in a magenta diamond, which is generated by the algorithm and focused on energy optimisation. The elevation change data is plotted with a lower interval of height change. It requires the rover to overcome a total of 4.01m, from the lowest point at 78.85m to the highest point at 82.86m, shown in Figure 103 (b).

Figure 104 shows when a straight path is followed by the Rover. The height change data plotted has a higher interval that the rover needs to overcome of 5.63m, from the lowest point at 78.85 m to 84.48m.

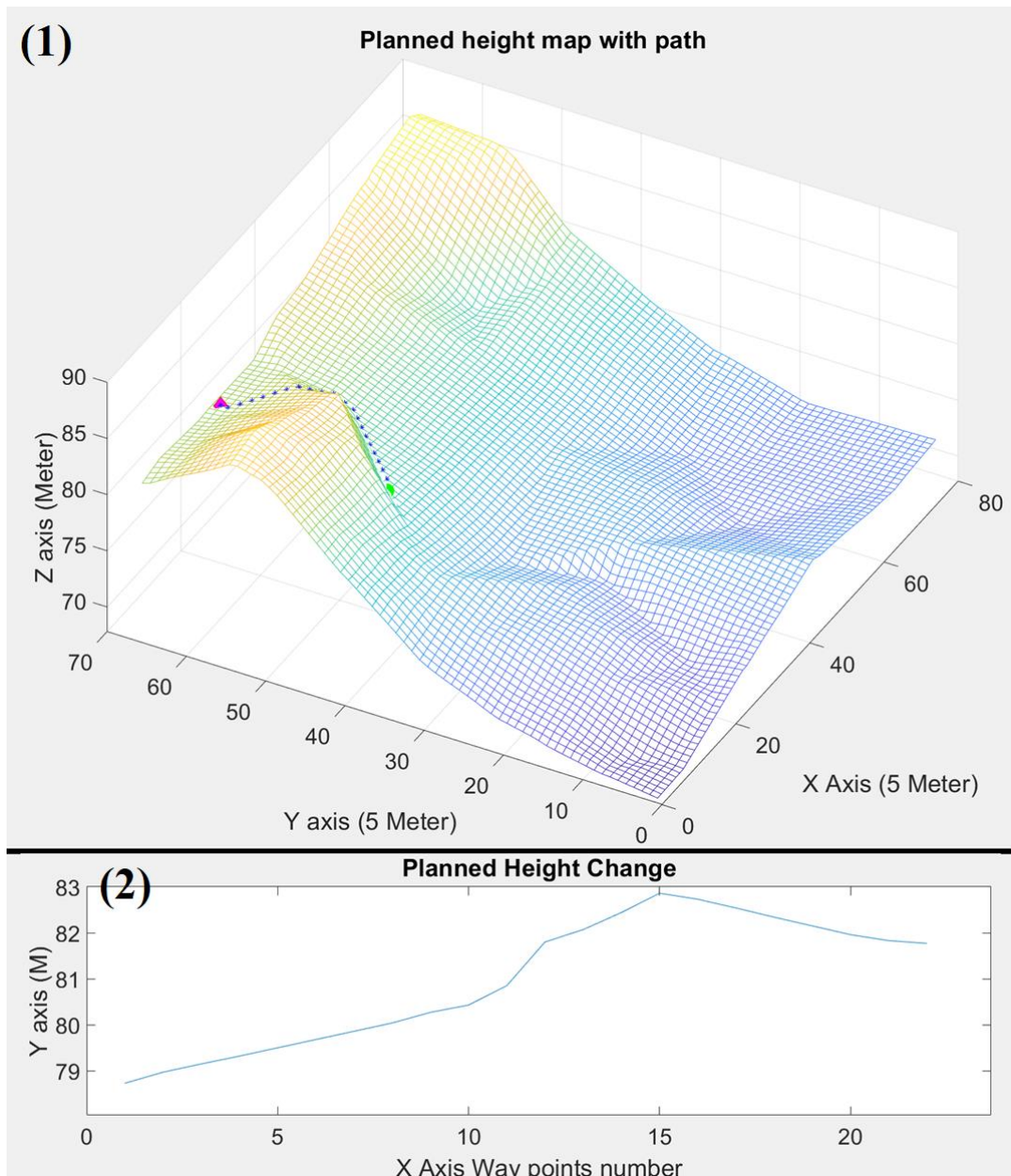


Figure 103. Energy optimised path and height change

As the shown, the height change that the rover needs to overcome with the energy optimised path is 4.01m, compared to the straight path which is 5.63m. This is over 28% of the height change wasted, which is unnecessary and can be avoided.

Furthermore, the energy that is required to overcome such a height change difference will be more than 28%, due to the internal friction of the driving system having a positive correlation with the load. Thus, with a higher torque output required

to climb a steeper slope, the efficiency of the driving system will decrease. The possibility of skating will also increase. That is why dynamic modelling and simulation of the system is required to determine a more accurate result, which has been completed in chapter 8.

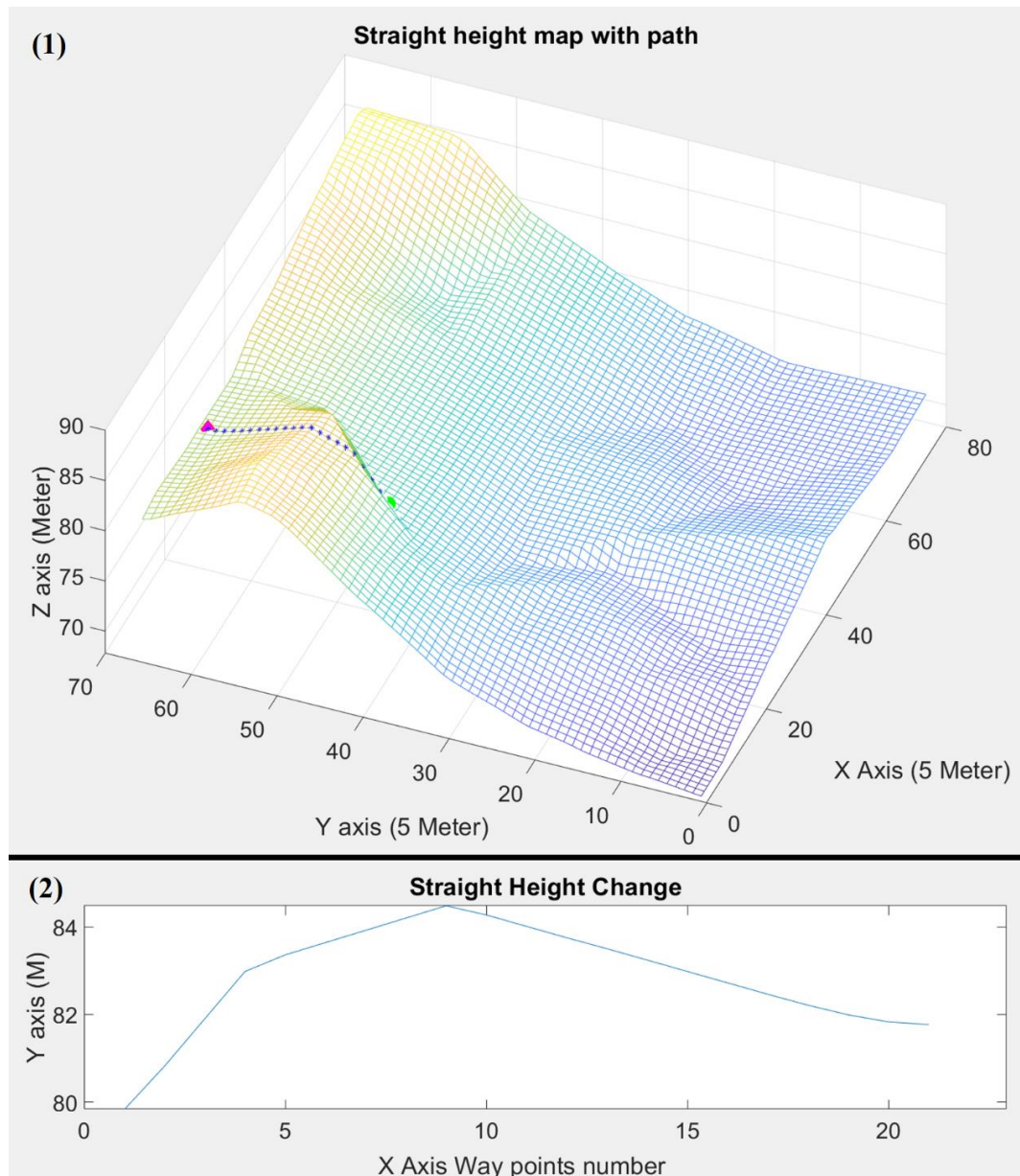


Figure 104. Straight path and height change

Lastly Table 15 shows the coordinates generated by the straight path, and Figure 105 shows the straight path with the coordinates plotted on a satellite map.

Table 15. Straight path waypoint set

<b>Points</b>	<b>Latitude</b>	<b>Longitude</b>	<b>Points</b>	<b>Latitude</b>	<b>Longitude</b>
1	55.90356	-4.182678	12	55.90354	-4.183557
2	55.90356	-4.182758	13	55.90354	-4.183637
3	55.90356	-4.182838	14	55.90354	-4.183717
4	55.90355	-4.182918	15	55.90354	-4.183797
5	55.90355	-4.182998	16	55.90354	-4.183877
6	55.90355	-4.183078	17	55.90354	-4.183957
7	55.90355	-4.183158	18	55.90354	-4.184037
8	55.90355	-4.183238	19	55.90353	-4.184117
9	55.90355	-4.183318	20	55.90353	-4.184197
10	55.90355	-4.183398	21	55.90353	-4.184277
11	55.90355	-4.183477			



Figure 105. Straight path with waypoints plotted on satellite map

### 9.3.2 Multiple Target Point Path Planning

The Centre for Information Technology in Agriculture (NERCITA) has an experimental base called National Demonstration Base for Precision Agriculture Research at Xiatoangshan in Beijing.

Plans for soil sampling have been prepared based on the initial information given by NERCITA, which roughly defines the field to be tested and the selected fields advised by NERCITA. In this case, all 32 blocks of 3-by-3 meter areas have been applied with different amount of fertilisers, hence it is important that a path passing all the centre points of these 32 blocks is generated, so that soil can be collected and the quality measured, in the form of nitrogen. Several plans have been created based on the farms' location, in order to optimise the efficiency of the soil sampling.

The process of planning is described below. Using Google maps, a plan can be created and the location coordinates of each sampling point can be obtained. Following this, several plans have been created using the Google maps. Complying with the best practice in the UK, the soil sampling route is planned in a W-shape, with the distance between each soil sample drilling point being about 20 meters. The exact coordinates of each drilling point can be obtained using a Google map function. The coordinates of each position shown in Figure 106 for a target sampling point can be defined based on its distance from the previous point or the user's choice. Once selected, its coordinates are obtained and recorded.

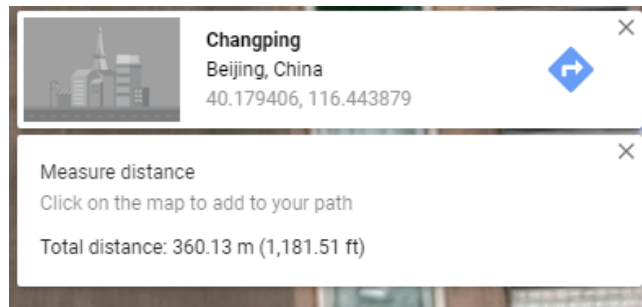


Figure 106. An example plan for soil sampling generated for a target farm at NERCITA

Figure 107 shows an example of a W shape robotic path plan for sampling the targeted farm fields at NERCITA's National Demonstration Base, where as Figure 108 shows an alternative plan for sampling the same targeted fields.



Figure 107. Plan for soling sampling at NERCITA’s National Demonstration Base



Figure 108. An alternative AgriRover robotic path plan

After initial planning, an optimal solution was obtained based on the least effort required by the AgriRover to go over all the waypoints within the defined field, as shown in Figure 109.



Figure 109. A complete robotic soil sampling plan for the NERCITA selected farms

All target points are defined using measurement tools and compiled in a table which could then be used by the AgriRover's soil sampling planner to control the soil sampling and drilling process in the field. Table 16 shows most of the coordinates of the planned sampling points.

Table 16. A potential plan for soil sampling, consists of GPS coordinates and distance information between points.

Sampling Point No.	Distance from Start Point (M)	Position	
Start Point	0	40.179406	116.443879
Point 1	20	40.179376	116.443681
Point 2	40	40.179319	116.443436
Point 3	60	40.179297	116.443210
Point 4	80	40.179252	116.442950
Point 5	100	40.179207	116.442961
Point 6	120	40.179168	116.443215
Point 7	140	40.179153	116.443435
Point 8	160	40.179124	116.443667
Point 9	180	40.179095	116.443915
Point 10	200	40.179066	116.443682
Point 11	220	40.179053	116.443441
Point 12	240	40.179000	116.443208
Point 13	260	40.178971	116.442981
Point 14	280	40.178924	116.442971
Point 15	300	40.178895	116.443205
Point 16	320	40.178859	116.443438
Point 17	340	40.178810	116.443672
Point 18	360	40.177771	116.443892
Point 19	380	40.178634	116.443915
Point 20	400	40.178591	116.443684
Point 21	420	40.178530	116.443460
Point 22	440	40.178475	116.443236
Point 23	460	40.178436	116.443004
Point 24	480	40.178385	116.443012
Point 25	500	40.178350	116.443243
Point 26	520	40.178313	116.443462
Point 27	540	40.178271	116.443711
Point 28	560	40.178237	116.443934
Point 29	580	40.178181	116.443700
Point 30	600	40.178150	116.443470
Point 31	620	40.178106	116.443240
Finish Point	640	40.178053	116.443003

Through further discussion with NERCITA, it became clear that the initial selected field has been divided into 32 small blocks, and each of these blocks have had different fertilisers applied for experimental purposes over several years. It is therefore desirable

to sample each of these blocks, so that a comparison and link to the yield could be made. A new set of plans has thus been developed.

Plan 1, shown in Figure 110, is designed to cover all 32 points in the centre of each block in a sequential manner, following a vertical path. This plan requires the rover to turn 14 times and it never passes any sampling points twice. The total distance the rover travels is 530 meters. The advantage with this plan is that it will travel the least distance.

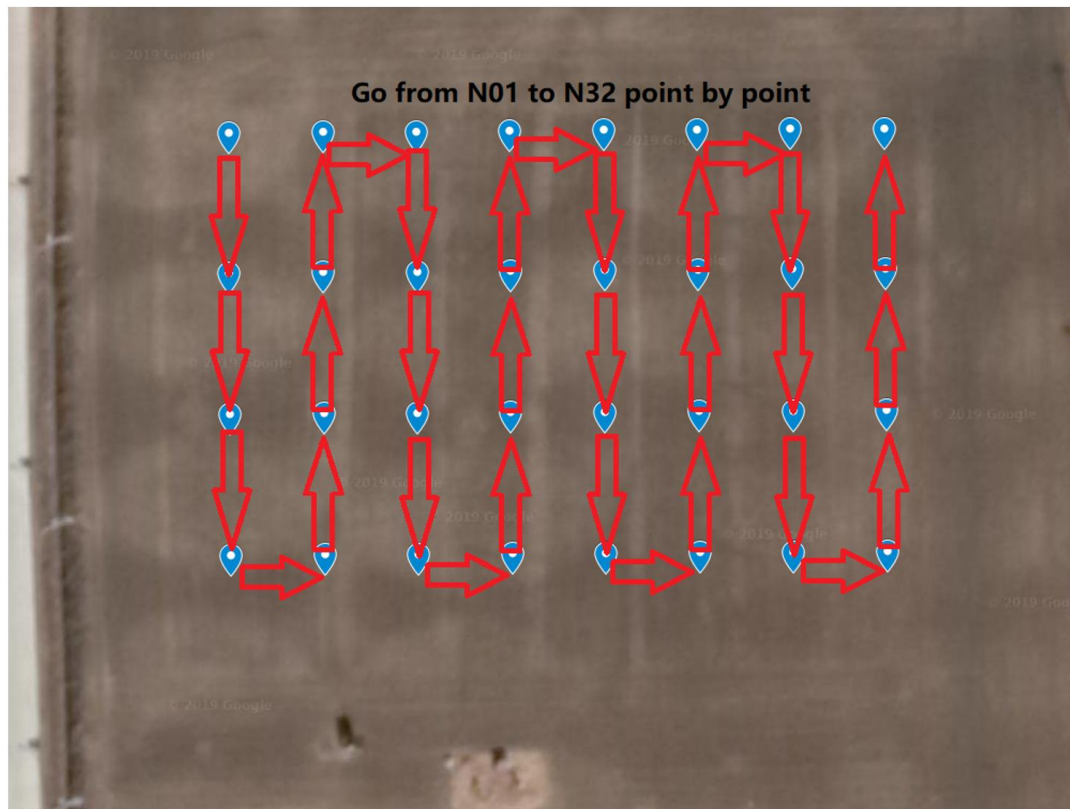


Figure 110. A complete robotic soil sampling plan for the NERCITA selected farms

Plan 2, shown in Figure 111, is also designed to cover all 32 points in the centre of each block in a slightly more complicated pattern along the diagonal direction of each of the blocks. This plan requires the rover to turn 11 times, and it passes twice two sampling points at the bottom left corner. The total distance travelled is 576.9 meters, and this is 46.7 meter or 8.8% more than Plan 1. Based on this, it was decided the Plan 1 was chosen for the field trials.

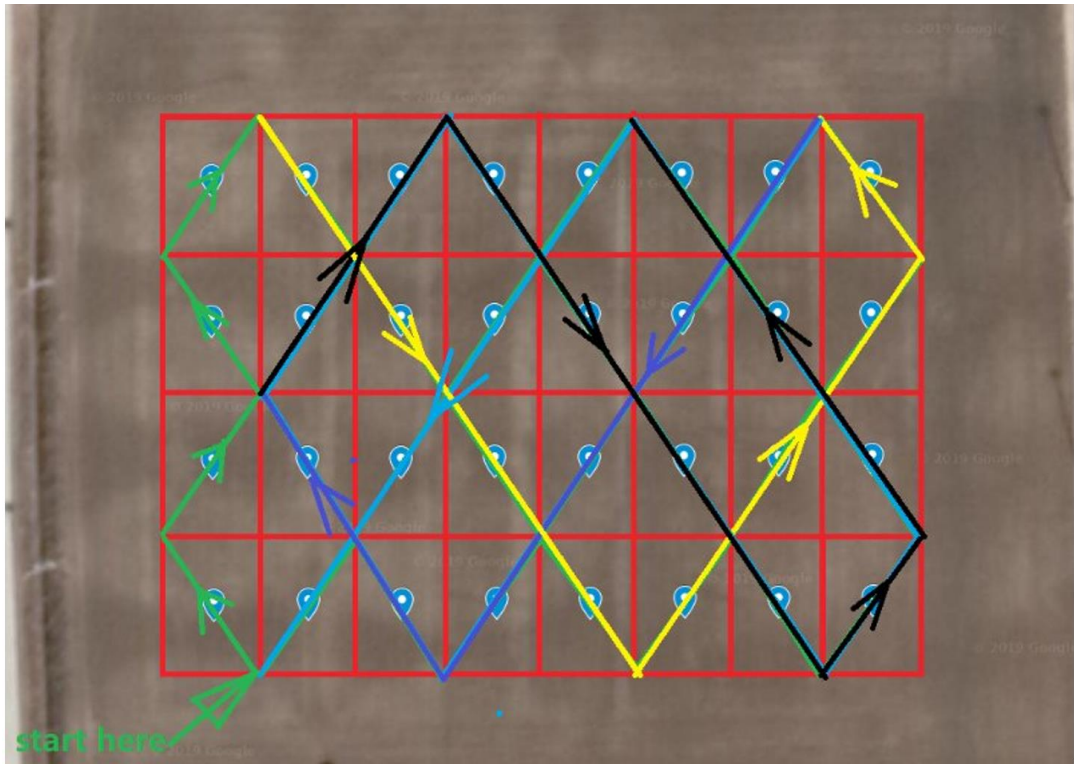


Figure 111. A complete robotic soil sampling plan for the NERCITA selected farms

## 9.4 Overview of the Rushyhill Farm Field Test

The field tests took place in Rushyhill farm, during a sunny winter day without cloud coverage, wind speeds are less than 5 mph, which is considered to be insignificant for the purpose of the tests. The setting of the tests, including the field terrain surface of the remaining stumps of the crops, are shown in Figure 112.



Figure 112. Rushyhill farm field test setting

Temperature on this day was cold at  $-2^{\circ}\text{C}$ , with ice and water on some parts of the test field, as shown Figure 113. This may cause some slippage issues.



Figure 113. Rushyhill farm field test with water and ice.

## 9.5 Result and Data Analysis

### 9.5.1 Rushyhill Farm field Test

The data from the field tests are collected by deploying an onboard data capture system, and the data related to the energy consumption are stored mostly in the computer onboard for offline processing. This is to save the bandwidth required to transfer more important data, such as the measured nitrogen values of the sampled points and their locations, in real-time. The energy related data is processed with a code written to do both the filtering and calculations. First, the data is imported from the '.bag' file, which is extracted from the ROS (Robot Operating System). This contains all the telemetry data of the rover and the contents is customisable. However, with more types of data selected to be captured, the ROS system will have the tendency to lag, which makes the whole system unresponsive and therefore degrades the controllability of the Rover. The telemetry data collected in the .bag file only includes all the motor driving and steering currents, duty cycles and time. This imported data

contains random numbers, which could be caused by the problem of the cross-talking of these numbers outside of the driver communication protocol. For the current, the range is from 0 to 255 in Decimal, which is 0 to 0xFF in Hexadecimal. The current value from 0 to 255 corresponds to 0 to 3 Amperes, according to the datasheet of the motor driver. Duty cycles range from -600 to +600. For the duty cycle the + and – dictates the direction, and the number 0 to 600 corresponds to 0 to 100%. The duty cycle is correlated to the voltage of the battery, which is averaged to 25V during the whole test.

Secondly, all the data is filtered and the number that is not inside of the range is removed. The negative numbers are recovered because of the data overflow, when the number is -1, then the data is 65535, which is 0xffff in hexadecimal, 0b1111 1111 1111 1111 in binary, or 0d65535 in decimal. The real number is the number shown, minus 65534. After all the data is corrected, they are rescaled according to the data sheet from the driver manufacturer.

Then all the data is processed and the power is calculated in Watt, by multiplying the voltage by the duty cycle and current. An example of the power is shown in Figure 114. Figure 114 (1) shows the power needed for the steering motion of the AgriRover, whereas Figure 114 (2) indicates the power needed for the driving motion of the rover from 4 wheels. Both Figure 114 (1) and (2) are for when the rover is following the planned path. Figure 114 (3) and (4) are the result of the power needed for the steering and driving motion of the rover going in a straight line, respectively.

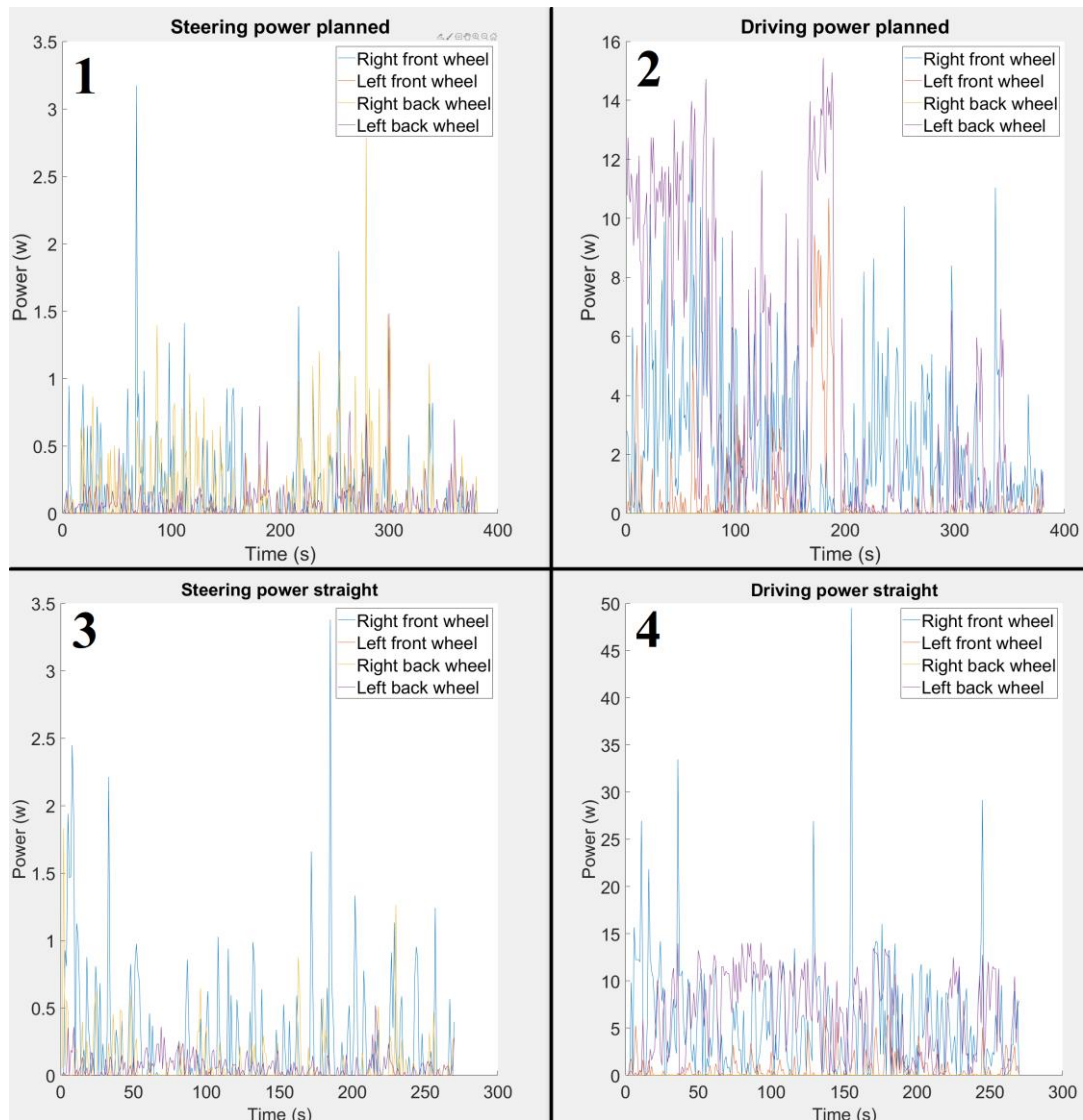


Figure 114. Field test power output from each driving and steering module, planned path compared to the straight path

From these test results, the following analyses are undertaken. First the standard deviation of Figure 114 (2) is lower than that of Figure 114 (4), which suggests the driving system of the AgriRover experiences less change in the power consumption than that of the straight line path. Figure 114 (2) also demonstrates a lower overall peak power required. Observation shows that when driving uphill with a higher incline angle, sometimes only three or four of the wheels have contact with ground, resulting in certain increases of power required on a single wheel. However, for Figure 114 (2) with the energy optimised path, due to the lower incline needed for rover to overcome,

there is less likely a moment where only three out of four wheels are in contact with the ground. Furthermore, the time required to complete is more in Figure 114 (2) for the energy optimised planning when compared to Figure 114 (4) for the straight path.

This is due to the total length of the path having a relationship close to  $1/\sqrt{2}$ .

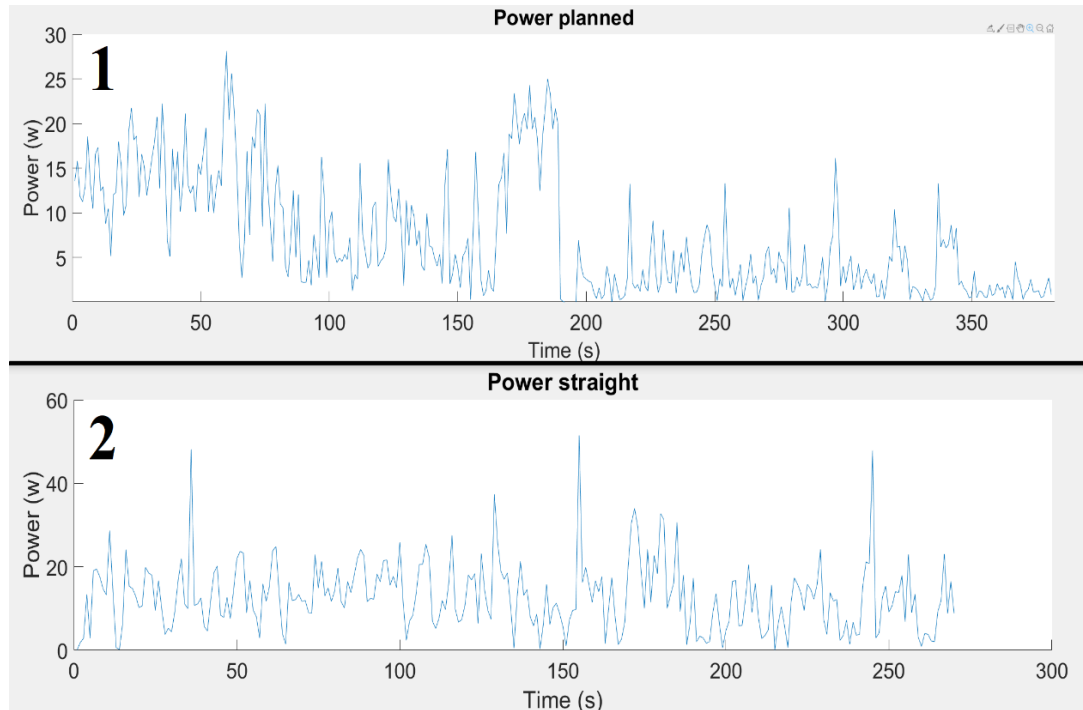


Figure 115. Field test power at a given time for the planned and straight paths

The total power consumed by all the wheels for an optimised path shown in Figure 102, is plotted in Figure 115 (1), which has the output power at a given time. Figure 115 (1) is the planned path, which has the maximum of less than 30 Watts at any given moment, with a standard deviation of 6.53.

Figure 115 (2) is the output power at a given time of the straight path. The figure shows that with the straight path, the maximum power at a given time has been over 50 Watts in multiple instances. A standard deviation of 8.2180 is observed, and this suggests the set of output powers at a given time have a higher randomness.

Finally, the power consumption of the rover is calculated with trapezoidal numerical integration. Shown in Figure 116 is the segments at a given time that are

ready to be processed. Zooming in shows the segmentation of the planned power. As Figure 116 shows, they are all segmented into trapezoidal shapes and can be calculated with integration in the last step of calculation.

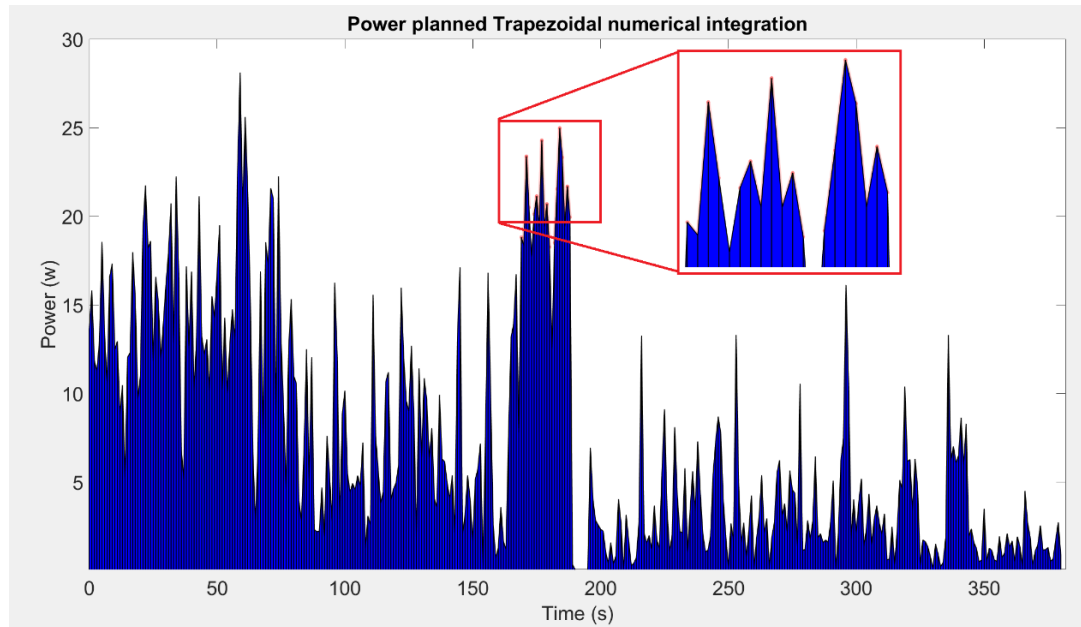


Figure 116. Trapezoidal numerical integration zoomed in

The last step of the calculation is applied to the integral to the power, which will give a final value of total power consumption in joules. For the planned path this is  $3.6405e+03$ , which is 3640.5 joules. The total distance travelled on map is 144.33 m, which is 25.223 joules/meter.

For the straight path, despite it taking less time with a shorter distance travelled, the total power consumption is  $4.6283e+03$ , which is 4628.3 joules. The total distance travelled on the map is 100 m, which is 46.283 joules/meter.

In conclusion, a 21.34% total energy consumption reduction is demonstrated by comparing the total energy consumed on a travelled straight-line path with an energy optimised planned path.

Considering the energy consumed, based on comparing the energy consumption between the energy optimised path of 25.223 joules/meter with the 46.283 joules/meter

for a straight line, it can be concluded that a reduction of 45.50% power per unit distance travelled is shown through these tests. This demonstrated that the proposed modelling and simulation approach is effective in producing an optimised path, as demonstrated in the field tests.

### 9.5.2 Field Test in China

The field test in China was conducted with more difficulties, as the AgriRover was broken during transit and testing, and therefore unfortunately the field test in China is not fully completed, hence there were no test data and results that can be processed. Simulation results are however presented in Section 9.3.2, which suggests a generated energy efficient path plan.

## 9.6 Summary

As mentioned previously in section 8.7, the simulation shows a 38.12% total energy saving with 1,568.54 joules for the planned path and 2,532.33 joules for the straight path. Compared to the field test of 3640.5 joules for the planned path and 4628.3 joules for the straight path, the result of 21.34% of the energy is saved, which is due to a few reasons. The energy consumption reduction rate with unit distance travelled is 45.5%.

First, all the fields have remaining bits of harvest plants, shown previously in Figure 112, which result in different resistance on different parts of the field, and this is denser on some parts of the field. Furthermore, the farmland field in the real world condition has variable rolling resistance, due to the condition of the soil moisture content and the temperature, some parts of the field is muddy and some has ice coverage, which all introduce more randomness to the whole system.

Secondly, as the simulation of the system is based on a static rolling resistance factor, the total power consumption will be different to the real world, as the rolling

resistance is set in the simulation to lower overall values in comparison with the real world. Thus, the overall power consumption in the simulation compared to the field test will be lower. Due to the calculation resource requirement of the ADAMS and MATLAB collaborative simulation, the randomly generated rolling resistant coefficient matrix was not implemented. The full run with the simplified model mentioned in chapter 8, required three days to complete with a computer that is equipped with a 4 core, 8 thread processor and 32GBs of ram. By adding more complexity, the simulation will have a higher rate of crashing, which makes it very difficult to complete in a reasonable time frame.

In addition, there was 2 days of raining before testing, so the farmland around that area, with lower elevation, was muddy and some parts were frozen solid due to the low temperature during the test. This makes it more difficult time for the rover to transverse in the field, due to the increased friction and slippage from the terrain.

## **10 Discussion and Conclusion**

In this chapter a discussion is provided to reflect on the undertaken work and review the work critically. Contribution to knowledge is first presented and further analysed to show the outcome of the research, with detailed description of the contribution presented. In the next section, the discussion of the research outcomes and results are presented. Based on these, conclusions of this research is summarised to provide an outline of the findings of the research. Future research work, which was not completed in this study, is then presented to provide some pointers to advance the energy optimised path planning and mobile robotic modelling in the future.

### **10.1 Contribution to Knowledge**

This research made the following contribution to knowledge:

A comparison and grading of mainstream path planning algorithms from an energy optimisation perspective is undertaken, using detailed evaluation criteria, including required computational power, extendibility, flexibility and more criteria that is relevant for the energy optimised planning purpose. These algorithms have not been compared from an energy optimisation angle before, and research for energy optimised planning under complex terrain environments had not been investigated.

Addressing these knowledge gaps, a methodology of designing, modelling, and simulating a mobile platform system is proposed to facilitate an energy optimised path planning. This leads to a new approach of a path planning algorithm that uses the terrain data available, and that reduces unnecessary energy spent in climbing the terrain. Such a methodology derives several novel methods:

A method for avoiding the local minimum problem for artificial potential field path planning, using the approach of approximation;

A method of achieving high expandability of the path planning algorithm, where this method is capable of generating a path through a large map in a short time period;

A novel method of multi-perspective dynamic simulation, which is capable of simulating the behaviour of internal mechanisms and the overall robotic mobile platform, with the fully integrated control, and the dynamic simulation enables prediction of energy consumption;

A novel method of modelling and analysing the kinematics and motions of a mobile robotic platform; A novel method of mathematically modelling and simplifying a steering mechanism for the wheel-based mobile vehicle was further investigated.

All the above is summarised in Figure 117, and shows the relationships between each contribution, where the blue boxes show the category, and the inner green boxes show the simplified points of contribution to knowledge. The yellow arrows demonstrate the relationships

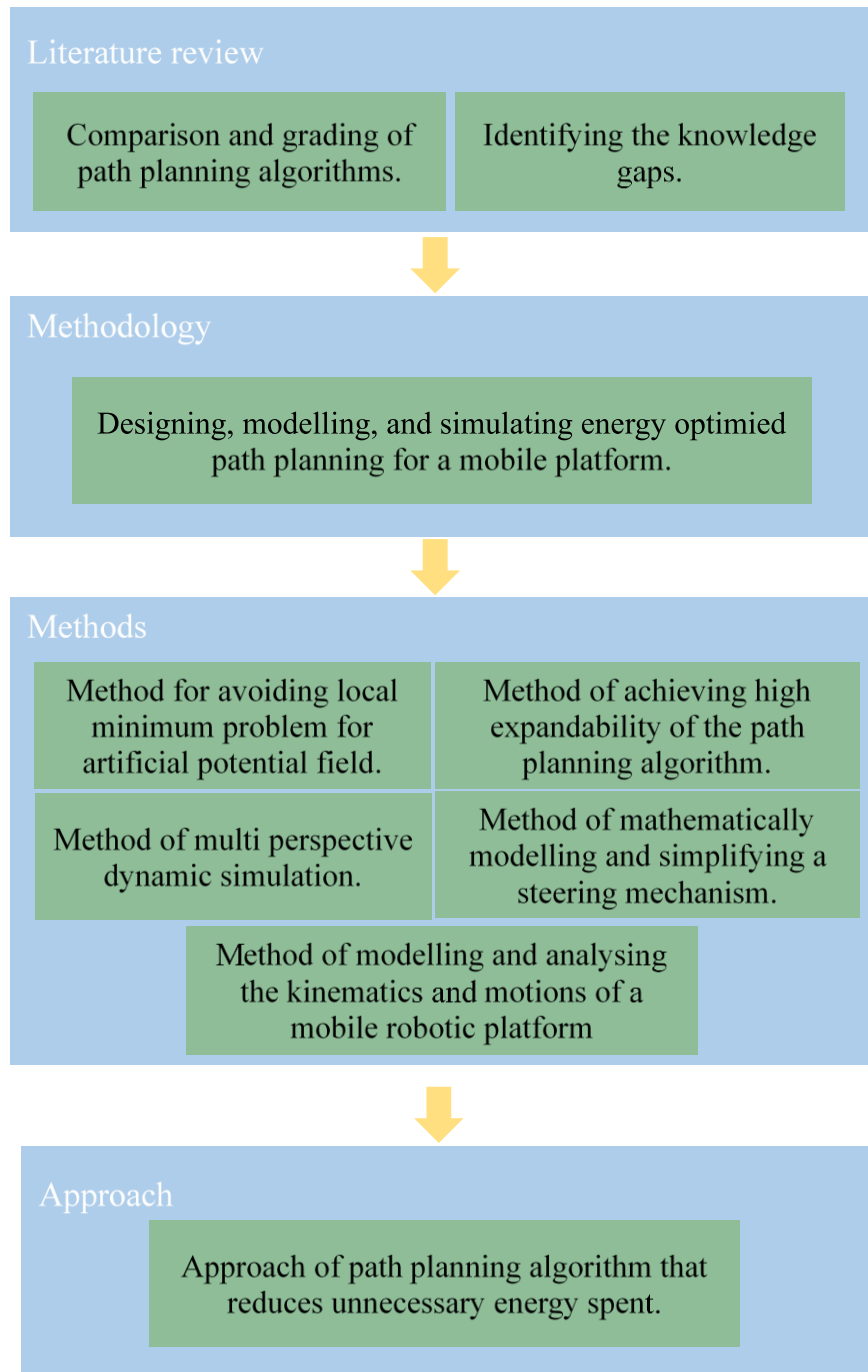


Figure 117. Relationships between each contribution  
Detailed explanation for contribution to knowledge is show as follows:

**A novel approach for the path planning algorithm that reduces unnecessary over crossing of the terrain, using the terrain data available for the public.**

The new approach of the path planning method for energy optimised planning tasks, for a wheel-based rover, have not been proposed before, which is concluded as discussed in Chapter 2. The function of utilising the terrain data for the wheel-based rover to avoid unnecessary over crossing is also enabled, which is adaptable for any terrain, with minimum modifications required. No such method and solution was previously proposed.

**A novel comparison and grading of mainstream path planning algorithms for the purpose of energy optimised planning.**

A complete and comprehensive comparison and review was done in Chapter 2 for all the mainstream path planning methods and algorithms, where the suitability for the task of energy optimisation of the path planning was evaluated and levelled in multiple perspectives. These included ‘Terrain and ground roughness modelling suitability’, ‘Extendibility’, ‘Flexibility’ and ‘Robustness’. This has not been done before for the purpose energy optimised path planning.

**A novel method of mathematically modelling and simplifying a steering mechanism for the wheel-based mobile vehicle.**

A mathematical model of the steering mechanism for the AgriRover was established according to the characteristics of the wheel-based rover, where the electrical and mechanical balance equations were joined, and a system transfer equation was concluded. Then, the system transfer equation was presented in block diagrams, with the simplification of the steering mechanism expressed as a mass spring damper

model. A complete step of modelling and simplification of a physical steering mechanism for the wheel-based rovers is shown in Chapter 5.

**A novel methodology of designing an energy optimised path planning algorithm.**

A new methodology for designing an energy optimised path planning algorithm is proposed in Chapter 3, which gives a guideline and reference for any researchers that will need to develop an energy optimised path planning algorithm for further improvement. The methodology presented is not only suitable for designing the energy optimised path planning algorithm for the AgriRover, but also will work for the purpose of designing an energy optimised path planning algorithm for any mobile robotic platform.

**A novel method for avoiding the local minimum problem for the artificial potential field path planning algorithm.**

The modified artificial potential field path planning method introduces a novel approach to tackling the problem of the local minimum by utilisation of an approximation algorithm. When every step is taken, the intermediate matrix that has the problem of the local minimum will become more and more uni-polarised, and the step size is decided according to the length between the start and destination points. This method solves the problem of the local minimum, which will guarantee a path that can be found with minimum loss of performance. This method of solving the problem of the local minimum for the artificial potential field path planning algorithm has never been presented before.

**A novel method of achieving high expandability of the energy optimised path planning algorithm, that can be extended to**

**include the variables of distance, terrain, uncrossable obstacles and surface materials, which is the characteristics of the practical mobile robotic platform's application environment.**

This is shown in Figure 16 and proposed in Chapter 4. By utilising a global artificial potential field calculation equation, where each of the required inputs is merged into a single artificial potential field, that was done by converting each physical matrix and then applying a weight factor. Therefore, the expandability of the algorithm is achieved. This high expandability for the energy optimised path planning algorithm has not been presented before.

**A novel method of simulating the behavior of the robotic mobile platform, with full integration of the control algorithm, and which gives the energy consumption.**

A novel method of simulating the control algorithms running in parallel, and utilising the collaborative simulation platform of ADAMS and Simulink for a robotic mobile platform has been introduced in Chapter 8. The simulation has been run using the real world terrain, and has the capability of following a generated path by the energy optimised path planning algorithm, which has not been achieved before.

**A novel method of modelling and analysing the kinematics and motions of the AgriRover, under different levels of ISO 8608 surface conditions, obstacles, loads, and speed and torque changes on the farmland field, sand and cement.**

Modelling and simulation of the AgriRover gives a resulting change of speed when running on different surface levels and shaped obstacles, which is discussed in Chapter

6. Furthermore, speed and torque changes are logged when the AgriRover is operating in a farmland field, sand and cement, as discussed in Chapter 7.

## **A novel approach to path planning that reduces unnecessary energy spent in a rich terrain environment.**

The path planning approach that can reduce the unnecessary energy used running in a rich terrain environment was designed, implemented, tested, validated, and evaluated under the guidance of systematic methods and methodologies. This is a unique and generic approach to such a problem with very low computational demand that gives a good result.

All the approaches and methods presented give a detailed process and methodologies, which can be used as reference for researchers who will be working on solutions that is related to all the problems that have been solved in this thesis.

## **10.2 Discussion**

### **10.2.1 Hypothesis Discussion**

First, the hypothesis that is introduced in Section 1.4.3 is discussed. The last stage of the hypothesis was set as:

The total energy costs of the same planning task when using the energy optimised path planning algorithm, utilising the AgriRover in an undulating terrain environment, is lower than when the AgriRover is running in a straight-line.

This hypothesis is proved by running the simulations and field experiments with the AgriRover, using the path generated by the energy optimised planning algorithm in the farming field.

As mentioned previously in Section 8.7, the collaboratively dynamic simulation shows a 38.12% total energy saving, with 1568.54 joules for the cooperative planned path and 2532.33 joules for the straight-line path. Compared to the field tests in Chapter 9, 3640.5 joules for the planned path and 4628.3 joules for the straight-line path, resulting in 21.34% of the energy being saved, which is different due to a few reasons. The energy consumption reduction rate, with unit distance travelled, is a 45.5% reduction, which proves the energy optimised path has successfully reduced the energy consumption by avoiding unnecessary terrain overcrossing.

Comparing the energy consumption saved for the simulation results of 38.12% and field test results of 21.34%, a difference of 16.78% is observed. The difference is mainly caused by the following: the collaborative simulation's coefficient of rolling friction is set to 0.2, which was discussed in Section 7.1. However, on the day of the field test, the ground surface condition was wet and muddy, as shown in Figure 113, and therefore the coefficient of the rolling friction was actually higher. Subsequently, the base energy cost is higher than in the simulation when the rover is running in the farm field. This is the major reason for the difference in energy savings between the simulation and field test. Also, it is the reason of the energy cost difference between the 1568.54 joules for the simulation and 3640.5 joules for the field test of the energy optimised path, and the 2532.33 joules for the simulation and 4628.3 joules for the field test of the straight-line path. More detailed discussion is in Section 9.6. So, overall the hypothesis is proved as the result showed.

The null hypothesis was set as:

Even with the energy optimised path planning algorithm utilised by the AgriRover, the total energy cost is the same or higher than the straight-line planning under the same planning task running in an undulating terrain environment.

This is not true as the simulation and field test result proved, as mentioned above.

## 10.2.2 Aims Discussion

For the aims proposed in section 1.4.4, the first aim is completed by a new proposed energy optimised path planning method, which is capable of generating a path for the AgriRover, while simultaneously avoiding the problem of unnecessary terrain overcrossing when running in terrain rich environment.

The second aim is that the expandability of the algorithm is insured by a comprehensive review of all the major path planning methods for the purpose of an energy optimised path planning, which was completed in Chapter 2. This was where the expandability of each type of mainstream algorithm is rated according to the literature reviewed. Furthermore, the design of the algorithm used a modified and improved artificial potential field, where the expandability is a part of the consideration introduced in Chapter 3. The additional input matrix, such as obstacles or windspeeds, can be used to construct the potential field according to the physical properties and task requirements if necessary, which is discussed in Chapter 4.

The third aim is about the adaptability of the algorithm if the new platform is a wheel-based rover. The designed algorithm is adaptable with minimal modifications required, due to the design of the algorithm where only the size, weight and power need to be modified. Also enabled is the function of utilising the terrain data and thus is adaptable for any terrain.

The last aim was to make complete and comprehensive modelling and simulations of the AgriRover, which is achieved and discussed in Chapters 5, 6, 7 and 8, each focused on a different aspect. The modelling and simulation of the AgriRover gives an understanding of the mathematical and physical characteristics of the AgriRover, therefore providing a guideline for the design and evaluation of the path planning algorithm.

The objectives of the project are proposed in Section 1.4.4. The objectives of the energy optimised designing focus are achieved, as mentioned before. Secondly, the terrain data for the farmland field test is used as the major consideration when designing the energy optimised path planning algorithm. Thirdly, the modelling and simulating of the energy consumption is done with the results for both compared in this Chapter and Chapter 9, as well as the result of the field test that has been compared and evaluated. Finally, the evaluation and conclusions are proposed on the total energy saved and energy saved per unit during the field test.

### 10.2.3 Overall Discussion

This thesis shows a complete process of developing an energy optimised path planning algorithm that covers a definition of needs, complete and comprehensive modelling of the rover, designing of the algorithm, collaborative simulation that is both capable of representing a detailed model of the AgriRover and capable of implementing a control algorithm for trajectory, and a field test that was carried out with data that has been analysed and concluded.

As discussed before, the field test shows a result of 21.34% total energy saved, which is a significant amount of energy saved. As shown in Figure 114, the peak power of the planned path is less than 16 Watt, but the straight path is close to 50 Watt, during the field test. This is the other benefit of utilising an energy optimised path that minimises the unnecessary overcrossing of the terrain. A lower peak output needed for the motor means less required torque to complete the path, which means a less steep terrain, and therefore less possibilities for the AgriRover to get stuck on the terrain. Furthermore, lower and less frequent torque peaks will extend the lifespan of the mobility systems, which include the motors, gearbox, steering mechanism, suspension, wheel and tires. This results in a lower cost of maintenance and thus lowers the

operational costs and overall total cost, which will give new technology, such as the AgriRover, an even better feasibility for mass production and adoption.

## **10.3 Future Work and Improvement**

### **10.3.1 An Energy Optimised Path Planning Method for Multiple Robots**

As mentioned previously, the path learning algorithm utilises an artificial potential field as the evidence for pathfinding, therefore it is practical to introduce an additional matrix field containing the real-time positioning of multiple rovers. As evaluated before, the path planning algorithm that utilises the artificial potential field, uses less computational requirement compared to other path planning algorithms, such as reinforcement learning and genetic algorithms. This makes it possible to be implanted in the onboard computer of the rover, and running the path planning algorithm in real time.

Such architectures can be made as a centralised or decentralised cluster, depending on the application. For a centralised cluster architecture, there will be structure master and slaves. The master can be a ground-station or a particular rover where all the other rover report to. Then a current position matrix can be generated and broadcasted to all the rovers. For a decentralised cluster architecture, each rover will have their own position sent via a data link, where only the neighbouring rovers, or rovers within a certain radius, will have the position data around them, which is enough to avoid collision.

Both of the architectures have their benefits and limitations. For the centralised cluster architecture, the planning algorithm will have a real-time position of each rover, and therefore is more controllable for planning a task. The limitations include the communication distance of the radio equipment being limited, therefore the

performance of the task solving capability of the cluster will degrade when the size of the cluster or the distance between them increases. For the decentralized cluster architecture, this problem is avoided because each member of the cluster only needs to communicate within a certain radius, but the capability of the centralised planning will be hard to achieve.

To solve this problem, the architecture of the rovers can be working in hybrid mode, where the control centre sends the tasks to the rovers that is within the communication radius, then the task is passed to all the rovers via a data-link, and the position of the rovers are sent back. Although this will increase the load on each of the rover due to the additional data that needs to be repeated, which may require a hardware upgrade, this is a solution for a collaborative multi-rover architecture that can be researched in the future.

### 10.3.2 AgriRover Hardware Update

Although the design of the AgriRover is not part of the research, there is involvement of fabrication improvement parts for the AgriRover during the research. However due to the reason of being a prototype there was undesirable electronic and mechanical anomalies which include backlashes of the wheels and steering mechanisms. The electronic anomalies is mostly costed by the interconnection of the AgriRover where a control and communication signal is communicated over wire via USB and the USB port on the motherboard of the AgriRover is directly connected to the central processing chip with a logic level transformer without additional protection, therefore the charge is from outside generated by friction have a direct unprotected path to the CPU chip and all the other unprotected USB devices. This problem was solved by introducing a USB anti-static protection board. For the anomalies generated with the mechanical system there is a few cost first it's the motor gearbox in combination selected has a backlash of  $\pm 2$  deg therefore the steering motion of the

vehicle has a hard time of keeping straight, second the encoder that that been used has a limited resolution which further increased the possibility of a anomaly during the operation. This is solved with a new version of AgriRover using better positioned motors gearboxes combination and encoders that has better resolution.

### 10.3.3 GPS Accuracy

The GPS accuracy of the Rover is sometimes unstable, which was improved by adding a stationary GPS receiver and by sending the data back to the rover. Also, a differential algorithm has been implemented to improve the accuracy, but the result of the GPS accuracy is still sometimes unstable. The other problem of the GPS is drifting, which happens sometimes during the normal running off the rover. An attempt to fix this was made with an additional onboard inertia measurement unit, or other sensors, such as cameras for terrain feature matching could be used. However, by introducing more complexity, the overall system has a reduction in the communication speed, as the Robot Operating System used is not a real-time system and has a reduction of reliability, thus a balance must be found.

## 10.4 Conclusion

This thesis has demonstrated a complete methodology and process of designing, modelling, simulating and testing an energy optimised path planning method for mobile robotic platforms. Not only does this thesis give a systematic approach to solving the problem of energy optimised path planning in a terrain rich environment, but also a model of corresponding methodology is proposed, followed and evaluated through a design on an established mobile robotic platform, named the AgriRover. The modelling and simulation is established, which shows a result of 38.12% total energy saved compared to a straight path. This energy saving is particularly high, because slipping occurred when following the straight-line path. Due to the soil and weather condition of the experimentation, a lower result of 21.34% total energy saved, in

comparison to a straight path, is saved. This 21.34% total energy saving demonstrates the effectiveness of the new approach of the energy optimised path planning method.

The time consumption between the map size of 5,000 points, which cost 0.638s, and with 1,000,000 points, which cost 2.08s, presented in Section 4.9, shows the expandability of the energy optimised path planning algorithm. This result difference of 16.78% energy saved between the simulation and experimentation proves the viability and practicality of the modelling, simulation and experimentation processes. Furthermore, with all the satisfactory results, the methodology for designing an energy optimised path planning method is proved and demonstrated to be able to bring much benefits of saving energy in other energy-crucial applications.

Several future research directions have also been identified and it is believed that further investigation in these areas will provide further knowledge to advancing the mobile platform energy optimised design and control. This complies and meets the current energy efficiency drive worldwide, as exemplified by the push for net-zero in 2050. The proposed work has the potential to be exploited in applications where there is rich terrain features and there is a demand for energy optimisation.

# References

## Uncategorized References

- Agostinacchio, M., Ciampa, D. and Olita, S. (2014) 'The vibrations induced by surface irregularities in road pavements—a Matlab® approach'. *European Transport Research Review*, 6 (3), pp. 267-275.
- Agrawal, A., Simon, G. and Karsai, G. (2004) 'Semantic translation of simulink/stateflow models to hybrid automata using graph transformations'. *Electronic Notes in Theoretical Computer Science*, 109 43-56.
- Albers, D., Radlmayr, J., Loew, A., Hergeth, S., Naujoks, F., Keinath, A. and Bengler, K. (2020) 'Usability Evaluation—Advances in Experimental Design in the Context of Automated Driving Human–Machine Interfaces'. *Information*, 11 (5), pp. 240.
- Amidi, O. and Thorpe, C.E. (1991) Published. 'Integrated mobile robot control'. *Mobile Robots V*, 1991. International Society for Optics and Photonics, pp.504-523.
- Andren, P. (2006) 'Power spectral density approximations of longitudinal road profiles'. *International Journal of Vehicle Design*, 40 (1-3), pp. 2-14.
- Ángel, L., Pérez, M., Díaz-Quintero, C. and Mendoza, C. (2012) Published. 'Adams/matlab co-simulation: Dynamic systems analysis and control tool'. *Applied Mechanics and Materials*, 2012. Trans Tech Publ, pp.527-531.
- Arras, K.O., Tomatis, N., Jensen, B.T. and Siegwart, R. (2001) 'Multisensor on-the-fly localization:: Precision and reliability for applications'. *Robotics and Autonomous Systems*, 34 (2-3), pp. 131-143.
- Bačík, J., Ďurovský, F., Biroš, M., Kyslan, K., Perdukova, D. and Padmanaban, S. (2017) 'Pathfinder–development of automated guided vehicle for hospital logistics'. *Ieee Access*, 5 26892-26900.
- Bansal, J.C. (2019) 'Particle swarm optimization'. *Evolutionary and swarm intelligence algorithms*. Springer, pp. 11-23.
- Bechtel, R. (2013) 'Multi-mission radioisotope thermoelectric generator (MMRTG)'. *Fact Sheet, NASA*.
- Benton, J., Coles, A. and Coles, A. (2012) Published. 'Temporal planning with preferences and time-dependent continuous costs'. *Proceedings of the International Conference on Automated Planning and Scheduling*, 2012.
- Bhounsule, P.A., Cortell, J. and Ruina, A. (2012) 'Design and control of Ranger: an energy-efficient, dynamic walking robot'. *Adaptive Mobile Robotics*. World Scientific, pp. 441-448.
- Bing, H., Gang, L., Jiang, G., Hong, W., Nan, N. and Yan, L. (2011) Published. 'A route planning method based on improved artificial potential field algorithm'. *2011 IEEE 3rd International Conference on Communication Software and Networks*, 2011. IEEE, pp.550-554.
- Blum, C. (2005) 'Ant colony optimization: Introduction and recent trends'. *Physics of Life reviews*, 2 (4), pp. 353-373.
- Borg, J.C., Yan, X.-T. and Juster, N.P. (2000) 'Exploring decisions' influence on life-cycle performance to aid “design for Multi-X”’. *Artificial Intelligence for Engineering Design, Analysis and Manufacturing*, 14 (2), pp. 91-113.

- Boroujeni, Z., Goehring, D., Ulbrich, F., Neumann, D. and Rojas, R. (2017) Published. 'Flexible unit A-star trajectory planning for autonomous vehicles on structured road maps'. *2017 IEEE international conference on vehicular electronics and safety (ICVES)*, 2017. IEEE, pp.7-12.
- Bounini, F., Gingras, D., Pollart, H. and Gruyer, D. (2017) Published. 'Modified artificial potential field method for online path planning applications'. *2017 IEEE Intelligent Vehicles Symposium (IV)*, 2017. IEEE, pp.180-185.
- Bradley, D.A., Seward, D., Dawson, D. and Burge, S. (2000) *Mechatronics and the design of intelligent machines and systems*. Crc Press.
- Canfield, S.L., Hill, T.W. and Zuccaro, S.G. (2019) 'Prediction and experimental validation of power consumption of skid-steer mobile robots in manufacturing environments'. *Journal of Intelligent & Robotic Systems*, 94 (3), pp. 825-839.
- Carreno, Y., Pairet, E., Ardón, P., Petillot, Y. and Petrick, R.P. (2020) 'Task Allocation and Planning for Offshore Mission Automation'.
- Chen, T., Zhang, G., Hu, X. and Xiao, J. (2018) Published. 'Unmanned aerial vehicle route planning method based on a star algorithm'. *2018 13th IEEE Conference on Industrial Electronics and Applications (ICIEA)*, 2018. IEEE, pp.1510-1514.
- Cheraghpour, F., Vaezi, M., Jazeh, H.E.S. and Moosavian, S.A.A. (2011) Published. 'Dynamic modeling and kinematic simulation of Stäubli© TX40 robot using MATLAB/ADAMS co-simulation'. *2011 IEEE International Conference on Mechatronics*, 2011. IEEE, pp.386-391.
- Christophe, F., Coatanea, E. and Bernard, A. (2014) 'Conceptual Design'. In: Laperrière, L. and Reinhart, G. (eds.) *CIRP Encyclopedia of Production Engineering*. Berlin, Heidelberg: Springer Berlin Heidelberg, pp. 275-281.
- Cochran, L.D., Hunt, B.D. and Laiche, T.P. (2020) 'FRMAC Assessment Manual Volume 2: Pre-assessed Default Scenarios-RTG Scenario for Mars 2020 Launch'.
- Conley, D.J., Paerl, H.W., Howarth, R.W., Boesch, D.F., Seitzinger, S.P., Havens, K.E., Lancelot, C. and Likens, G.E. (2009) 'Controlling eutrophication: nitrogen and phosphorus'. *Science*, 323 (5917), pp. 1014-1015.
- Coulter, R.C. (1992) 'Implementation of the pure pursuit path tracking algorithm'.
- Crick, F. and Clark, J. (1994) 'The astonishing hypothesis'. *Journal of Consciousness Studies*, 1 (1), pp. 10-16.
- Crisp, J.A., Adler, M., Matijevic, J.R., Squyres, S.W., Arvidson, R.E. and Kass, D.M. (2003) 'Mars exploration rover mission'. *Journal of Geophysical Research: Planets*, 108 (E12), pp.
- Curran, P. (1983) 'Multispectral remote sensing for the estimation of green leaf area index'. *Philosophical Transactions of the Royal Society of London. Series A, Mathematical and Physical Sciences*, 309 (1508), pp. 257-270.
- Das, S.S., Parhi, D.R. and Mohanty, S. (2018) 'Insight of a six layered neural network along with other AI techniques for path planning strategy of a robot'. *Emerging trends in engineering, science and manufacturing (ETESM-2018)*, IGIT Sarang, India.
- Datouo, R., Motto, F.B., Zobo, B.E., Melingui, A., Bensekrane, I. and Merzouki, R. (2017) Published. 'Optimal motion planning for minimizing energy consumption of wheeled mobile robots'. *2017 IEEE International Conference on Robotics and Biomimetics (ROBIO)*, 2017. IEEE, pp.2179-2184.

- Davidson, E.J. (2005) *Evaluation methodology basics: The nuts and bolts of sound evaluation*. Sage.
- Dodds, C. and Robson, J. (1973) 'The description of road surface roughness'. *Journal of sound and vibration*, 31 (2), pp. 175-183.
- Domenech, A., Domenech, T. and Cebrian, J. (1987) 'Introduction to the study of rolling friction'. *American Journal of Physics*, 55 (3), pp. 231-235.
- Dorigo, M., Birattari, M. and Stutzle, T. (2006) 'Ant colony optimization'. *IEEE computational intelligence magazine*, 1 (4), pp. 28-39.
- Dréo, J. and Siarry, P. (2002) Published. 'A new ant colony algorithm using the heterarchical concept aimed at optimization of multim minima continuous functions'. *International Workshop on Ant Algorithms*, 2002. Springer, pp.216-221.
- Farnham, T., Jones, S., Aijaz, A., Jin, Y., Mavromatis, I., Raza, U., Portelli, A., Stanoev, A. and Sooriyabandara, M. (2021) Published. 'UMBRELLA Collaborative Robotics Testbed and IoT Platform'. *2021 IEEE 18th Annual Consumer Communications & Networking Conference (CCNC)*, 2021. IEEE, pp.1-7.
- French, M.J., Gravdahl, J. and French, M. (1985) *Conceptual design for engineers*. Springer.
- French, R.H. (1985) *Open-channel hydraulics*. McGraw-Hill New York.
- Gajic, Z. and Lelic, M. (1996) *Modern control systems engineering*. Prentice-Hall, Inc.
- Galvagno, E., Velardocchia, M. and Vigliani, A. (2011) 'Dynamic and kinematic model of a dual clutch transmission'. *Mechanism and machine theory*, 46 (6), pp. 794-805.
- Gao, H., Deng, Z., Ding, L. and Wang, M. (2012) 'Virtual simulation system with path-following control for lunar rovers moving on rough terrain'. *Chinese Journal of Mechanical Engineering*, 25 (1), pp. 38-46.
- Gaskell, M. and Smith, R. (2007) 'Nitrogen sources for organic vegetable crops'. *HortTechnology*, 17 (4), pp. 431-441.
- Georgakopoulos, D. and Jayaraman, P.P. (2016) 'Internet of things: from internet scale sensing to smart services'. *Computing*, 98 (10), pp. 1041-1058.
- Gerland, P., Raftery, A.E., Ševčíková, H., Li, N., Gu, D., Spoorenberg, T., Alkema, L., Fosdick, B.K., Chunn, J. and Lalic, N. (2014) 'World population stabilization unlikely this century'. *Science*, 346 (6206), pp. 234-237.
- Golnaraghi, F. and Kuo, B.C. (2017) *Automatic control systems*. McGraw-Hill Education.
- Govaers, F. (2019) *Introduction and Implementations of the Kalman Filter*. BoD—Books on Demand.
- Gregar, J. (1994) 'Research Design (Qualitative, Quantitative and Mixed Methods Approaches)'. *Book published by SAGE Publications*, 228.
- Haslum, P., Lipovetzky, N., Magazzeni, D. and Muise, C. (2019) 'An introduction to the planning domain definition language'. *Synthesis Lectures on Artificial Intelligence and Machine Learning*, 13 (2), pp. 1-187.
- Hassan, R., Cohanim, B., De Weck, O. and Venter, G. (2005) Published. 'A comparison of particle swarm optimization and the genetic algorithm'. *46th AIAA/ASME/ASCE/AHS/ASC structures, structural dynamics and materials conference*, 2005. pp.1897.
- Hirahara, S., Oliveira, I.C. and Santhanam, R. (2018) Published. 'NP-hardness of minimum circuit size problem for OR-AND-MOD circuits'. *33rd Computational Complexity Conference (CCC 2018)*, 2018. Schloss Dagstuhl-Leibniz-Zentrum fuer Informatik.

- Hoffmann, J., Hermanns, H., Klauck, M., Steinmetz, M., Karpas, E. and Magazzeni, D. (2020) Published. 'Let's Learn Their Language? A Case for Planning with Automata-Network Languages from Model Checking'. *Proceedings of the AAAI Conference on Artificial Intelligence*, 2020. pp.13569-13575.
- Hou, L., Zhang, L. and Kim, J. (2019a) 'Energy modeling and power measurement for mobile robots'. *Energies*, 12 (1), pp. 27.
- Hou, L., Zhang, L. and Kim, J. (2019b) 'Energy Modeling and Power Measurement for Three-Wheeled Omnidirectional Mobile Robots for Path Planning'. *Electronics*, 8 (8), pp. 843.
- Howe, K. and Eisenhart, M. (1990) 'Standards for qualitative (and quantitative) research: A prolegomenon'. *Educational researcher*, 19 (4), pp. 2-9.
- Huete, A., Didan, K., Miura, T., Rodriguez, E.P., Gao, X. and Ferreira, L.G. (2002) 'Overview of the radiometric and biophysical performance of the MODIS vegetation indices'. *Remote sensing of environment*, 83 (1-2), pp. 195-213.
- Hulley, S.B. (2007) *Designing clinical research*. Lippincott Williams & Wilkins.
- Hussain, R. and Zeadally, S. (2018) 'Autonomous cars: Research results, issues, and future challenges'. *IEEE Communications Surveys & Tutorials*, 21 (2), pp. 1275-1313.
- Hwang, Y.K. and Ahuja, N. (1992) 'A potential field approach to path planning'. *IEEE Transactions on Robotics and Automation*, 8 (1), pp. 23-32.
- ISO (1995) 'Mechanical vibration—road surface profiles—reporting of measured data'. *International Organization for Standardization, Switzerland*.
- Iwashita, K. and Oda, M. (1998) 'Rolling resistance at contacts in simulation of shear band development by DEM'. *Journal of engineering mechanics*, 124 (3), pp. 285-292.
- Jayaraman, P., Yavari, A., Georgakopoulos, D., Morshed, A. and Zaslavsky, A. (2016) 'Internet of things platform for smart farming: Experiences and lessons learnt'. *Sensors*, 16 (11), pp. 1884.
- Jones, R. and Lee, G.F. (1982) 'Recent advances in assessing impact of phosphorus loads on eutrophication-related water quality'. *Water Research*, 16 (5), pp. 503-515.
- Kani, A.N. (1998) *Control systems*. RBA Publications.
- Keidar, M. and Kaminka, G.A. (2012) Published. 'Robot exploration with fast frontier detection: Theory and experiments'. *Proceedings of the 11th International Conference on Autonomous Agents and Multiagent Systems-Volume 1*, 2012. pp.113-120.
- Kempenaar, C., Lokhorst, C., Bleumer, E., Veerkamp, R., Been, T., van Evert, F., Boogaardt, M., Ge, L., Wolfert, J. and Verdouw, C. (2016) 'Big Data analysis for smart farming: results of TO2 project in theme food security'.
- Kennedy, J. and Eberhart, R. (1995) Published. 'Particle swarm optimization'. *Proceedings of ICNN'95-international conference on neural networks*, 1995. IEEE, pp.1942-1948.
- Khan, A., Noreen, I. and Habib, Z. (2018) Published. 'An energy efficient coverage path planning approach for mobile robots'. *Science and information conference*, 2018. Springer, pp.387-397.
- Khatib, O. (1986) 'Real-time obstacle avoidance for manipulators and mobile robots'. *Autonomous robot vehicles*. Springer, pp. 396-404.
- Kleinbort, M., Solovey, K., Littlefield, Z., Bekris, K.E. and Halperin, D. (2018) 'Probabilistic completeness of RRT for geometric and kinodynamic planning with forward propagation'. *IEEE Robotics and Automation Letters*, 4 (2), pp. x-xvi.

- Kleppner, D. and Kolenkow, R. (2014) *An introduction to mechanics*. Cambridge University Press.
- Kothari, C.R. (2004) *Research methodology: Methods and techniques*. New Age International.
- Kumar, K.N., Ranga, V.P. and Govind, K.S. (2019) 'Design and Development of Dual Arm Mobile Robotic Platform for Warehouse Applications'. *Congress of Indian Society of Theoretical and Applied Mechanics*. India, Available at: [https://203.110.246.133/resources/2019/proceedings/Paper\\_Full/124fullpaper.pdf](https://203.110.246.133/resources/2019/proceedings/Paper_Full/124fullpaper.pdf).
- Kusuma, M. and Machbub, C. (2019) Published. 'Humanoid robot path planning and rerouting using A-Star search algorithm'. *2019 IEEE International Conference on Signals and Systems (ICSigSys)*, 2019. IEEE, pp.110-115.
- Lakshmanan, A.K., Mohan, R.E., Ramalingam, B., Le, A.V., Veerajagadeshwar, P., Tiwari, K. and Ilyas, M. (2020) 'Complete coverage path planning using reinforcement learning for tetromino based cleaning and maintenance robot'. *Automation in Construction*, 112 103078.
- Le, A.V., Prabakaran, V., Sivanantham, V. and Mohan, R.E. (2018) 'Modified a-star algorithm for efficient coverage path planning in tetris inspired self-reconfigurable robot with integrated laser sensor'. *Sensors*, 18 (8), pp. 2585.
- Lee, G.F., Rast, W. and Jones, R.A. (1978) 'Water Report: Eutrophication of water bodies: Insights for an age old problem'. *Environmental Science & Technology*, 12 (8), pp. 900-908.
- Lee, M.C. and Park, M.G. (2003) Published. 'Artificial potential field based path planning for mobile robots using a virtual obstacle concept'. *Proceedings 2003 IEEE/ASME International Conference on Advanced Intelligent Mechatronics (AIM 2003)*, 2003. IEEE, pp.735-740.
- Li, M. (2019) *An investigation of haptic assisted robotic manipulating and planning for high accuracy control*. University of Strathclyde.
- Lines, J.A. (1991) *The suspension characteristics of agricultural tractor tyres*. Doctoral Cranfield Institute of Technology.
- Liu, C., Lee, S., Varnhagen, S. and Tseng, H.E. (2017) Published. 'Path planning for autonomous vehicles using model predictive control'. *2017 IEEE Intelligent Vehicles Symposium (IV)*, 2017. IEEE, pp.174-179.
- Liu, G., Li, T., Peng, Y. and Hou, X. (2005) Published. 'The ant algorithm for solving robot path planning problem'. *Third International Conference on Information Technology and Applications (ICITA'05)*, 2005. IEEE, pp.25-27.
- Liu, S. and Sun, D. (2013) 'Minimizing energy consumption of wheeled mobile robots via optimal motion planning'. *IEEE/ASME Transactions on Mechatronics*, 19 (2), pp. 401-411.
- Łukowska, A., Tomaszuk, P., Dzierżek, K. and Magnuszewski, Ł. (2019) Published. 'Soil sampling mobile platform for Agriculture 4.0'. *2019 20th International Carpathian Control Conference (ICCC)*, 2019. IEEE, pp.1-4.
- Martinez, J.L., Pozo-Ruz, A., Pedraza, S. and Fernandez, R. (1998) Published. 'Object following and obstacle avoidance using a laser scanner in the outdoor mobile robot Auriga-/spl alpha'. *Proceedings. 1998 IEEE/RSJ International Conference on Intelligent Robots and Systems. Innovations in Theory, Practice and Applications (Cat. No. 98CH36190)*, 1998. IEEE, pp.204-209.

- Maxongroup (2021) *Maxon 203126 Gearbox Catalog page*. Available at: [https://www.maxongroup.com/medias/sys\\_master/root/8882781224990/EN-21-405-406-407.pdf](https://www.maxongroup.com/medias/sys_master/root/8882781224990/EN-21-405-406-407.pdf).
- Millea, N. (2003) 'National progress report of Great-Britain 2000-2002'.
- Mollazade, K., Omid, M. and Arefi, A. (2012) 'Comparing data mining classifiers for grading raisins based on visual features'. *Computers and Electronics in Agriculture*, 84 124-131.
- Montes, N., Mora, M.C. and Tornero, J. (2007) Published. 'Trajectory generation based on rational bezier curves as clothoids'. *2007 IEEE Intelligent Vehicles Symposium*, 2007. IEEE, pp.505-510.
- Morris, B., Medyckyj-Scott, D. and Burnhill, P. (2000) 'EDINA Digimap: new developments in the Internet Mapping and Data Service for the UK Higher Education community'. *Liber Quarterly*, 10 (4), pp. 445-453.
- NASA, J.-C., Univ. of Arizona (2013) *Southbound Opportunity, June 2013*. Available at: <https://www.jpl.nasa.gov/images/southbound-opportunity-june-2013>.
- Nguyen, T.M., Vu, L.D. and Nguyen, Q. (2019) Published. 'Evaluation Motion Comfort of Sleeper Coach, the Type of Vehicle Is Manufactured and Assembled at Vietnam, Effect of Random Road Profile Based on Standard ISO 8608'. *International Conference on Engineering Research and Applications*, 2019. Springer, pp.303-309.
- Niu, C. and Yan, X. (2018) Published. 'Energy optimization path planning for battery-powered agricultural rover'. *MATEC Web of Conferences*, 2018. EDP Sciences, pp.02001.
- Noreen, I., Khan, A., Asghar, K. and Habib, Z. (2019) 'A path-planning performance comparison of RRT\*-AB with MEA\* in a 2-dimensional environment'. *Symmetry*, 11 (7), pp. 945.
- Ooi, C.C. and Schindelbauer, C. (2009) 'Minimal energy path planning for wireless robots'. *Mobile Networks and Applications*, 14 (3), pp. 309-321.
- Orozco-Rosas, U., Montiel, O. and Sepúlveda, R. (2019) 'Mobile robot path planning using membrane evolutionary artificial potential field'. *Applied Soft Computing*, 77 236-251.
- Pahl, G. and Beitz, W. (1996) 'Embodiment design'. *Engineering design*. Springer, pp. 199-403.
- Pahl, G., Beitz, W., Feldhusen, J. and Grote, K.-H. (2007) *Engineering design: a systematic approach*. London: Springer.
- Pamosoaji, A.K. and Hong, K.S. (2013) 'A Path-Planning Algorithm Using Vector Potential Functions in Triangular Regions'. *Ieee Transactions on Systems Man Cybernetics-Systems*, 43 (4), pp. 832-842.
- Papadimitriou, G., Saigol, Z. and Lane, D.M. (2015) Published. 'Enabling fault recovery and adaptation in mine-countermeasures missions using ontologies'. *OCEANS 2015-Genova*, 2015. IEEE, pp.1-7.
- Peralta, F., Arzamendia, M., Gregor, D., Reina, D.G. and Toral, S. (2020) 'A comparison of local path planning techniques of autonomous surface vehicles for monitoring applications: The ypacarai lake case-study'. *Sensors*, 20 (5), pp. 1488.
- Pinzi, M., Galvan, S. and y Baena, F.R. (2019) 'The Adaptive Hermite Fractal Tree (AHFT): a novel surgical 3D path planning approach with curvature and heading constraints'. *International journal of computer assisted radiology and surgery*, 14 (4), pp. 659-670.

- Prathibha, S., Hongal, A. and Jyothi, M. (2017) Published. 'IoT based monitoring system in smart agriculture'. *2017 International Conference on Recent Advances in Electronics and Communication Technology (ICRAECT)*, 2017. IEEE, pp.81-84.
- Qi, N., Ma, B., Zhang, Z. and Ren, D. (2008) Published. 'A modified artificial potential field algorithm for mobile robot path planning'. *2008 7th World Congress on Intelligent Control and Automation*, 2008. IEEE, pp.2603-2607.
- Qixin, C., Yanwen, H. and Jingliang, Z. (2006) Published. 'An evolutionary artificial potential field algorithm for dynamic path planning of mobile robot'. *2006 IEEE/RSJ International Conference on Intelligent Robots and Systems*, 2006. IEEE, pp.3331-3336.
- Rabinowicz, E. (1951) 'The nature of the static and kinetic coefficients of friction'. *Journal of applied physics*, 22 (11), pp. 1373-1379.
- Raja, R., Dutta, A. and Venkatesh, K.S. (2015) 'New potential field method for rough terrain path planning using genetic algorithm for a 6-wheel rover'. *Robotics and Autonomous Systems*, 72 295-306.
- Reiter, C., Wildfeuer, L., Wassiliadis, N., Krahl, T., Dirnecker, J. and Lienkamp, M. (2019) Published. 'A holistic approach for simulation and evaluation of electrical and thermal loads in lithium-ion battery systems'. *2019 Fourteenth International Conference on Ecological Vehicles and Renewable Energies (EVER)*, 2019. IEEE, pp.1-17.
- Rödel, C., Stadler, S., Meschtscherjakov, A. and Tscheligi, M. (2014) Published. 'Towards Autonomous Cars'. 2014. Association for Computing Machinery.
- Samuel, M., Hussein, M. and Mohamad, M.B. (2016) 'A review of some pure-pursuit based path tracking techniques for control of autonomous vehicle'. *International Journal of Computer Applications*, 135 (1), pp. 35-38.
- Scharf, L.L., Harthill, W.P. and Moose, P.H. (1969) 'A comparison of expected flight times for intercept and pure pursuit missiles'. *IEEE Transactions on Aerospace and Electronic Systems*, (4), pp. 672-673.
- Serway, R.A. (1986) *Study Guide with Computer Exercises to Accompany Physics for Scientists and Engineers, [and] Physics for Scientists and Engineers with Modern Physics*. Saunders College Pub.
- Sharma, K. and Palwalia, D.K. (2017) Published. 'A modified PID control with adaptive fuzzy controller applied to DC motor'. *2017 International Conference on Information, Communication, Instrumentation and Control (ICICIC)*, 2017. IEEE, pp.1-6.
- Sharpe, J.E. (2012) *AI System Support for Conceptual Design: Proceedings of the 1995 Lancaster International Workshop on Engineering Design, 27–29 March 1995*. Springer Science & Business Media.
- Shivgan, R. and Dong, Z. (2020) Published. 'Energy-Efficient Drone Coverage Path Planning using Genetic Algorithm'. *2020 IEEE 21st International Conference on High Performance Switching and Routing (HPSR)*, 2020. IEEE, pp.1-6.
- Shrivastava, P., Soon, T.K., Idris, M.Y.I.B. and Mekhilef, S. (2019) 'Overview of model-based online state-of-charge estimation using Kalman filter family for lithium-ion batteries'. *Renewable and Sustainable Energy Reviews*, 113 109233.

- Slowik, A. and Bialko, M. (2007) Published. 'Design and optimization of IIR digital filters with non-standard characteristics using particle swarm optimization algorithm'. *2007 14th IEEE International Conference on Electronics, Circuits and Systems*, 2007. IEEE, pp.162-165.
- Study, N.R.C.T.R.B.C.f.t.N.T.E. (2006) *Tires and passenger vehicle fuel economy: informing consumers, improving performance*. Transportation Research Board.
- Sun, B., Zhu, D., Tian, C. and Luo, C. (2018) 'Complete coverage autonomous underwater vehicles path planning based on gladius bio-inspired neural network algorithm for discrete and centralized programming'. *IEEE Transactions on Cognitive and Developmental Systems*, 11 (1), pp. 73-84.
- Tikhonov, A.N. and Samarskii, A.A. (2013) *Equations of mathematical physics*. Courier Corporation.
- Tipler, P.A. and Mosca, G. (2007) *Physics for scientists and engineers*. Macmillan.
- Tseng, F.H., Liang, T.T., Lee, C.H., Der Chou, L. and Chao, H.C. (2014) Published. 'A star search algorithm for civil UAV path planning with 3G communication'. *2014 Tenth International Conference on Intelligent Information Hiding and Multimedia Signal Processing*, 2014. IEEE, pp.942-945.
- Tudón-Martínez, J.C., Fergani, S., Sename, O., Martínez, J.J., Morales-Menendez, R. and Dugard, L. (2015) 'Adaptive road profile estimation in semiactive car suspensions'. *IEEE Transactions on Control Systems Technology*, 23 (6), pp. 2293-2305.
- Umari, H. and Mukhopadhyay, S. (2017) Published. 'Autonomous robotic exploration based on multiple rapidly-exploring randomized trees'. *2017 IEEE/RSJ International Conference on Intelligent Robots and Systems (IROS)*, 2017. IEEE, pp.1396-1402.
- Vadakkepat, P., Tan, K.C. and Ming-Liang, W. (2000) Published. 'Evolutionary artificial potential fields and their application in real time robot path planning'. *Proceedings of the 2000 congress on evolutionary computation. CEC00 (Cat. No. 00TH8512)*, 2000. IEEE, pp.256-263.
- Wallace, R.S., Stentz, A., Thorpe, C.E., Moravec, H.P., Whittaker, W. and Kanade, T. (1985) Published. 'First Results in Robot Road-Following'. *International Joint Conference on Artificial Intelligence*, 1985. Citeseer, pp.1089-1095.
- Warren, C.W. (1989) Published. 'Global path planning using artificial potential fields'. *Robotics and Automation, 1989. Proceedings., 1989 IEEE International Conference on*, 1989. IEEE, pp.316-321.
- Williams, G., Aldrich, A. and Theodorou, E.A. (2017) 'Model predictive path integral control: From theory to parallel computation'. *Journal of Guidance, Control, and Dynamics*, 40 (2), pp. 344-357.
- Williford, K.H., Farley, K.A., Stack, K.M., Allwood, A.C., Beaty, D., Beegle, L.W., Bhartia, R., Brown, A.J., de la Torre Juarez, M. and Hamran, S.-E. (2018) 'The NASA Mars 2020 rover mission and the search for extraterrestrial life'. *From habitability to life on Mars*. Elsevier, pp. 275-308.
- Wit, J.S. (2000) *Vector pursuit path tracking for autonomous ground vehicles*. FLORIDA UNIV GAINESVILLE CENTER FOR INTELLIGENT MACHINES AND ROBOTICS.
- Wong, C., Mineo, C., Yang, E., Yan, X.-T. and Gu, D. (2020) 'A novel clustering-based algorithm for solving spatially-constrained robotic task sequencing problems'. *IEEE/ASME Transactions on Mechatronics*.

- Xaud, M.F., Leite, A.C., Barbosa, E.S., Faria, H.D., Loureiro, G.S. and From, P.J. (2019) 'Robotic Tankette for Intelligent BioEnergy Agriculture: Design, Development and Field Tests'. *The XXII Brazilian Conference on Automation*.
- Yan, X.-T., Bianco, A., Niu, C., Palazzetti, R., Henry, G., Li, Y., Tubby, W., Kisdi, A., Irshad, R. and Sanders, S. (2020) 'The agrirover: a reinvented mechatronic platform from space robotics for precision farming'. *Reinventing Mechatronics*. Springer, pp. 55-73.
- Yan, X.-T. and Zante, R. (2010) 'A mechatronic design process and its application'. *Mechatronics in Action*. Springer, pp. 55-70.
- Yan, X.T., Donaldson, K.M., Davidson, C.M., Gao, Y., Wu, H., Houston, A.M. and Kisdi, A. (2018) 'Effects of sample pretreatment and particle size on the determination of nitrogen in soil by portable LIBS and potential use on robotic-borne remote Martian and agricultural soil analysis systems'. *RSC advances*, 8 (64), pp. 36886-36894.
- Zacherl, L., Radlmayr, J. and Bengler, K. (2020) Published. 'Constructing a mental model of automation levels in the area of vehicle guidance'. *International conference on intelligent human systems integration*, 2020. Springer, pp.73-79.

# Appendix A: Co-Simulation

## Notes for the Co-Simulation Setup for Future Reference

### Variable Setup

Only one variable for each type is selected for explanation in this section, as all variables of the same type will be setup in the same way.

Input variable: torque\_vr1

The driving torque variable, torque\_vr1, is the variable for the right front wheel's torque, as shown in Figure 118. Variable torque\_vr1 is an input variable which is set as shown in the window in Figure 119.

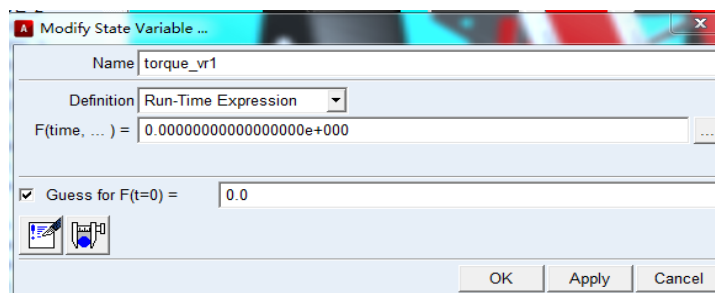


Figure 118. Variable torque\_vr1 setup

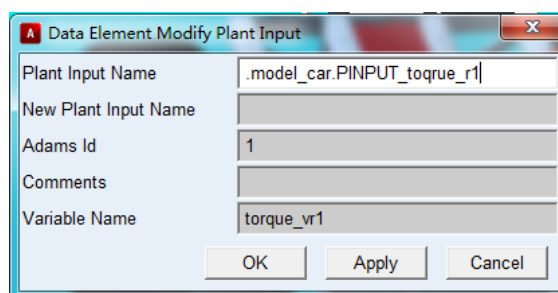


Figure 119. Set input variables

The last step is to connect the torque\_vr1 variable to the rover model. The input variable created in Figure 119 is used as the value of the control model torque as shown

in Figure 120. This completes the settings for the driving torque. The torque settings for the other wheels are completed in the same way.

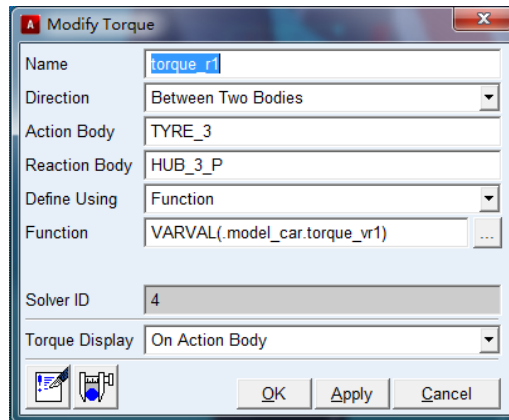


Figure 120. Set the torque

Input variable: angle\_v12

The establishment of the angle variables and setting of the input variables is the same as the steps shown in the last section. The difference for this variable type is the relationship with the rover model, because the control method before was for torque control, and the steering uses acceleration control. The simplest control method, due to the limited computational power, is to directly control the steering angles, but it had problems after several attempts.

A movement is created, as shown in Figure 121Figure 95. Then the rotation pair for the right front wheel created earlier was selected in the joint motion setting box, as shown in Figure 121. The parameters was set and the type is set to acceleration.

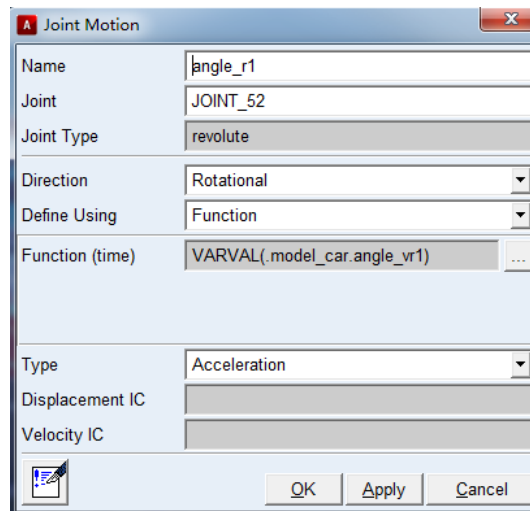


Figure 121. Acceleration settings

The two front wheels have been set with parallel constraints before, so no movement is defined for the left front wheel. Then, as the front wheel steering and driving is adopted in this example, the rear wheels will follow passively, so the rear wheels will not have any moving motion defined.

Input variable: torque\_pos

This variable is only used for data processing after the simulation, and it is not part of the input of the physical model of the rover, this can be set using the same method above.

Output variable: vposex

This variable was setup using the same method as before, with the difference in the F(time) section that DX(CONNECTING\_PLATE\_FRONT.cm,MARKER\_342) has to be selected, which links the markers and motions as shown in Figure 122

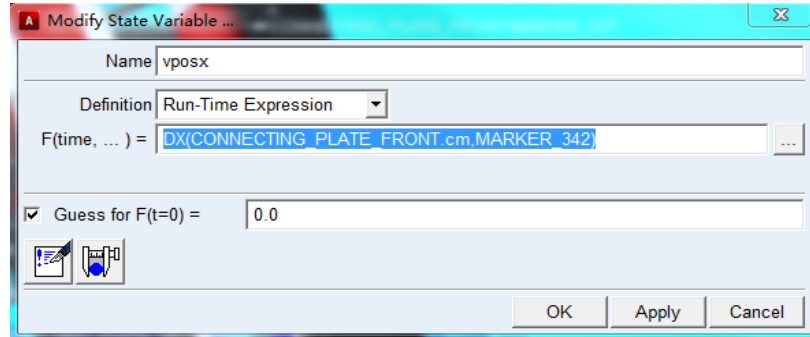


Figure 122. Link the model with the variable

## Links between MATLAB Simulink and ADAMS

In Controls\_Plant\_model.mdl, the window of the function block parameters in Simulink is opened and the ADAMS model and output prefix is set to ADAMS\_prefix, as shown in Figure 123.

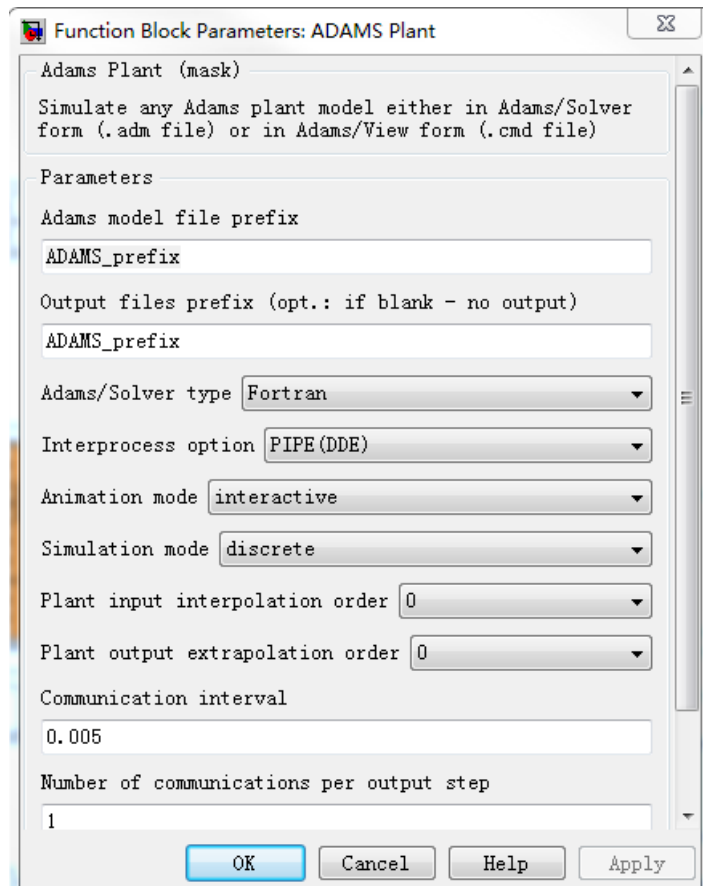


Figure 123. Function Block Parameter: ADAMS Plant window

The following settings is refined by proceeding with the simulation experiment debugging. The Interprocess is set to PIPE(DDE). If the two software are not running on the same computer, the Interprocess is set to TCP/IP, and a communication link will need to be setup. Adams/Solver is set to Fortran. The Communication Interval is set to 0.005, which means the data communication between ADAMS and MATLAB will happen every 0.005s. The Simulation Mode is set to discrete, if not the Rover will go through the terrain. The Animation mode is set to interactive, which enables interactive calculations between ADAMS and MATLAB, and while the co-simulation is running the ADAMS/View will show the simulation as the Rover moves through the path. If batch is selected, instead of interactive, the simulation will be in batch processing and no simulation animation will show. Finally, the simulation time is set to 800 in the Controls\_Plant\_model.mdl, so that there is enough time for all the rover's simulation to move through the path is completed.

## Co-Simulation Result Data Processing

1. After the co-simulation is finished, the ADAMS interface will automatically be closed and a .res file will be automatically generated.
2. Use the shortcut key F8 to enter the post/processor interface, select file>import>result file, select the newly generated controls\_plant\_1.res file under the file name, and select model\_car under the model's name. Finally Click OK.
3. Right-click anywhere on the result processing area, then select load animation, select the corresponding res file, and then the animation will start play. Note that when playing the animation, the frame increments have to be a larger value, such as 100, otherwise due to the amount of data being too large, it could result in insufficient computer memory.
4. Right-click the simulation window in the data window shown below in Figure 124, and select as shown. The vehicle speed curve is then drawn.

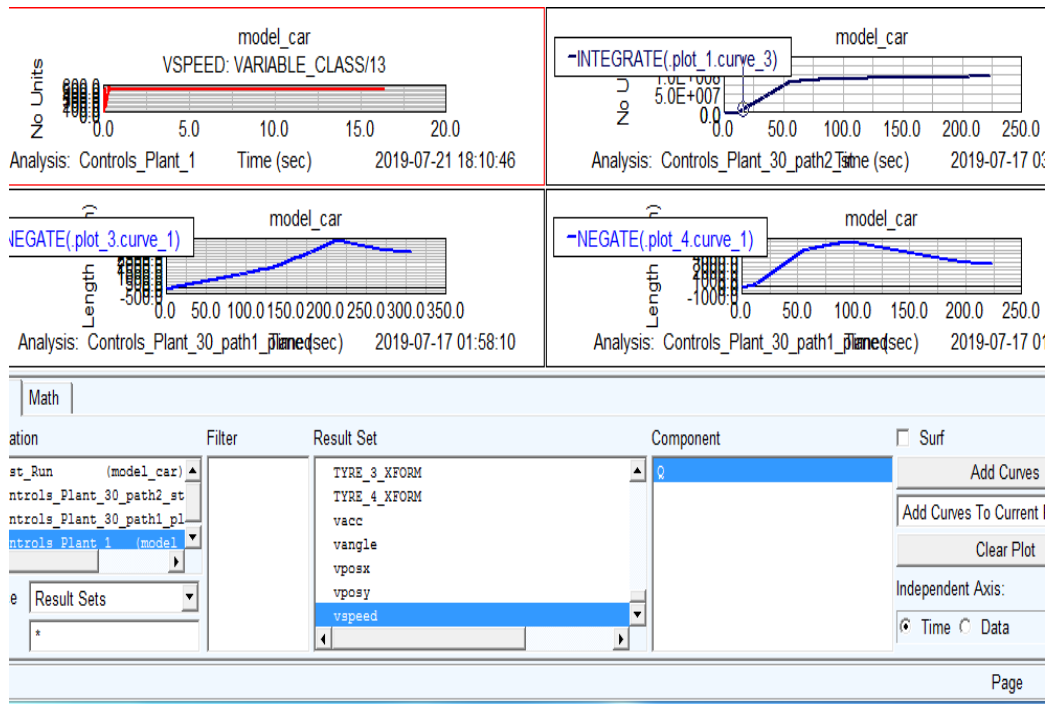


Figure 124. Simulation window

5. In the same window, add the torque value and change the content of the Result Set box to torque\_pos, as shown in Figure 125 below.

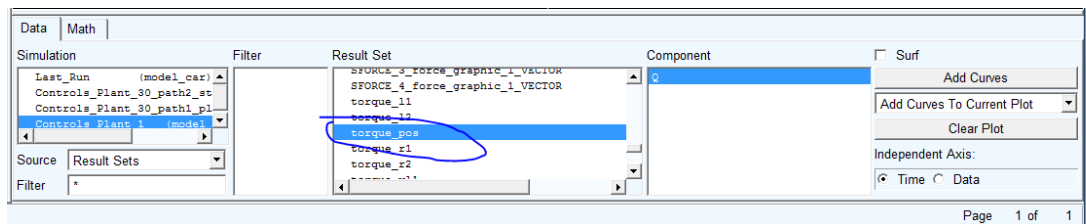


Figure 125. The Result Set box selecting torque\_pos

6. Then click the multiply button, set by the tool above, and select two curves torques and speeds to multiply. A new curve will appear, and this is the power curve ( $E=V \cdot F$ ), as shown in Figure 126.

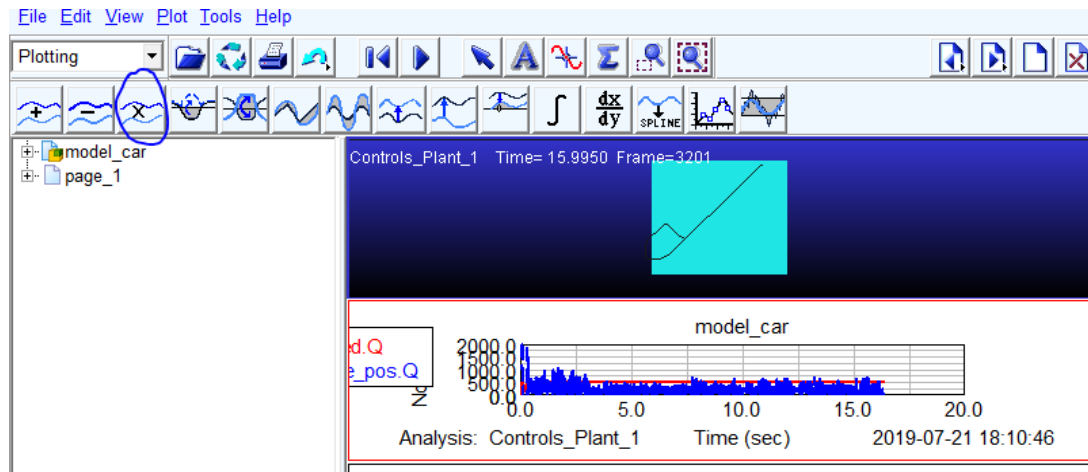


Figure 126. Power curve generation

7. By integral the third curve, the corresponding energy consumption can be obtained. There is a conversion relationship between the energy consumption calculated here and the real energy consumption. Because the above is a single-wheel's torque, it is multiplied by the speed of the car. In the real word it should be the torque multiplied by the speed and by two wheels, so it is double of the one shown.

## Problems and Solutions of Co-Simulation

### Path is Too Long

If the planned path is too long, the amount of simulation data will be too large, resulting in the inability to post-process the data. Increasing the control cycle can reduce the amount of data, but the effect of the control result will be worse. To solve this, a long path can be broken down to shorter paths, and thus the co-simulations can be done with shorter paths.

### Animation Playback Needing More RAM

During animation playback, increase the frame increment, otherwise it is easy to run out of memory, even with 64GB computers. This can be accounted for by increasing the system memory.

### Co-Simulation Contact Force Invalid

The four wheels of the vehicle define the contact force on the road surface entity, which can be simulated normally when using ADAMS alone. However, when using MATLAB for joint co-simulation, it is found that the contact force fails and the model directly passes the terrain and falls through. To solve this, the user can set the Simulation Mode to discrete in ADAMS in the export control parameters set.

### Robot Wheel Skidding

If the contact set between the wheel and the terrain is not set correctly, slipping is likely to occur. Changing the contact method from friction to impact will solve this problem.